NUREG/CR-6369, Vol. 3
SEA 97-3105-A:17

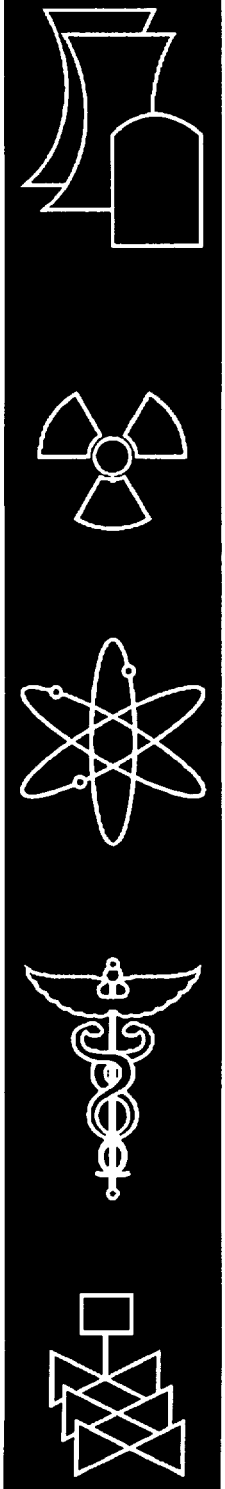

Drywell Debris Transport Study: Computational Work

Final Report

Science and Engineering Associates, Inc.

U.S. Nuclear Regulatory Commission
Office of Nuclear Regulatory Research
Washington, DC 20555-0001

AVAILABILITY NOTICE

Availability of Reference Materials Cited in NRC Publications

NRC publications in the NUREG series, NRC regulations, and *Title 10, Energy,* of the *Code of Federal Regulations,* may be purchased from one of the following sources:

1. The Superintendent of Documents
   U.S. Government Printing Office
   P.O. Box 37082
   Washington, DC 20402–9328
   <http://www.access.gpo.gov/su_docs>
   202–512–1800

2. The National Technical Information Service
   Springfield, VA 22161–0002
   <http://www.ntis.gov/ordernow>
   703–487–4650

The NUREG series comprises (1) brochures (NUREG/BR-XXXX), (2) proceedings of conferences (NUREG/CP-XXXX), (3) reports resulting from international agreements (NUREG/IA-XXXX), (4) technical and administrative reports and books [(NUREG-XXXX) or (NUREG/CR-XXXX)], and (5) compilations of legal decisions and orders of the Commission and Atomic and Safety Licensing Boards and of Office Directors' decisions under Section 2.206 of NRC's regulations (NUREG-XXXX).

A single copy of each NRC draft report is available free, to the extent of supply, upon written request as follows:

Address: Office of the Chief Information Officer
Reproduction and Distribution
Services Section
U.S. Nuclear Regulatory Commission
Washington, DC 20555–0001
E–mail: <DISTRIBUTION@nrc.gov>
Facsimile: 301–415–2289

A portion of NRC regulatory and technical information is available at NRC's World Wide Web site:

<http://www.nrc.gov>

All NRC documents released to the public are available for inspection or copying for a fee, in paper, microfiche, or, in some cases, diskette, from the Public Document Room (PDR):

NRC Public Document Room
2120 L Street, N.W., Lower Level
Washington, DC 20555–0001
<http://www.nrc.gov/NRC/PDR/pdr1.htm>
1–800–397–4209 or locally 202–634–3273

Microfiche of most NRC documents made publicly available since January 1981 may be found in the Local Public Document Rooms (LPDRs) located in the vicinity of nuclear power plants. The locations of the LPDRs may be obtained from the PDR (see previous paragraph) or through:

<http://www.nrc.gov/NRC/NUREGS/SR1350/V9/lpdr/html>

Publicly released documents include, to name a few, NUREG-series reports; *Federal Register* notices; applicant, licensee, and vendor documents and correspondence; NRC correspondence and internal memoranda; bulletins and information notices; inspection and investigation reports; licensee event reports; and Commission papers and their attachments.

Documents available from public and special technical libraries include all open literature items, such as books, journal articles, and transactions, *Federal Register* notices, Federal and State legislation, and congressional reports. Such documents as theses, dissertations, foreign reports and translations, and non-NRC conference proceedings may be purchased from their sponsoring organization.

Copies of industry codes and standards used in a substantive manner in the NRC regulatory process are maintained at the NRC Library, Two White Flint North, 11545 Rockville Pike, Rockville, MD 20852–2738. These standards are available in the library for reference use by the public. Codes and standards are usually copyrighted and may be purchased from the originating organization or, if they are American National Standards, from—

American National Standards Institute
11 West 42nd Street
New York, NY 10036–8002
<http://www.ansi.org>
212–642–4900

NUREG/CR-6369, Vol. 3
SEA 97-3105-A:17

Drywell Debris Transport Study: Computational Work

Final Report

Manuscript Completed: February 1998
Date Published: September 1999

Prepared by
C. Shaffer, D. V. Rao, J. Brideau

Science and Engineering Associates, Inc.
6100 Uptown Blvd. NE
Albuquerque, NM 87110

Prepared for
Division of Engineering Technology
Office of Nuclear Regulatory Research
U.S. Nuclear Regulatory Commission
Washington, DC 20555-0001
NRC Job Code W6325

For sale by the U.S. Government Printing Office
Superintendent of Documents, Mail Stop: SSOP, Washington, DC 20402-9328
ISBN 0-16-050194-6

Abstract

This report describes various analyses conducted as part of the drywell debris transport study. The primary objective of these analyses was to identify controlling phenomena and critical data requirements. A secondary objective was to explore various options available to model debris transport in the drywell, and make judgements regarding the degree of accuracy to which each phenomenon should be modeled. These analyses decomposed the problem into several components that were amenable to resolution by well-proven analytical models. The analyses specifically addressed the following phenomena that significantly impact debris transport: pressure vessel blowdown, containment thermal-hydraulics (e.g., structural wetness, flow velocities in the drywell), debris removal by various capture mechanisms and debris transport in the water pools formed on the drywell floor. The analytical tools used in the study included RELAP, MELCOR and CFD-2000. The results of some of the analyses were used to design the experiments conducted as part of the study and during the debris transport quantification process described in NUREG/CR-6369, Vol. 1.

Contents

Table of Contents (Continued)

List of Figures

List of Figures (Continued)

List of Tables

Executive Summary

A postulated LOCA in a BWR whose primary piping is insulated with fibrous material will generate fibrous debris in a region close to the break. This debris would be transported from the location of the break to vent pipes by a combination of steam and water components of the blowdown flow. During transport, a fraction of the generated debris may be removed from the flow by mechanisms such as gravitational settling, inertial capture and diffusion. Studies by SEA as well and the PIRT Panel assembled by NRC identified several key phenomena that were judged to significantly control debris transport. Among these were (a) flow rate and thermodynamic conditions[1] of the blowdown, (b) time and duration of debris generation, (c) local and bulk flow velocities, (d) containment thermal hydraulics (including structural wetness), (e) relative contributions of various capture/removal mechanisms and (f) transport of the debris in the water pools formed on the drywell floor. A realistic understanding of these phenomena is vital to estimate debris transport factors. A series of analyses were undertaken as part of drywell debris transport study to identify controlling phenomena and data required to quantify their impact on debris transport to the desired degree of accuracy. A secondary objective of these analyses was to explore various options available for modeling debris transport in the drywell and select those methods that best meet the goals of this study[2]. With these objectives, a series of calculations were undertaken. These calculations can be broadly divided into four groups according to the phenomenon they studied.

The first series of calculations addressed pressure vessel blowdown. These calculations were necessitated by the fact that blowdown flow rates given in the updated final safety analysis reports (UFSAR) were judged to be unrealistic for the purpose of debris transport estimation, especially for the postulated main steam line breaks (MSLB). The focus of the calculations was to obtain reasonable estimates for flow through the break, its thermodynamic state and its duration for breaks postulated in main steam line and recirculation line of small and large BWRs. SEA developed a scoping model based on a set of well-proven and widely used equations that govern critical flow through nozzles. Predictions of the model were verified by comparison with RELAP calculations, which were also used to derive some of the key parameters of the SEA model. The study suggested that no major difference exists between various plant types. In all cases blowdown occurs within the first 100 seconds following a LOCA. In the case of MSLB, the stagnation quality at the exit plane varies between 100-70%, although the void fraction is close to 99% all through the blowdown. Calculations also concluded that debris would likely be generated within the first few seconds when the dynamic pressures in the break vicinity are larger and debris would be steam-borne. In the case of a recirculation line break, initially the flow is nearly 100% water. Due to flashing within the vessel and the piping, flow quality steadily increases reaching as high as 38%. During the same time the stagnation void fraction changes from 0.05 to 80%. In this case, majority of the debris would be generated during later stages of the accident and would be water-borne.

The second series of calculations addressed thermal and hydraulic conditions that exist in the drywell following postulated breaks in the recirculation and main steam lines. The calculations relied primarily on MELCOR, an NRC code specifically developed and validated for such a purpose. In selected cases, the results of MELCOR were verified by hand calculations. Important conclusions of the study were that structures would become wet within the first second after a LOCA. It is unlikely that a water pool would form on the drywell floor during blowdown following a steam line break. On the other hand, pool formation and overflow is very likely following a recirculation line break. It would take less than a second for the

[1] The thermodynamic condition of particular interest is steam flow quality. Transport pathways for high quality steam flows would be quite different from those for low quality (primarily water) flows.

[2] The goal of this study (as noted in NUREG/CR-6369, Section 1) is not to develop a best-estimate predictive tool. But to derive reasonable upper bound estimates of debris transport factors employing models/methods that can be easily comprehended by engineers that are not necessarily experts in the field of particle transport.

drywell to reach a quasi-steady state and for the vents to be cleared of water. Thereafter, drywell atmosphere is purged through the downcomers to the suppression pool where it is condensed.

The MELCOR runs described above were also used to draw some insights into debris transport and explore the capability of particle transport models inherent to MELCOR. These calculations suggested that although MELCOR could be useful for conducting integrated debris transport calculations, its particle transport model would have to be modified and validated to facilitate such an application. Such an effort is justifiable only if a best-estimate predictive tool is the desired objective of DDTS. Otherwise, simpler models should be used to quantify the importance of each of the debris capture mechanisms. With this view, a series of calculations were conducted to understand the relative importance of each capture mechanism as a function of the break type and debris size. The results of these analyses suggested that gravitational settling would be negligible for small and medium size debris, but could be dominant for large debris. Another, mechanism for capture of large debris is entrapment on floor gratings and vent entrances. On the other hand, dominant capture mechanisms for small and medium debris would likely be inertial capture and diffusionary processes. Calculations clearly established that small and medium size debris would impact structures located in their
pathways, but it was not clear if they would stick to wet surfaces or would be carried away by the steam flow. The analyses concluded that this was one area where further research was necessary. Another area identified for research included washdown of debris by containment sprays and break overflow. Experiments were conducted later in the study to investigate these areas.

The final set of calculations addressed the issue of debris transport in the water pool formed on the drywell floor. These calculations employed a commercially available computational fluid dynamics (CFD) code CFD-2000 to predict flow patterns that exist in the pool and their impact on debris transport. The calculations were conducted in two steps. In the first step, CFD-2000 was used to simulate past experiments to establish flow conditions that would be necessary to maintain debris of various sizes in suspension. The second step estimated actual flow conditions that would exist on the drywell floor as a result of containment sprays or break overflow, and used that information to judge if those flow conditions would be sufficient to keep the debris in suspension. The study clearly established that debris transport is strongly dependent on the accident scenario and drywell layout. The results of these calculations were directly used in NUREG/CR-6369 to quantify debris transport.

List of Acronyms

ANS	American Nuclear Society
ANSI	American National Standards Institute
ARL	Alden Research Laboratories, Inc.
BWR	Boiling water reactor
CEESI	Colorado
CFD	Computational fluid dynamics
DDT	Drywall Debris Transport Study
DEGB	Double ended guillotine break
ECCS	Emergency core cooling system
FSAR	Final Safety Analysis Report
HEM	Homogeneous equilibrium model
LOCA	Loss of coolant accident
LPCI	Low pressure core spray
LPCS	Low pressure core spray
MSIV	Main steam isolation valve
MSLB	Main steam line break
NRC	U.S. Nuclear Regulatory Commission
PIRT	Phenomena Identification and Ranking Table
PPL	Pennsylvania Power and Light Company
RECIR	Recirculation pipe
SEA	Science & Engineering Associates, Inc.
UFSAR	Updated Final Safety Analysis Report

1. Introduction

1.1 Background and Objectives

A LOCA in a BWR would generate piping insulation debris ranging in size from small fibrous shreds to partially torn insulation blankets. High velocity blowdown flows would transport these insulation fragments from the location of their generation to the suppression pool. During their transport, potentially that some of the fragments may be captured on various drywell structures (e.g., pipes, I-beams, and cable conduits). This potential is depends strongly on factors such as time and duration of debris generation, size and wetness of the debris, wetness of the structural surfaces and local and bulk flow patterns (i.e., flow velocity and direction). In turn, these factors are controlled by thermal-hydraulic phenomena, such as blowdown flow rate, vent clearing and condensation on structures. After blowdown is completed, water enters the drywell due to containment spray operation or overflow from the broken pipes. As the water cascades down from the location of its introduction, it washes down debris and deposits them in the pool formed on the drywell floor. In the pool, the debris may settle down or remain in suspension depending on the level of flow turbulence and pool flow patterns.

In February 1996, SEA completed a study to identify important phenomena that dominate debris transport in BWRs [Ref. 1-1]. Based on this study, SEA proposed a methodology by which debris transport could be predicted using a combination of analytical tools. In 1996, NRC assembled a PIRT panel to review SEA's proposed approach. After reviewing Reference 1-1 and other documents, the PIRT panel compiled a preliminary list of important phenomena and suggested that SEA should undertake simple analyses that would provide insights regarding the relative importance of each of the highly ranked phenomena [Ref. 1-2]. Many of the calculations documented in this report were initiated in response to this need. The focus of the analyses was to explore various options available for modeling important phenomena and identify critical data needs for quantification of each phenomenon [Ref. 1-2]. The scope of these calculations was to draw the necessary insights that could be used to develop the scaling rationale for the experiments conducted as part of the study or during quantification of the transport factors. The analyses that were conducted are generally tractable and can be easily comprehended.

1.2 Program Overview and Report Outline

Four different types of independent calculations were performed as part of this study. These calculations can be categorized by the following four phenomena:

Reactor Pressure Vessel Blowdown: The objective of these calculations was to obtain realistic estimates for the blowdown flow rates and their thermodynamic characteristics as a function of the type of postulated break. These calculations were necessitated by the fact that UFSAR values for blowdown flow rates were judged to be unrealistic for the purpose of debris transport estimation. The calculations relied primarily on a simple model developed as part of the study. But some of the key parameters in the model were derived after comparison with RELAP calculations for similar breaks. Model predictions were used effectively to draw insights related to debris generation and debris transport. These calculations and their results are presented in Section 2.

Containment Thermal Hydraulics: The objective of these calculations was to estimate prototypical structural wetness in the drywell. The primary tool used for these calculations was MELCOR, although several hand calculations were conducted to provide the required input and verify the predictions. The results of the calculations provided insights related to: (a) containment pressurization and vent clearing, (b) condensation on structures located at various distances from the break as a function of time, and (c) time-scales associated with drywell pool buildup. The results were effectively used to design the experiments conducted in the DDTS. These calculations and their results are presented in Section 3.

End-to-End Debris Transport Phenomena: A series of calculations, termed as end-to-end calculations, were undertaken to examine the integrated nature of debris transport and identify critical data needs for quantifying effects of important phenomena and plant features. These calculations employed methods that are easily understood by a trained engineer, who is not necessarily an expert in particle transport. The

emphasis of the calculations was to obtain order-of-magnitude estimates, rather than very accurate best-estimate predictions. Various insights provided by these calculations were effectively used during debris transport quantification. These calculations and their results are presented in Section 4.

Debris Transport in the Drywell Pools: Transport of debris washed down by sprays and deposited in the pools formed on the drywell floor was examined using detailed simulations of the flow. A commercially available Computational Fluid Dynamics code (CFD-2000) was used to predict the flow patterns that exist as a result of accumulation containment spray water or ECCS overflow. The predicted flow fields were then used in conjunction with experimental data to determine likelihood of debris transport. Predictions were obtained for three drywell types (Mark I, II and III) and for a variety of accident scenarios. These calculations and their results are presented in Section 5.

1.3 References

1-1 D.V. Rao, C. Shaffer, A. Johnson, and G. Hecker, "Proposed Methodoloty by Modeling LOCA Debris Transport in BWR Drywalls," SEA 96-970-01-A:6, February 1996.

1-2 G. E. Wilson, et al., "BWR Drywell Debris Transport Phenomena Identification and Ranking Tables (PIRT)," Initial Issue, June 28, 1996.

2. Blowdown Flow Characteristics

2.1 Introduction

A postulated DEGB in the primary system piping results in blowdown of pressure vessel inventory until the vessel pressure falls below the LPCI and LPCS pumps shut-off heads. The duration and contents of the blowdown depend on a variety of factors, including break area, discharge coefficient, and systematic considerations. Because, the duration and characteristics of blowdown strongly influence debris generation and transport, it was vital that they be estimated as accurately as possible.

The accident analysis sections of the UFSAR provide the blowdown history for the design basis accidents analyzed by the utility. However, the break flow parameters given in the UFSAR are derived employing very conservative models, which are designed to maximize rate of energy release to the containment following a LOCA. For example, one UFSAR of a large BWR/4 with Mark I containment lists two sets of blowdown flow rates following a large break MSLB. The first set is obtained based on the homogeneous equilibrium model[3] (HEM) and the second one is based on a modified version of HEM developed specifically by the utility. Figure 2-1 compares these flow rates. Also plotted on the figure is a more realistic estimate of flow rates. As evident from this figure, both the FSAR and HEM predictions overestimate vessel pressure (psi), liquid flow rate (lb/s) and underestimate steam flow rate (lb/s). According to these models, a MSLB discharge consists mainly of water, which is quite contrary to the existing experimental evidence, which is closer to the third curve. This difference could have significant implications to debris transport, considering that water-borne debris transport is substantially different from steam-borne transport. Therefore, it was concluded that usage of the UFSAR values to estimate thermal hydraulics conditions for the purpose of evaluating debris transport was inappropriate for a DEGB in the main steam line. A scoping model was developed by SEA to more realistically predict estimates of blowdown flow characteristics following a postulated large break LOCA. The intent of the model was not to provide very accurate predictions of the blowdown flow rates, but more realistic (although still somewhat conservative) predictions. The model is empirical in nature and some of the key parameters (e.g., loss coefficients) in the model were derived after comparing its predictions with those of RELAP computer code. The results of the model were provided as input to the CFD calculations and MELCOR calculations described in the following sections.

[3] HEM was traditionally used for recirculation line break. Some utilities, however, employed HEM also to predict blowdown following MSLB.

2.2 SEA Scoping Model

A simple model developed by SEA [Ref. 2-1] for vessel blowdown included the following equation:

$$G_{cr} = (\rho_{cr})\sqrt{2(h_o \bullet \chi_{cr} \bullet h_g^{cr} - (1 \bullet \chi_{cr}) \bullet h_f^{cr})} \qquad (2\text{-}1)$$

where

G_{cr} = critical flow rate (lbm/ft^2/s)
x_{cr} = flow quality at critical plane
h_g^{cr} = gas phase enthalpy at critical plane (Btu/lbm)
h_f^{cr} = fluid phase enthalpy at critical plane (Btu/lbm)
h_o = stagnation enthalpy (Btu/lbm)

and the critical density ρ_{cr} is given as:

$$\rho_{cr} = \left[\frac{\chi}{\rho_g} + \frac{(1-\chi)S}{\rho_f}\right]\left[\frac{\chi}{S^2}\right] \qquad (2\text{-}2)$$

S is slip ratio. Assuming a slip ratio of 1.0, the above equation can be simplified as

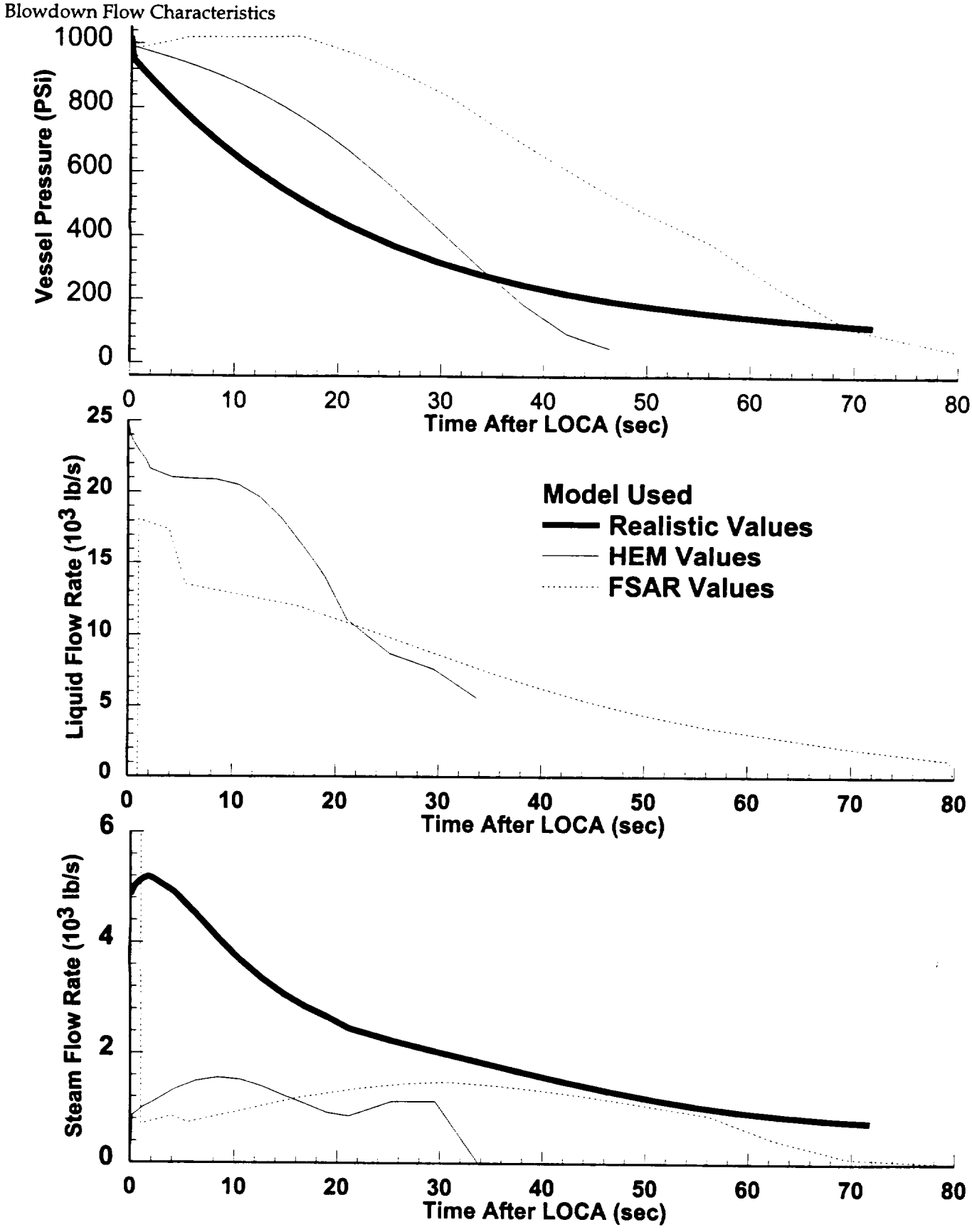

Figure 2-1. Various Model Predictions for MSLB Blowdown

$$\rho_{cr} = \left[\frac{\chi_{cr}}{\rho_g^{cr}} + \frac{(1 - \chi_{cr})S}{\rho_f^{cr}} \right]^{-1} \quad (2\text{-}3)$$

The void fraction at the critical plane can be estimated by:

$$\alpha_{cr} = \frac{1}{1 + \frac{(1 - \chi_{cr})}{\chi_{cr}} \bullet \frac{v_f}{v_g}} \quad (2\text{-}4)$$

where υ_f, υ_g are specific volumes of liquid and gas.

The critical properties are calculated at critical pressure. For pure steam the critical pressure can be calculated from the following equation:

$$P_{cr} = P_o \left[\frac{2}{\gamma + 1} \right]^{\frac{\gamma}{(\gamma - 1)}} \quad (2\text{-}5)$$

where γ is the ratio of specific heats and P_o is the stagnation pressure. Using a γ of 1.12, per for pure steam can be estimated as

$$P_{cr} = 0.58\, P_o \quad (2\text{-}6)$$

For two-phase mixture with qualities in the range of 0.1 - 0.3.

$$\frac{P_{cr}}{P_o} = 0.2 - 0.3 \quad (2\text{-}7)$$

The energy and mass balances for the core are given by:

$$\frac{dM_i}{dt} = - A_B \bullet G_{cr}$$

$$\frac{\Delta h_o}{\Delta t} = (Q_{decay} + Q_{relaxation} - A_B \bullet G_{cr} \bullet h_o^{t-1} \pm Q_{fg})$$

$$P(t) = fn(\chi, v_f, v_g, M_i) \quad (2\text{-}8)$$

where,

A_B is break area (ft^2)

Q_{decay} is decay heat rate (Btu/s)

$Q_{relaxation}$ is relaxation heat rate (Btu/s)

Q_{fg} is heat loss/gain due to phase change (Btu/s)

SEA developed a simple model using these equations and performed calculations for the three different reactor types described above. The model has several drawbacks:

1. Entrainment of water by flow steam is not mechanistically modeled. Instead, correlations provided in Ref. 1 and the RELAP calculation curve used to estimate entrainment.

2. 3-D effects of vessel fluid mixing was not modeled.

The systems performance following a MSLB was assumed as follows:

- MSLB occurs upstream of the flow restrictors
- MSIV close in 2-3 seconds after the DEGB
- The feed water and HPCI pumps are disabled
- Recirculation pumps trip immediately after scram.

For a recirculation line break, the following assumptions were used:

- Feedwater pumps trip after 2-3 seconds when MSIVs close
- Scram occurs on containment pressure
- Recirculation pumps and isolation valves close after scram.

2.3 Comparison with RELAP

RELAP is an NRC code developed for transient analysis of BWRs after a LOCA [Ref.2-2]. In this study, comparison with the RELAP computer code results was sought for two reasons:

- To validate the predictions of SEA model and examine its applicability to this problem, and

- To obtain some the input data (e.g., loss coefficients) that can be used to refine SEA model estimates.

The RELAP results were obtained for two postulated LOCAs:

1. A DEGB LOCA in the Main Steam Line ahead of the flow restrictors in a large BWR/4 with Mark I containment.
2. A DEGB LOCA in the suction end of Recirculation Line in a medium BWR/4 with Mark I containment.

Figure 2-2 compares the SEA scoping model predictions with RELAP for the same plant. As evident from this figure, both the SEA model and RELAP predict blowdown flow rates within the same order of magnitude. The SEA Model predicted slightly higher flow rates for the first ten seconds, while the RELAP runs predicted slightly higher flow in the later part of the accident. These differences are attributable to systems response assumed and the obviously better modeling in RELAP. Nevertheless, this comparison shows that the SEA model predictions are reasonable for a MSLB.

Figure 2-3 provides similar comparison for a postulated break in the recirculation line. Once again, reasonable agreement was noted between SEA model predictions and RELAP predictions.

2.4 Blowdown Predictions

The blowdown predictions were obtained for four different plants:

1. A small BWR/4 with Mark I Containment
2. A Medium BWR/4 with Mark I Containment
3. A Large BWR/4 with Mark I Containment
4. A Large BWR/6 with Mark III Containment.

The objective of this exercise was to examine if the plant types significantly impact accident time scales or containment thermal hydraulic conditions. If significant deviations were noted, then they would be accounted for adequately in the later analyses.

Table 2.1 lists some of the geometric and flow parameters used in the analysis. As pointed out previously, other parameters such as loss coefficients were taken directly from RELAP runs.

Figures 2-4 through 2-11 present the results of these calculations for each plant type.

Important conclusions are as follows:

1. No major difference exists between various plant types. In all cases blowdown occurs within the first 100 seconds following a LOCA. These time scales are comparable to those assumed in the NUREG/CR-6224 study.

2. In the case of MSLB (Figures 2-4, 2-6, 2-8 and 2-10):
   2.1. Vessel pressure decays rapidly.
   2.2. The flow rate varies from the initial value of about 6, 700 lbm/s to 2, 000 lbm/s.
   2.3. During the same time, the stagnation quality at the exit plane varies between 100-70%, although the void fraction is close to 99% all through the accident. Therefore, the flow behaves essentially as steam
   2.4. The quantity of water discharged during blowdown is small and will not result in formation of a drywell pool during blowdown.

3. In the case of a recirculation line break (Figures 2-5, 2-7, 2-9 and 2-11):
   3.1. The vessel pressure decreases more slowly compared to a MSLB. Even towards the end of the accident, exit plane pressure is still large.
   3.2. Initially the flow is nearly 100% water. But with time, due to flashing within the vessel and the piping, flow quality increases steadily with time reaching as high as 38%. During the same time the stagnation void fraction changes from 0.05 to 80%.
   3.3. The flow rate is typically much larger than a MSLB, reaching as high as 26,000 lbm/sec.
   3.4. The quantity of water discharged is large, and it is likely that water-borne transport of debris may dominate. It is also likely that the drywell pool will overflow into the vents during blowdown itself.

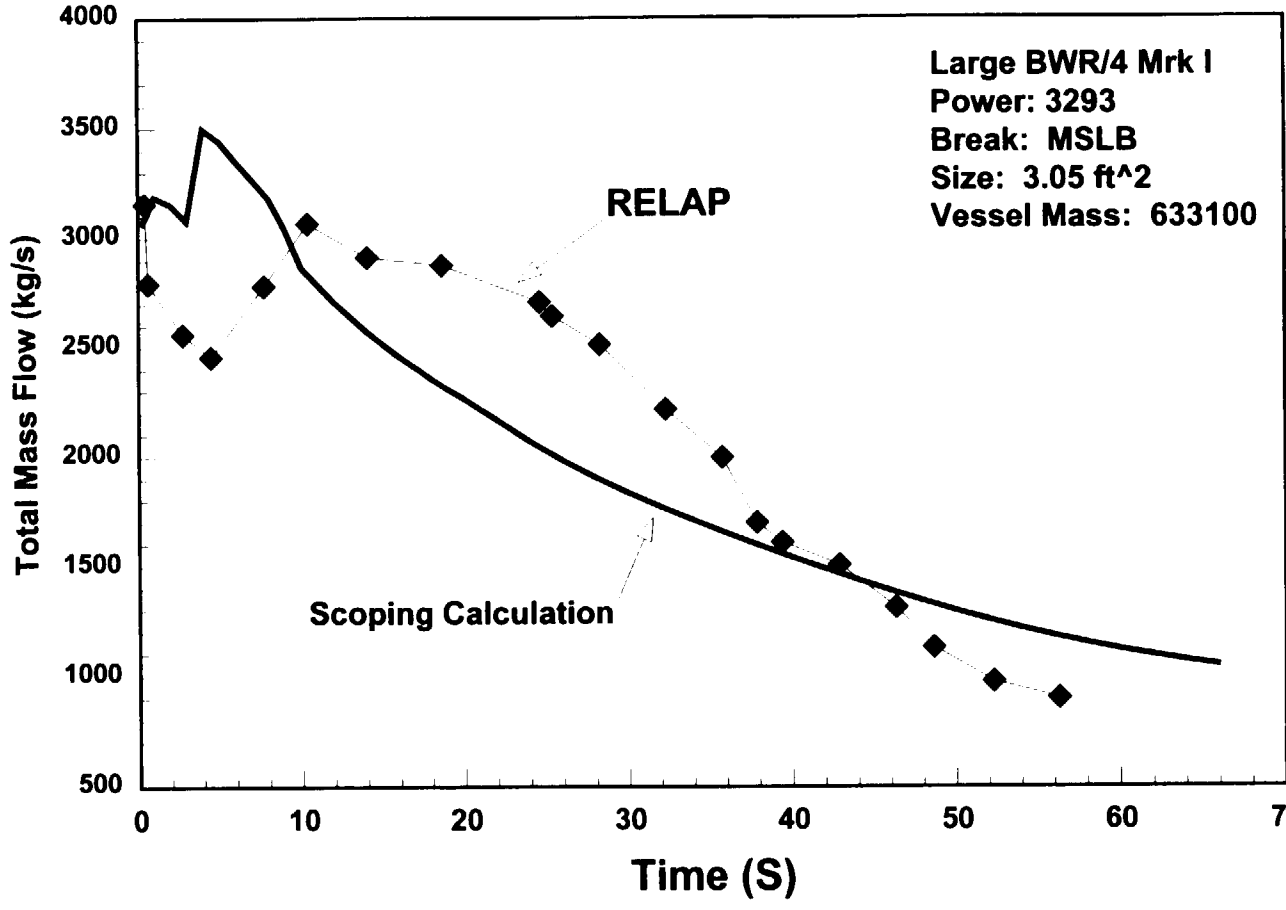

Figure 2-2. Comparison of SEA Model Predictions with those of RELAP for MSLB.

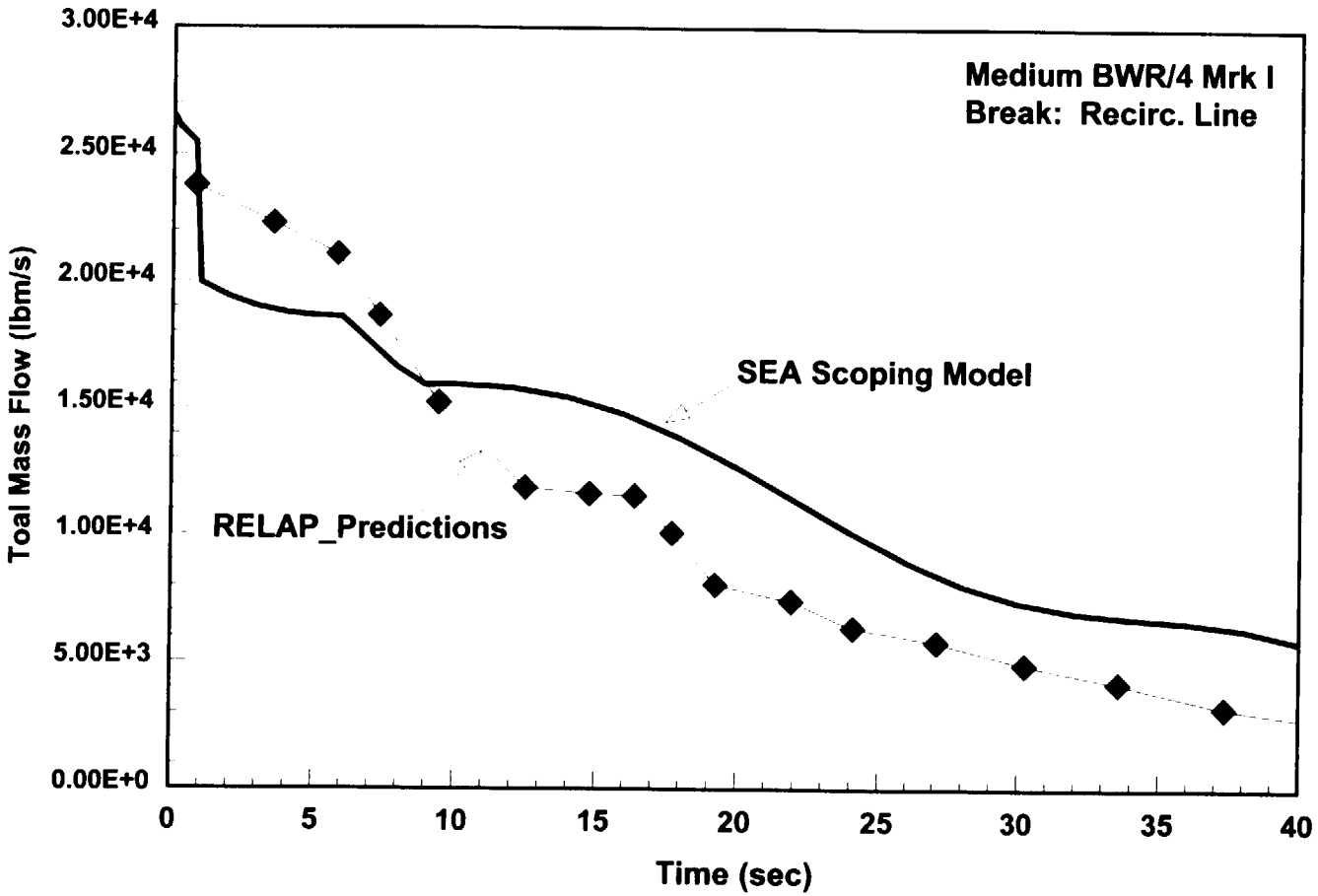

Figure 2-3. Comparison of SEA Model Predictions with RELAP predictions for Recirculation Line Brake.

Table 2-1 Geometric Parameters of Representative BWRs

	Duane Arnold	Hope Creek	NMP-2	Perry
MSLB Break Area (ft^2)	3.05	3.05	3.96	3.05
Recirc Break Area (ft^2)	2.575	4.1	3.147	3.197
Liquid Inventory (lbm)	286,435	633,100	660,088	613,400
Vapor Inventory (lbm)	9,000	10,000	25,414	12,791
Steam from Decay and Relaxation (lbm)	29,067	57,350	59,588	68,747

2.5 Usage of Calculational Results

The blowdown model predictions were used in the DDTS primarily to draw insights related to the following phenomena: Debris Generation, Containment Thermal Hydraulics and Prototypical Wetness.

2.5.1 Implications for Debris Generation

Figures 2-12 and 2-13 present predicted two-phase velocities at the exit plane following a DEGB in a main steam line and recirculation line, respectively. Also plotted in the figures are ratios of dynamic pressure in the center line of the jet originating from the break and expanding into the drywell. These dynamic pressures were estimated using the ANSI/ANS Jet expansion model. As evident from Figure 2-12, the fluid velocity, remains nearly sonic for up to 40 seconds after a LOCA. However, during the same time the dynamic pressure, decreases rapidly with time, falling to 30% of its original value within the first 10 seconds. On the other hand, in the case of a recirculation line break, the fluid velocity as well as the dynamic pressure are low initially, and increase with time as the fluid exit quality increases as a direct result of flashing inside the pipes and pressure vessel. These figures clearly suggest that debris generation occurs primarily within the first 10 seconds following a main steam line break, but over a prolonged period of time (up to 30 seconds) following a recirculation line break.

2.5.2 Structural Wetness and Containment Thermal Hydraulics

The source-term values (i.e., Figures 2-4 through 2-11) were provided as input to MELCOR and its predictions are provided in the following sections.

One of the inputs required for MELCOR calculations is the droplet size of the liquid component suspended in steam flow. Estimates of the drop size were obtained as follows.

Consider a water/steam jet expanding into infinite space. The water and steam volumetric rate after expansion is Q_f and Q_g, respectively. For such a flow, the mean diameter of the broken droplet is given by the following correlation:

$$d(\mu m) = \frac{585}{V_o}\sqrt{\frac{\sigma}{\rho_o}} + 597\left(\frac{\mu_f^2}{\rho_f \cdot \sigma}\right)^{0.225}\left(\frac{10^3 \cdot Q_f}{Q_g}\right)^{1.5} \qquad (2\text{-}9)$$

where

V_o = velocity of the fluid mixture in pipe (m/sec);
σ = surface tension (dynes/cm);
ρ_f = density of water (1.0 g/cc);
ρ_g = density of steam (10^{-3} g/cc0;
μ_f = 0.196 X 10^{-2} POISE

$$\Rightarrow \frac{Q_f}{Q_g} = \frac{(1-\chi)}{\chi} \cdot \frac{\rho_g}{\rho_f} \qquad (2\text{-}10)$$

A. Pure Water

$\chi = 0$ and $Q_g = 0$

=> d (μm) $\rightarrow \infty$

In other words, the water jet (non-flashing) breaks up into very large droplet sizes for which this correlation is not applicable.

B. Recirculation Line Break

χ = 0.15 to 0.30

Vo = 211 m/sec (700 ft/sec)

For these conditions, the estimated droplet diameter is 217 μm.

C. Steam Break

χ = 0.9 - 0.75

Vo = 302.4 m/sec (1,000 ft/sec)

For these conditions, the above equation predicts a droplet diameter of 16.8 μm.

These calculations suggest that water would be suspended in steam in the form of fine droplets, approximately 15 μm in diameter. It is possible that the droplets would be even smaller. On the other hand, the recirculation breaks will produce relatively much larger droplets.

2.6 References

2-1 D.V. Rao, et al., "Drywell Debris Transport Study," Draft Phase I Letter Report, SEA 96-3105-010-A:2, September 1996.

2-2 C.M. Allison, et al., "SCDAP/RELAP5/MOD 2 Code Manual," NUREG/CR-5273-Vol. 1, September 1989.

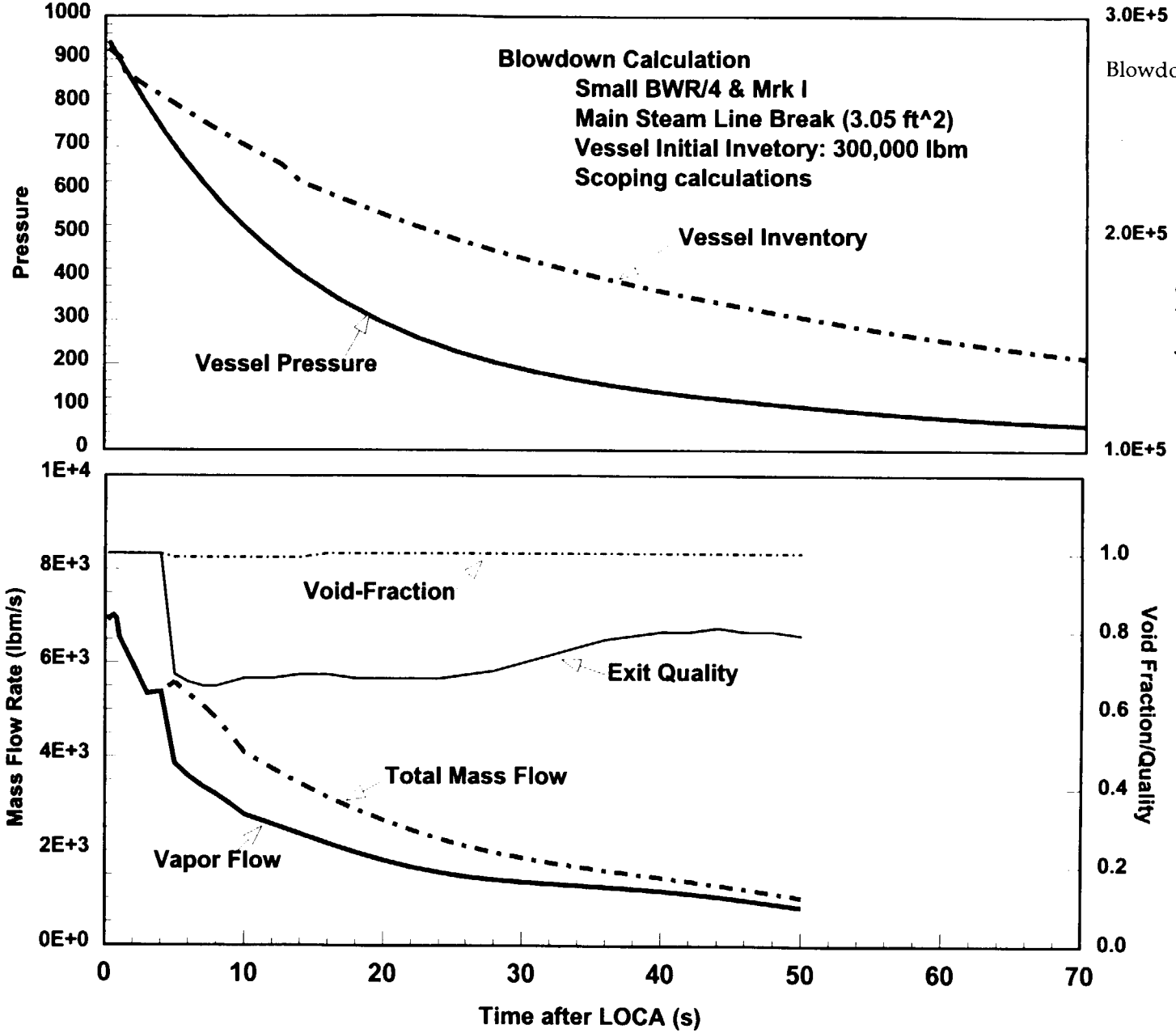

Figure 2-4. SEA Model Predictions for a Small BWR/4 Blowdown Following a MSLB.

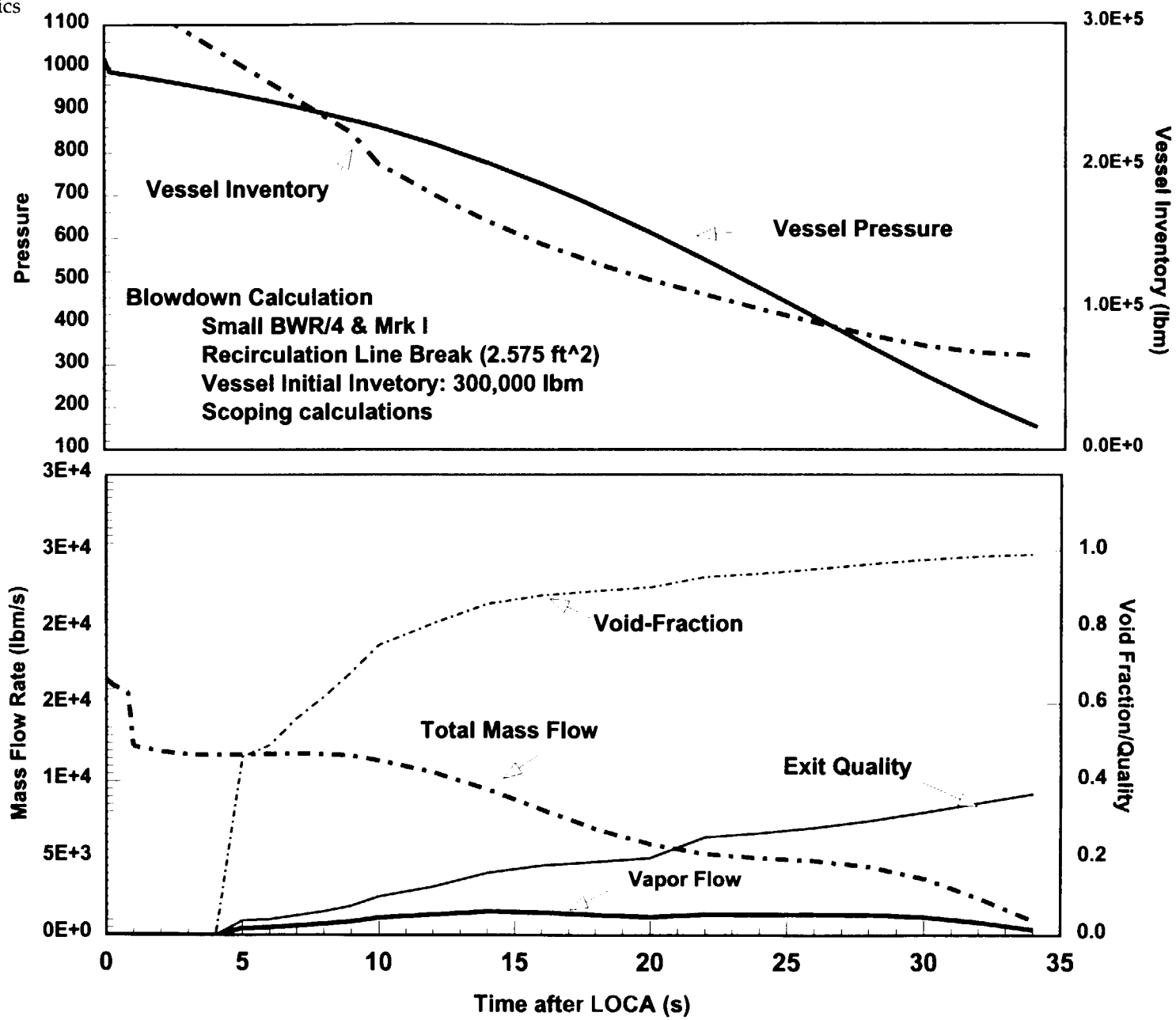

Figure 2-5. SEA Model Predictions for Small BWR/4 Vessel Blowdown Following a Recirc. Break.

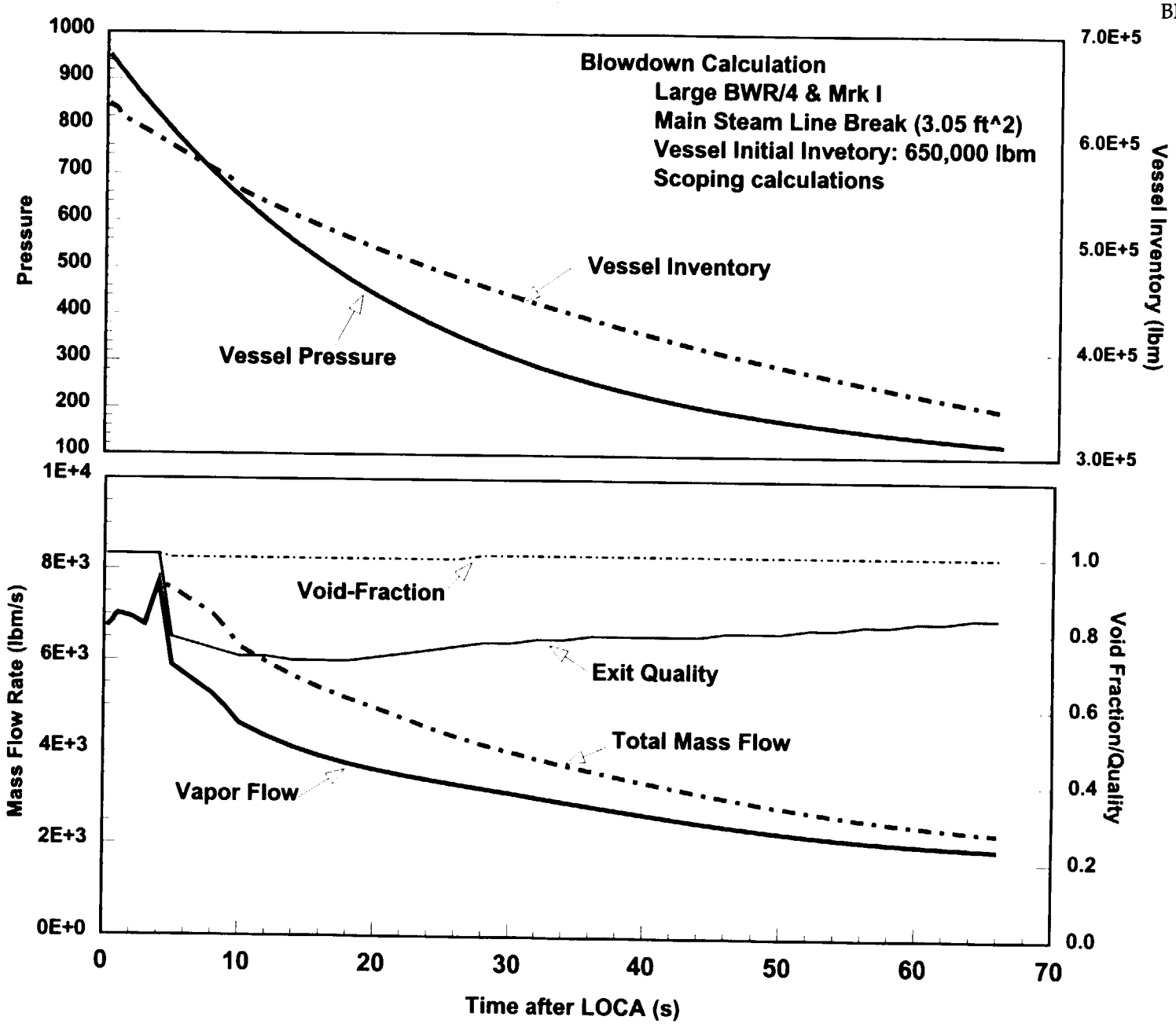

Figure 2-6. SEA Model Predictions for a Large BWR/4 Vessel Blowdown Following a MSLB.

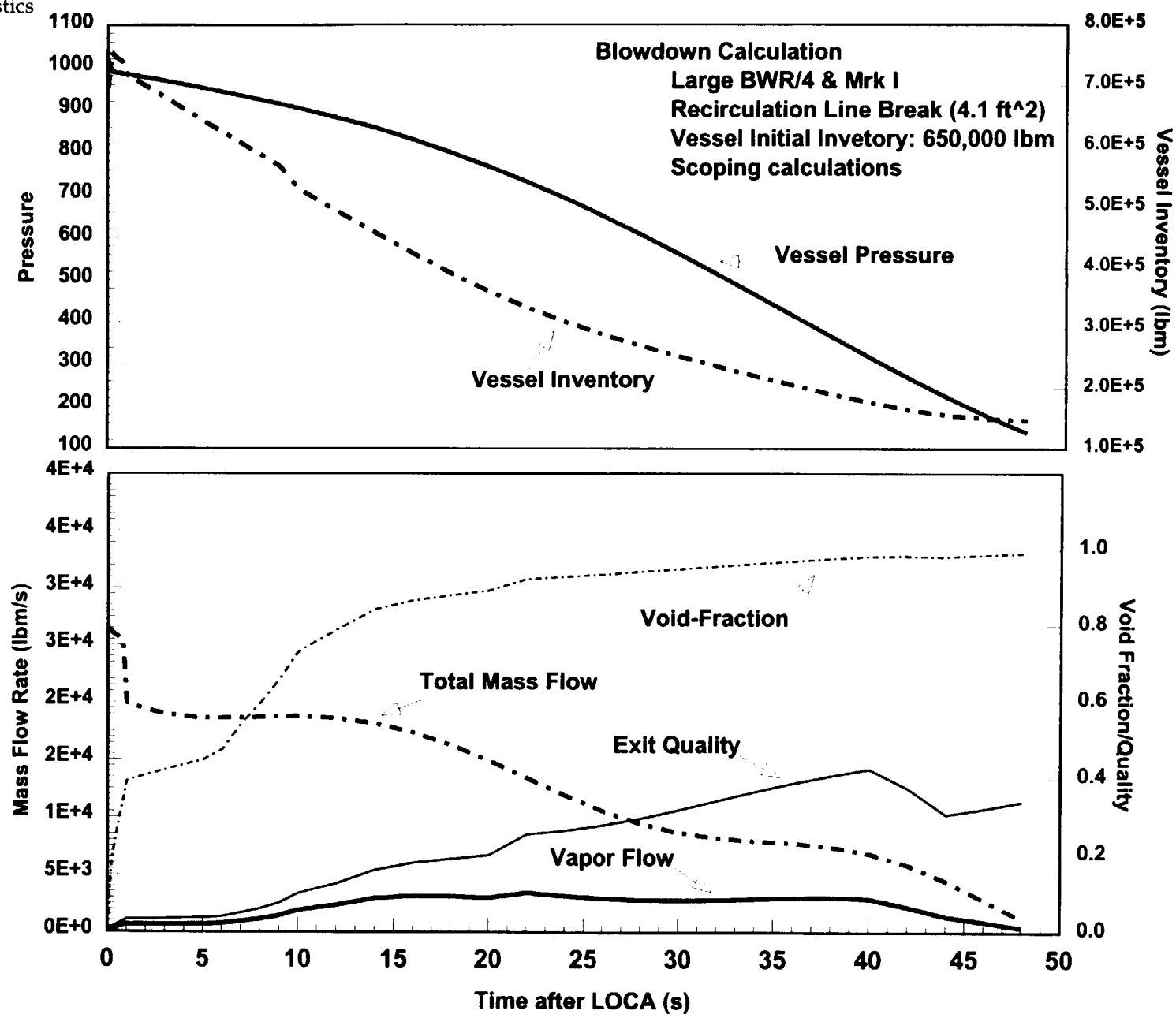

Figure 2-7. SEA Model Predictions for Large BWR/4 Vessel Blowdown Following a Recirc. Break.

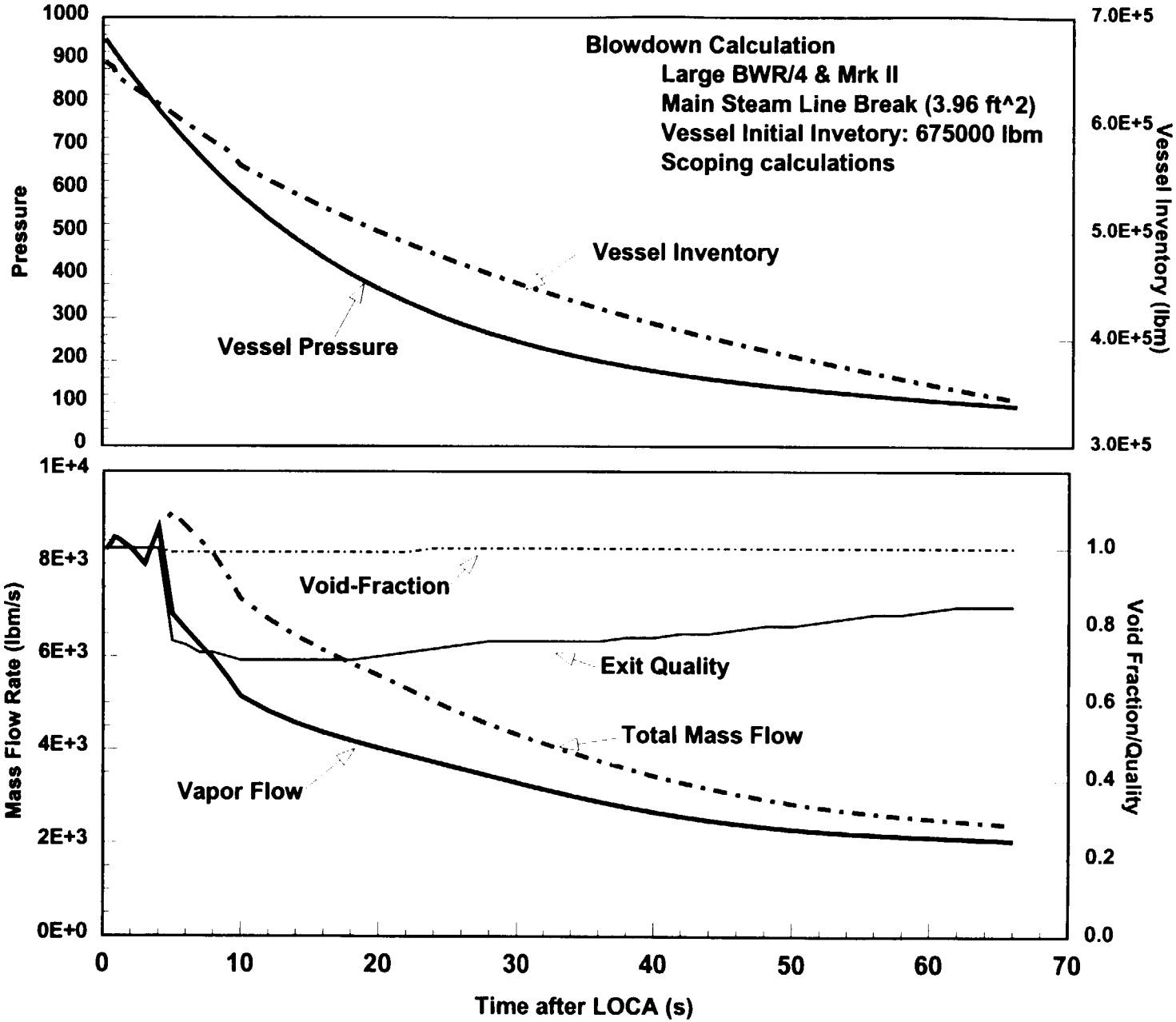

Figure 2-8. SEA Model Predictions for a Large BWR/4 Vessel Blowdown Following a MSLB.

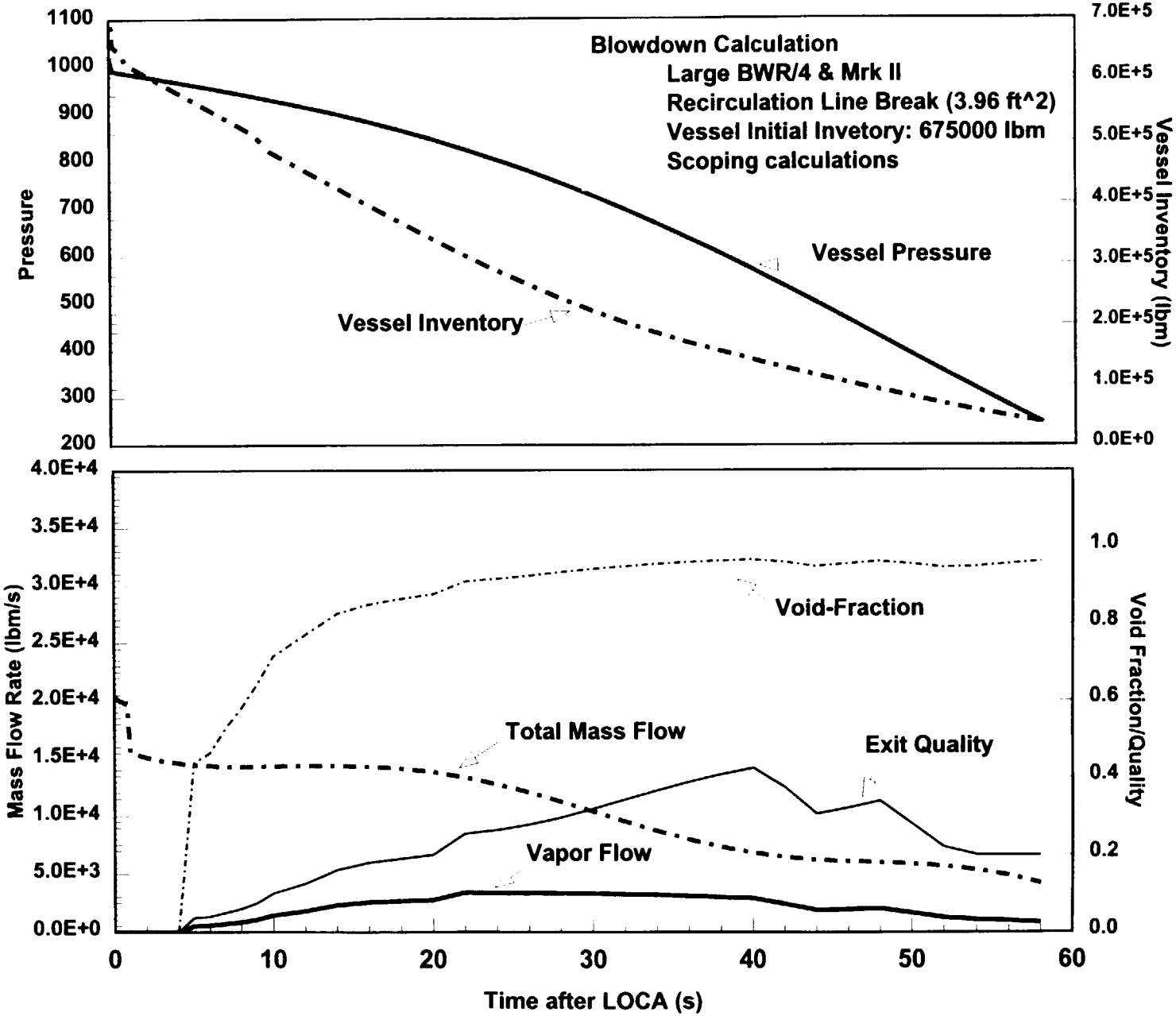

Figure 2-9. SEA Model Predictions for Large BWR/4 Vessel Blowdown Following a Recirc. Break.

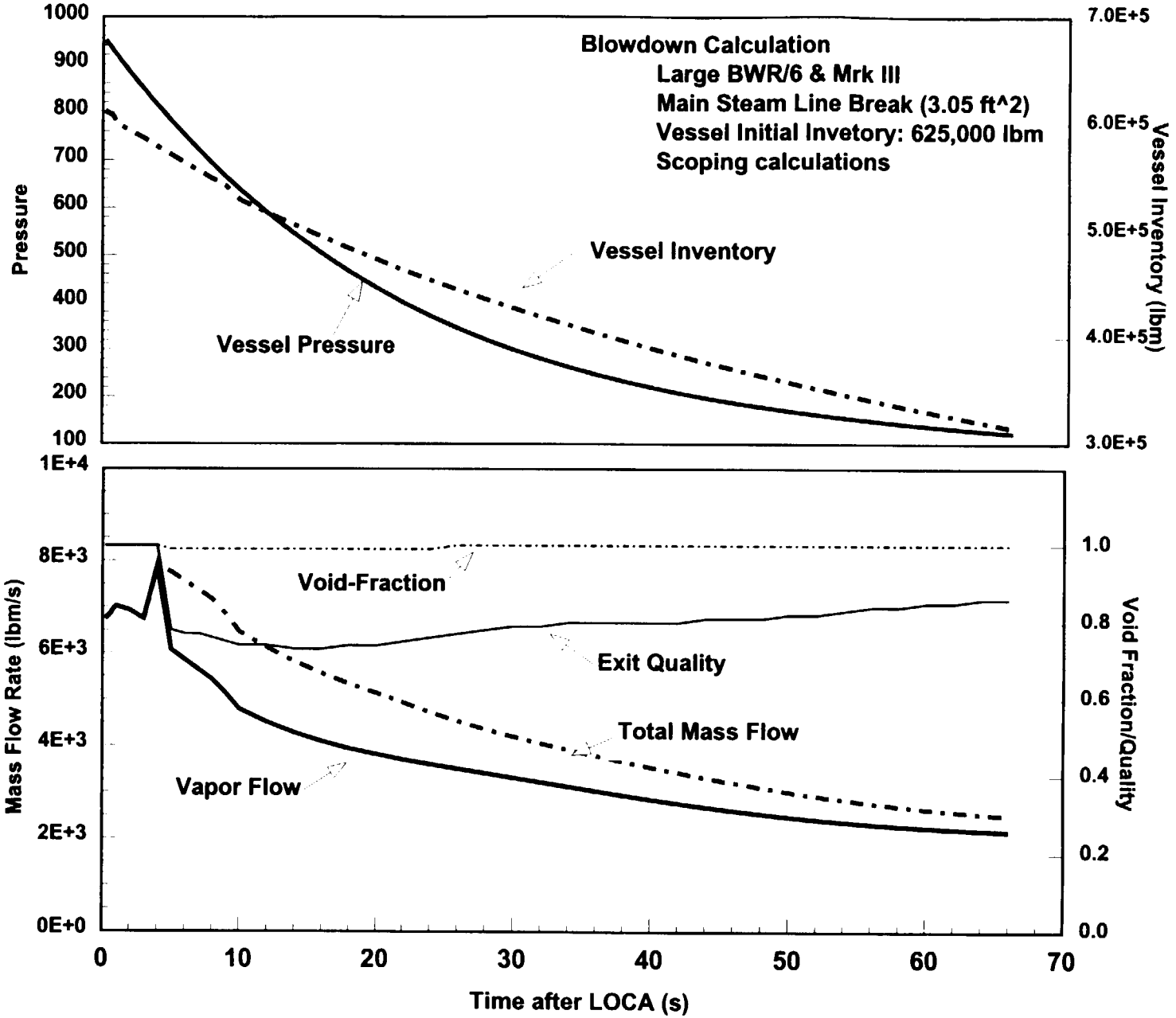

Figure 2-10. SEA Model Predictions for BWR/6 Vessel Blowdown Following a MSLB.

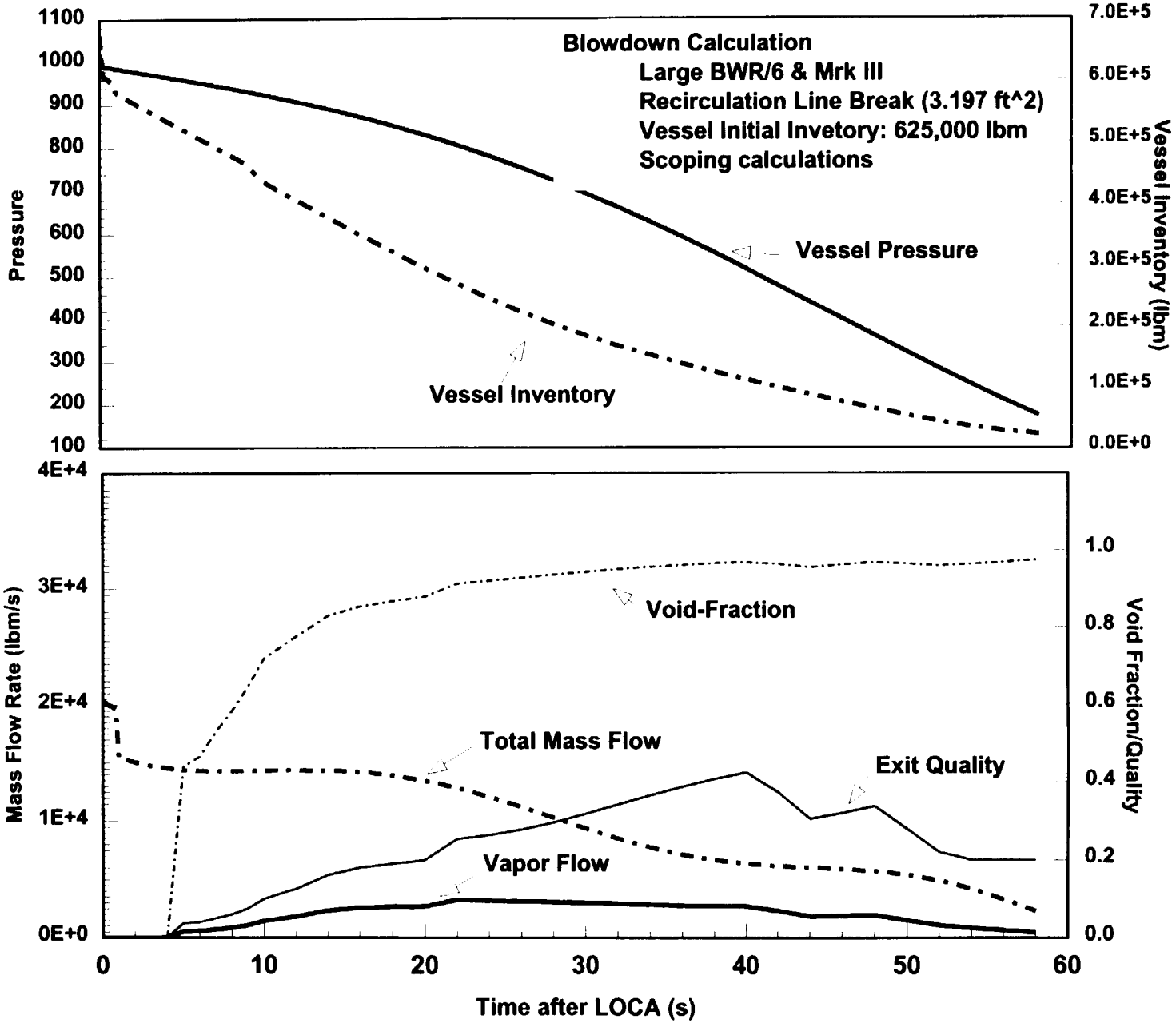

Figure 2-11. SEA Model Predictions for BWR/6 Vessel Blowdown Following a Recirc. Break.

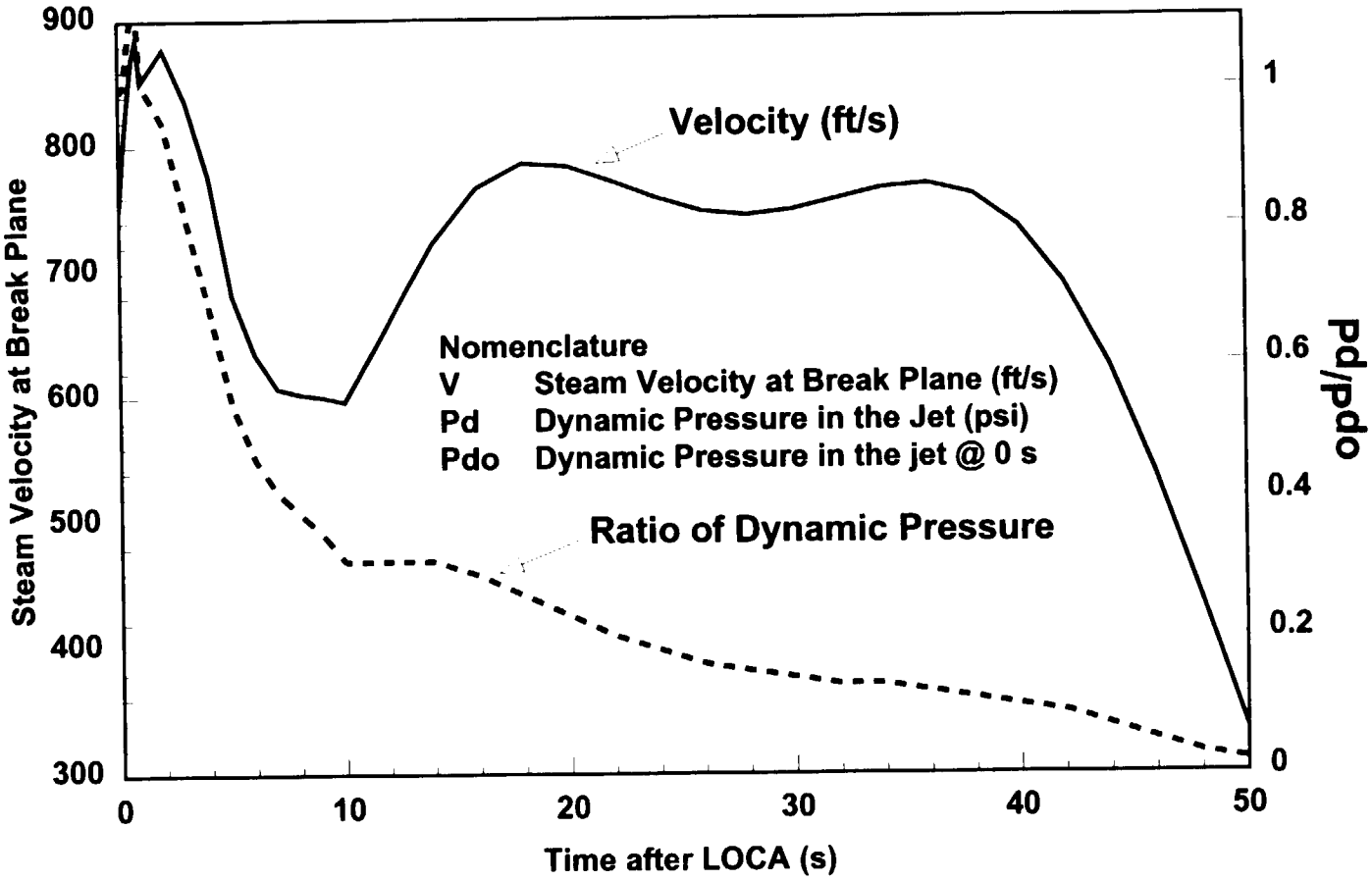

Figure 2-12. Velocity and Dynamic Pressure in the Vicinity of the break following a MSLB in a large BWR/4 with Mark I Containment.

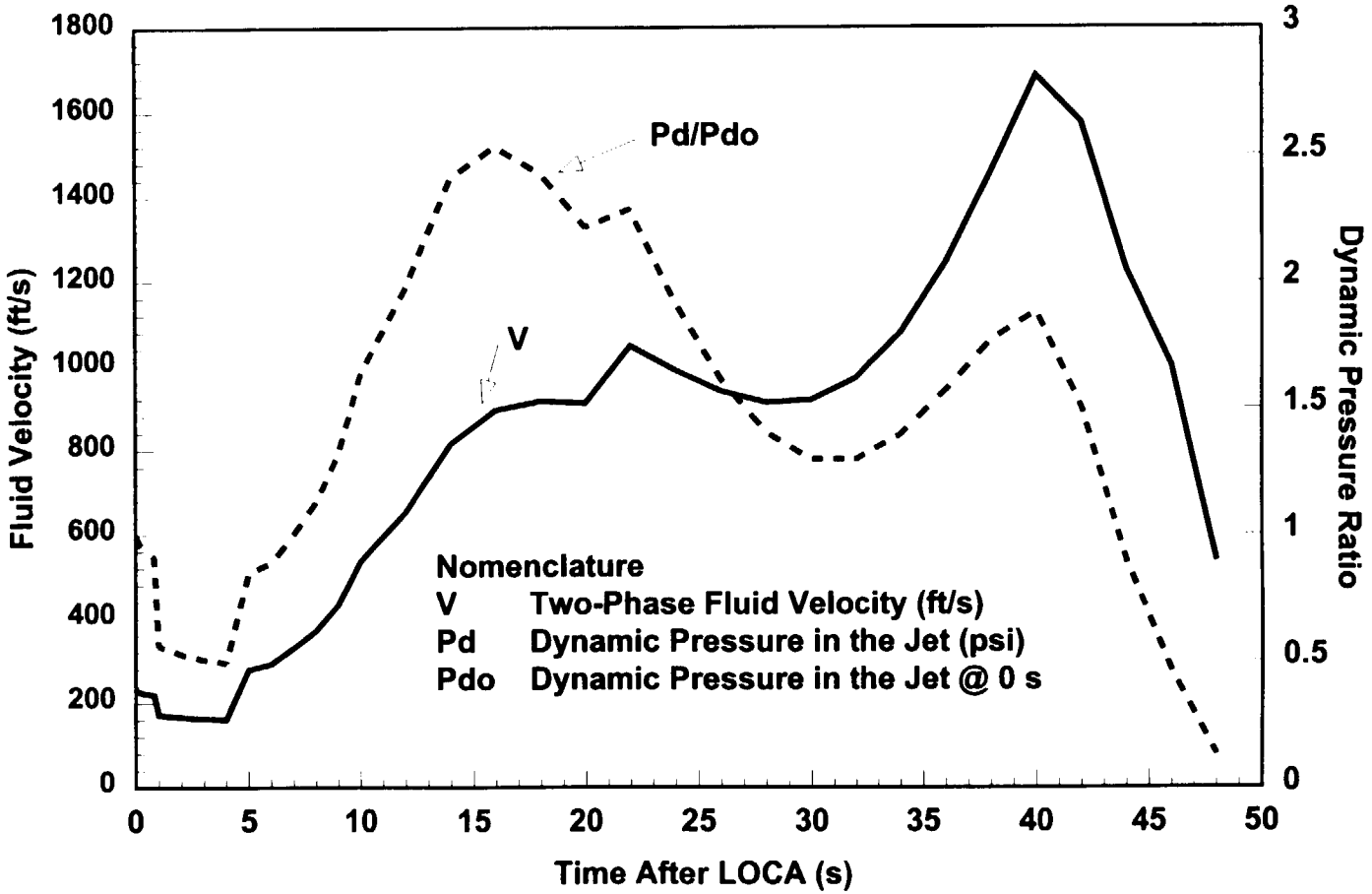

Figure 2-13. Velocity and Dynamic Pressure in the vicinity of the break following a Recirculation Break in a large BWR/4 with Mark I Containment.

3. MELCOR Analyses and Results

3.1 Study Objective

Preliminary MELCOR calculations were performed to support the first phase of the analytical study of the transport of insulation debris to the wetwell following a MSL or a RECIR break. These calculations helped quantify the importance of some of the phenomena ranked high by the PIRT panel [Ref. 3-1] and supported simplified scoping calculations performed by hand. Key thermal-hydraulic information determined from these calculations included the containment pressure and temperature response, the flow velocities throughout the drywell and the vent downcomer system, the rate of steam condensation on drywell structures, the rate of accumulation of water on the drywell floor, the time required to clear the downcomer pipes of water, and the transport of noncondensable gases to the wetwell. Plausible debris transport results were calculated to demonstrate the capability of the MELCOR code to provide analytical support for the study of debris transport once the characteristics of the debris are better understood. To conduct these calculations, a scoping-level MELCOR input model was developed for the reference plant in the NUREG/CR-6224 strainer blockage study [Ref. 3-2].

3.2 Summary Of Findings

This study simulated the following four pipe break scenarios where the calculations were driven by break source terms determined using a simplified calculational break flow model described in Section 2. One source term which simulated a MSL break was used for both steam line breaks and another source term that simulated a RECIR break was used for both recirculation pipes breaks. Recirculation flows were not included in these source terms.

- Main steam line break located in the cylindrical neck of the containment (high),
- Main steam line break located where the steam pipes exit the containment (low),
- Recirculation pipe break located at the top of the recirculation system (high),
- recirculation pipe break located near the drywell floor (low).

Debris transport characteristics based on the successful MELCOR simulation of the Karlshamn experiment [4-3] were used to perform the debris transport analysis. The characteristics referred to herein as wet debris would predict essentially the same gravitational settling rates as the Karlshamn simulation. An alternative set with debris characteristics referred to as dry debris was also studied for comparison purposes. Debris transport by condensate or recirculation washdown flows was not studied, i.e., the MELCOR model which normally predicts debris transport from surfaces due to water film flow was deactivated. The debris transport was calculated with and without a simplified inertial deposition model.

The MELCOR thermal-hydraulic input model subdivided the containment into 6 levels and had separate control volumes for the reactor cavity and the shield wall annulus. The containment and the downcomer vent system were then further subdivided into 4 quadrants to look for asymmetrical effects (a total of 31 volumes).

3.2.1 Key Thermal-Hydraulic Findings

Several key thermal-hydraulic findings were determined from these preliminary MELCOR calculations:

- Water in the downcomer vent pipes was purged from the pipes in about a second.

- Containment pressures increased rapidly following the postulated pipe break to about 3 atmospheres in about 1 second, roughly corresponding to the clearing of the downcomer vents, further pressurization was prevented by the pressure suppression system. After a relatively short period of 5 to 10 seconds, the pressures decrease again.

- Steam immediately condensed upon contact with surface structures until the temperature of the surface equilibrated with the steam environment. The total rate of condensation within the drywell for the high MSLB break, for example, peaked at 530 kg/sec at about 2.5 seconds.

second, depending upon the location of the surface relative to the pipe break.

- Peak flow velocities as high as 250 m/sec (820 ft/sec) were found near the break and flow velocities through the vent downcomer pipes exceeded 200 m/sec (660 ft/sec). Elsewhere in the drywell the velocities varied considerably from one location to another. The peak velocities generally occurred almost immediately following the pipe break then decreased with time as was expected. (Velocity distributions at 5 sec are provided in Section 4.7.)

- The majority of the nitrogen gas initially located in the drywell was forced into the wetwell in about 3 seconds (some gases were essentially trapped in the reactor cavity). The average residence time for a tracer gas injected into the drywell along with the insulation debris source ranged from about 0.5 seconds to 2 seconds following its injection into the flow stream. This residence time, which was break type and location dependent, was an indicator of the time available for debris deposition to occur.

- A pool of water accumulated on the drywell floor and in the reactor cavity sumps, as was expected. In the MSL breaks, the pool was much too shallow to overflow into the downcomer vent pipes, i.e., the depth of the water was only about a quarter of the depth required to overflow. In the RECIR pipe break, the results were considerably different, here the overflow began at 5 seconds for the low RECIR break. The asymmetrical pressures acting on the drywell floor pool pushed the accumulated water to the back side of the pedestal from the break and after the drywell pressures peaked, the pool became two-phased. The swollen water level caused the water to overflow into the vents at the back side of the pedestal. The drywell pool of course leveled out again after the primary system was depressurized.

Additional thermal-hydraulic information is shown in Section 3.7.

3.2.2 Key Debris Transport Findings

The debris transport results provided plausible transport fractions based on modified particle transport models inherent in the MELCOR code and the debris characteristics that successfully simulated the Karlshamn experiment. The transport fractions calculated ranged from 0.3 to 0.9, depending upon the conditions applied to the calculation. The transport fraction is defined as all the debris transported into the vent pipes included the debris deposited within the vent downcomer system. Assuming a recirculation line break near the entrance to a couple of the vent downcomers, small dry debris, and taking no credit for inertial capture, the transport fraction was 0.90. Alternatively, assuming a steam line break located in the neck of the drywell, wet debris (similar to Karlshamn), and taking credit for inertial capture by using a simple inertial capture model, the transport fraction was 0.33.

The debris transport findings are summarized in Figures 3-1 and 3-2. Figure 3-1 shows the results when a simplified inertial deposition model was employed and Figure 3-2 shows the results without the inertial model. Each figure shows the results of the four LOCA scenarios run with both the wet and the dry debris characteristics. The two dominant deposition mechanisms identified were gravitation for large pieces and inertial processes for small pieces. Additional debris transport information is provided Section 3.7.

These results were not used in the final quantification undertaken later in the study.

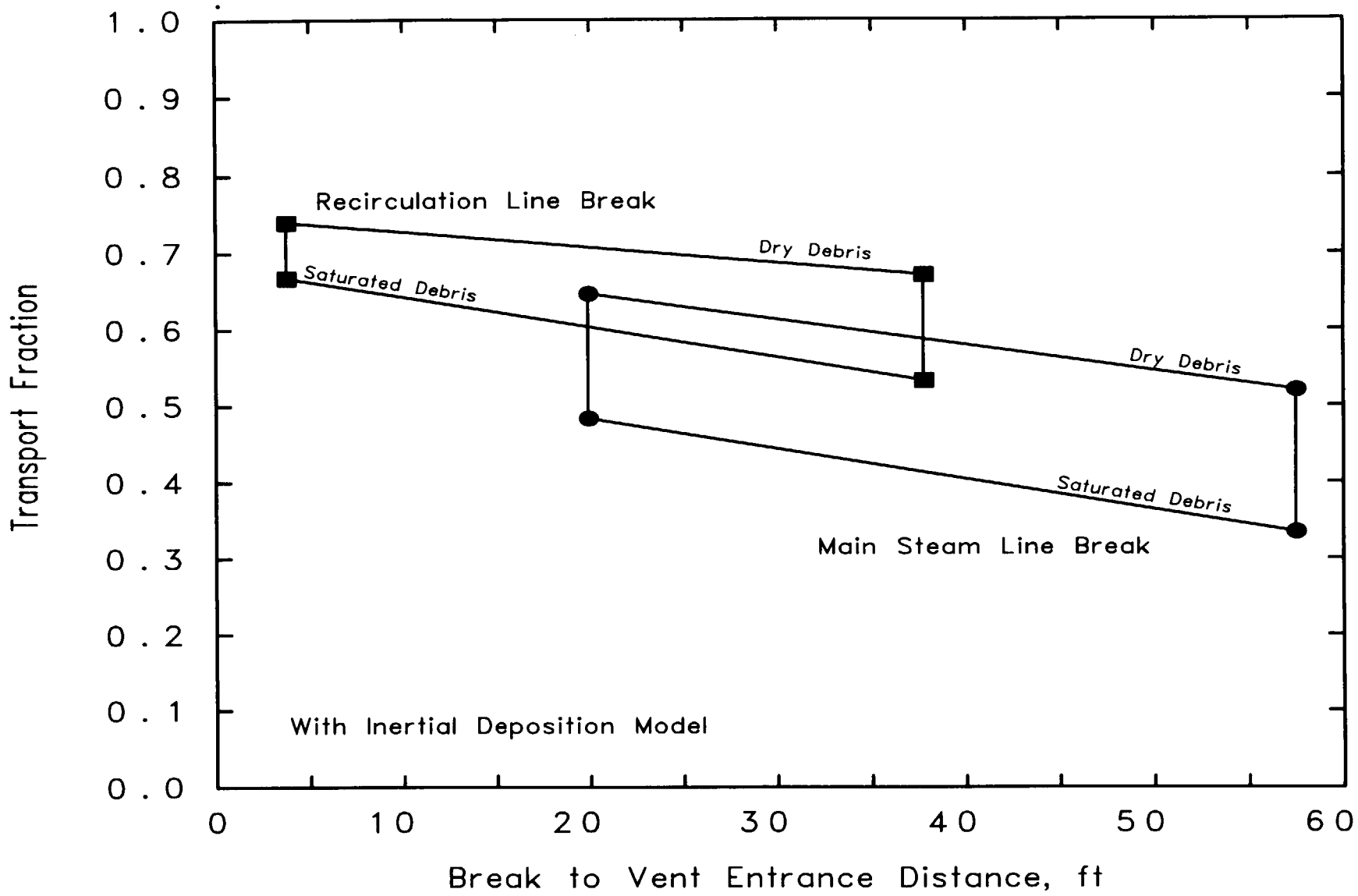

Figure 3-1. Debris Blowdown Transport Fractions

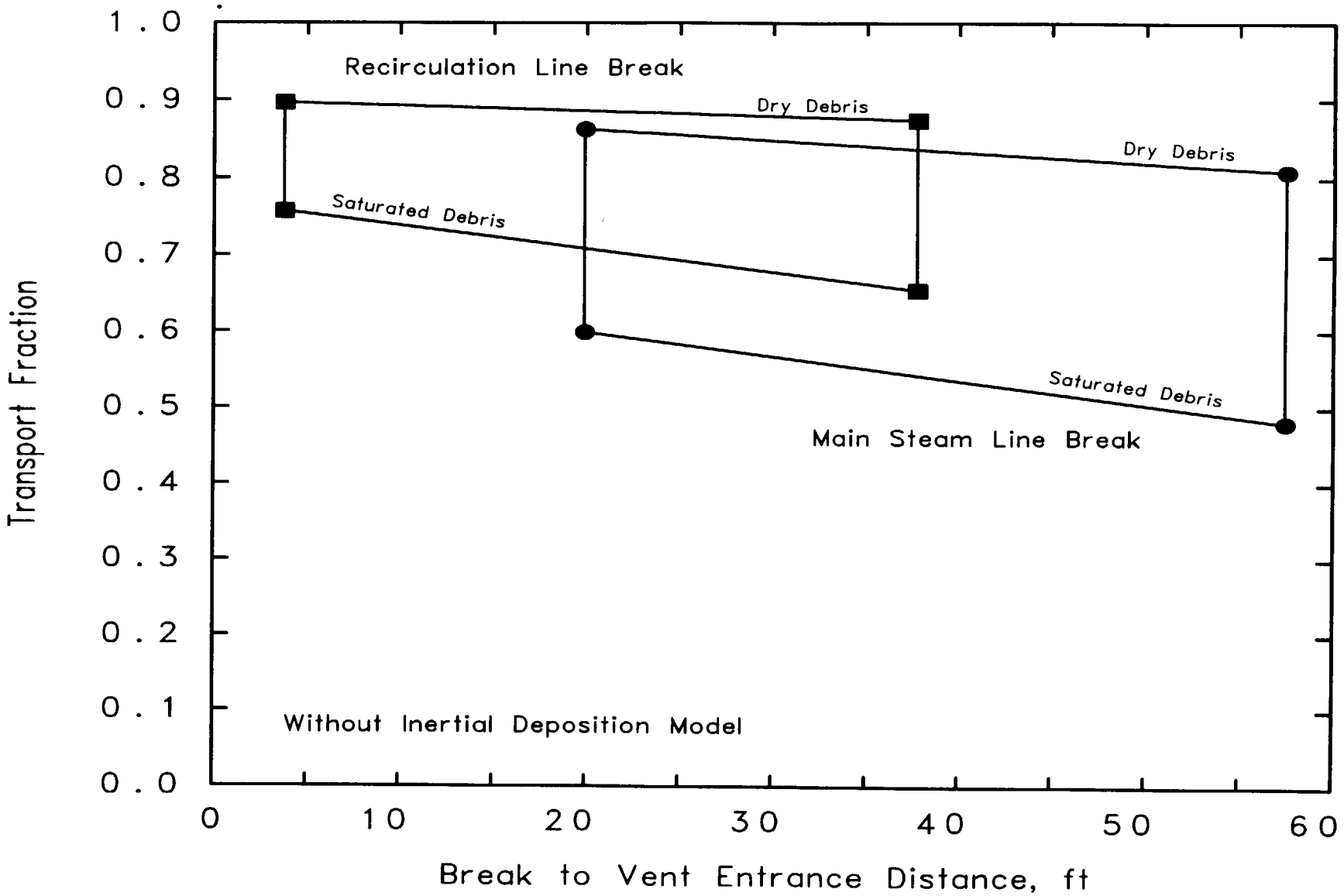

Figure 3-2. Debris Blowdown Transport Fractions

3.3 Thermal-Hydraulic Models

The containment was subdivided into a total of 31 lump-parameter control volumes. First the drywell was subdivided into six levels to define the geometry in the vertical direction and then each of these levels waste subdivided into four quadrants to look for asymmetrical effects. The vent downcomer was modeled with four volumes, i.e., one for each quadrant. The reactor cavity, the space between the reactor vessel and the shield wall, and the wetwell were each modeled with a single volume.

The six levels of the drywell are shown in Figure 3-3. The spherical portion of the drywell was subdivided into three levels by the two major platforms (gratings). The upper cylindrical portion was also subdivided into three levels. These levels were defined by the top of the shield wall and bottom of the cap as shown.

The volume of each of these control volumes was determined from the total water and free volumes obtained from the FSAR and the dimensions of the containment boundary, reactor vessel, and pedestal and shield walls. First the gross volumes were calculated from the dimensions and then uniformly adjusted to obtain the correct free volume. The ratio of the FSAR free volume of 109450 ft^3 minus the free vent volume of 7743 ft^3 to the calculated gross volumes of 139600 ft^3 minus the vent volume was 0.77.

Assumption: The volume of the internal structures, i.e., pipes, gratings, pumps, ladders, pipe hangers, etc., was assumed uniformly distributed throughout the drywell but not in the vent system. Therefore the gross volume for each control volume was simply multiplied by 0.77 of obtain its free volume. This was deemed adequate for these scoping calculations.

These control volumes were interconnected with a total of 65 flow paths.

Assumption: The flow areas of these flow paths were determine from calculated gross cross-sectional areas uniformly adjusted for obstructions. The flow path form loss coefficients for each path connecting drywell volumes was specified at 2.5.

Assumption: Vertical flow areas between levels in the drywell were assumed to be 50% of their associated gross cross-sectional areas and the lateral areas between quadrants were assumed to be 75% of the gross areas.

Assumption: The reactor cavity was assumed to be connected to the drywell by a 3 ft by 6 ft open hatch located in the quadrant containing the pipe break. Water was allowed to flow into the reactor cavity and cavity sump through this hatch.

Assumption: The shield wall annulus in only connected to the Level 5 control volumes.

The spillover elevation was determined so that the pool volume would equal 1955 ft^3 [FSAR value] before water could overflow into the vent system. The vent downcomer piping was assumed to not have any obstructions. The wetwell water level was 3 ft above the bottom of the downcomer pipes. The loss coefficient of 4.4 [FSAR value] was applied to the vent system.

Surfaces areas were estimated for each of these control volumes resulting in a total of 138 separate heat structures, i.e., 138 separate 1-D heat conduction calculations. The surface areas associated with the containment boundary, the reactor vessel, and the pedestal and shield walls were calculated from their dimensions. The total calculated surface area of the these boundary structures was 38622 ft^2 and this area was appropriately associated with the various control volumes. The surface area of the internal structures was estimated at 61000 ft^2 for a total area of 99622 ft^2. The internal surface areas were estimated by calculating the area for the larger pipes within the drywell such as the steam lines, recirculation and feedwater pipes, the ventilation ducts visible in the available drawings and the gratings and structural I-beams of the upper platform and then extending the estimate judiciously to include a contribution for similar items and items not visible in the drawings. The surface area was deemed underestimated by 10 to 20%.

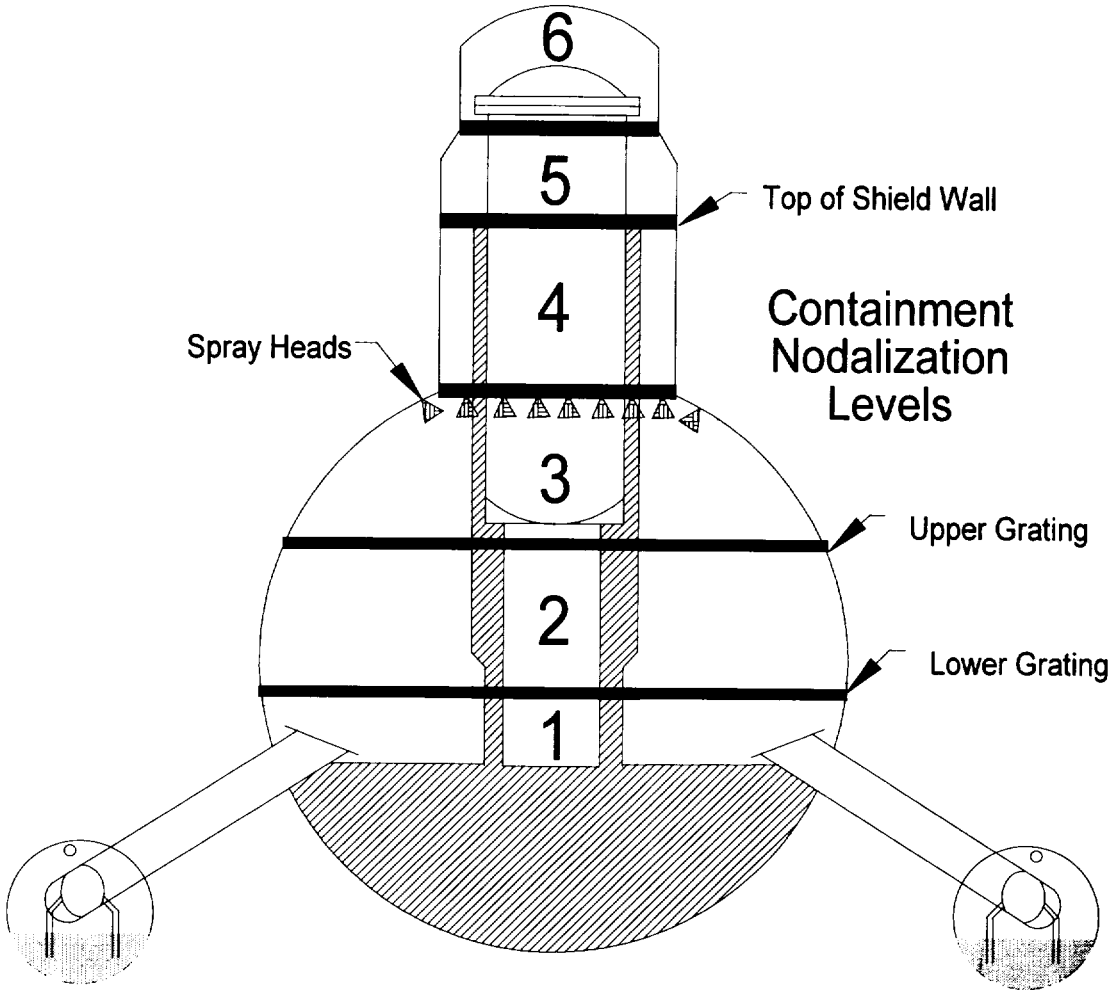

Figure 3-3. Containment Nodalization

The boundary surface areas were oriented per their actual position, i.e., floor, ceiling, or vertical. Only floor areas, horizontally facing upwards, can accumulate gravitationally deposited debris.

Assumption: The 61000 ft^3 of internal surface area was uniformly distributed inside the drywell volumes (not including the vent system), i.e., ~0.6 ft^2 of area per ft^3 of volume.

Assumption: 15% of the internal area was modeled as a floor, 15% as ceiling, and 70% as vertical walls. This distribution was based on the surface estimates made for various structures.

Assumption: The internal structures were all modeled as ¼ inch base steel. Actually, about 9000 ft^2 was associated with insulated pipes but for these calculations, modeling the insulation was not important.

Pipe break flows were introduced into the calculation as mass and energy source terms to the control volume designated as the break volume.

3.4 Debris Transport Models

A primary set of debris characteristics was originally selected for this study that would reasonably well reproduce the results of the Karlshamn experiment. Since these characteristics were intended to simulate wet debris, an alternative set of characteristics were selected to simulate dry debris. The parameters selected for the primary debris characteristics are listed in Table 3-1.

Since the amount of water carried along with insulation debris is not known, this study was originally intended to bound the wetness using a fully saturated wet debris and a dry debris, i.e., with wet debris, all of its interstitial spaces are completely filled with water whereas dry debris contains no water. The effective particle densities of fully wet and dry debris were 1025 kg/m^3 (64 lbm/ft^3) and 38.4 kg/m^3 (2.4 lbm/ft^3), respectively.

Since the actual size distribution of the debris particles is not known and a lognormal distribution was used in the Karlshamn simulation, a lognormal distribution was used herein. The Karlshamn simulation assumed a lognormal size distribution with a mass medium diameter of 130 microns and a standard deviation of 2; a particle density of 2800 kg/m^3 (175 lbm/ft^3); and dynamic and coagulation shape factors of 2 [Ref. 3-3]. The 180 micron MMD distribution used here provided similar debris transport to the Karlshamn for the conditions of the Karlshamn experiment.

Table 3-1: Debris Transport Parameters

Transport Parameter	Value
Debris Size	180 • MMD with • of 2
Dynamic Shape Factor	1.4 for Wet Debris 4.2 for Dry Debris
Coagulation Shape Factor	1.0
Particle Density	1025 kg/m^3 for Wet Debris 38.4 kg/m^3 for Dry Debris
Source Mass	120 kg
Source Timing	Constant Rate Over 5 seconds
Film Solubility	0

The dominant deposition process in the Karlshamn simulation was gravitational deposition as predicted by the Stoke's equation as follows:

$$U_{stokes} = \frac{\rho_p \cdot g \cdot d_p^{\,2} \cdot C}{18 \cdot \mu \cdot \chi} \qquad (3\text{-}1)$$

where

U_{stokes}	=	the gravitational deposition velocity
ρ_p	=	the particle density
g	=	the acceleration of gravity
d_p	=	the particle diameter
C	=	the slip correction coefficient
μ	=	the gas viscosity
χ	=	the dynamic shape factor

In the Karlshamn simulation, the gas parameters were well known but the particle diameter, the particle density, and the dynamic shape factor were not known. However, the same general results could be expected for any reasonable combination of these three parameters that produce the ratio of $\rho_p \cdot d_p^{\,2} / \chi$ that is the same as that given by the Karlshamn simulation. Table 3-2 lists several of these combinations.

It has been clearly noted that the Stokes equation is not the most appropriate equation for insulation debris transport in the highly turbulent flows that would be present in the drywell following a postulated pipe break [B-4]. Newton's equation for gravitational settling has been proposed as the more applicable equation. This equation is:

$$U_{newt} = \left[\frac{4 \cdot d_p^{\,3} \cdot g \cdot (\rho_p - \rho_g)}{3 \cdot d_e^{\,2} \cdot \chi \cdot \rho_g \cdot C_D(d_e)} \right]^{\frac{1}{2}} \qquad (3\text{-}2)$$

where

U_{newt}	=	the deposition velocity
d_p	=	the diameter of the volume of an equivalent sphere
d_e	=	the characteristic or envelope diameter of the particle
C_D	=	the drag coefficient that depends on the Reynolds number.

ARL measured terminal settling velocities for samples of insulation debris [Ref. 3-5]. Debris transport parameters were deduced from one group of these data which indicated that the settling velocity was about 2 ft/sec for a debris particle with the mass of 2 to 5 milligrams. The work of Brockmann [B-6, B-7] was used in deducing these parameters. These parameters are shown in Table 3-3.

The debris characteristics deduced from the ARL data clearly indicate that the realistic mass diameter is much larger the mass diameters used to successfully simulate the Karlshamn experiment with MELCOR., 1000 microns compared to 130 microns. The primary reason for this difference is that the MELCOR code employs the Stoke's equation which overpredicts the settling velocities for particles of this size. The settling velocities and particle masses for the two sets of debris characteristics studied herein and for the Karlshamn simulation are shown in Table 3-4.

Table 3-2: Debris Characteristic Producing Results Similar to Karlshamn

Debris Type	Particle Diameter microns	Particle Density kg/m^3	Dynamic Shape Factor
Karlshamn	130	2800	2
Wet	180	1025	1.4
50% Wet	287	531.5	1.74
Dry	785	38.4	1
Dry	1608	38.4	4.2

Table 3-3: Debris Characteristics Deduced from ARL Data

Parameter	Value
Particle Material Density	2800 kg/m^3
Effective Particle Density	38.4 kg/m^3
Mass Diameter	1000 microns
Mass	1.5 milligrams
Envelope Diameter	4180 microns
Aerodynamic Diameter	820 microns
Dynamic Shape Factor	4.2
Settling Velocity Predicted by Stoke's Equation	87.4 ft/sec
Settling Velocity Predicted by Newton's Equation	2.4 ft/sec
Particle Reynolds Number	310
Drag Coefficient	0.66

Table 3-4: Settling Velocities and Particles Masses for This Study

Parameter	Karlshamn	Wet Debris	Dry Debris
Mass Diameter, micron	130	180	180
Particle Density, kg/m^3	2800	1025	38.4
Dynamic Shape Factor	2	1.4	4.2
Stoke's Settling Velocity, ft/sec	3.1	3.1	0.03
Particle Mass, milligram	0.0031	0.0031	0.00012
Envelope Diameter, micron	540	750	750

Note that the settling velocities for the Karlshamn simulation have Stoke's predicted settling velocities near that of the ARL data and that the wet debris data used herein has the same settling velocity as does the Karlshamn simulation. This effectively ties the Karlshamn data to ARL data in that both reasonably predict nearly the same settling velocity. This implies that the debris characteristics deduced from the ARL data could well predict the Karlshamn experiment if the Stoke's equation in MELCOR were replaced with the Newton's equation.

The coagulation shape factor was kept at a nominally small value of 1 in these calculations to prevent over predicting the rate of coagulation. Coagulation would be dominated by the gravitational process where particles that fall faster over take slower particles. A shape factor of 1 is deemed conservative, i.e., under predicting deposition in the drywell.

Insulation debris was sourced into each calculation at a constant rate over a period of 5 seconds. Since the debris transport in these calculations was so rapid, this assumption could have significant impact on the transport results. One calculation was run with the debris sourced into the calculation during the first 0.1 seconds and this calculation indicated a higher debris retention because more of the debris was propelled into the upper reaches of the drywell before the water in the vent downcomer cleared. The total mass of debris introduced into each calculation was 120 kg which corresponded to the predicted debris generated for the postulated break of the RCAS-J006 weld in the reference plant [Ref. 3-2].

The film solubility parameter is a MELCOR code parameter defined as that fraction of deposited debris that is dissolved in the surface water film. This parameter is obviously not directly applicable to this study but it does allow the user to force the debris to remain on the structures where deposited and keeping the debris where deposited means that the results will provide information as to where debris is deposited within the containment.

The deposition processes that effected the transport fractions calculated in this study are gravitational, inertial, and to a lesser extent diffusiophoresis (condensation driven). The deposition processes as determined by the MAEROS equations, except for inertial, are shown in Figure 3-4. MAEROS is the

aerosol transport model implemented into MELCOR. Gravitational deposition clearly dominated over diffusiophoresis for insulation debris transport and the thermophoresis and diffusion processes were not significant.

A simplified turbulent diffusion inertial deposition model was implemented in MELCOR as part of another study performed for Sandia. This model is also known as a free-flight model and the model was included in SEA's response to the PIRT Panel request for information [3-4]. The deposition velocity predicted by this model tends to reach a maximum and remain there when the dimensionless particle relaxation time exceeds about 10. This maximum value is a dimensionless deposition velocity of about 0.1 and it valid to a dimensionless relaxation time of at least 1000. Some experimental data show this trend to dimensionless relaxation times of about 50000. The dimensionless relaxation times for the debris characteristics and drywell conditions of this study are in the general range of a few thousand to a few tens of thousands, certainly much larger than 10. Thus the inertial deposition velocity becomes:

$$U_{inertial} = u_o \left[\frac{0.0225 \rho_g \cdot V_{flow}^2 \cdot \left(\frac{\nu}{V_{flow} \cdot \delta} \right)^{\frac{1}{4}}}{\rho_g} \right]^{\frac{1}{2}} \quad (3\text{-}3)$$

where

$U_{inertial}$ = the deposition velocity
u_o = the dimensionless deposition velocity of 0.1
ρ_g = the gas density
V_{flow} = the flow velocity
ν = the gas kinematic viscosity
δ = the boundary layer thickness

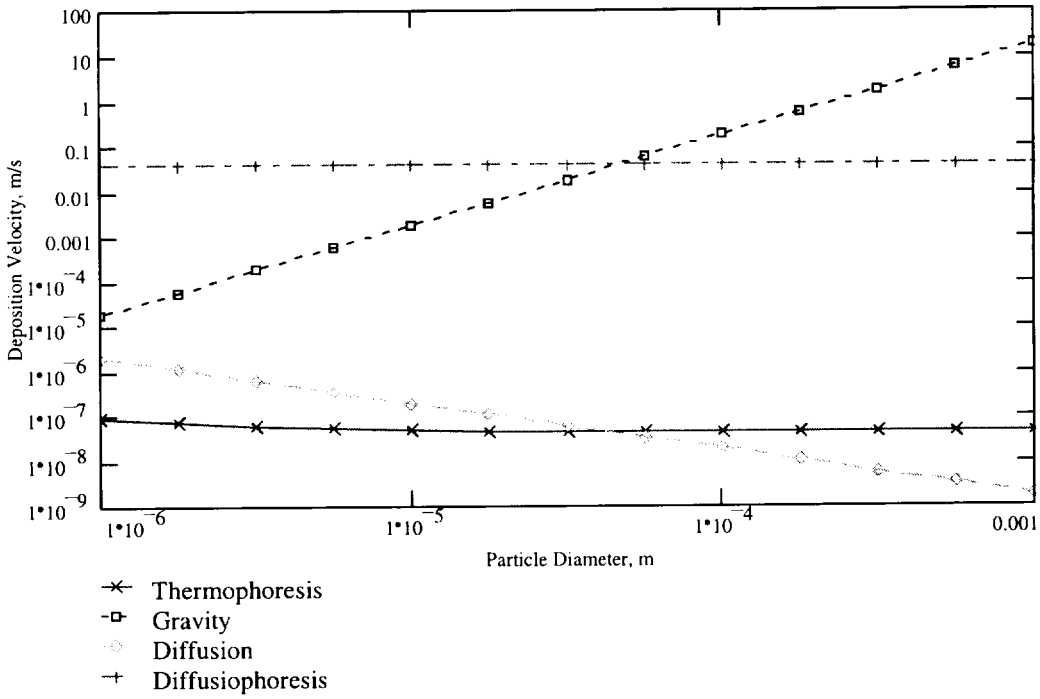

Figure 3-4. Debris Deposition Processes

The numerator of this equation is the surface shear stress and the term in brackets is known as the friction velocity. The inertial deposition velocity for the expected drywell conditions and a boundary layer thickness of 10^{-5} m is shown as a function of the flow velocity in Figure 3-5.

This inertial correlation was implemented into MELCOR in a crude 'patch' method by replacing the term associated with the non-significant diffusion deposition with the inertial deposition. Further, the inertial deposition velocity was implemented as a constant value of 0.1 m/sec. This patch implementation was intended only to scope the value of the correlation to this application. As shown in Figure 3-5, the correlation predicts a deposition velocity of 0.1 m/sec when the flow velocity is about 9 m/sec.

The flow velocities encountered in the drywell, as determined by this study, vary considerably with both time and location. Thus, the correlation as implemented will underpredict the deposition at certain time and locations but overpredict at others. However, it is deemed to provide a reasonable indication of the effectiveness of the correlation for the purposes of a scoping calculation.

3.5 Residence Time Scoping Model

A simple debris particle density decay model was used to compare the results of this study with the Karlshamn and the CEESI experiments [3-8] by means of an effective overall deposition velocity. The idea of the overall effective deposition velocity is that the effect of all of the deposition and resuspension processes active during an experiment or a calculation can be combined into a single number. Starting with the basic exponential decay equation.

$$M(t) = M_o \cdot e^{-\lambda \cdot t} \tag{3-4}$$

where

$M(t)$	=	the time-dependent mass of airborne debris
M_o	=	the initial mass of airborne debris
λ	=	the decay constant
t	=	the time

and

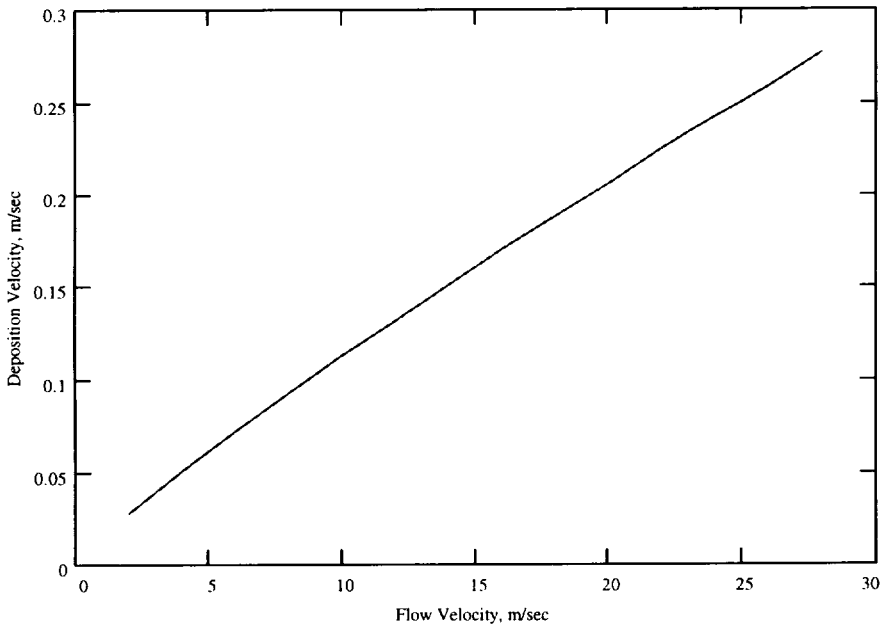

Figure 3-5. Inertial Deposition Velocity

$$\lambda = u_d \cdot \frac{A}{V} \tag{3-5}$$

where

u_d = the overall effective deposition velocity

A = the surface area

V = the volume.

The fraction deposited, f_d, as a function of time becomes

$$f_d = 1 - e^{-\lambda \cdot t} \tag{3-6}$$

If the total debris deposited in an experiment, f_{exp}, and the residence time of the gases carrying the debris, t_{res}, is known then an experimental overall effective deposition velocity can be determined by

$$u_d = \left(-\frac{V}{A}\right) \cdot \frac{\ln(1 - f_{exp})}{t_{res}} \tag{3-7}$$

An equation for the transport fraction is:

$$TF = e^{-u_d \cdot \frac{A}{V} \cdot t} \tag{3-8}$$

This transport fraction equation is shown in a contour plot in Figure 3-6 where the residence time (sec) is shown on the horizontal axis, the deposition velocity (m/sec) on the vertical axis, and the contour shows the resulting transport fractions. If this equation could be validated then an approximate transport fraction could be deduced from an experimentally determined deposition velocity and a calculationally determined residence time.

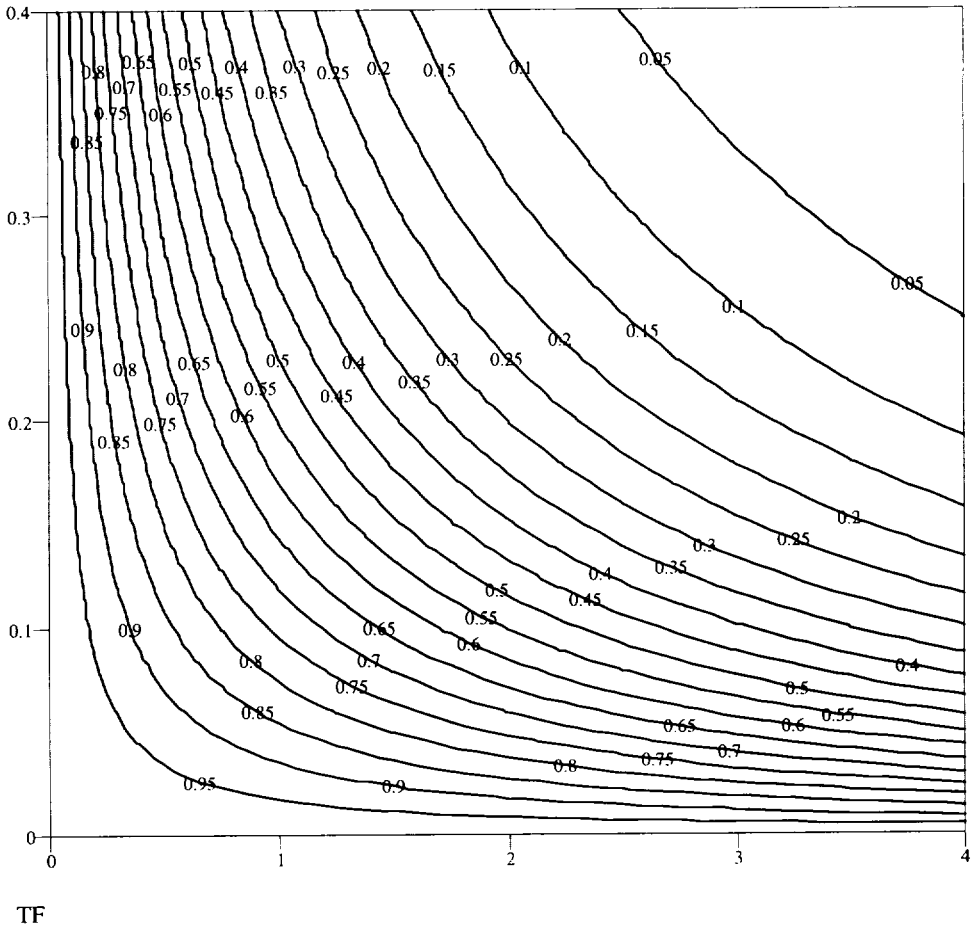

Figure 3-6. Debris Transport Fraction

3.6 Simulation Of Experiments

Two experiments, the Karlshamn and the CEESI experiments, have been simulated using MELCOR. Both of these experiments provide sufficient data to estimate an effective overall deposition velocities.

3.6.1 Karlshamn Simulation

The primary results of the Karlshamn simulation were presented in Reference 3-3 but are shown again here in Table 3-5. Table 3-5 shows the final location of deposited debris. The Karlshamn transport fraction was 0.0096.

The flow velocity in the upper room of the Karlshamn experiment was about 1 m/sec and the flow length of the room was 3-1/3 m. Thus the debris residence time was about 3-1/3 seconds. The area to volume ratio for the upper room was 3.98 m^{-1}. With a deposition fraction of 0.77 and a residence time of 3-1/3 seconds, the overall deposition velocity was calculated at 0.113 m/sec.

3.6.2 CEESI Air Blast Simulation

The CEESI test chamber was 21.6 m long, the area to volume ratio was 1.35 m^{-1}, and the flow velocity was estimated at about 8.4 m/sec. The residence time was then about 2.6 seconds. Observation of the final debris deposition indicated that about 90% of the debris was deposited on the exit screen at the far end of the test chamber. Thus the overall deposition velocity was about 0.03 m/sec which is only about 25% of that determined for Karlshamn. The tests did not involve steam or water, therefore the debris and the surfaces were completely dry.

The CEESI test chamber was modeled with MELCOR to simulate the debris deposition and 4 test cases were run. The results of these simulation cases are shown in Table B-6.

The CEESI test case, designated Base Simulation using the dry debris characteristics of this study without taking credit for inertial deposition reproduced the test results, however the debris characteristics were not very realistic. The other cases all indicated significant debris deposition. One plausible explanation could be that the dry debris deposited on the dry surfaces was actually reentrained into the flow whenever deposited. If the surfaces were wet, as expected in a pipe break scenario, the debris could stick to the wet surfaces resulting in significant deposition.

Table 3-5: Results of Karlshamn Simulation

Location	Karlshamn Experiment	MELCOR Simulation
Room 1 - Upper	77.8%	76.7%
Room 1 - Int.	10.6%	11.8%
Room 1 - Lower	10.7%	8.9%
Downcomer	0.06%	0.003%
Room 2	0.9%	2.6%

Table 3-6: Results of CEESI Simulations with MELCOR

Case	Debris Condition	Dynamic Shape Factor	Particle Density kg/m^3	Transport Fraction
Base Simulation	Dry	4.2	38.4	.9190
Dry Inertial Deposition	Dry	4.2	38.4	.6950
Wet w/o Inertial	Wet	1.4	1025	.4764
Wet with Inertial	Wet	1.4	1025	.3794

3.7 Additional Results

3.7.1 Additional Debris Transport Results

A total 18 calculational cases were performed for the reference plant and the results of these calculations are shown in Table 3-7. The reference plant results are also compared directly to the Karlshamn and CEESI experiments. Four calculational scenarios were repeated for each of the four break scenarios, i.e., wet and dry debris and with and without the inertial deposition model. A separate low recirculation calculation was run where the debris was introduced into the calculation during the first one-tenth of a second (DA-R1-Instant). A separate low MSL calculation was run where Stoke's gravitational deposition was effectively deactivated but the simplified inertial deposition model with a constant deposition velocity of 0.1 m/sec was active (DA-MSL-2).

Table 3-7 shows the calculated and experimental transport fractions, effective residence times, and decay constants and overall effective deposition velocities estimated using the residence time scoping model. The effective residence times for the reference plant calculation were determined by injecting a point-source tracer gas into the break control volume and then measuring the time required for 50% of that tracer gas to transport to the wetwell. For the bulk of the calculations where the debris source was introduced over a five second period, the tracer gas was introduced at 2 seconds. For the single calculation where the debris was introduced in the first one-tenth seconds, the tracer gas was also introduced in the first one-tenth seconds.

Figure 3-7 shows the fractions of the tracer gas located in the drywell as a function of time for the five distinct scenarios reported in Table 3-7. The shortness of these residence times illustrates how rapidly the debris transport would occur for these scenarios. A comparison of the two low recirculation pipe break calculations which differ only in the timing of the debris and tracer gas source clearly indicate the near instantaneous debris generation can increase debris resident time and therefore debris deposition fraction because more of the debris was propelled into the upper reaches of the drywell before flow to the wetwell commenced.

The times required for one-half of the tracer gas to transport to the wetwell are:

- MSLB - High Break 1.79 sec
- MSLB - Low Break 1.04 sec
- RECIR - High Break 1.06 sec
- RECIR - Low Break
  - Source 5 sec 0.55 sec
  - Source 0.1 sec 1.77 sec

A very interesting result shown in Table 3-7 is the groupings of the overall deposition velocities. The overall deposition velocities for the calculation with wet debris and without inertial deposition are all very similar to the velocity from Karlshamn. This is good indication that the debris in these calculations is depositing in a manner similar to Karlshamn despite their differing flow velocities. The dry debris calculations without inertial deposition all group with the CEESI experiment. The inertial deposition model then enhances the overall deposition velocities. The residence time scooping model appears to correlate well with the calculated MELCOR results.

The flow velocity in the Karlshamn was only about 1 m/sec whereas in the reference plant drywell the velocity were generally much higher. The low velocity in Karlshamn indicates that inertial deposition was probably not very important to the overall deposition, whereas in the reference plant inertial deposition likely would be very important if debris sticks to wet surfaces, and these calculations clearly indicate that the surfaces all build a substantial film almost immediately following exposure to steam. Therefore, there is a substantial possibility that the results associated with the wet debris characteristics as defined herein and inertial deposition could be valid. Note again that the debris characteristics for wet debris were specified to essentially reproduce the Karlshamn simulation.

The dry debris without inertial deposition appears to be more applicable to the air blast experiment where the walls were dry and debris inertially impacted onto the surfaces probably was reentrained.

The calculation where the gravity deposition model was deactivated shows that significant deposition could occur even if gravitational deposition were to be found invalid for this application provided that inertially deposited debris were to stick to surfaces

Table 3-7. Calculate Effective Deposition Velocities

Break	Inertial Model	Conditions	Area/Vol m2/m3	Transport Fraction	Deposition Fraction	Effective Residence Time	Decay Constant 1/sec	Deposition Velocities m/sec
Karlshamn Upper Level	Experimetal	Steam	3.98	0.222	0.778	3.33	0.452	0.113
DA - MSL-4	no	Wet	2.98	0.479	0.521	1.79	0.412	0.138
DA - MSL-2	no	Wet	2.98	0.598	0.402	1.04	0.497	0.167
DA - RECIR-3	no	Wet	2.98	0.653	0.347	1.06	0.403	0.135
DA - RECIR-1	no	Wet	2.98	0.756	0.244	0.55	0.506	0.170
DA-R1-Instant	no	Wet	2.98	0.566	0.434	1.77	0.322	0.108
DA - MSL-4	yes	Wet	2.98	0.333	0.667	1.79	0.615	0.206
DA - MSL-2	yes	Wet	2.98	0.482	0.518	1.04	0.704	0.236
DA - RECIR-3	yes	Wet	2.98	0.532	0.469	1.06	0.598	0.200
DA - RECIR-1	yes	Wet	0.91	0.667	0.334	0.55	0.734	0.806
CEESI	Experimetal	Air	1.35	0.900	0.100	2.58	0.041	0.030
DA - MSL-4	no	Dry	2.98	0.808	0.192	1.79	0.119	0.040
DA - MSL-2	no	Dry	2.98	0.862	0.138	1.04	0.143	0.048
DA - RECIR-3	no	Dry	2.98	0.874	0.126	1.06	0.127	0.043
DA - RECIR-1	no	Dry	2.98	0.897	0.103	0.55	0.197	0.066
DA - MSL-4	yes	Dry	2.98	0.519	0.481	1.79	0.367	0.123
DA - MSL-2	yes	Dry	2.98	0.646	0.354	1.04	0.423	0.142
DA - RECIR-3	yes	Dry	2.98	0.670	0.330	1.06	0.379	0.127
DA - RECIR-1	yes	Dry	2.98	0.739	0.261	0.55	0.547	0.183
DA - MSL-2	U=0.1 m/s	No-Grav	2.98	0.506	0.494	1.79	0.381	0.128

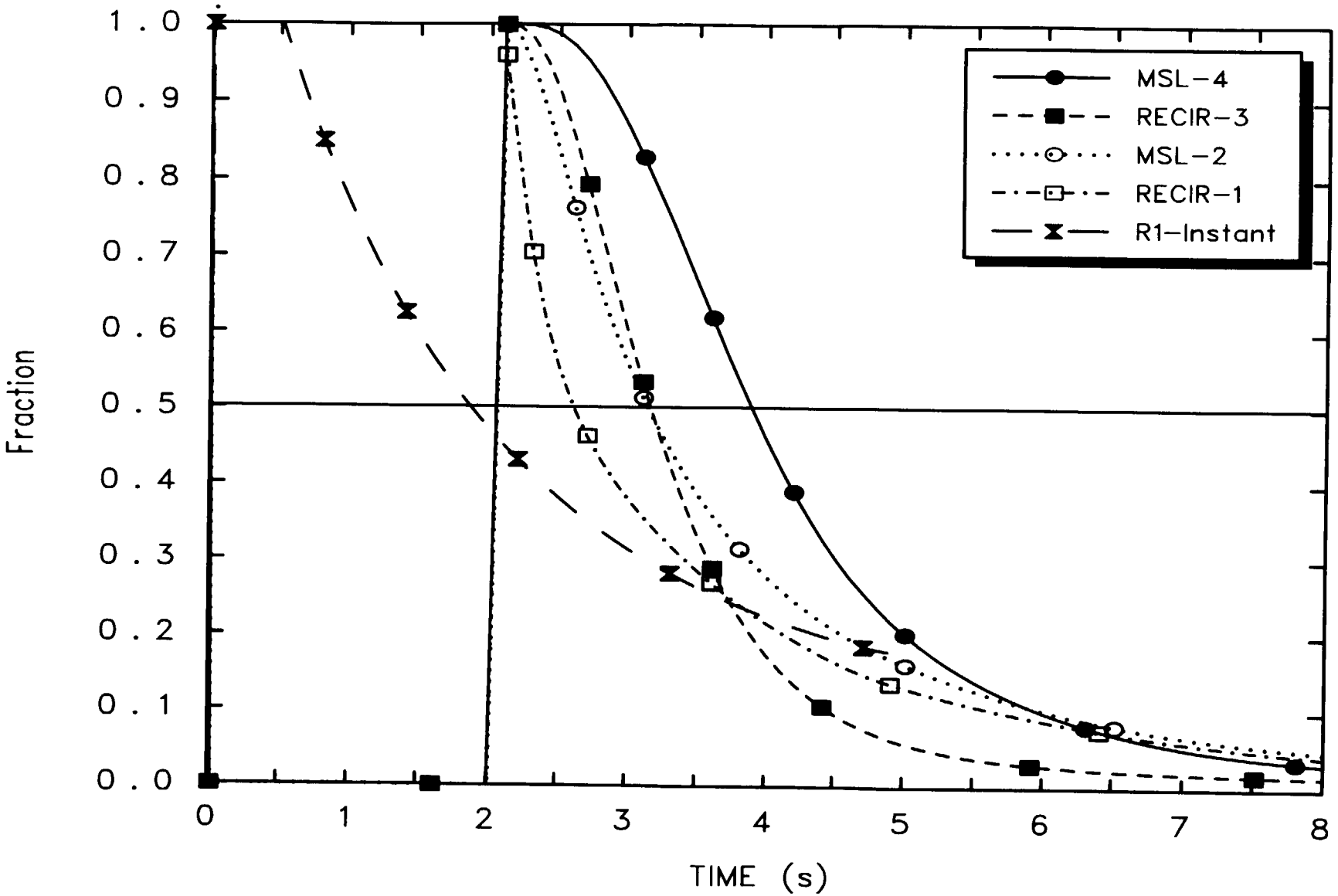

Figure 3-7. Fraction of the Tracer Gas in Drywell

once deposited. The calculation also shows good agreement with simple residence time scoping model since constant inertial deposition velocity of 0.1 m/sec plus a small contribution for condensation driven deposition was essentially returned from the residence time scoping model as 0.128.

Table 3-8 shows the final distribution of debris for the higher MSL break for both wet and dry debris and with and without inertial deposition. The distributions are shown by vertical levels, then by horizontal (facing upwards) versus vertical surfaces, and then by azimuthal quadrant.

Some debris was deposited in each of the 31 control volumes which 10 to 15% deposited in the neck regions of the drywell and 1 to 2% in the reactor cavity and shield wall annulus spaces. A few percent was deposited in the drywell-side of the vent downcomer system piping but this debris was included in the overall transport fractions. When debris was predominantly on the horizontal surfaces, it clearly indicates the relative importance of the gravitational deposition process for that calculation because most of the surface area was vertical. More debris was deposited in the quadrant associated with the break than in the other quadrants. Only one of the two side quadrants is shown in Table 3-8 since their deposition fractions were identical because of the symmetrical flows.

Selected time-dependent debris transport results are presented in Appendix A.

3.7.2 Additional Thermal-Hydraulic Results

Flow velocity distribution throughout the drywell at a time of 5 seconds after the break are provided in Figures 3-8 through 3-11 for the 2 MSL breaks and the 2 recirculation line breaks. Two type of velocities are shown, i.e., control volume averaged velocities and velocities though the flow junctions which connect the control volumes.

The velocities shown in the boxes are the control volume averaged velocities as calculated by the following MELCOR algorithm.

$$V_{cv} = \frac{A_{cv}}{2} \cdot \sum_{j} |Q_j| \qquad (3\text{-}9)$$

where

V_{cv} = the volume averaged velocity
A_{cv} = the area associated with the volume (typically volume/height)
Q_j = the volumetric flow though connecting junction j.

The numbers between the boxes show the junction flow velocities between the control volumes going both vertically and azimuthally. Note that only one side quadrant is shown because the flows were symmetrical around the pedestal. The junction velocities are:

$$V_j = \frac{Q_j}{A_j} \qquad (3\text{-}10)$$

where

V_j = the junction velocity
A_j = the junction flow area
Q_j = the volumetric flow though connecting junction j

Selected time-dependent thermal-hydraulic results are presented in Appendix B.

3.8 Conclusions And Recommendations

The debris transport results provided plausible transport fractions based on the debris transport models inherent in the MELCOR code and the debris characteristics that successfully simulated the Karlshamn experiment. The transport fractions calculated ranged from 0.3 to .9 depending upon the conditions applied to the calculation. Assuming a recirculation line break near the entrance to a couple of the vent downcomers, small dry debris, and taking no credit for inertial capture, the transport fraction was 0.90. Alternatively, assuming a steam line break located in the neck of the drywell, wet debris (similar to Karlshamn), and taking credit for inertial capture, the transport fraction was 0.33.

The uncertainties associated with these MELCOR calculations include the debris characteristics, such as the size distribution of the debris, the potential moisture of the debris, and the debris shape factors; the validity of the debris deposition and capture

Table 3-8. Final Insulation Debris Deposition Distribution for Level 4 MSL Break

	Calculational Assumptions			
	Saturated Debris without Inertial Deposition	**Saturated Debris with Inertial Deposition**	**Dry Debris without Inertial Deposition**	**Dry Debris with Inertial Deposition**
Vertical Orientation				
Level 6	2.38%	2.61%	0.85%	2.29%
Level 5	3.46%	4.88%	1.26%	3.41%
Level 4	5.73%	8.81%	2.05%	5.55%
Level 3	11.32%	15.96%	4.39%	11.37%
Level 2	12.64%	16.78%	5.77%	14.32%
Level 1	15.09%	16.07%	4.14%	9.64%
Cavity	1.43%	1.58%	0.74%	1.53%
Vents	2.77%	3.44%	0.63%	3.24%
Wetwell	45.17%	29.87%	80.17%	48.65%
Surface Orientation				
Horizontal Facing Upwards	77.12%	52.59%	17.93%	14.04%
Vertical & Horizontal Downwards	22.88%	47.41%	82.07%	85.96%
Azimuthal Orientation				
Break Quadrant	34.01%	32.90%	26.44%	26.99%
Side Quadrant	23.56%	24.70%	26.45%	26.66%
Back Quadrant	18.88%	17.70%	20.66%	19.70%

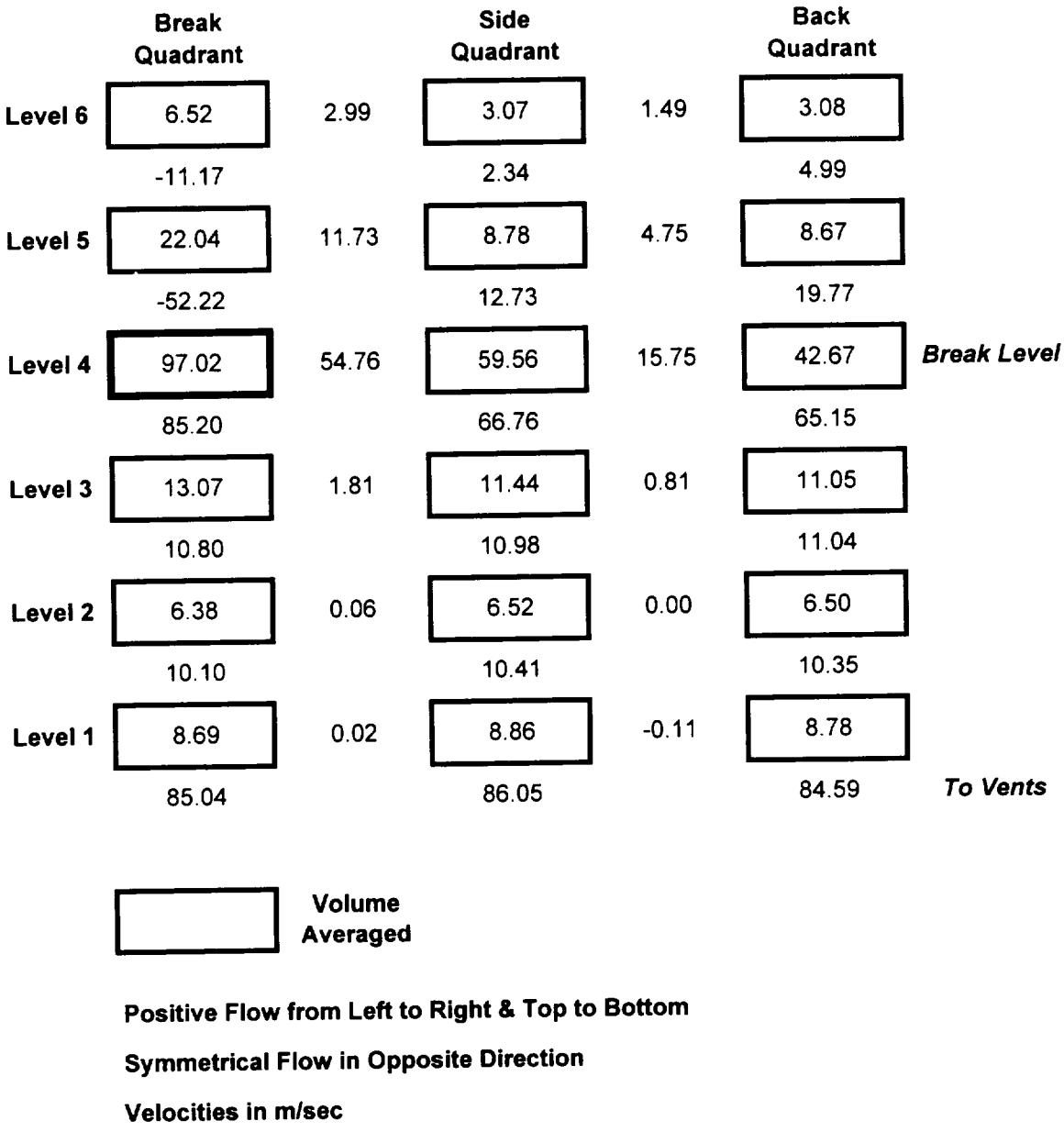

Figure 3-8. Velocity Distribution in Drywell at 5 sec for Main Steam Line Break – Level 4

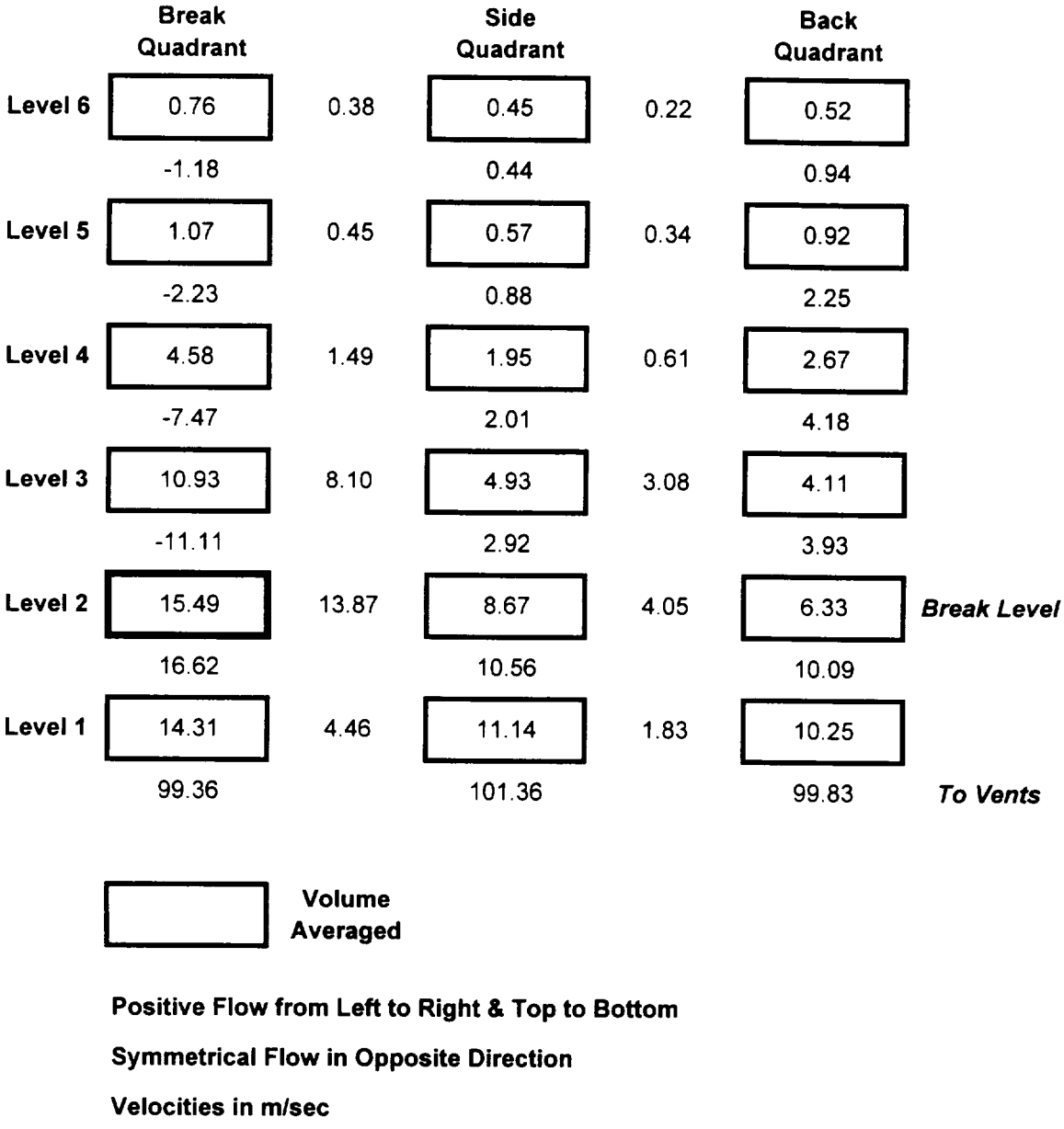

Figure 3-9. Velocity Distribution in Drywell at 5 sec for Main Steam Line Break – Level 2

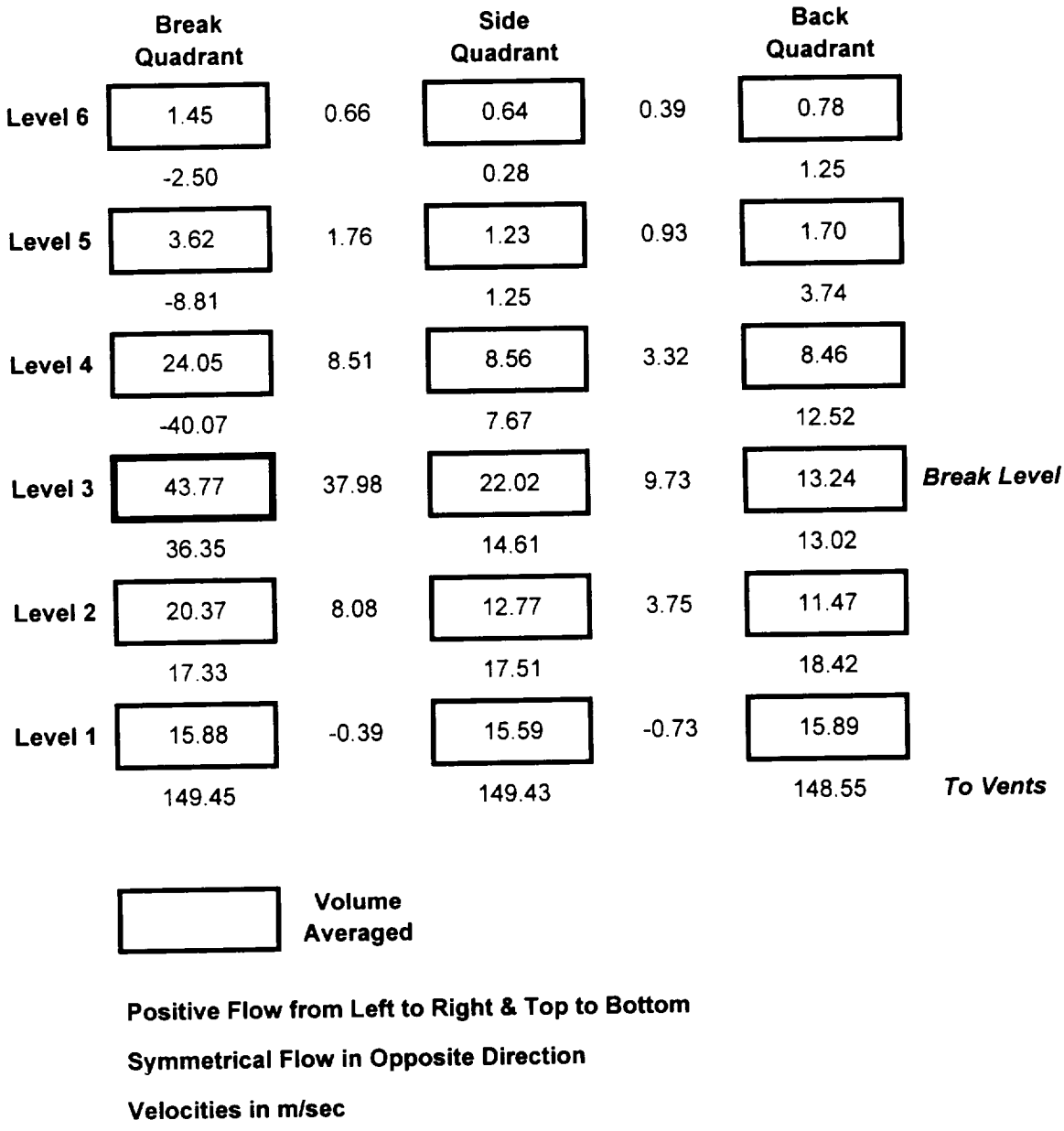

Figure 3-10. Velocity Distribution in Drywell at 5 sec for Recirculation Pipe Break – Level 3

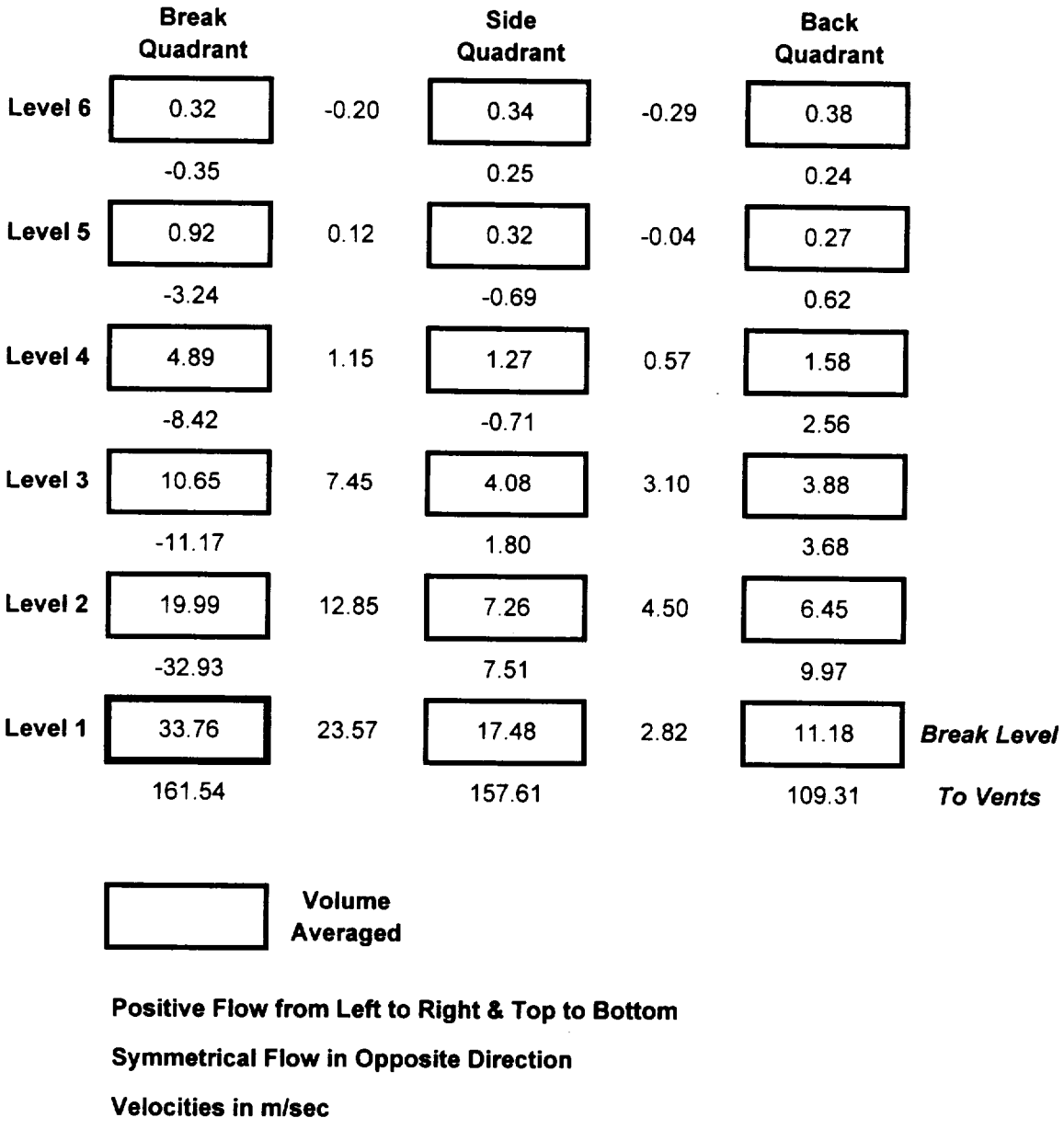

Figure 3-11. Velocity Distribution in Drywell at 5 sec for Main Steam Line Break – Level 1

models; and the rate at which the insulation target would be destroyed. The two apparent dominant deposition mechanism were gravitation settling and inertial capture processes. Among the objectives of the proposed experiments, are the determinations of whether or not gravitational deposition can play a significant role in capturing debris given the high level of turbulence expected in the drywell following a LOCA and whether or not debris inertially captured onto wet drywell surfaces will stick to those surfaces and not be resuspended. The comparative rates of target destruction and vent clearing can play a significant role in how much of the debris is propelled into the upper reaches of the drywell prior to the onset of flow to the wetwell. Debris propelled into the upper portion of the drywell would have a longer residence time for the deposition processes to work. Most of these calculations assumed that target destruction took five seconds, whereas experiments indicated that a fraction of a second may be more reasonable.

Proposed experiments may point to the validity of using an inertial capture correlation such as a the turbulent diffusion deposition model (also referred to as a free-flight model) which is a direct function of the flow velocities. These preliminary calculations merely assumed a constant inertial deposition velocity of 0.1 m/sec when credit was taken for inertial capture. A more appropriate implementation of this inertial capture correlation would make the deposition rate a function of a characteristic control volume velocity.

A simple calculation model based on the traditional decay rate equation and the residence time of the gases propelling the debris was used to compare the MELCOR calculations to the experimental results of the Karlshamn and CEESI air blast experiments. The model was used to estimate an effective overall deposition velocity from the experiments and each of the calculations. The idea of the overall effective deposition velocity is that the effect of all of the deposition and resuspension processes active during an experiment or a calculation can be combined into a single number. The experimental and calculational results compared reasonably well to the experimental results using the simple model. This simple model and/or MELCOR code simulations of the experiments should be explored as a means of backing out an effective deposition velocity from the proposed experiments.

In summary, this study indicates that the MELCOR code could be a useful tool to examine the experimental results of the proposed experiments. It could for example be used to deduce overall deposition velocities from the distribution of debris deposits. Once the experimental results are understood, the MELCOR code could be used to apply the new data to nuclear plants.

3.9 References

3-1 Gary E. Wilson, et. al., "BWR Drywell Debris Transport Phenomena Identification and Ranking Tables (PIRT)," PIRT Panel Report to the USNRC, June 28, 1996.

3-2 G. Zigler, et. al., "Parametric Study of the Potential for BWR ECCS Strainer Blockage Due to LOCA Generated Debris," NUREG/CR-6224, SEA 93-554-06-A:1, October 1995.

3-3 C. J. Shaffer, "Demonstration of MELCOR Code Capability to Simulate Insulation Debris Transport Within a BWR Drywell," SEA 94-970-01-A:5, October 23, 1995.

3-4 D.V. Rao, et. al., "Drywell Debris Transport Methodology, Responses to PIRT Panel Request for Information," SEA96-3104-06-A:1, May 1996.

3-5 Letter to G. Zigler of SEA from A. Johnson of ARL, May 24, 1996.

3-6 J. E. Brockmann and D. J. Radar, "APS Response to Nonspherical Particles and Experimental Determination of Dynamic Shape Factor," Aerosol Science and Technology 13:162-172, 1990.

3-7 R. J. Lipinski, et. al., "Uncertainty in Radionuclide Release Under Specific LWR Accident Conditions," DRAFT, SAND84-0410, February 1985.

3-8 NRC Memorandum to Charles Z. Serpan, Jr., from Michael L. Marshall, Jr., "Trip Report July 9 through 11, 1996,: Observations of BWROG Air Jet Tests."

4. Debris Transport In The Drywell

In Section 3, MELCOR was used to examine its applicability to predict debris transport in the drywell. These analyses showed that MELCOR can be a useful tool to conduct integrated analyses. However, it has to be modified to incorporate appropriate models for debris capture by inertial means and debris transport in the water pools. This section explores the possibility of using simpler models to predict and transport to rank capture mechanisms for each debris size and obtain an order-of-magnitude transport factors. In this section the debris wave catagorized into classes one through six as described in NUREG/CR-6224 [Ref. 4.1].

4.1 Containment Thermal-Hydraulic Conditions

Containment thermal and hydraulic conditions influence debris transport significantly. The calculations presented in the previous sections were used to evaluate thermal-hydraulic conditions that exist in the drywell following (a) a main steam line break, and (b) a recirculation line break. The following paragraphs present the most important results.

4.1.1 Main Steam Line Break

Following a main steam line break (MSLB), essentially dry steam expands into the containment. The mass flow rate of steam falls from an initial value of close to 6,000 lbm/s (assuming blowdown from both ends of the broken pipe) to about 1,000 lbm /s within a period of 50 seconds, while the steam flow velocity remains essentially at the sonic velocity of 700 ft/s. Water enters the drywell in the form of fine droplets (≈ 5-15 μm) produced from isentropic expansion of the steam jet and a thin condensate layer on the structural surfaces. However, the water content is not likely to be large enough to completely wet the debris during their generation. Additional experiments were conducted to confirm this finding. During the first few seconds, wetness is primarily going to be due to steam condensation on relatively cold structures, enhanced by droplet deposition.

The expected drywell atmosphere flow velocities depend on the region in the drywell of interest and the location of the break. The flows peak early and decrease with time. The approximate flow velocities (averaged over the first five seconds) for a break assumed to occur in the upper region of the containment are presented in Table 4-1. These flow velocities were estimated based on: (a) CFD simulation of the drywell flows by the PIRT panel [Ref. 4.2], (b) MELCOR calculations for pressure-driven flows.

The scoping calculations suggested that the vents clear in less than one second into the accident. After the vents are cleared, the containment atmosphere turns over into the suppression pool in about 4 s, implying that several drywell atmosphere turn over occur within the first 15 seconds after the MSLB.

4.1.2 Recirculation Line Break

During a RECIR break, initially mainly water exits the broken pipe. At about 5 to 10 s into the accident, a mixture of water and steam is discharged at high velocities. During this phase, the dynamic pressures far outweigh the corresponding pressures during the initial 5 s after the break. Table 4-2 summarizes the expected flow conditions and dynamic pressures following a RECIR. Since the debris generation is proportional to the dynamic pressure, these results suggest that for a RECIR most of the fibrous insulation debris will be produced in the later stages of the accident.

The total mass flow rate remains fairly high (≈20,000 lbm/s) throughout the blowdown phase of a RECIR compared to a similar size MSLB. However, the water content of the exit flow is very large. But during the later stage, the steam void fraction is also large and, given the velocities of the two-phase mixture, it is likely that the slip would be minimal. In these circumstances, the flow would consist of water droplets, 200 μm in average diameter, suspended in the jet flow.

Table 4-1. Expected Flow Velocities in the Drywell during a MSLB

Time (s)	Velocity in the neck (ft/s) [m/s]	Velocity in the upper grating (ft/s) [m/s]	Velocity in the lower grating (ft/s) [m/s]	Velocity in the vents (ft/s) [m/s]
0 - 2	100 [30]	45 [14]	53 [16]	59 [18]
2 - 5	100 [30]	45 [14]	53 [16]	60 [18]
5 - 10	85 [26]	36 [11]	42 [13]	46 [14]
10 - 15	68 [21]	29 [9]	34 [10]	37 [11]

Table 4-2. Expected Flow Conditions and Dynamic Pressures during a RECIR.

Time (s)	Velocity (ft/s) [m/s]	Dynamic Pressure (psi) [MPa]	Steam Quality at Break
0 - 1	> 200 [61]	> 200 [1.4]	≈ 0
1 - 5	160 [49]	130 [0.9]	≈ 0
5 - 10	800 [244]	637 [4.4]	0.15

Corresponding to these conditions, it is expected that all of the structures located in the path of the jet will be drenched with water. An additional insight gained from these analyses is that the insulation materials in the vicinity of the break are likely to be thoroughly wet prior to the time when the break jet would produce significant debris. The scoping calculations also suggest that a recirculation line break will fill up the drywell floor with water in less than 5 s. Several pool turnovers are expected to occur within the first 15-20 seconds.

4.2 Implications for Drywell Debris Transport

4.2.1 Accident Scenario

4.2.1.1 Main Steam Line Break

Based on available data, it is reasonable to assume that all debris would be generated and mixed with containment atmosphere within the first one second before the vents are cleared. After that, the debris would undergo the following processes:

(a) Deposit on structures by inertial means
(b) Deposit on walls, etc., by turbulent inertial/diffusionary means
(c) Deposit on floors by gravitational forces
(d) Filtered out (trapped) by gratings, etc., or
(e) Be advected to the suppression pool.

Independent calculations were performed to evaluate the potential of each of these processes. The calculations are summarized in the following section.

4.2.1.2 Recirculation Line Break

It is very likely that debris would be generated over several seconds following a recirculation line break. It is very likely that this debris would be transported with water. However, a fraction may be carried by steam flow depending on where the debris was generated. The fraction that is entrained and transported by steam would behave in a manner very similar to the previous case with the following exceptions:

(a) The structure will be more likely to be wet
(b) The debris would be possibly larger

The fraction transported by the water will be carried to the floor immediately, where it will mix

with the pool water. Thereafter, it will undergo any of the following processes:

(a) Settle on the floor under influence of gravity
(b) Deposit on walls and structures by inertial means, and
(c) Advection to suppression pool.

Independent calculations below demonstrate the potential for each of these processes.

4.2.2 Baseline Calculations

4.2.2.1 Main Steam Line Break

(i) Advection to Suppression Pool:

Assume:

- In the first second, the drywell has reached its maximum pressure and the debris were generated and thoroughly mixed with drywell atmosphere.

- During the quasi-steady state that exists,
- $\dot{m}_{break}$ enters the drywell, while the same amount leaves the core.

Under these conditions, the debris concentration is given by:

$$C^t = \frac{M_{total} \bullet C^{t-\Delta t} - \dot{m}_{break}\, C^{t-\Delta t} \bullet \Delta t}{M_{total}} \qquad (4\text{-}1)$$

where

C^t is concentration at time t (kg-debris/kg-steam)

C^{t-dt} is concentration at t - Δt

M_{total} is total steam mass at t, (kg-steam)

$\dot{m}_{break}$ is break flow rate (kg/s)

$$C^t = C^{t-\Delta t} - \frac{\dot{m}_{break}}{M_{total}} C^{t-\Delta} \bullet \Delta t \qquad (4\text{-}2)$$

$$\frac{\Delta C}{\Delta t} = -\frac{\dot{m}_{break}}{M_{total}} C \qquad (4\text{-}3)$$

$$\int \frac{1}{C} dC = -\int \frac{\dot{m}_{break}}{M_{total}} dt \qquad (4\text{-}4)$$

$$\log C = -\frac{1}{\tau}\int dt = -\left[\frac{t}{\tau}\right] + [k] \qquad (4\text{-}5)$$

Where the turn-over (or flushing) time,

$$\tau = \left[\frac{\dot{m}_{break}}{M_{total}}\right]^{-1} \qquad (4\text{-}6)$$

when

$$t = 0;\ C = C_o$$

$$-\log C_o = +k \qquad (4\text{-}7)$$

$$-\log C = -\frac{t}{\tau} + \log C_o \qquad (4\text{-}8)$$

$$\log\frac{C}{C_o} = -\frac{t}{\tau} \qquad (4\text{-}9)$$

$$\frac{C}{C_o} = e^{-\frac{t}{\tau}} \qquad (4\text{-}10)$$

Table 4-3 presents concentration as a function of time. For these calculations, the turnover time was assumed to be 4 seconds.

Table 4-3 Variation in the concentration due to advection.

t (s)	t/τ	C/Co
4	1	0.37
8	2	0.135
12	3	0.05

This effectively shows that about 95% of all suspended debris would be advected to suppression pool in first 12 seconds if they are not removed from the flow by one of the following mechanisms.

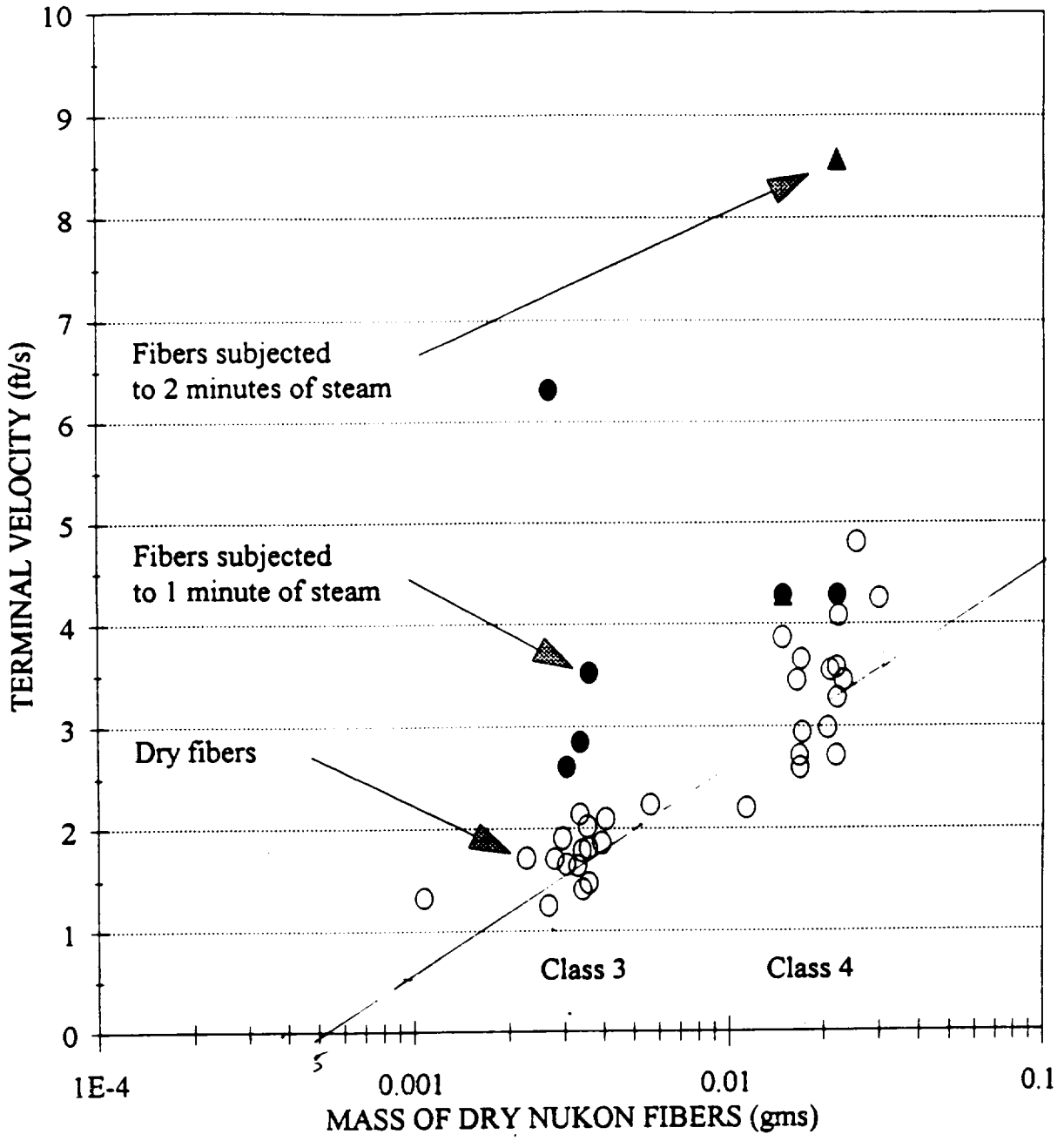

Figure 4-1. Terminal Velocity of Dry and Steam-Wetted NUKON Fibers in Still Air.

(ii) Potential for Gravitational Settling

For these calculations it is essential to understand the sensitivity of this deposition mechanism to the debris particle size. The settling velocities for classes 3 and 4 were measured and plotted in Figure 4-1. These measurements were made for the following conditions:

(a) totally dry
(b) wetted by 1 min. of steam exposure
(c) wetted by steam for 2 minutes

From this data, SEA obtained the following equations:

$$U_o = 16\sqrt{m} \quad \text{totally dry} \qquad (4\text{-}11)$$

$$U_1 = 24\sqrt{m} \quad \text{1 minute steam} \qquad (4\text{-}12)$$

$$U_2 = 44\sqrt{m} \quad \text{2 minute steam} \qquad (4\text{-}13)$$

where,

U is deposition velocity (ft/s)

m is mass in gms (g).

Using the information provided above, settling velocities can be derived for different debris sizes. Table 4-4 presents these calculated settling velocities. In this table, U_o, U, and U_2 correspond to estimate settling velocities for dry, exposed to 1-min of steam and exposed to 2-min of steam.

If is assumed that (a) residual turbulence and (b) flow patterns do not impede debris settling, then it is likely that substantial settling will occur. However, in reality, large containment velocities close to 30-50 ft/s exist and high levels of turbulence are likely. As a result, it is unlikely that this mechanism dominates. For relative importance, the concentration change due to settling alone are estimated from rate equations and shown in Table 4-5. A residence time of 30 seconds was assumed to develop these estimates.

Table 4-4. Calculated Settling Velocities for Debris Classes 3, 4, 5, and 6.

Class[4]	Approx. Size[1]	Mass	U_o	U_1	U_2
3	¼ x ¼ x ¼	0.003	0.87	1.3	2.4
4	1 x 1 x ¼	0.02	2.3	3.5	6.3
5	2 x 2 x ¼	0.09	4.8	7.2	13.2
6	2 ½ x 2 ½ x ¼3 x 3 x ¼	0.15	6.196	9.3	17

[4]Classification and weights for debris were provided by ARL (P. Murthy) as part of NUREG/CR-6224 study.

Table 4-5. Estimated Concentration Changes Due to Settling Alone.

V_o	Area	Volume	C/C_o (4 sec.)	Quantity Deposited
0.87	2,463 ft^2	150,000 ft^3	0.94	6%
2.3			0.86	14%
4.8			0.72	28%
6.2			0.66	34%

If turbulence does not impede settling as shown in Table 4.4, then up to

≈ 0% of Class 1 and 2,
≈ 3% of Class 3,
≈ 7% of Class 4,
≈ 10% of Class 5,
≈ 15% of Class 6

debris would settle down in the drywell.

However, all the evidence suggests that very high levels of turbulence exists in the drywell following a LOCA [Ref 4.2]. Such conditions will impede settling. Further experiments are needed. If experimental data suggests that gravitational settling is possible, then appropriate models can be developed. Until shown otherwise, gravitational settling should be ignored in small and medium pieces.

(iii) Inertial Capture on Structures

In general, stokes number is a good indicator of the inertial capture, defined as

$$Stk = \frac{\tau V}{D} \qquad (4\text{-}14)$$

where,

τ is relaxation time (U/g)

U is gravitational velocity (m/s)

g is acceleration due to gravity (m/s^2)

V is fluid velocity (m/s)

D is pipe (structure) diameter (m).

Stokes numbers estimated for different debris sizes are presented in Table 4-6. These estimates are based on a flow velocity of 30 ft/s transported across a pipe 12" in diameter.

The previous tables suggested that debris particles would come in contact with structural surfaces. Whether they stick to the surface or not depends on debris wetness and flow velocity. The following engineering analyses can be used to estimate potential for debris adhesion.

Potential for adhesion:

For a flow over a rectangular piece of insulation located on a surface, the force balance for its removal is drag by flow ≥ surface forces.

If it is assumed that the piece is stuck to the surface by surface tension of water, then surface force is given as

$$2(A+B)\sigma \neq F_{surface} \qquad (4\text{-}15)$$

The drag force is given as

$$F_{drag} = (A)(B) \bullet \frac{1}{2} \rho_g V_g^2 \bullet C_f \qquad (4\text{-}16)$$

Table 4-6. Stokes Numbers for Different Debris Sizes.

Class	U (m/s)	τ(s)	Stk @ 10 m/s and 0.3048 pipe
1	0.003	0.0003	0.01
2	0.03	0.003	0.10
3	0.27	0.027	0.89*
4	0.70	0.07	2.35*
5	1.46	0.15	4.90*
6	1.89	0.193	6.32*

*This debris will hit surfaces.

where

A and B are length and width of the fiber piece

V_g is flow velocity

ρ_g is flow density

σ is water surface tension

C_f is drag coefficient.

Using the force balance, it can be shown that

$$V_g = \sqrt{\frac{4(A+B)\sigma}{C_{fx} AB \rho_g}} \qquad (4\text{-}17)$$

For a 2" x 2" piece

A = 5 cm, B = 5 cm

σ = 50 dynes/cm

ρ_g = 3 x 10^{-3} g/cc at 45 psi

C_{fx} = 0.0576 for rough surfaces

$$V_g = \sqrt{\frac{4(10)(50)}{(0.0576)(25)(3x\,10^{-3})}} = 680 \text{ cms or } 6.8 \text{ m/s} \qquad (4\text{-}18)$$

Certainly, flow above 6.8 m/s will likely dislodge the debris from surfaces. Note also that a gas velocity of 10 m/s (or 30 ft/s) is commonly known as the critical velocities for entrainment where a water film on the surface would be broken up and entrained by steam flowing across it.[5] Thus, it is likely that whenever the flow velocities across a surface are larger than 10 m/s or so, the debris would be reentrained. This value may be much larger if the gravity acts against the debris movement.

Conclusions:

- Most of the debris will likely hit the structures, but they may not stick to them. Calculations suggest that debris size classes 3, 4, 5, and 6 possess Stokes numbers far in excess of the 1.0 needed to ensure that a fraction of them hit surfaces located in their path. On the other hand, Classes 1 and 2 would not probably approach surfaces.
- Calculations suggest that even large pieces may not stay on surfaces because of associated large drag forces. Our analyses suggest that at a flow velocity of

[5]Most steam/water separation equipment is designed to operate at steam velocities below 30 ft/s to minimize water entrainment.

about 10-15 m/s, debris would be entrained and carried off the structures.

- In the containments, such velocities exist in the majority of the local regions. As a result, it is likely that only a small fraction would ultimately stick to surfaces. This fraction can not be easily determined in the present calculations.

- Further experimentation is needed in this area. In particular, we need to establish whether or not a particular piece of fiberglass adheres to a surface at a given flow velocity and direction.

- For this scoping analysis, it was assumed that inertial capture contribution is negligible.

⇒Inertial capture neglected

(iv) Turbulent Diffusion Means

For small particles, the turbulent diffusion is a likely deposition mechanism. Deposition by *turbulent diffusion* occurs when the particles are transported from the turbulent core of the fluid through the boundary layer to a diffusion sublayer whose thickness is approximately one "stopping distance" from the surface. At this point, the particle follows a free path to the surface. The stopping distance is the product of the particle relaxation time and the mean velocity of the particle. There are various theories to model turbulent diffusion, but most of them only differ in the way in which they estimate the mean particle velocity at the beginning of the free flight to the surface.

The available experimental data [Ref. 4.1] indicates that the deposition velocity for turbulent diffusion of spherical particles is proportional to the square of the dimensionless relaxation time, τ^+, for $\tau^+ < 10$, but is essentially independent of the dimensionless relaxation time for particles with τ^+ in the range between 10 and 1000. The *dimensionless relaxation time*, τ^+, is defined as:

$$\tau^+ = S\, d^{+2} / 18 \qquad (4\text{-}19)$$

where

$d^+ = dp\, u^* / \nu$ is the *dimensionless particle diameter* and u^* is the friction velocity.

For particles with $\tau^+ < 10$, turbulent diffusion effects dominate the deposition behavior. Motion of particles characterized by $10 < \tau^+ < 10^3$ is entirely governed by inertia and their deposition velocity is independent of τ^+. Particles characterized by $\tau^+ > 10^3$ are unaffected by the turbulent gas phase eddies due to their high momentum, and their destination is determined by the initial release process, i.e., by the movement of the average gas flow. Particles characterized by $\tau^+ > 10^6$, on the other extreme, are dominated by gravitational sedimentation.

For comparison purposes, note that for fibrous insulation debris and average flow velocities of about 30 ft/s (9 m/s), $\tau^+ = 10$ corresponds to a particle with characteristic diameter in the order of 10 μm, whereas $\tau^+ = 1000$ corresponds to a particle with a characteristic diameter in the order of 100 μm. In these circumstances, gravitational sedimentation will become important (i.e., $\tau^+ > 10^6$) for particles in the order of 1000 μm.

Scoping calculations suggest that approximately 20% by mass of the fibrous debris particles corresponding to Classes 1 and 2 can be deposited on structures in the drywell by turbulent diffusion. Again, additional experimental efforts are needed to investigate the potential for debris particle deposition due to turbulent diffusion following a main steam line break.

(v) Filtration at Gratings

All the steam line breaks are located above the lower grating and some are located even above the higher grating. In these configurations, debris generated by a postulated break must pass through the gratings before it reaches the vents. These gratings are typically made of 3 in. length by 1 in. width clearances shown below.

As the debris hits these gratings, it may become physically trapped on it.[6] Clearly, the quantity trapped would depend on the size of the debris and the local flow velocity. If the debris is large enough to get stuck, it may (a) stay on the grating, or (b) be forced through the grating.

The mechanism for forcing the debris through will require sufficient pressure drop induced to by the flow of air through the debris that will cause the debris to go through the hole.

The magnitude of pressure drop across a blanket 2.5 cm in thickness can be given as [Ref. 4.2].

$$\Delta H = 0.057\, \rho_g V_g^2 \bullet (\Delta L) \qquad (4\text{-}20)$$

where

ρ_g = density of air (3 x 10-3 g/cc)

V_g = flow velocity (103 cm/s)

ΔL = 2.5 cm

ΔH = pressure drop in cm-water

$\Delta H = (\Delta L)\, cm\text{-}water$

$= 5.6\ (\Delta L)\, ft\text{-}water.$

Thickness	ΔH (ft-water)
1 cm	1.6
2.5 cm	14
0.5 cm	2.8

How debris piece would behave when subjected to such stresses is unknown. This needs to be determined.

Conclusions:

A large fraction of the large pieces may be removed initially from the flow at the gratings. However, sufficient pressure drop may force these pieces down through the holes. It is not clear what would happen to them in reality because it depends entirely on the structural strength of the material and resulting air flow patterns.

(vi) Vent Cover/Jet Plate

The flow undergoes bending around the vent plate. Once again, for Stk >>1, a substantial fraction of debris are expected to be deposited on the vents. Given the fact that vents are many and located at strategic locations, a large fraction could be removed. The fractions in Table 4-7 are estimated from available engineering data/equations.

As evident from Table 4-7 further experimental data is needed to estimate removal fraction for size classes 3 and 4. It is likely that capture efficiency is large for sizes 5 and 6, and minimal for size classes 1 and 2.

Table 4-7. Estimated Removal Fractions

Size Class	Stk	ε (removal fraction)
1	0.06	≈ 0
2	0.32	≈ 0.1
3	2.85	$\approx$?? (No Data)
4	7.54	$\approx$?? (No Data)
5	15.74	≈ 1.0
6	20.32	≈ 1.0

(vii) Conclusions

Depending on debris size, a large fraction may be removed from the flow. However, it is very dependent on the type of debris generated. Based on our analyses, the insights in Table 4-8 can be drawn.

4.2.2.2 Recirculation Line Break

The CFD calculations suggested that water flows at high velocities on the drywell floor for Mark I reactors. At such high velocities, it is unlikely that any debris would remain in the drywell floor pool. The only possibility may be debris entering the sump located in the center of

[6] Note CEESI experiment did not show any evidence of this. Likely no 5 and 6 class debris was generated.

Table 4-8. Insight by Debris Class

Debris Size	Insights
Classes 1 and 2	• For these, flow relaxation times and Stokes numbers are very small. Therefore, potential for large scale inertial capture is minimal except in the areas where eddies form. Assume fraction removed by this as 0. Additional experiments are needed. • Gravitational settling velocities are negligible even for quiescent flows. Very unlikely that this debris would settle under the influence of gravity. • Turbulent diffusion may remove debris and coat some of the structures. However, given the residence time of 4 s, the debris may reach the suppression pool in large quantities. Assume a removal fraction of 21%. • No debris will be filtered by the gratings because they are very small. • Stokes number are very small for deposition on vent covers, etc. • Net fraction assumed is to be part of turbulent diffusion. This rate is ≈ 21%
Classes 3 and 4	• Stokes numbers are large enough that the debris would impact the drywell structures. But they may not stay attached as the ambient flow velocities are very large. Further experimental data is needed to quantify this potential. For this study, it is assumed that all debris would be reentrained. A removal fraction of 0.0 is assigned. • Gravitational settling velocities are large for calm flows. But for turbulent condition, they are minimal. • The vent plates are a good location for some of the debris to deposit, as well as structures located around. For now, since BWROG tests showed otherwise, we neglect that potential. • Removal by turbulent conditions may not be large considering that the debris would stick out into the ambient flow. Net fraction for the present study = 0 This is an overly conservative number.
Classes 5 and 6	• Large Stokes numbers, but they may not stick to surfaces. Further experimental data needed. A removal fraction of 0.0 is assigned. • A large fraction will be filtered at the gratings. We assume this fraction to be 50%. • A good fraction may also be deposited on the vent cover. We assume the fraction to be 10%. • No other mechanisms play an important role. • Total deposition is • 60%.

the drywell which may settle down in the sump. The following calculations were used to establish these factors.

(i) Will the Debris Remain Suspended?

The PP&L tests [Ref. 4-3] suggested that for specific energy inputs higher than 1.0 most likely all debris will remain suspended. Specific energy input is expressed as

$$E = \frac{\rho_w \bullet Q_w \bullet H}{dw\ \ell} \qquad (4\text{-}21)$$

where

E is specific energy (lbm-ft/s/ft^3)

ρ_w is density (lbm/ft^3)

Q_w is flow velocity (ft^3/s)

H is static head between downcomer and pool (ft)

$dw\ell$ is total volume of water (ft^3)

For Mark I,

$dw\ell \approx 2{,}000$ ft^3

$\rho_w \approx 62$ lbm/ft^3

$$Q_w = \frac{25{,}000\ lbm/s}{62\ lbm/ft^3} = 403.2\ ft^3/s$$

$H \approx 1$ ft-water (this is minimum)

$$E = 12.5 \frac{lbm - ft/s}{ft^3}.$$

Figures 7 and 8 of the PPL report suggest that all debris would remain entrained at these high specific velocities.

Also note that the NRC suppression pool chugging tests [Ref. 4-5] showed that even lower specific energies would be needed to resuspend debris and even to destruct them.

(ii) Will the Debris be Transported?

Assuming no turbulence dissipation, the flume velocities can be calculated for the Mark I plant based on the following calculations.

For an idealized geometry, assume that flow is added uniformly to the pool around the pedestal. For all practical reasons, flow then proceeds uniformly to the vents. At an imaginary plane located 5 ft from the vents, the flow velocity is calculated as:

$$V_w = \frac{Q_w}{A_{plane}}$$

$$Q_w = 600\ ft^3 \qquad (4\text{-}22)$$

$$A_{plane} = 1{,}256\ ft^2$$

$$V_w = 0.32\ ft/s$$

At the vent entrance

$$V_{vent} = \frac{Q_w}{A_{vent}} = \frac{400}{8\ x\ 17.75} = 2.8\ ft/s \qquad (4\text{-}23)$$

Given these conditions, it is likely that flow will transport debris.

(iii) Transport Fractions

Based on these analyses, it was assumed that all debris reaching the drywell floor would be carried to the suppression pool. The only exception is for that fraction that enters the reactor cavity. The best scenario for that is if the debris and water mixture enters the sump at time 0 and never comes out thereafter.

For such a condition, the fraction entering the cavity can be estimated as

$$F_{cavity} = \frac{V_{cavity}}{V_{pool}} \qquad (4\text{-}24)$$

$$\approx 20\%$$

Thus, it is likely that about 80% of debris would be transported.

4.3 References

4-1 G. Zigler, et al., "Parametric Study of the Potential for BWR ECCS Strainer Blockage Due to LOCA Generated Debris," NUREG/CR-6224, U.S. Nuclear Regulatory Commission, October 1995.

4-2 K. Williams, "CFD Simulation of BWR Drywell Response to MSLB Event," Presentation to the PIRT Panel, 1996.

4-3 Paavergos and Hedley, "Particle Deposition Behavior from Turbulent Flows," Chem. Eng. Des., Vol. 62, September 1984.

4-4 K. W. Brinchman, "Results of Hydraulic Tests on ECCS Strainer Blockage and Material Transport in a BWR Suppression Pool," EC-059-1006, Rev. 0, May 1994.

4-5 F. J. Souto and D. V. Rao, "Experimental Investigation of Sedimentation of LOCA-Generated Fibrous Debris and Sludge in BWR Suppression Pools," NUREG/CR-62368, U. S. Nuclear Regulatory Commission, December 1995.

5. Drywell Floor Pool Debris Transport

This section documents a computational study of the potential for postulated LOCA generation fibrous insulation debris to be captured and retained by a pool of water forming on the floor of a BWR drywell following a pipe break accident.

5.1 Objective

Substantial quantities of insulation debris could be either deposited on the drywell floor during the period of primary system depressurization or could be washed down to the drywell floor from drywell structures where the debris was captured during depressurization. This debris could then be subsequently transported from the floor into the vent downcomers. Therefore, determining the potential for debris to remain captured on the floor was a necessary step in the overall debris transport study.

The primary objective of this calculation was to examine the potential for debris to settle in drywell pools and to estimate debris transport fractions (both central and upper bound estimates, see NUREG/CR-6369 for definitions of these estimates). The transport fraction was defined as the fraction of debris entering a drywell pool that would transport into the downcomer vents. The study considered Mark I, II, and III designs and it examined some variations in the pool depth and the entrance conditions to the pools.

5.2 Debris Transport Considerations

5.2.1 Drywell Pool Geometries

The three basic BWR designs each have uniquely different geometries. Each of these three basic designs then varies somewhat from plant to plant. Of course, thoroughly studying debris transport in all of the possible design configurations was beyond the scope and resources of the study. Nevertheless, an attempt was made to examine the debris transport in the full spectrum of BWR drywell floor geometries, at least to some extent. The drywell size and subsequently their diameters at the floor level vary substantially from plant to plant. The height from the drywell floor to the downcomer vent entrances (depth of pool once formed) generally ranges from about 0.5 to about 1.5 ft for Mark I and Mark II plants. The overflow heights for a Mark III are much higher, (e.g., order of 15 ft). Further, the downcomer vents for each of the three designs are completely different. The Mark I design has eight slanted downcomers while the Mark II has on the order of 98 vertical downcomers (the number and size also varies somewhat from plant to plant). The Mark III, instead of downcomers, has a weir wall that completely circumscribes the drywell. The basic features of these designs will be illustrated in the nodalization diagrams presented herein. The reader, not already familiar with these designs, can refer to numerous other documents such as plant Safety Analysis Reports, for further details.

5.2.2 Post-LOCA Thermal-Hydraulic Conditions

The floors of the BWR drywell are dry during the normal operation of the plant. Following a postulated LOCA pipe break water would accumulate on the floor until the level of this water reached the lower lip of the vent downcomers, or the weir wall in a Mark III, where the water would subsequently flow into the suppression pool. Sources of water accumulating on the floor include water from the pipe break, ECCS water overflow from the break, condensate, and the containment sprays.

During the very dynamic primary system depressurization, water on the drywell floor would be very turbulent, in fact, it would likely be skewed asymmetrically to the side of the drywell opposite the pipe break and the pool would most likely be a flashing two-phase pool. This pool condition, which was beyond the capability of the CFD code employed herein, was examined for a small Mark I plant using the MELCOR code (reported in an earlier section). The debris transport related conclusions drawn from the MELCOR analysis pertinent to this study were:

- Debris would be entrained and relatively well mixed by the highly turbulent pool.

- A pool forming on the drywell floor during this depressurization period would likely overflow during a postulated recirculation line (RL) break but not during a main steam line (MSL) break.

- For a RL break, the overflow would start as early as 5 second after pipe rupture, would cease when the depressurization became much less dynamic, at about 25 sec, and approximately one-half of the water accumulating on the floor would overflow into the vents. After 25 sec, the pool would level out across the floor so overflow ceases.
- It was likely that about 50% of the debris deposited onto the floor would almost immediately transport to the suppression pool following a RL break.

- Only a small amount of debris, less than 5%, would be trapped in the reactor cavity sump.

ECCS recirculation water flows from the break would completely fill the pool (also referred to as turnover time) in the range of 30 to 60 sec for Mark I and Mark II designs when operated at full rated capacity. For a Mark III, the fill time was more like 10 minutes. Flows conditions within these drywell floor pools maintained by full ECCS flows can be generally characterized as highly turbulent.

Following a MSL break, assuming that the operators throttle the ECCS flows so that only steam exits the broken pipes, the floor pool would form from condensate accumulation and containment sprays, if operated. If the sprays were not operated, it would take a substantial amount of time for the pool to fill to the overflow level. The condensation rate for the MELCOR calculation discussed above would take about 9 hours for the pool to overflow for that plant. This implied that any debris trapped on the drywell floor would remain trapped.

If the spray were operated, overflow would happen in about 2 to 3 minutes in the Mark I and Mark II plants. Note that this study assumed that Mark III plants do not have containment sprays. Pools formed by containment sprays were found to be much less turbulent, in general, than pools formed by full ECCS break flow.

5.2.3 Characteristics of Fibrous Insulation Debris

Several important characteristics of fibrous insulation debris must be considered when estimating whether or not debris would likely settle and remain in a drywell pool. These characteristics, which have been reported in other documents, are now summarized here.

The size and condition of the debris must be considered. The debris classifications herein included small and large pieces of insulation and erosion products. Erosion products were generally individual fibers or small groups of fibers.

Dry insulation debris was buoyant when initially introduced to a water pool due to air trapped between its fibers. A significant period of time was required for complete water saturation of the debris. Basically, in still water, dry debris floated, completely saturated debris settled, and partially saturated debris did something in between the dry and saturated conditions. Partially saturated debris, for example, can simply hover with neutral buoyancy.

The time required for debris to saturate was highly dependent upon water temperature and turbulence, as well as size. Intact insulation can float for days in 50 °F water but at temperatures characteristic of the drywell following a LOCA (120 to 140 °F), the debris would sink much more rapidly. One study [Ref. 5-1] documents that shreds, pieces measuring 4 inch square, and half-pillows sank in 20 to 30 sec. In a simple desk top experiment, a small piece of insulation dropped into a cup of hot water from a coffee dispenser took 45 sec to sink. In conclusion, insulation debris saturates in a relatively short period of time at drywell pool water temperatures; however, this period of time could be important should debris drop into an established pool near the vent entrances.

Debris settling velocities for small water-saturated debris in still water have been measured and documented [Ref. 5-2]. The settling velocity for small debris generally ranges from about 0.05 ft/sec to 0.15 ft/sec. Very small debris, such as erosion products would not settle, at least for the purposes of this study. Larger pieces of relatively intact insulation (3 in by 3 in by 1 in) can settle at velocities up to about 0.2 ft/sec but 0.2 ft/sec appeared to be

the upper limit for settling velocities. Even larger pieces (6 in by 6 in by 1 in) were found to settle slower at about 0.1 ft/sec due to a type of fluttering motion. Settling velocity was somewhat dependent on water temperature but a calculation indicated that the dependency was on the order of 10% or less.

The capability of debris to resuspend once it has settled onto the floor was also a consideration, however there was no available data on resuspension of insulation debris. Resuspension would depend upon such parameters as shape and orientation relative to the flow. Further, debris could simple roll along across the floor without becoming completely resuspended.

5.2.4 Source of Debris Entering Drywell Pool

When and how the debris would enter the drywell pool was an important consideration. Debris deposited during the depressurization of the primary system could saturate and settle to the floor prior to pool overflow, whereby this debris would be more likely to remain than debris that was washed down into an established pool. Washed down debris could float long enough to reach a vent entrance even if pool turbulence was low enough allow the debris to settle.

Debris washed down by pipe break ECCS water flows could consist of both small pieces of debris and erosion products from the erosion of large debris trapped on a grating. Further, this debris would enter the pool directly below the break where the pool turbulence would most certainly be higher.

Debris washed down by either containment sprays or steam condensate drainage could again consist of small pieces of debris and erosion products except that the expected quantity of erosion products would be substantially less due to the reduce capability of eroding insulation by spray flows. This debris would generally enter the pool more uniformly because the washdown process would go on throughout the entire containment.

5.2.5 Drywell Debris Transport/Capture Mechanisms

Debris transport through a drywell pool depends primarily upon it buoyancy and the turbulence level of the water. Debris may be suspended in the water, floating on the pool surface, or settled onto the floor where it can be pushed along the floor by the flow. Debris settling within the pool depends upon both the turbulence level and the particle transit time from its point of entry to the vent entrance.

Debris may be trapped within the pool by one of two mechanisms. First debris could become entangled on an underwater structure such as a piping support. Secondly, debris could settle in a relatively non-turbulent portion of the pool and remain there.

5.3 Methodology

A computer simulation that modeled all pertinent aspects of drywell pool debris transport was not possible, at least within the constraints of project resources. The methodology used herein was based on computational fluid dynamics (CFD) code simulations of various drywell pool configurations to determine characteristic flow patterns, velocities, and turbulence levels. Then relying upon engineering judgment to assess the likelihood of debris capture by the pool. The level of conservatism applied to the engineering judgments was based on the type of estimate under consideration, i.e., central or upper bound estimates.

The CFD code employed in this study was the CFD2000 code, Version 2.2, developed by Adaptive Research [5-3]. The CFD2000 code provided a complete integrated environment for the modeling and analysis of complex flow patterns.

5.3.1 Methodology Overview

The process of applying this methodology is illustrated graphically in Figure 5-1. The available knowledge based, shown at the top of the figure, included data from one applicable series of tests as well as theoretical CFD knowledge, plant data, and the characteristics of fibrous insulation debris. The experimental data came from a series of tests performed by ARL of PPL [Ref. 5-4] to determine the transport and entrainment characteristics of different kinds of insulation materials in a small laboratory flume. Considerable knowledge

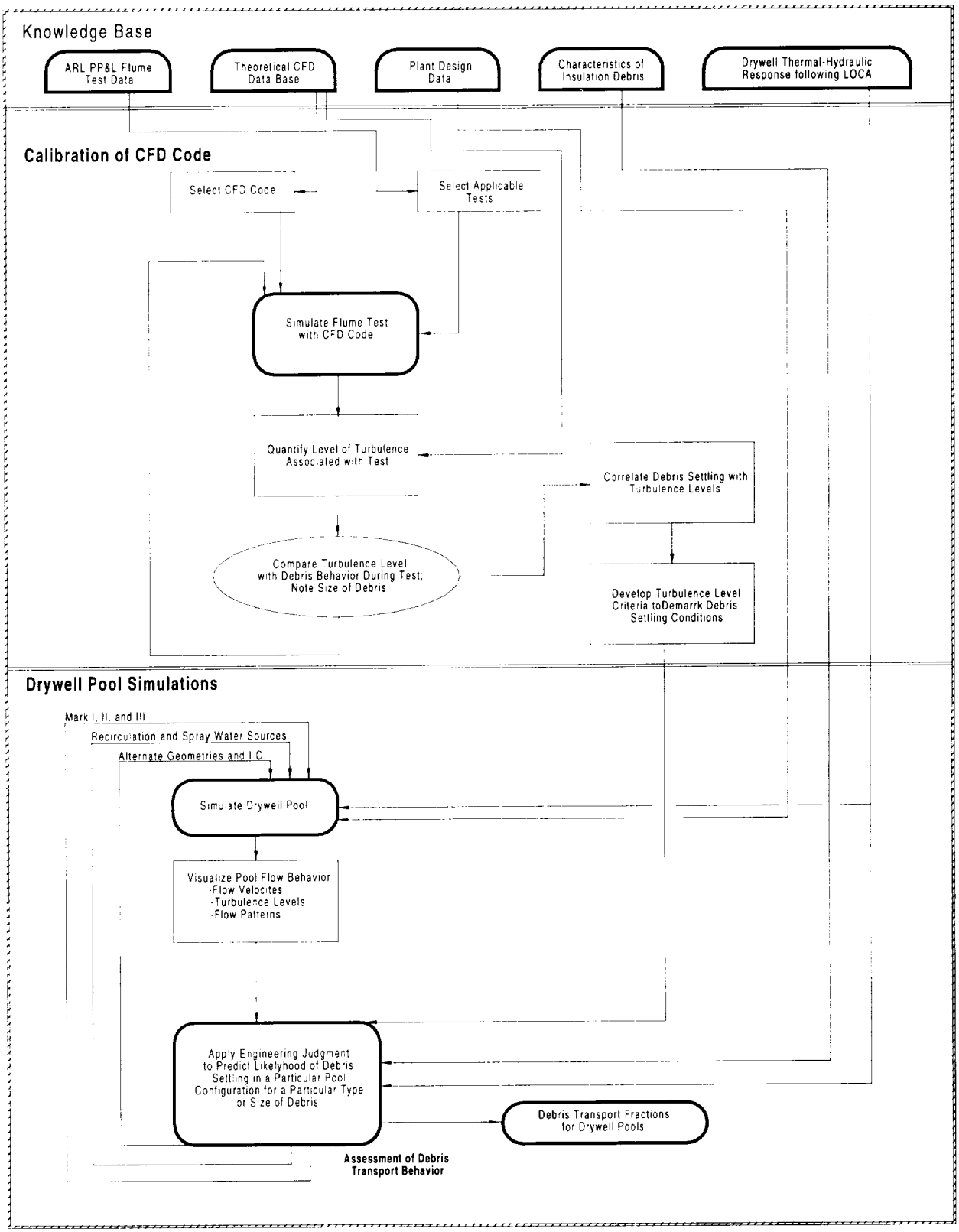

Figure 5-1: Drywell Floor Pool Debris Transport Methodology

exists regarding the quantification of turbulence levels in water pools using CFD tools. Existing safety analysis reports document the plant designs and thermal-hydraulic conditions in a BWR drywell following a LOCA.

Anchoring the analytical results to prototypical experimental data was needed to correlate pool turbulence levels with conditions that allowed debris to settle. This was accomplished by simulating the ARL PPL flume tests with the CFD code and then correlating the code predicted turbulence level for a given test with the test results showing whether or not debris actually settled in that test. Maximum levels of turbulence whereby debris could settle were determined an applied to the drywell floor pool simulation results. Two maximum levels were determined; one for small debris and one for large debris. This step is shown in the figure as the calibration of the CFD code.

The results of each of the drywell floor pool simulations consisted of graphical pictures showing pool flow behavior such as two and three-dimensional pictures of flow velocities and flow turbulence in the form of specific kinetic energy. These turbulence levels were then compared to the maximum levels for debris settling determined by the code calibration. If the pool turbulence was higher than a maximum level, then debris would not likely to settle.

With all of this information at hand, a team of project engineers discussed the likelihood for debris settling for each pool configuration. The team then arrived at estimates for the debris transport fractions. These debris transport fractions were implemented into the overall debris transport study.

5.3.2 Turbulence Level Quantification

Pool turbulence levels were related to the specific kinetic energies of the water, i.e., the kinetic energy per unit volume (units of ft^2/sec^2). Relating debris transportability to specific kinetic energy is a widely used method of correlating particle suspension with pool turbulence. The CFD code automatically calculated non-isotropic three-dimensional specific kinetic energies from the root mean square of the turbulent velocities, U_{rms}, using the following equations:

$$KE_{turb} = \frac{1}{2} \cdot U_{rms}^2 \qquad (5\text{-}1)$$

$$U_{rms} = \sqrt{\frac{\left(u_x^2 + u_y^2 + u_z^2\right)}{3}} \qquad (5\text{-}2)$$

5.3.3 Calibration of CFD Code

The CFD code was calibrated by simulating the ARL PP&L flume tests. In other words, the maximum turbulence levels, as predicted by the code, that would allow fibrous insulation debris to settle were determined by comparing the code predicted turbulence levels in the flume test simulations to experimentally determined debris settling results. The simulations of the ARL PP&L flume tests are reported in Appendix C of this report. The following is a brief summary of the results of those simulations.

Several of the ARL PP&L flume tests, that tested the transportability of fibrous insulation debris, were judged applicable to drywell pool transport study, i.e., test conditions were prototypical of a BWR drywell floor. The flume used in these tests was 22 inches wide, 16 inches, deep, and 18 ft long. A weir wall, one foot high, was installed at the end of the flume to simulate flow over the top of the downcomer vent pipes. Flow velocities for debris transport ranged up to 1 ft/sec. Flow turbulence levels were controlled using flow straighteners on the main inlet flow and small downcomer pipes that injected turbulent flow at specified positions and flow rates. The judging of the prototypicality of these tests was based on the pool depth, the flow velocities and turbulence levels studied, and the type and size debris studied. These parameters were very much in the range of expected parameters for the drywell floor pool in Mark I and Mark II plants. The results of the CFD simulations of the flume tests are summarized in Table 5-1.

Table 5-1: Results of the CFD Simulations of the ARL PP&L Flume Tests

Test No.	Flume Transport Flow Velocity (ft/sec)	Turbulence Introduced by Downcomer Pipes	Weir Wall Used	Debris Transport Results		CFD Code Predicted Turbulence Level (ft^2/sec^2)
				Small Pieces	Large Pieces	
1	0.27	No	No	Settled	Settled	K.E. < 0.0012
2	0.56	No	No	Settled	Settled	K.E. < 0.0012
3	1.00	No	No	Transported	Settled	0.0012 < K.E. > 0.014
4	0.27	Yes	No	Transported	Settled	0.0012 < K.E. > 0.014
5	0.56	Yes	No	Transported	Transported	K.E. > 0.014
6	0.27	No	Yes	Settled	Settled	K.E. < 0.0012
7	0.56	No	Yes	Transported	Settled	0.0012 < K.E. > 0.014

The conclusions drawn from the flume test simulations regarding debris transport in a drywell pool were:

- If the CFD code predicted value for specific kinetic energy was greater than about 0.01 ft^2/sec^2, then both large and small debris would remain suspended and well mixed in the drywell floor pool
- If the predicted value was less than about 0.001 ft^2/sec^2, then all debris would settle to the drywell floor with settling velocities akin to the settling velocities measured for insulation debris settling in still water.
- If the predicted value was between 0.001 and 0.01 ft^2/sec^2, then the small debris would settle but the large debris would remain suspended.

These conclusions are summarized in Table 5-2.

Table 5-2. Debris Behavior Based on Turbulence Levels

Specific Kinetic Energy (ft2/sec2)	Behavior of Small Debris	Behavior of Large Debris
K.E. < 0.001	Settles	Settles
0.001 < K.E. > 0.01	Suspended	Settles
K.E. > 0.01	Suspended	Suspended

5.3.4 Common CFD Modeling Assumptions

Several assumptions were used throughout these calculations to simulate the various drywell floor pool configurations. The motivations for these assumptions were the limitations of the CFD code and project resources. All of the drywell floor simulations were solved using the cylindrical coordinate system and assumed steady state turbulent flow conditions.

5.3.4.1 Boundary Conditions

In reality, any pool formed on the drywell floor would have a freestanding surface defined by hydrodynamic forces. The depth of the pool could vary with location relative to the flow inlets and outlets and the pressure at the water surface would essentially be the drywell atmospheric pressure. The CFD code employed in these simulations, however, did not have the capability of modeling a freestanding surface, i.e., a boundary with water on one side and a gas on the other. The pool surface was therefore modeled using a solid wall surface without surface friction. The primary disadvantage of this modeling assumption was of course that the depth of the pool was fixed at constant user specified value.

Pool boundaries defining by the inner and outer walls and the drywell floor were simulated using wall friction. The wall friction provided drag on the water flows thereby creating a flow boundary layer next to the wall.

Flow obstructions, such as piping supports, were not modeled although these supports would tend to introduce turbulence into the flow. A review of a series of photos showing the drywell floor and surrounding equipment of a Mark I plant indicated that drywell equipment was supported up off of the floor by relatively narrow support structures. The potential effect that obstructions would make on flow turbulence was considered in the engineering judgment portion of the study.

5.3.4.2 Fluid Properties

Since the simulations were performed without heat being transferred or phase change, the only fluid properties affecting the results were the density and viscosity of water at an appropriate temperature. Fluid properties for saturated water at 100 °C were obtained from the CFD code properties library.

5.3.4.3 Symmetry

The flow simulations were simplified where possible using the symmetry of the flows along the floor. This simplification of the input model assumed that the flow patterns in one portion of the floor were either identical or mirror images of another section of the floor. The exact geometries will be discussed as each calculation is presented.

5.3.5 Modeling of Inlet Flows

Water flows introduced into the drywell floor pool simulations were defined by:

- the volume rate of flow
- the specific kinetic energy of the flow
- the entrance area into the pool.

The rate of flow, of course, was determined by the ECCS design of the plant simulated. Note that each plant generally has different design flow rates.

Flows from the broken pipes would be dispersed upon falling from the break to the floor. How much the flows would be dispersed would depend upon a number of variables including the distance the water must fall to reach the floor and the quantity, location, and orientation of structures below the break. Thus, a spectrum of dispersions may be possible ranging from a relatively tightly focused flow falling directly to the floor to a completely broken up flow spread out over a large area. The level of turbulence associated with the flow entering the pool would also vary with the dispersion of the flow.

For simulations of ECCS recirculation flows from the broken pipe, the flow inlet to the pool was modeled two ways in an attempt to bracket the impact of the inlet flow on the turbulence in the pool. In the first method, the flow was introduced into a relatively small area at a relatively high level of turbulence. In the second method, the flow was assumed dispersed over one-quarter of the total drywell floor and the flow entered the pool with a relatively low level of turbulence. These methods are illustrated in Table 5-3.

Table 5-3. Method of Introducing ECCS Recirculation Flows into Pool

Modeling Method	Entrance Area	Inlet Turbulence
Focused	Small	High
Dispersed	¼ of Drywell Floor	Low

The CFD code required two input numbers to specify the inlet level of turbulence. These were the incoming turbulence kinetic energy, KE_{inlet}, and the incoming turbulence dissipation rate, ϵ_{inlet}. A code option that allowed these two numbers to be calculated by the code was used, whereby the user simply specified the turbulence as a percentage of the incoming flow that was turbulent. KE_{inlet} then was this percentage (divided by 100) times the square of the inlet face normal velocity. The code calculated ϵ_{inlet} from the following equation.

$$\varepsilon_{inlet} = C_{\mu}^{\frac{3}{4}} \cdot \rho \cdot \frac{KE_{inlet}^{2}}{\mu_{t}} \qquad (5\text{-}3)$$

Where

$C\mu$ = a turbulence model constant (0.09 assumed)

ρ = the density of the incoming flow

μ_t = the turbulent viscosity estimated at 100 times the incoming laminar viscosity.

Flow was introduced as a mass flux by specifying constant uniform velocity over the entrance area and specifying the water density from the code's properties library. Containment spray flows were assumed uniformly dispersed throughout the drywell and were modeled as entering the floor pool at a uniform inlet velocity.

5.3.6 Drywell Pool Configurations Simulated

The drywell floor pools simulated in this study are shown in Table 5-4. Pools formed and maintained by flows from broken pipes were simulated for all three basic BWR designs using both inlet methods shown in Table 5-3. A high level of turbulence was specified as 100% of the incoming flow being turbulent (see discussion above) and a low level of turbulence was specified as 2%.

Pools formed by the operation of containment sprays were simulated for the Mark I and Mark II designs. The base Mark I pool depth was 17 inch and the base Mark II depth was 6 inches. Alternate calculations were then performed at the alternate depths to determine if the conclusions drawn from the base calculations would be altered if the depths were difference. Again note that these depths differ from plant to plant.

Table 5-4: Drywell Pool Configurations Simulated

Plant Design	Water Source	Pool Depth	Entrance Area	Inlet Turbulence	Inlet Flow
Mark I	Break Overflow	17 inches	Focused	100%	25000 GPM
			Dispersed	2%	
	Containment Sprays	17 inches	Uniform	2%	4800 GPM
		6 inches			
Mark II	Break Overflow	6 inches	Focused	100%	28600 GPM
			Dispersed	2%	
	Containment Sprays	6 inches	Uniform	2%	7400 GPM
		17 inches			
Mark III	Break Overflow	15.5 ft	Focused	100%	27410 GPM
			Dispersed	2%	

The remainder of this report documents the results of these simulations consisting primarily of two and three-dimensional color graphics. The content of these graphics is discussed leaving it to the reader to visualize the flow patterns.

5.4 Mark I Simulations

5.4.1 Full Recirculation Flow from Break

The drywell floor pool sustained by a recirculation water flow from a broken pipe of 25000 GPM was simulated. This flow would cascade down to the drywell floor and accumulate until the water level reached the bottom of the vent downcomers where it then would overflow into the suppression pool.

5.4.1.1 Geometrical Layout and Initial Conditions

Since the recirculation water flows from the LOCA break would cascade down from the pipe break on one side of the drywell, the water flows across the drywell floor would be symmetrical around the reactor pedestal from that location. Therefore, the flow simulation was preformed on only one-half of the drywell floor to allow a more detailed nodalization of that half of the floor than would have been realistically possible simulating the full floor.

The geometrical layout is illustrated in the nodalization diagram shown in Figure 5-2. Only one-half of the drywell floor bounded by the pedestal wall, the drywell liner wall, the floor, and the pool free surface was modeled. The pool depth of 2 ft was modeled using a total of 9 vertical calculational cells. The radial distance between the pedestal wall and the drywell liner was modeled using 20 cells. The azimuthal direction (180°) was modeled with 80 cells. The inner and outer radii as modeled were 11.69 ft and 22.92 ft, respectively.

The flow was introduced into the calculation as a uniform constant velocity source over the pool surface area highlighted by blue in the nodalization diagram. The selection of this area was somewhat arbitrary but the selection was designed to focus the inlet flow over a relatively small portion of the floor area (19.1 ft^2, as it turned out) below the break. The uniform constant velocity associated with 25000 GPM of flow through this area was 1.46 ft/sec and its turbulence level was specified at 100%.

Four downcomer vent entrances were simulated using a pressure driven outlet boundary condition. Note that the BWR Mark I design has a total of 8 downcomer vents but due to symmetry only 4 entrances were simulated. The outlet boundaries were simulated as rectangular surfaces although the actual vent entrances are circular. The pool depth below the vent entrances was 1.4 ft.

The actual depth of water over the lip of these vent entrances would vary inversely with the flow velocity at the entrances. A calculation indicated that a depth of about 6 inches corresponding to an entrance velocity of about 6 ft/sec was reasonably depth for this simulation. At shallower depths, the velocities increased rapidly and at larger depths the velocities approached the drywell pool free stream velocities. The flow area corresponding to a depth of 6 inches was 1.1 ft^2 per vent entrance.

The pressure within the simulated drywell pool was controlled by the specification of the loss coefficient associated with the outlet boundaries. Each of the four outlet boundaries was treated identically and the resulting mass flow rates were nearly the same. Because the water flows were incompressible and at a constant temperature, the absolute value of the pressure was not important to these calculations, as long as the pressure drop across the outlets was substantially greater than the magnitude of the pressure drops within the drywell pool. The external pressure was specified as zero. The absolute pool pressures were typically about 10 psia and the internal pressure drops less than about 3 psi.

5.4.1.2 Base Case Results

The flow patterns, flow velocities, and kinetic energy levels are illustrated in following set of figures, i.e., Figures 5-3 through 5-7.

Figure 5-3. This figure shows the flow velocity in three dimensions in the form of velocity contours, i.e., lines of constant velocity. The figure consists of several layers of contours at discreet elevations within the pool. The color indicated the magnitude of the velocity at that particular location and the color scales are indicated in two ways at the left side of the figure. The velocities peaked at a little over 1.5 ft/sec. The flow inlet is seen near the top and the four flow outlets around the rim. As the downward moving inlet flow encountered the floor, it was

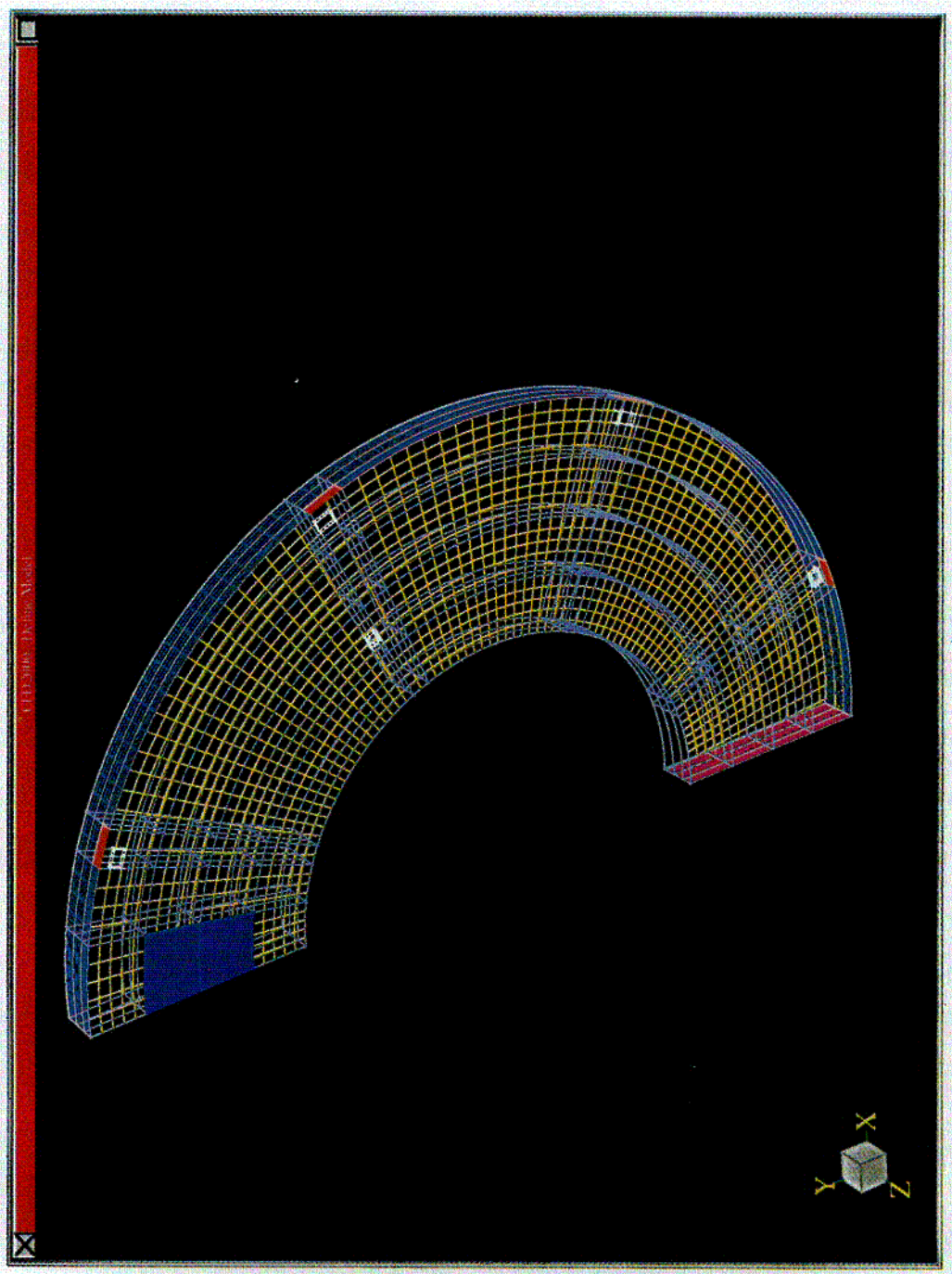

Figure 5-2: Nodalization Diagram for Full Recirculation Flow From Broken Pipe in Mark I

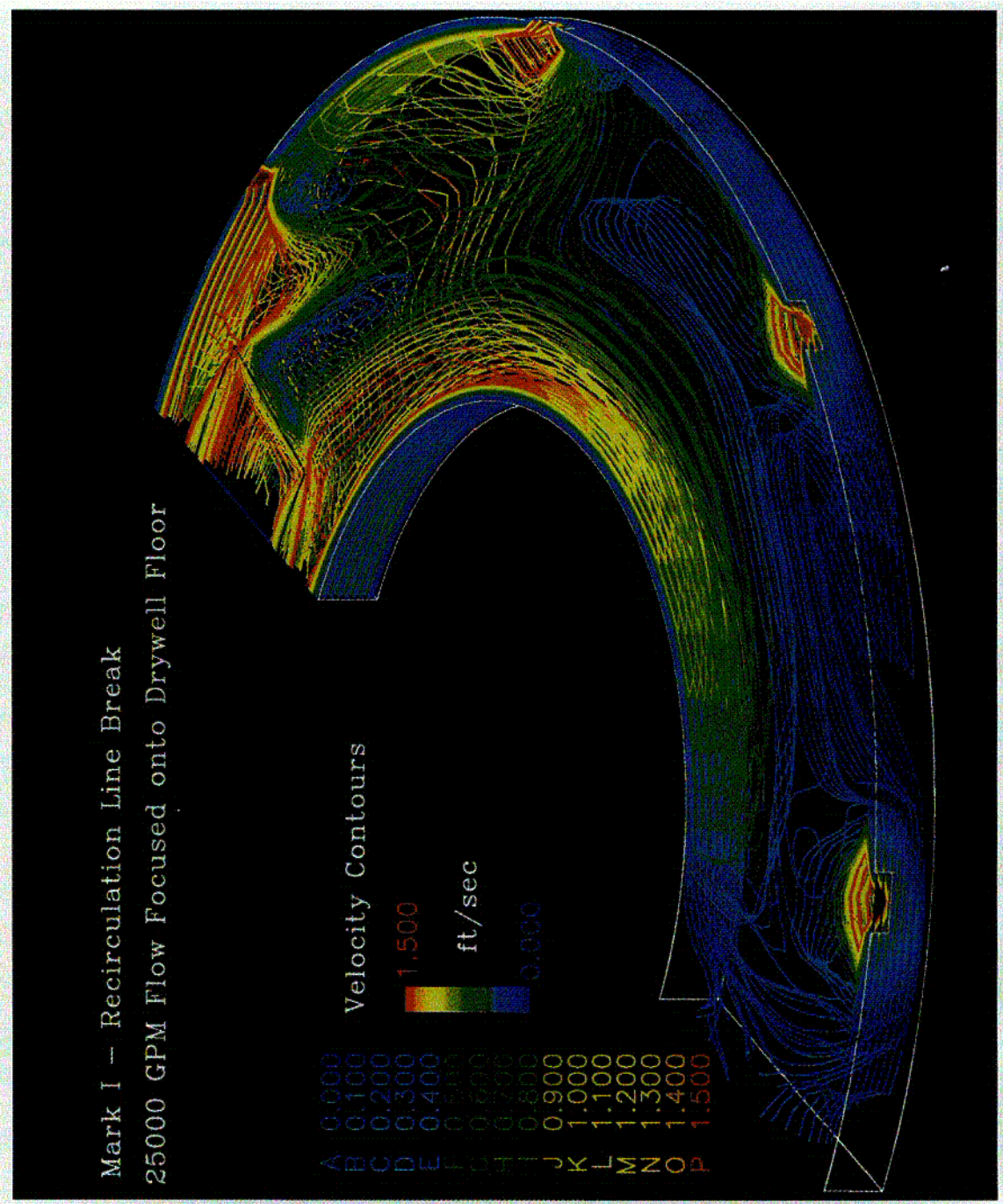

Figure 5-3: Flow Velocities for Full Recirculation Flow from Broken Pipe in Mark I

C.2

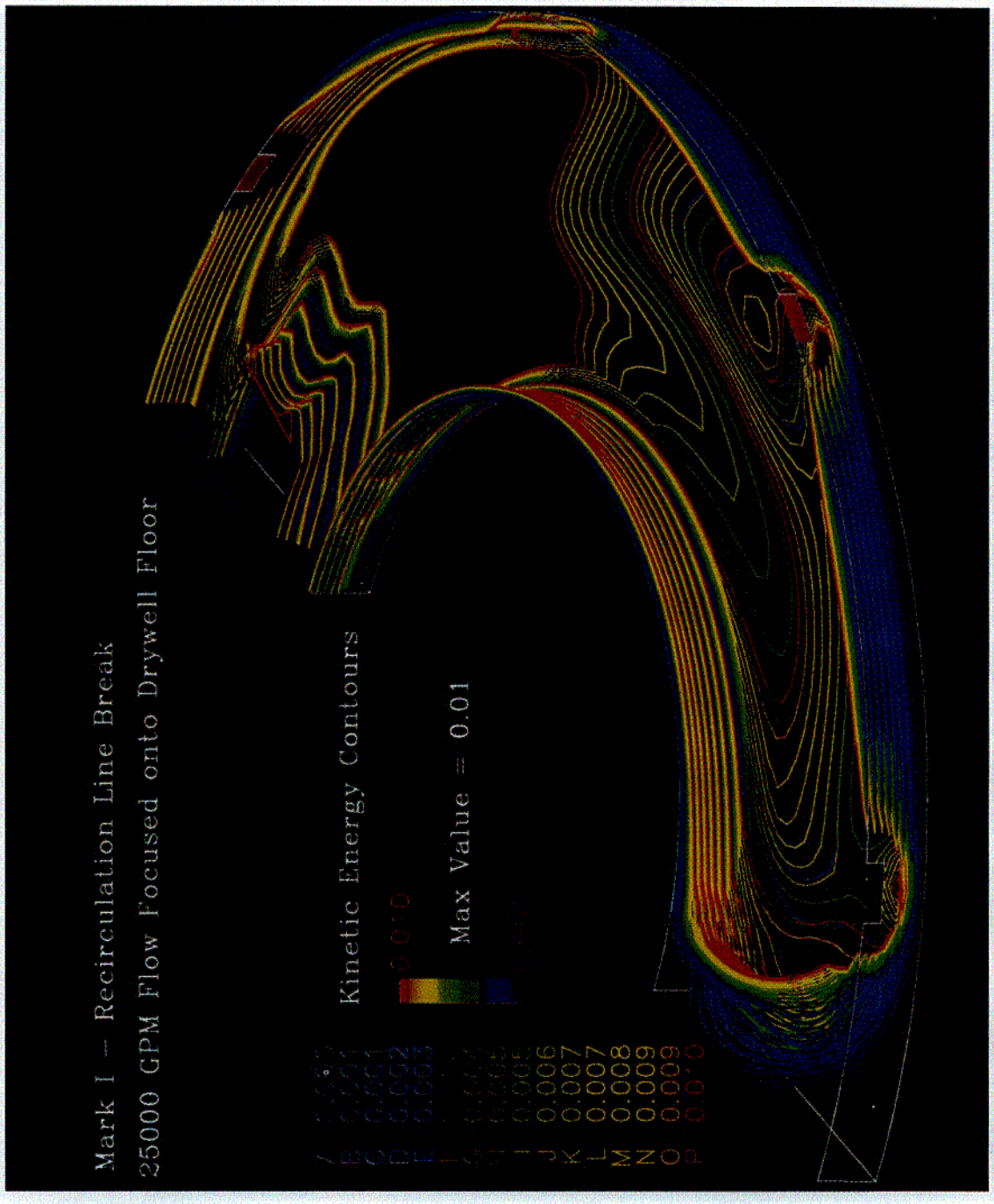

Figure 5-4: Specific Kinetic Energies for Full Recirculation Flow from Broken Pipe in Mark I

C-3

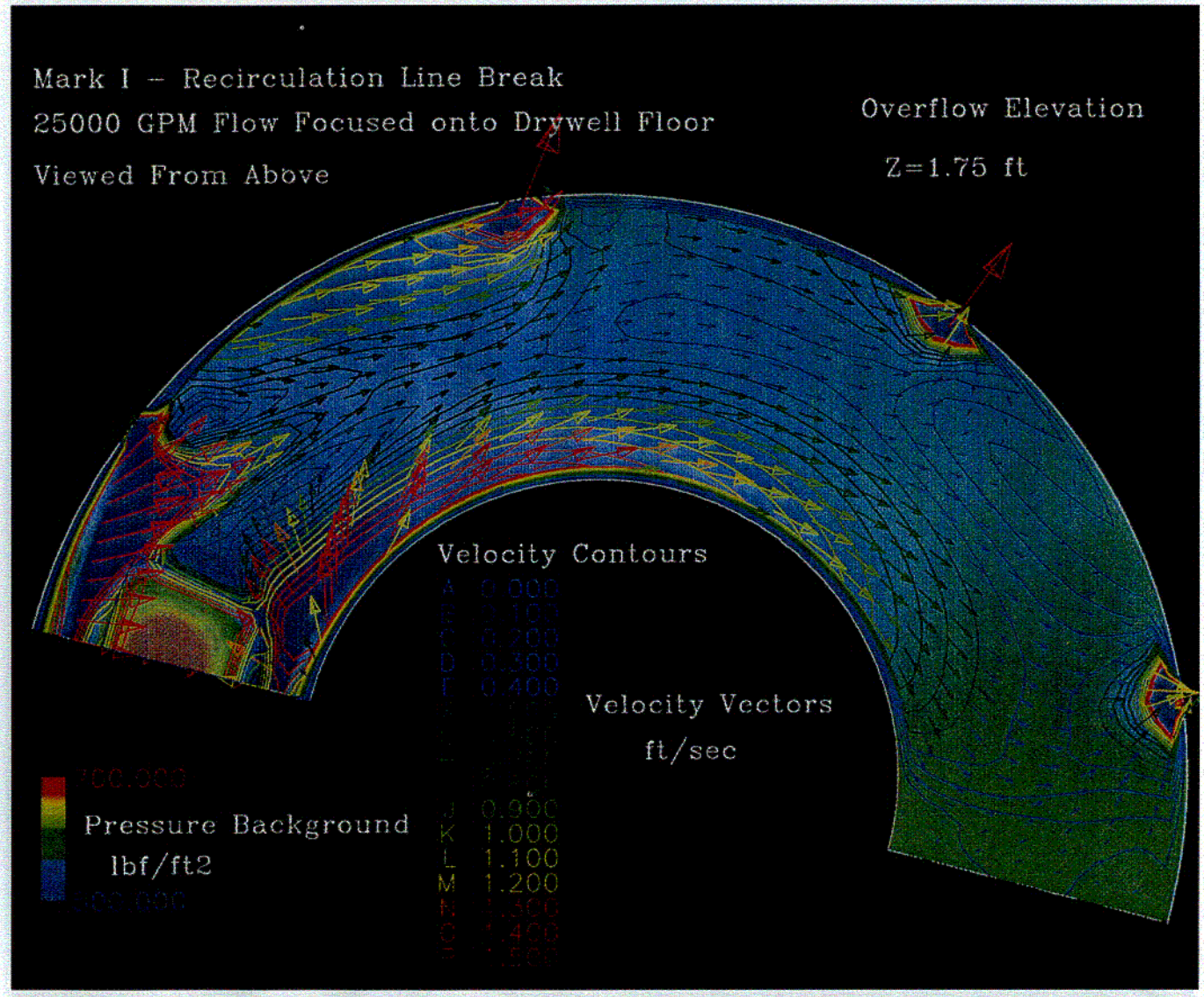

Figure 5-5: Flow Velocities at Overflow Level for Full Recirculation Flow from Broken Pipe in Mark I

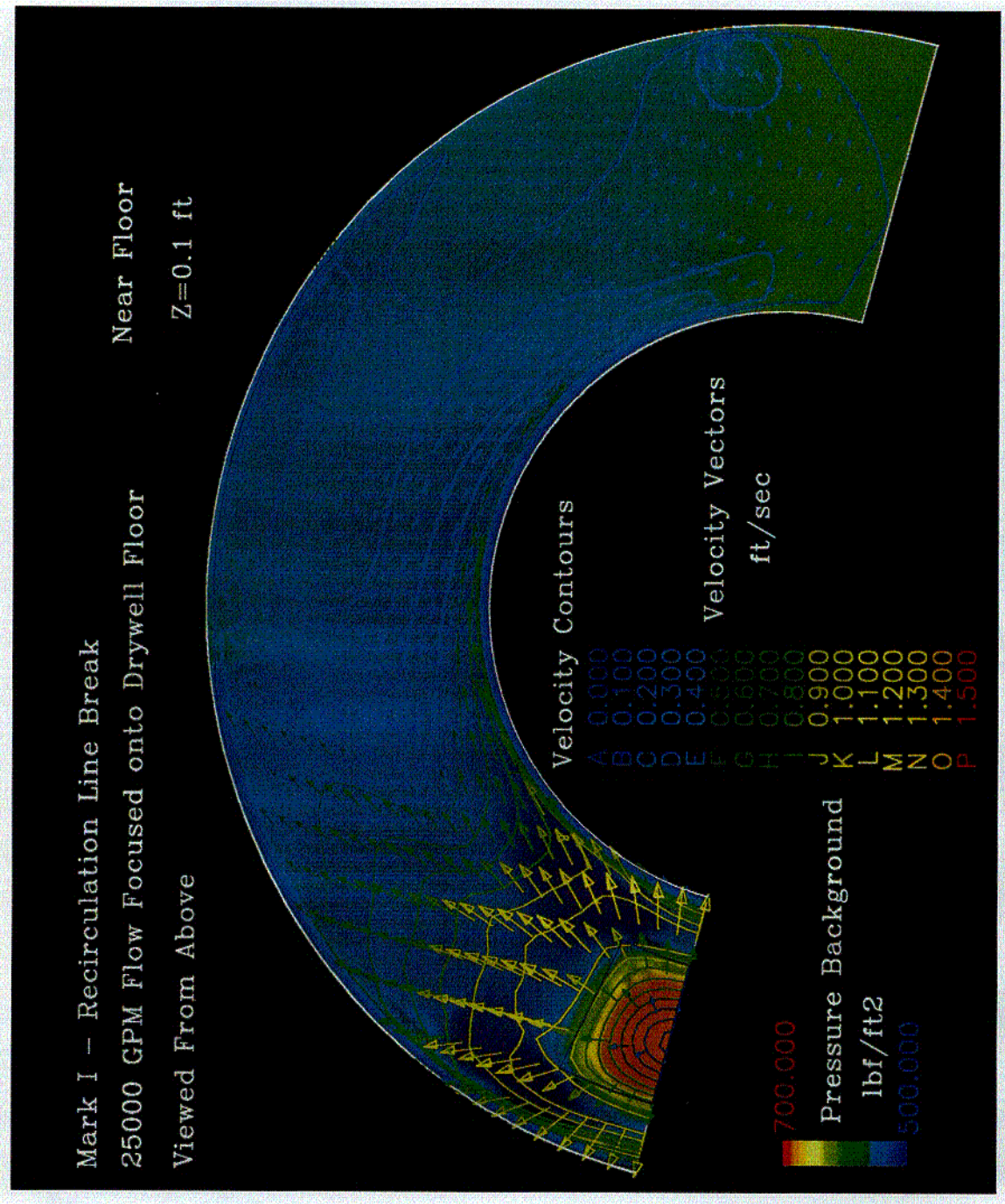

Figure 5-6: Flow Velocities Near Floor for Full Recirculation Flow from Broken Pipe in Mark I

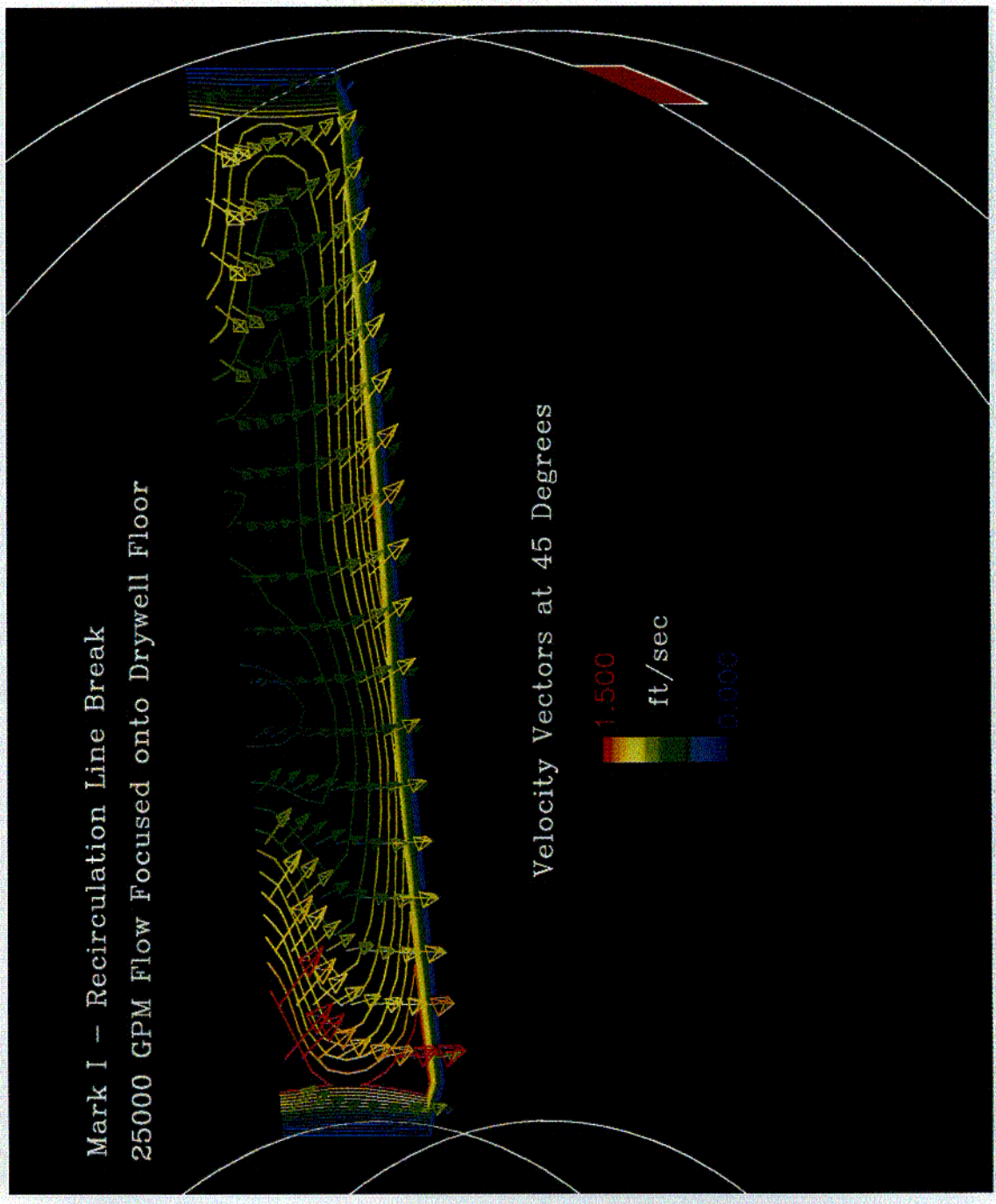

Figure 5-7: Flow Velocities in Vertical Cross-Section for Full Recirculation Flow from Broken Pipe in Mark I

generally deflected along the bottom of the floor. Higher velocities were indicated around the inlet region, across the pedestal wall, and near the outlets. Slower velocities were found at side opposite the break and near the floor.

Figure 5-4. The specific kinetic energies are shown in a similar manner in Figure 3-4. Here the maximum value plotted was fixed at 0.01 ft^2/sec^2. As shown, nearly the entire pool was predicted to have a kinetic energy greater than this value which corresponded to the maximum value that would allow even the large debris could settle. The lower kinetic energies at the far end of the pool are likely an artifact of the symmetry assumption.

Figure 5-5. Flow velocities and pool pressures are shown for one specific elevation of the pool. The elevation of 1.75 ft was 0.35 ft above the lower lip of the vent entrances and 0.25 ft below the top of the pool. Here the flow velocities are shown both as contours and as directional vectors. The color background shows the pressure throughout the pool at this elevation. Again, the color scales indicate their magnitude.

Figure 5-6. Flow velocities and pressures near the floor are shown. Here a boundary layer effect causes the flows to slow near the floor over a substantial portion of the floor.

Figure 5-7. This figure shows the flow velocity contours and vectors in a vertical cross-section located 45° from the break end of the pool. Wall boundary effects are illustrated.

5.4.1.3 Alternate Conditions

One alternate case was performed for the Mark I recirculation line pool. This alternate case assumed that the inlet flow was widely dispersed so that it entered over a full quarter of the drywell floor at relatively low levels of turbulence. The flow rate was still 25,000 GPM but the uniform flow inlet velocity was now only 0.18 ft/sec and the turbulence was 2%. The specific kinetic energies for the case are shown in Figure 5-8. Even at this much milder inlet condition, the turbulence level in the bulk of the pool was higher than at 0.01 ft^2/sec^2.

5.4.1.4 Conclusions Regarding Debris Transport

The predicted turbulence levels in a pool formed and maintained by a 25,000 GPM flow from the broken pipe in this Mark I design were likely much too high to allow substantial debris to settle, especially small pieces of debris. Some small credit might be taken for retaining large debris deposited during blowdown at the far end away from the break in a central estimate but not as an upper bound. Large pieces of debris deposited during blowdown could have sufficient time to saturate and settle onto the floor prior to vent overflow. Large pieces of saturated debris located in the floor boundary layer away from the break turbulence and laying flat against the floor could well remain there but the uncertainty associated with this conclusion prevented crediting retention in upper bound estimates.

5.4.2 Containment Spray Flow

A pool formed by the operation of the containment sprays was simulated for the same Mark I plant geometry as the preceding calculation. A total spray flow of 4800 GPM was assumed to fall uniformly to the floor where it would accumulate until the water level reached the entrances to the downcomer vents where it then would overflow into the suppression pool.

5.4.2.1 Geometrical Layout and Initial Conditions

Each of the eight downcomer vents and their associated floor area would behave identically under the uniform flow entrance condition assumed for this simulation. Therefore, only a one-eight section of the floor pool with one vent downcomer was modeled as shown in Figure 5-9. There were 9 vertical calculational cells, 20 radial cells, and 21 azimuthal cells.

The size of the vent outlet flow was sized to provide a somewhat arbitrary exit velocity of about 3 ft/sec resulting in an area of 0.22 ft^2 with a height of about 0.3 ft. Therefore, the total height of the pool was 1.7 ft (1.4 ft to the entrance lip plus 0.3 ft for the exit).

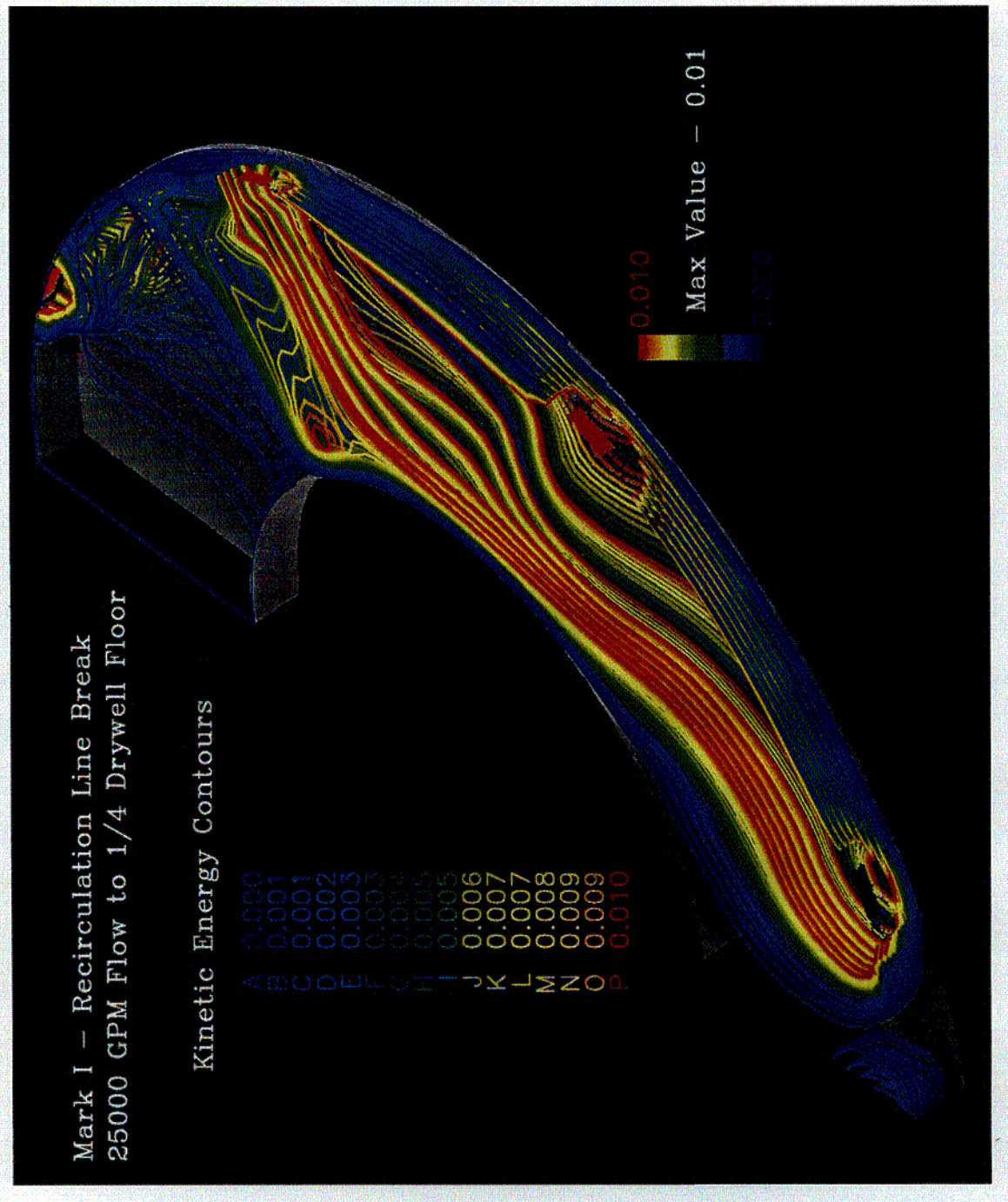

Figure 5-8: Specific Kinetic Energies for Full Recirculation Flow from Broken Pipe in Mark I (Dispersed)

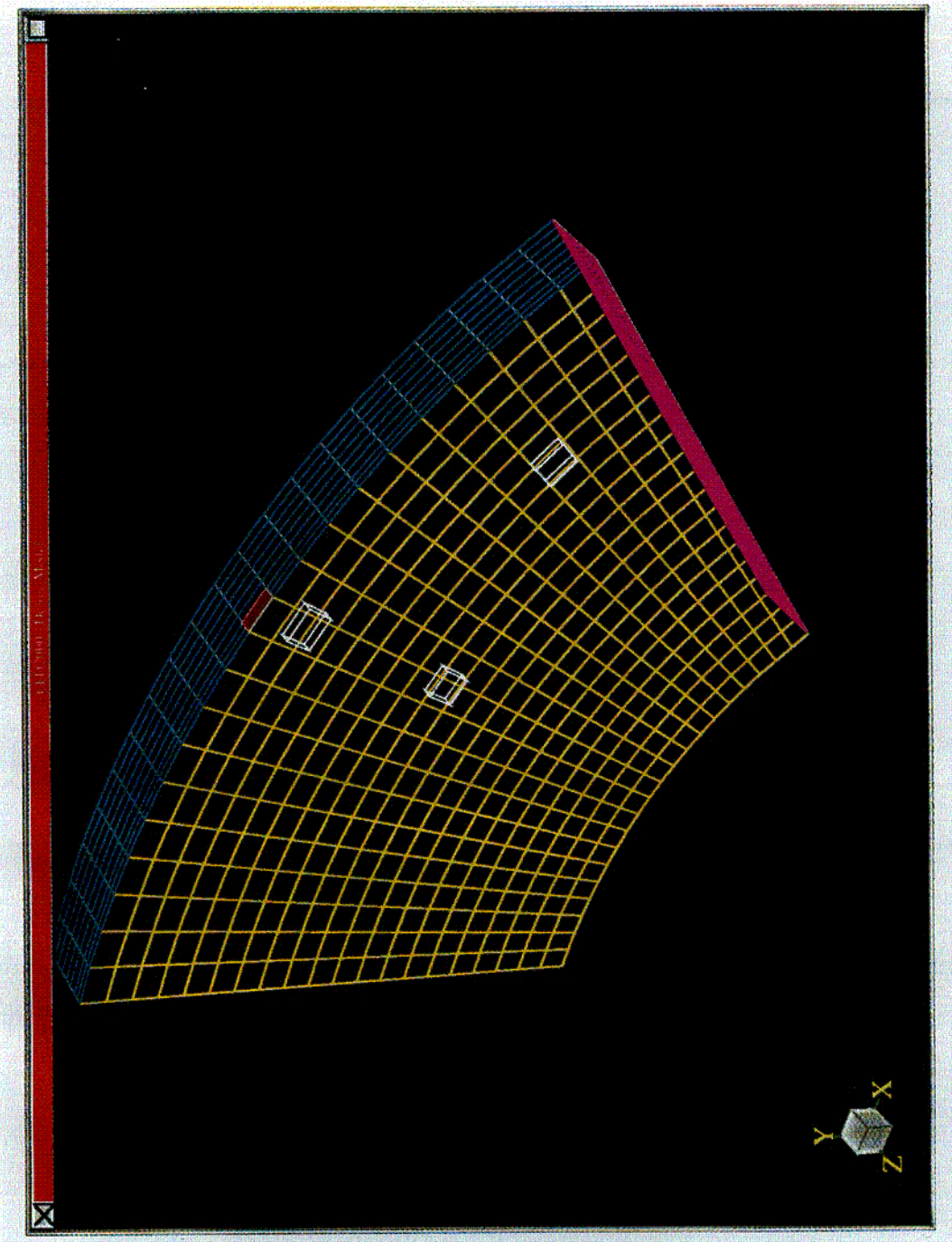

Figure 5-9: Nodalization Diagram for Containment Spray Pool in Mark I

The flow was introduced into the calculation at a constant velocity of 0.0087 ft/sec over the entire upper boundary.

5.4.2.2 Base Case Results

The flow patterns, flow velocities, and kinetic energy levels are illustrated in Figures 5-10 through 5-13. These figures are similar to those of the preceding calculation.

Figure 5-10. This figure shows velocity contours in three dimensions. As expected, the peak velocities occurred near the vent entrances. The highest velocity contour plotted was 0.1 ft/sec. Recall, insulation debris settles in still water at velocities ranging from about 0.05 to 0.2 ft/sec. Most the pool flowed at a velocity considerable slower than the flow near the exit.

Figure 5-11. The specific kinetic energies shown in this figure indicated a very low level of turbulence. The maximum value plotted was 0.00001 ft^2/sec^2. This level of turbulence was two orders of magnitude lower than the level that would allow small pieces of debris to settle.

Figure 5-12. This figure illustrates the direction of flows and magnitude of velocities at an elevation near the top of the pool.

Figure 5-13. The vertical behavior of the flow near the vent can be seem in this figure showing both velocity contours and velocity vectors for a vertical cross-section passing through the vent exit.

5.4.2.3 Alternate Conditions

Because the downcomer vent entrances in some Mark I plants are closer to the floor than the Mark I plant simulated herein, one alternate calculation was run to simulate a shallower pool to determine the effect of pool depth on debris transport. This alternate case assumed that the pool depth in this plant was only 6 inch rather than the actual 17 inches and the resulting kinetic energies are shown in Figure 5-14. As seen, the specific kinetic energies were still quite low, much lower than the levels needed to keep small pieces of from settling. These results do not indicate a strong dependency of pool turbulence and debris transport on pool depth for a Mark I.

5.4.2.4 Conclusions Regarding Debris Transport

The very low predicted turbulence levels and flow velocities of this simulation strongly indicated that debris would likely settle to floor of the pool and remain there. Debris washed down into the pool by the sprays after the pool reached overflow levels could be transported into the vents if the debris falls closed to the exit. Therefore, some transport of small washed down debris was considered in the upper bound estimate.

5.5 Mark II Simulations

5.5.1 Full Recirculation Flow from Break

The drywell floor pool sustained by a recirculation water flow from a broken pipe of 28,600 GPM was simulated. This flow would cascade down to the drywell floor and accumulate until the water level reached the tops of the vent downcomers pipes where it then would overflow into the suppression pool.

5.5.1.1 Geometrical Layout and Initial Conditions

As in the Mark I calculation, only one half of the drywell floor was simulated because the recirculation water flows from the LOCA break would cascade down from the pipe break on one side of the drywell. The Mark II geometrical layout is illustrated in the nodalization diagram shown in Figure 5-15. There were 10 vertical calculational cells, 23 radial cells, and 80 azimuthal cells.

The number of vertical downcomer vent pipes in Mark II plants, their arrangement, and their height above the floor vary from plant to plant. The sheer number of downcomer pipes in a Mark II made their simulation with a CFD code difficult. To provide the necessary symmetry to model the associated complexity, this simulation assumed that there were a total of 98 downcomers arranged uniformly in three concentric circles. In Figure 5-15, 48 of these downcomers are shown as ring segments that were approximately rectangular in shape. The shapes of the rectangles varied from ring-to ring, as shown in the figure, but their cross-sectional areas remained constant for all downcomers. The inner diameter of the downcomer modeled was nominally 2 ft and

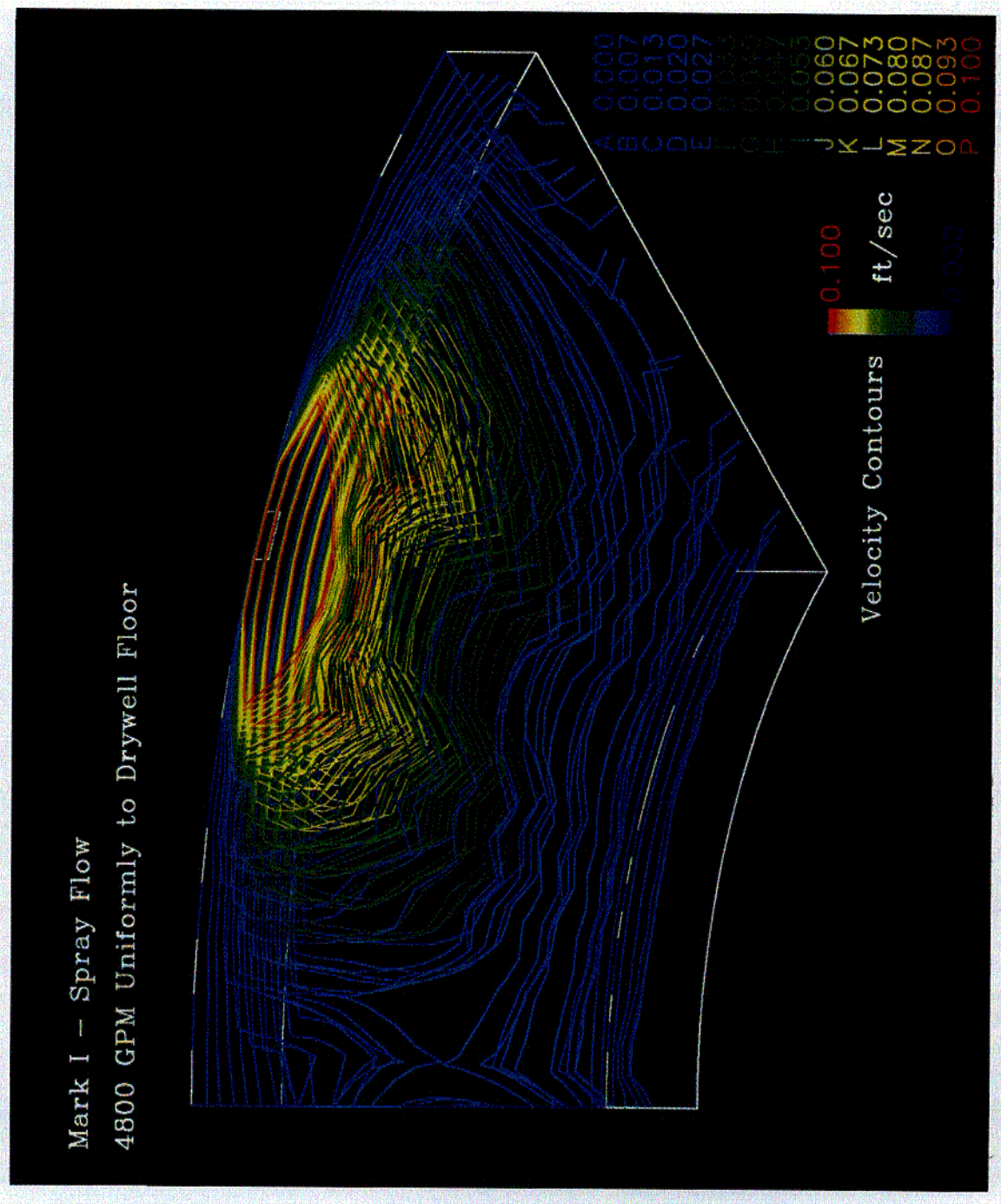

Figure 5-10: Flow Velocities for Containment Spray Pool in Mark I

C-9

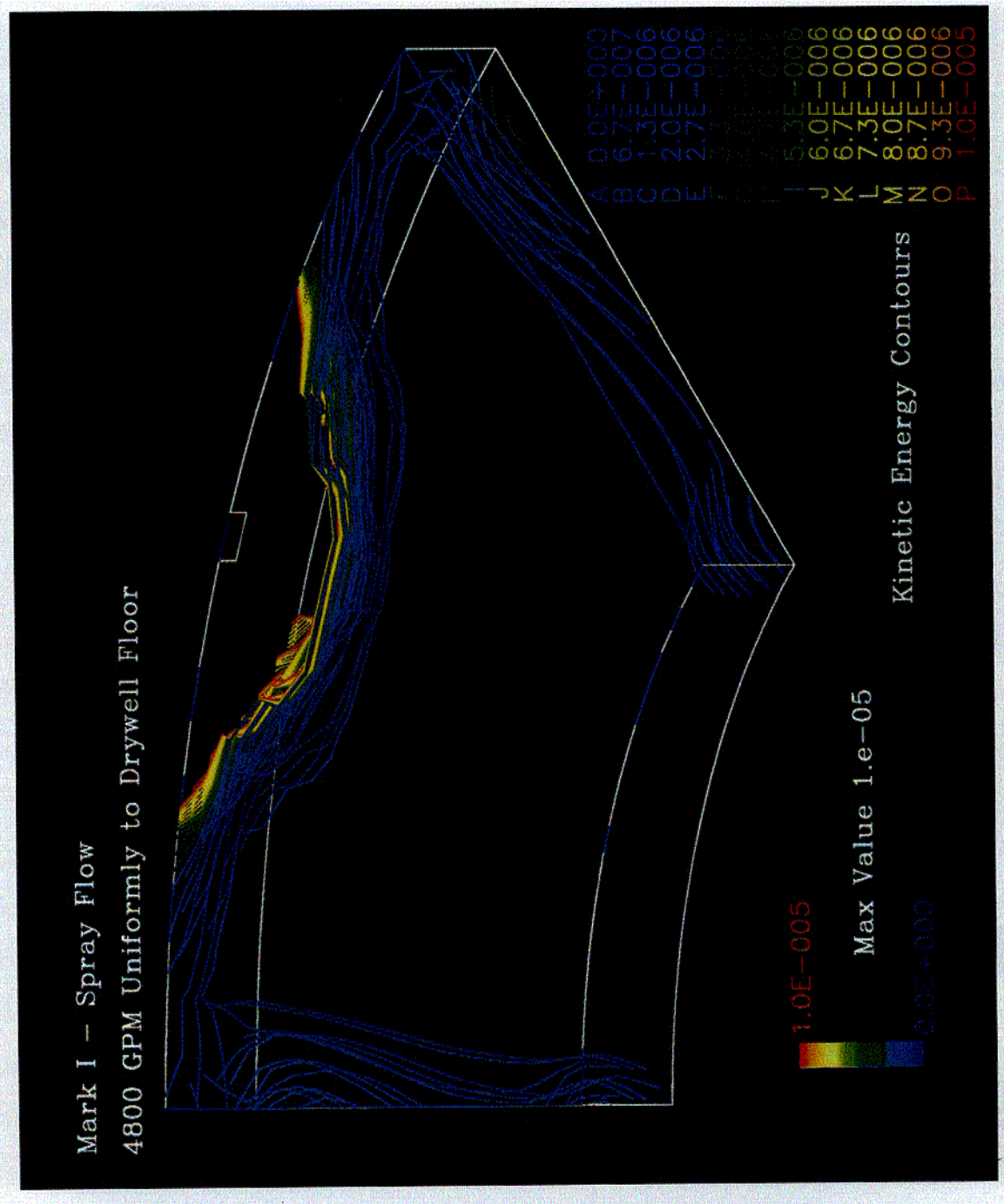

Figure 5-11: Specific Kinetic Energies for Containment Spray Pool in Mark I

C-16

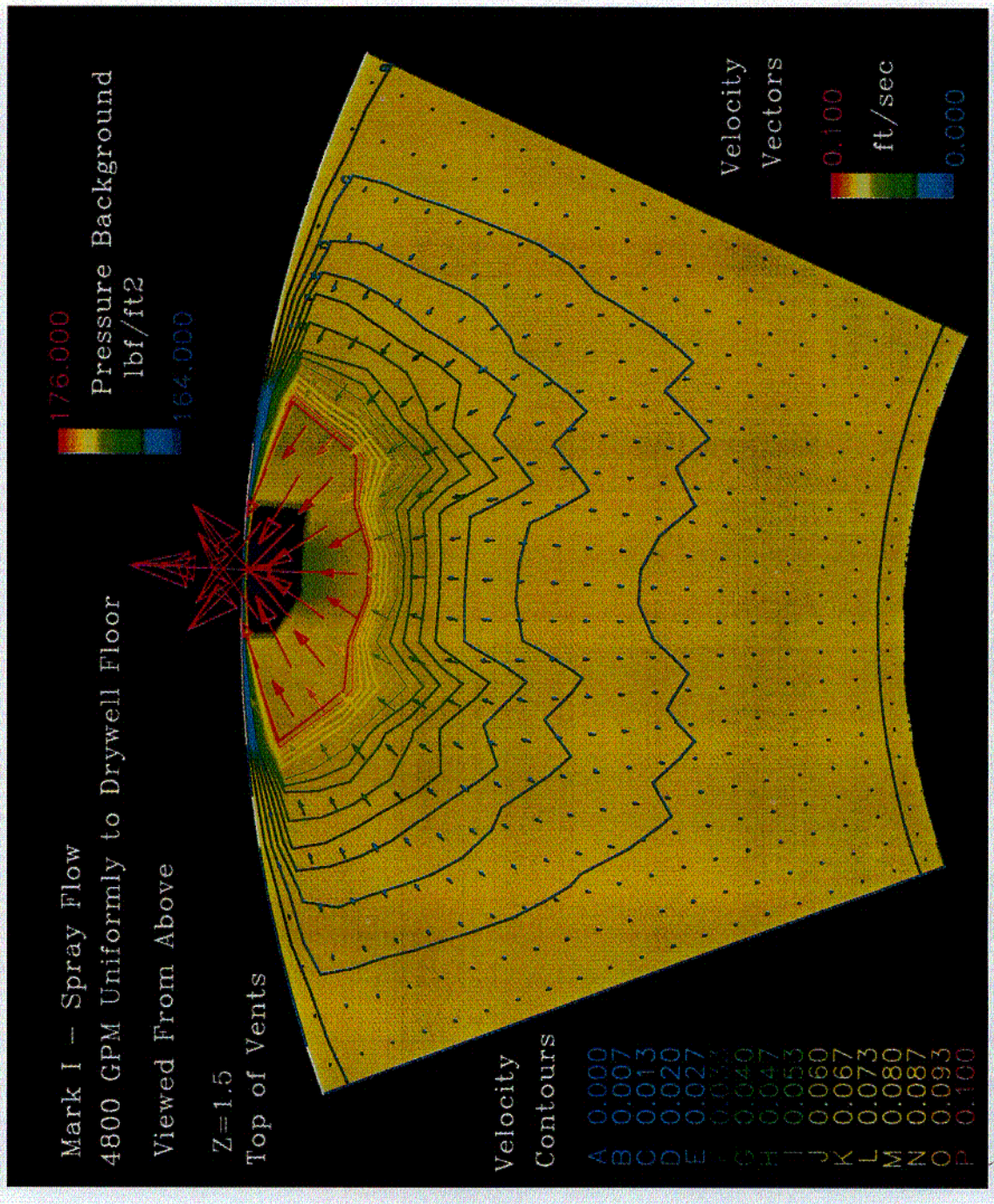

Figure 5-12: Flow Velocities at Overflow Level for Containment Spray Pool in Mark I

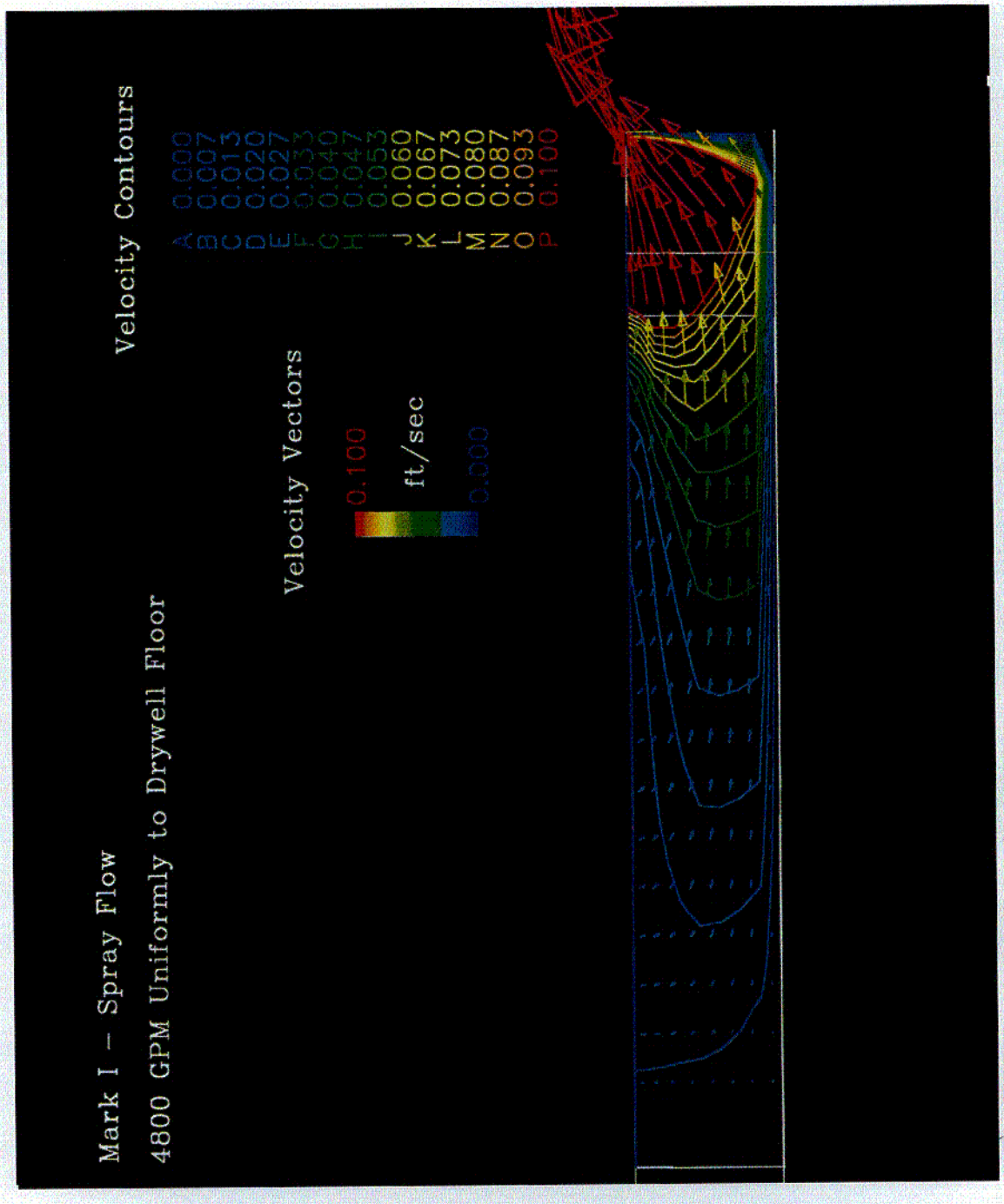

Figure 5-13: Flow Velocities in Vertical Cross-Section for Containment Spray Pool in Mark I

C-12

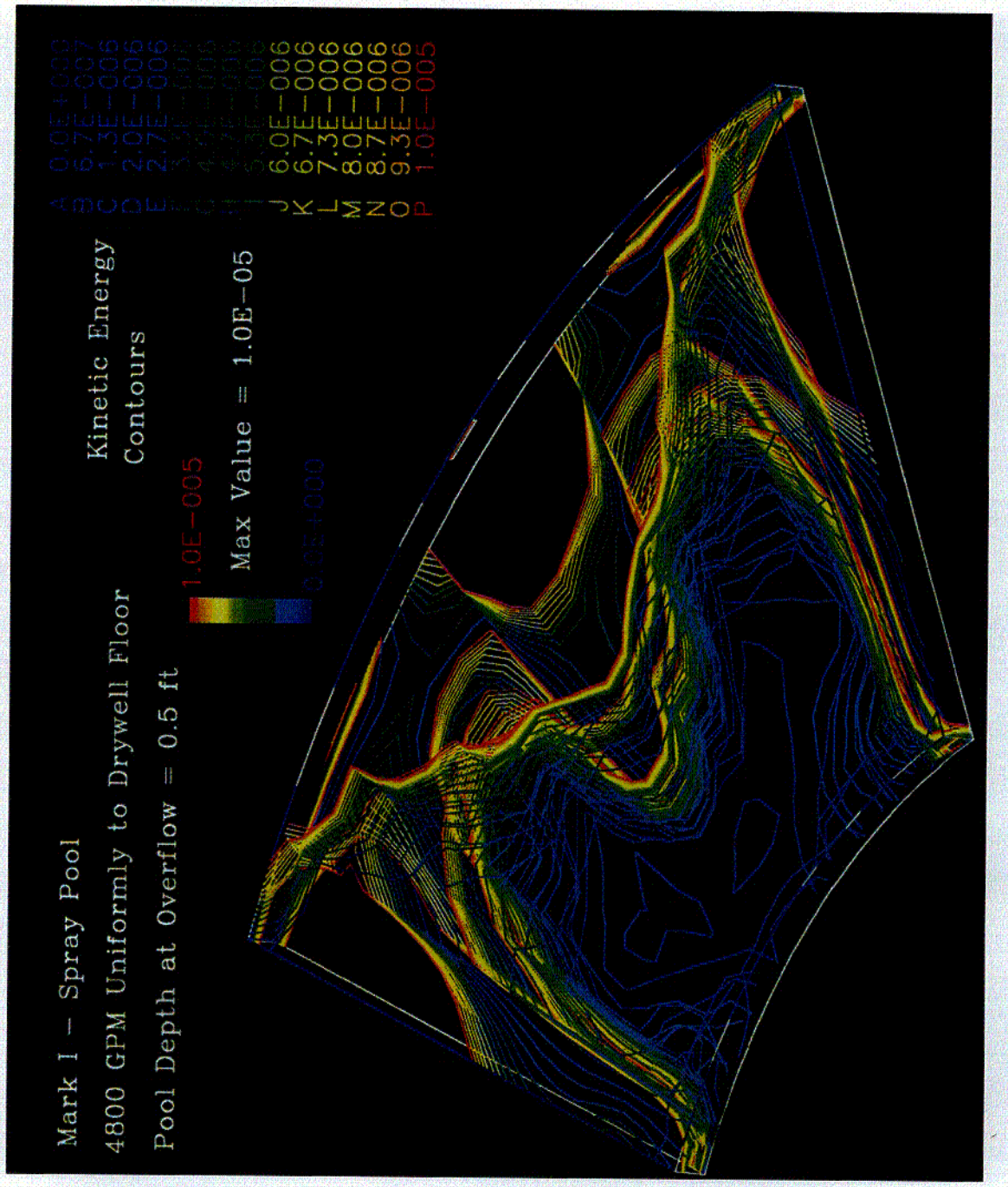

Figure 5-14: Specific Kinetic Energies for Containment Spray Pool in Mark I (6 inch Pool)

C-13

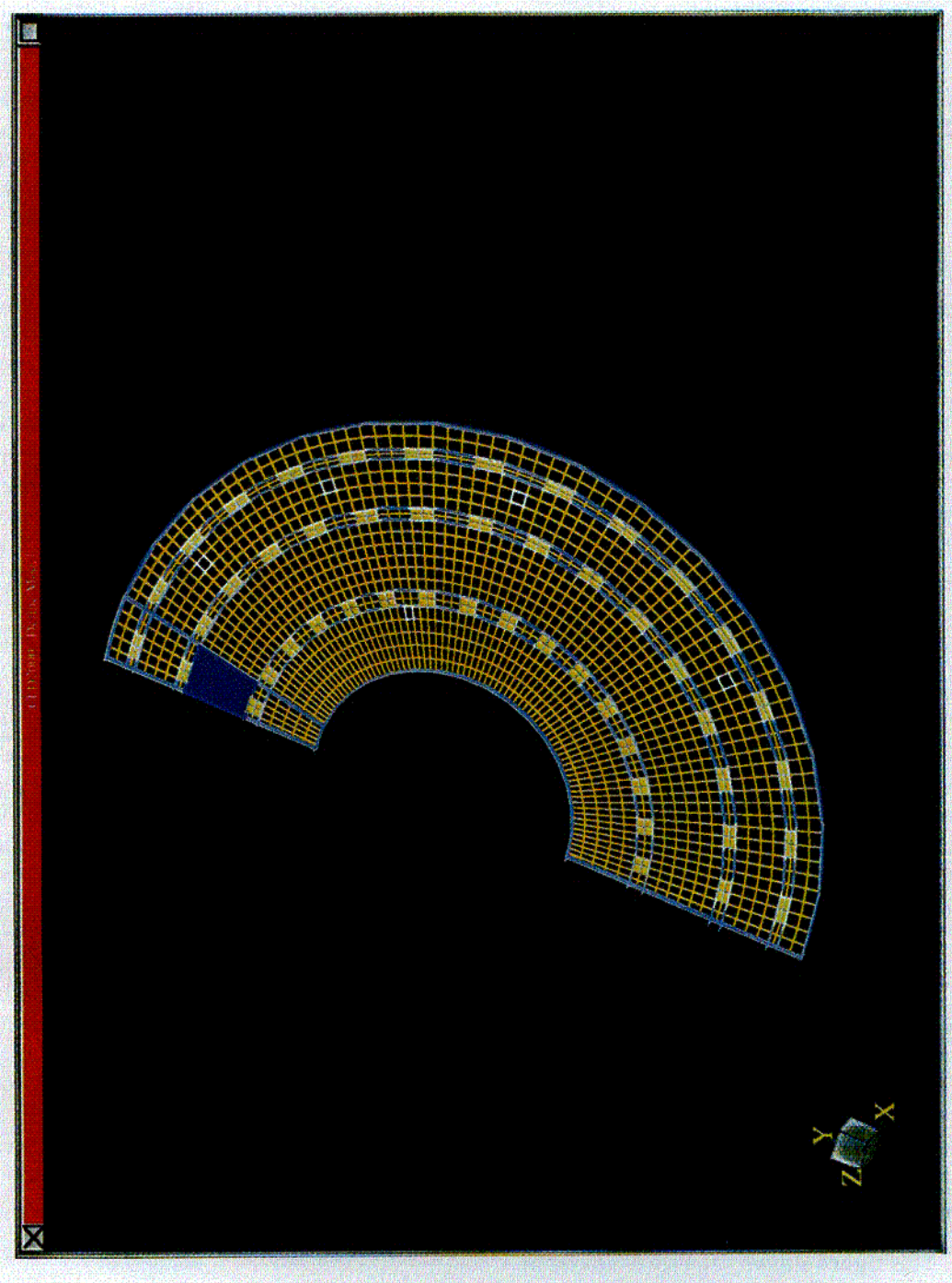

Figure 5-15: Nodalization Diagram for Full Recirculation Flow From Broken Pipe in Mark II

extended 6 inches above the floor. An extra 0.25 inches was added to the height of the pool to account for overflow into the pipe.

Although the CFD code was capable of modeling a single or a few downcomer standpipe with reasonable accuracy, modeling 48 of them would have required reconfiguring the code's dimension statements and recompiling the code. This was not considered practical for the scope of this project. Therefore, the model for the downcomer vents used in this simulation were kept very simple. In essence, the effect of the standoff pipe itself upon the flow was neglected. Only the exit of water at each location was modeled by placing an outlet boundary at the top of the pool for of the downcomers. Thus, water exited the pool at the downcomer locations on the basis of the pressure at that location. This simplification was a known deficiency in the simulation but still the results was considered adequate to draw general conclusions.

The flow was introduced into the calculation as a uniform constant velocity source over the pool surface area highlighted by blue in the nodalization diagram. The selection of this area was somewhat arbitrary but the selection was designed to focus the inlet flow over a relatively small portion of the floor area (41.1 ft^2, as it turned out) below the break. The uniform constant velocity associated with 28,600 GPM of flow through this area was 0.78 ft/sec and its turbulence level was specified at 100%.

5.5.1.2 Base Case Results

The flow patterns, flow velocities, and kinetic energy levels are illustrated in Figures 5-16 through 5-18. These figures are similar to those of the preceding calculation. In viewing these figures, remember that the standoff pipes were not modeled, therefore the flows are shown as moving through them.

Figure 5-16. This figure shows velocity contours in three dimensions. The peak velocities predicted were a little higher than 3.0 ft/sec. These higher velocities were located near the pedestal wall.

Figure 5-17. This figure shows the specific kinetic energies with the maximum value plotted fixed at 0.01 ft^2/sec^2. As shown, the majority of the pool was predicted to have a kinetic energy greater than this value which corresponded to the maximum value that would allow even the large debris could settle.

Figure 5-18. Flow velocities and pool pressures are shown for the pool elevation of the pool of 0.51 ft, near the top of the pool. Here the flow velocities are shown both as contours and as directional vectors. The color background shows the pressure throughout the pool at this elevation.

5.5.1.3 Alternate Conditions

One alternate case was performed for the Mark II recirculation line pool. This alternate case assumed that the inlet flow was widely dispersed so that it entered over a full quarter of the drywell floor at relatively low levels of turbulence. The flow rate was still 28,600 GPM but the uniform flow inlet velocity was now only 0.055 ft/sec and the turbulence was 2%. The specific kinetic energies for the case are shown in Figure 5-19. At this much milder inlet condition, the turbulence levels were significantly reduced for the pool on the opposite side of the break.

5.5.1.4 Conclusions Regarding Debris Transport

The predicted turbulence levels in a pool formed and maintained by a 28,600 GPM flow from the broken pipe in this Mark II design were likely much too high to allow substantial debris to settle, especially small pieces of debris. If the break flow was sufficiently dispersed prior to entering the pool, some possibility exits for debris, particularly larger debris, to settle in the pool at the backside of the pedestal. However, due to the uncertainty associated with these Mark II simulations, debris capture by the pool was not considered credible in either of the central or the upper bound estimates.

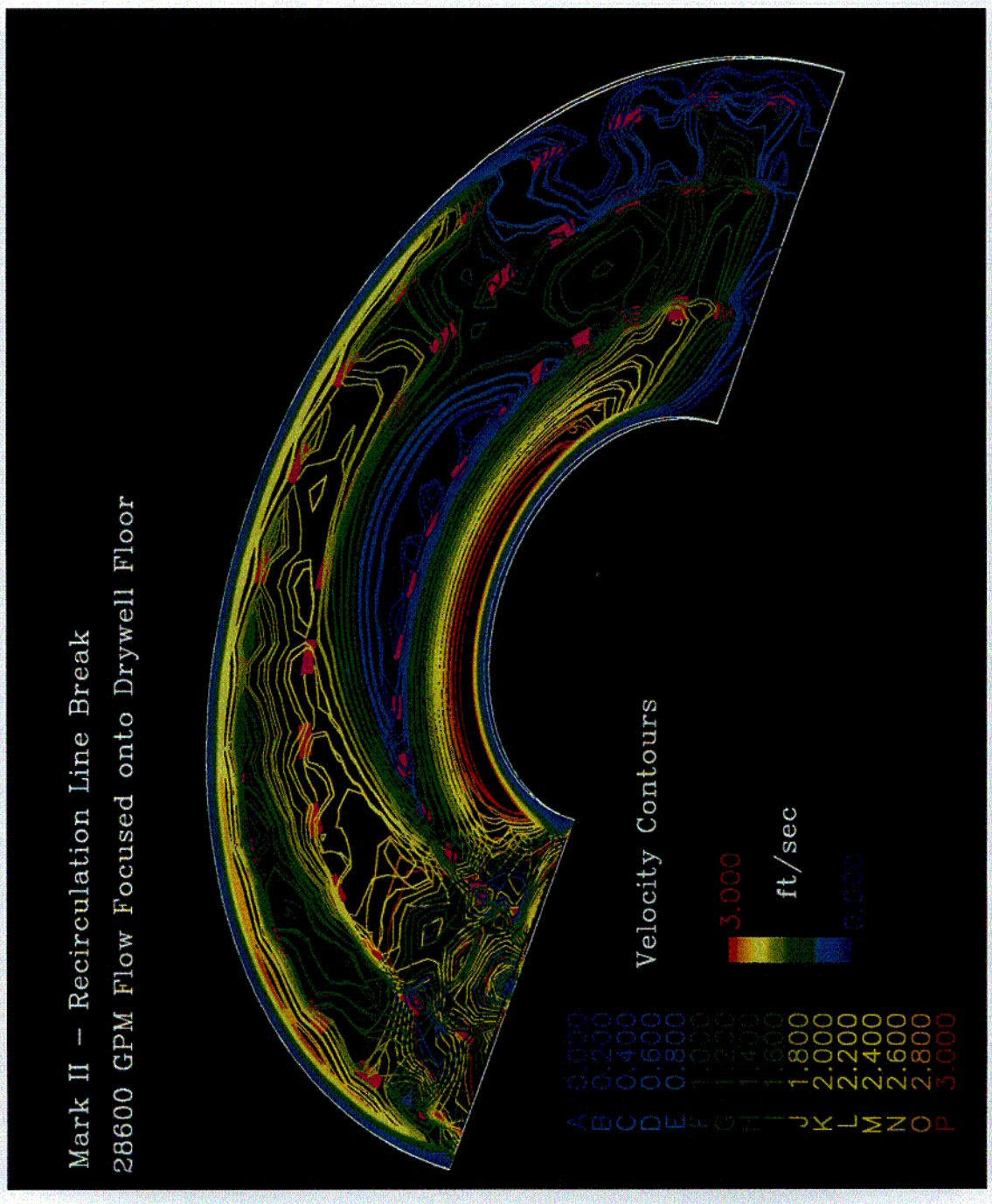

Figure 5-16: Flow Velocities for Full Recirculation Flow from Broken Pipe in Mark II

C-15

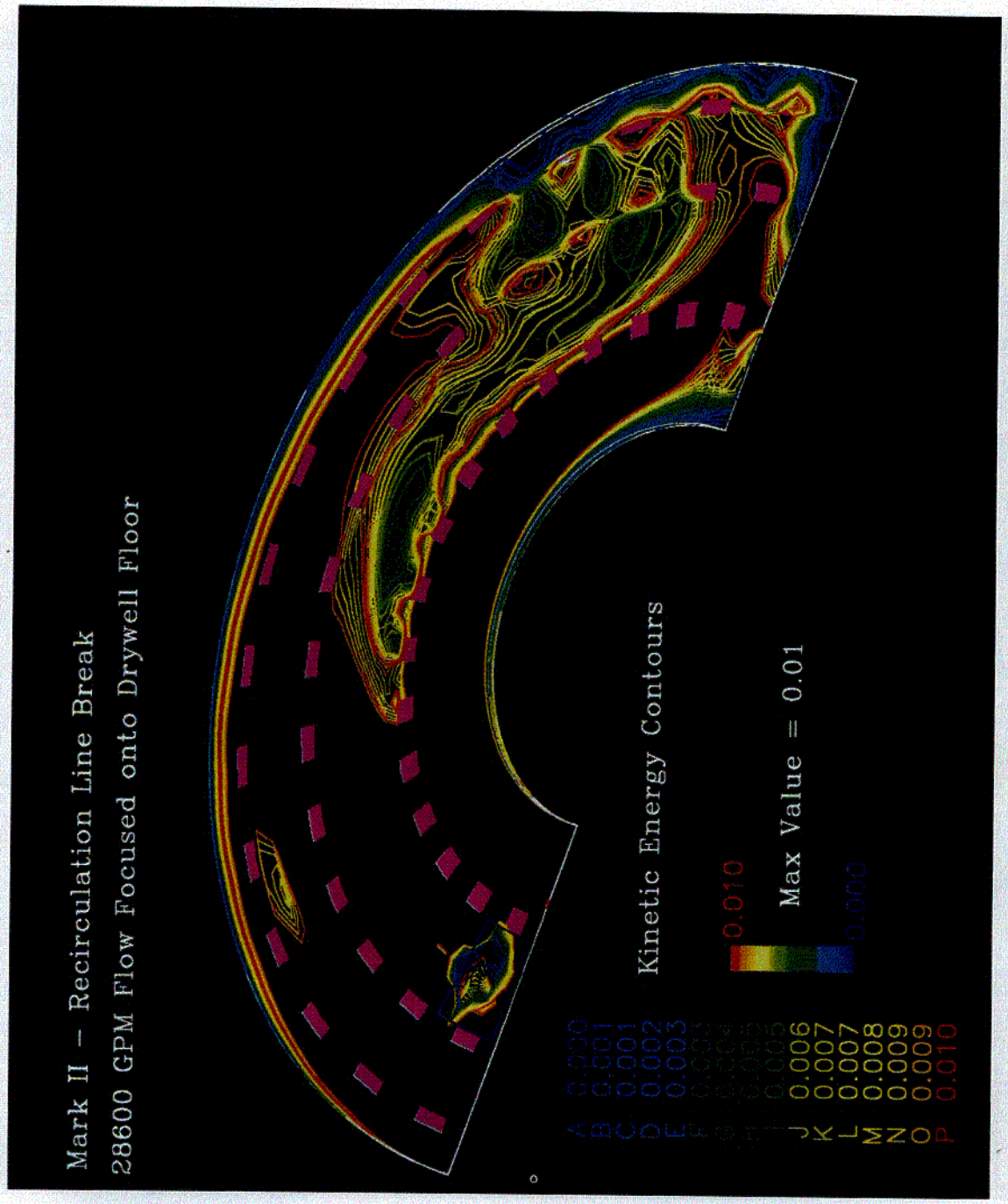

Figure 5-17: Specific Kinetic Energies for Full Recirculation Flow from Broken Pipe in Mark II

C-16

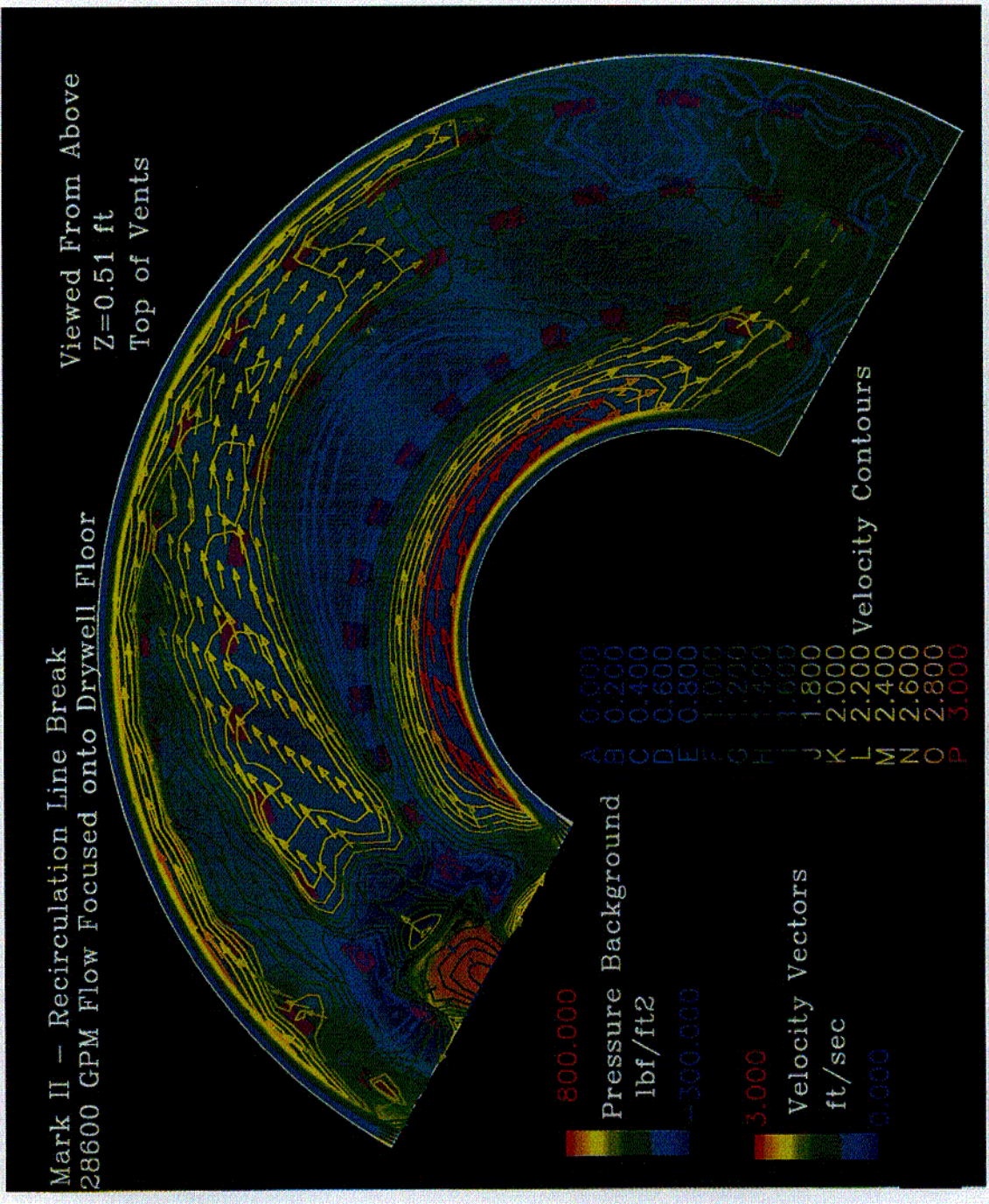

Figure 5-18: Flow Velocities at Overflow Level for Full Recirculation Flow from Broken Pipe in Mark II

C-17

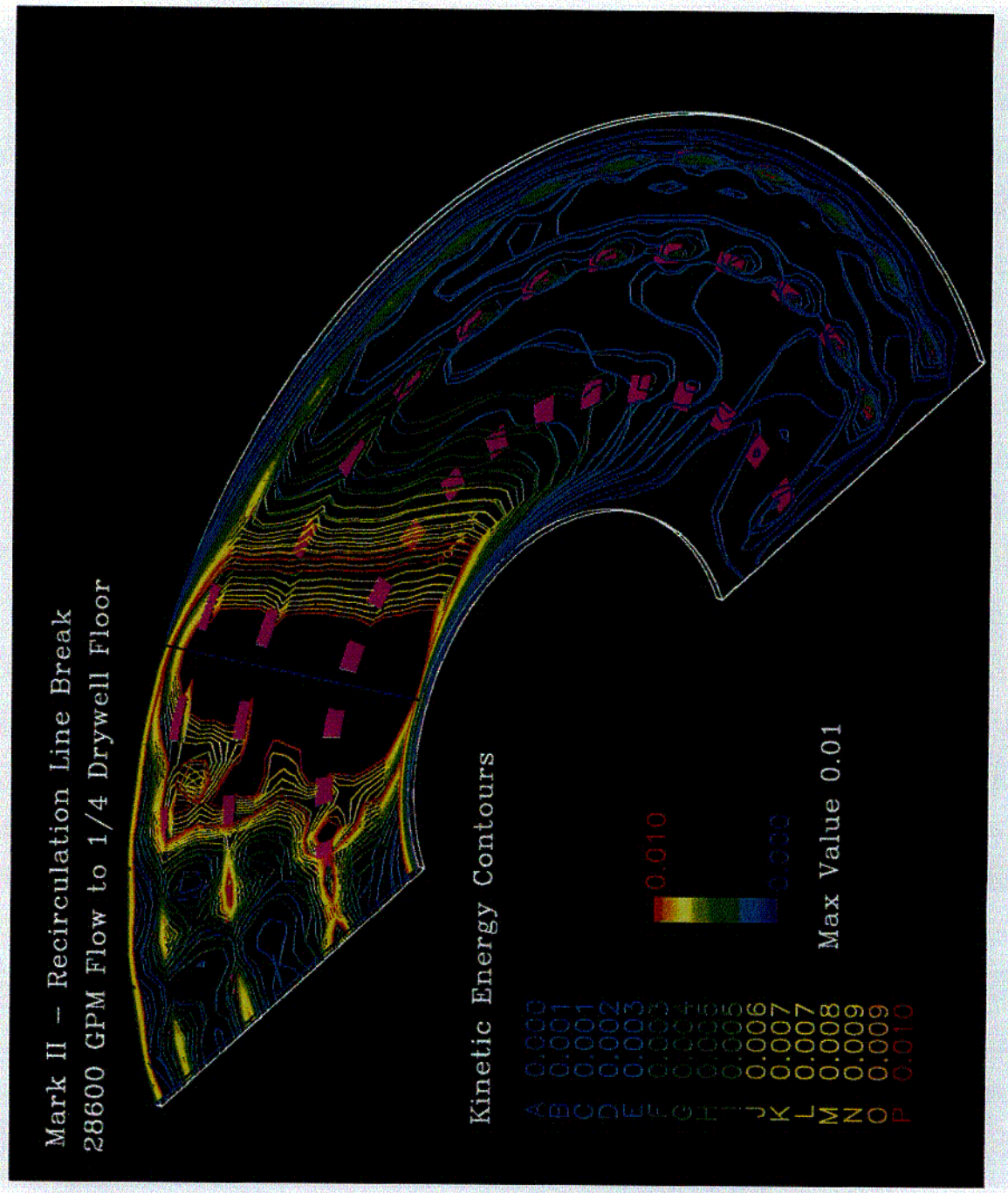

Figure 5-19: Specific Kinetic Energies for Full Recirculation Flow from Broken Pipe in Mark II (Dispersed)

C-18

5.5.2 Containment Spray Flow

A pool formed by the operation of the containment sprays was simulated for the same Mark II plant geometry as the preceding calculation. A total spray flow of 7400 GPM was assumed to fall uniformly to the floor where it would accumulate until the water level reached the entrances to the downcomer vents where it then would overflow into the suppression pool.

5.5.2.1 Geometrical Layout and Initial Conditions

The geometrical layout for this simulation was similar to that of the Mark II recirculation flow simulation previously discussed. Because the containment spray flow was assumed to fall through the drywell to the floor in a uniform manner, only a small section of the floor that contained nine downcomers was modeled as representing the entire floor pool. This modeled section of floor pool was actually 3/32 of the total floor pool. There were 10 vertical calculational cells, 23 radial cells, and 30 azimuthal cells. The nodalization for this simulation is shown in Figure 5-20.

Contrasting the previous simulation where the downcomer standoff pipes could not be modeled due to the complexity involved, the standoff pipes in this calculation were modeled because there were only nine of them. The rectangular approximation to the circular pipes was simulated using four wall boundary conditions each. The outlet boundaries were placed at the tops of the wall boundary such that water flowed into the pipes from above. Note the pool height was ¼ inch higher than the pipes that protruded 6 inches from the floor.

The flow was introduced into the calculation at a constant velocity of 0.0038 ft/sec at the elevation corresponding to the tops of the pipes. Inlet flows covered the entire floor except for the area excluded by the downcomers. The constant inlet velocity was 0.0038 ft/sec. The water was introduced into the calculation in this manner to prevent the incoming flows from flowing directly into the vents as would normally be prevented by covers installed on the top of the vents.

5.5.2.2 Base Case Results

The flow patterns, flow velocities, and kinetic energy levels are illustrated in Figures 5-21 through 5-23. These figures are similar to those of the preceding calculations.

Figure 5-21. This figure shows velocity contours in three dimensions. The water throughout most of the pool was moving relatively slowly. The flow velocities increased to about 0.5 ft/sec around the tops of the downcomer pipes where the water overflowed into the pipes.

Figure 5-22. This figure shows the specific kinetic energies with the maximum value plotted fixed at 0.01 ft^2/sec^2. A significant portion of the pool, at least at the higher levels, exceeded this energy level. When the maximum value was reduced to 0.001 ft^2/sec^2 (not shown), the predicted kinetic energies for nearly all of the pool exceeded this value.

Figure 5-23. The vertical behavior of the flow around the vents can be seen in this figure showing both velocity contours for a vertical cross-section passing through the center vents. This figure also further illustrates the scheme used to model the vents.

5.5.2.3 Alternate Conditions

Because the downcomer pipes in some Mark II plants extend further from the floor than those modeled in the previous Mark II simulations, one alternate calculation was run to simulate a deeper pool to determine the effect of pool depth on debris transport. This alternate case assumed that the pipes extended 18 inches above the floor rather than the 6 inches for the base case. The specific kinetic energies for this alternate calculation are shown in Figure 5-24. While the kinetic energies were reduced from those for the shallower pool, the turbulence levels were still rather high when considering the transport of small debris.

5.5.2.4 Conclusions Regarding Debris Transport

The turbulence levels for the Mark II spray pool were significantly higher than those predicted in the Mark I simulations. Although the inlet flow rate was 50% higher for the Mark II, the likely cause for

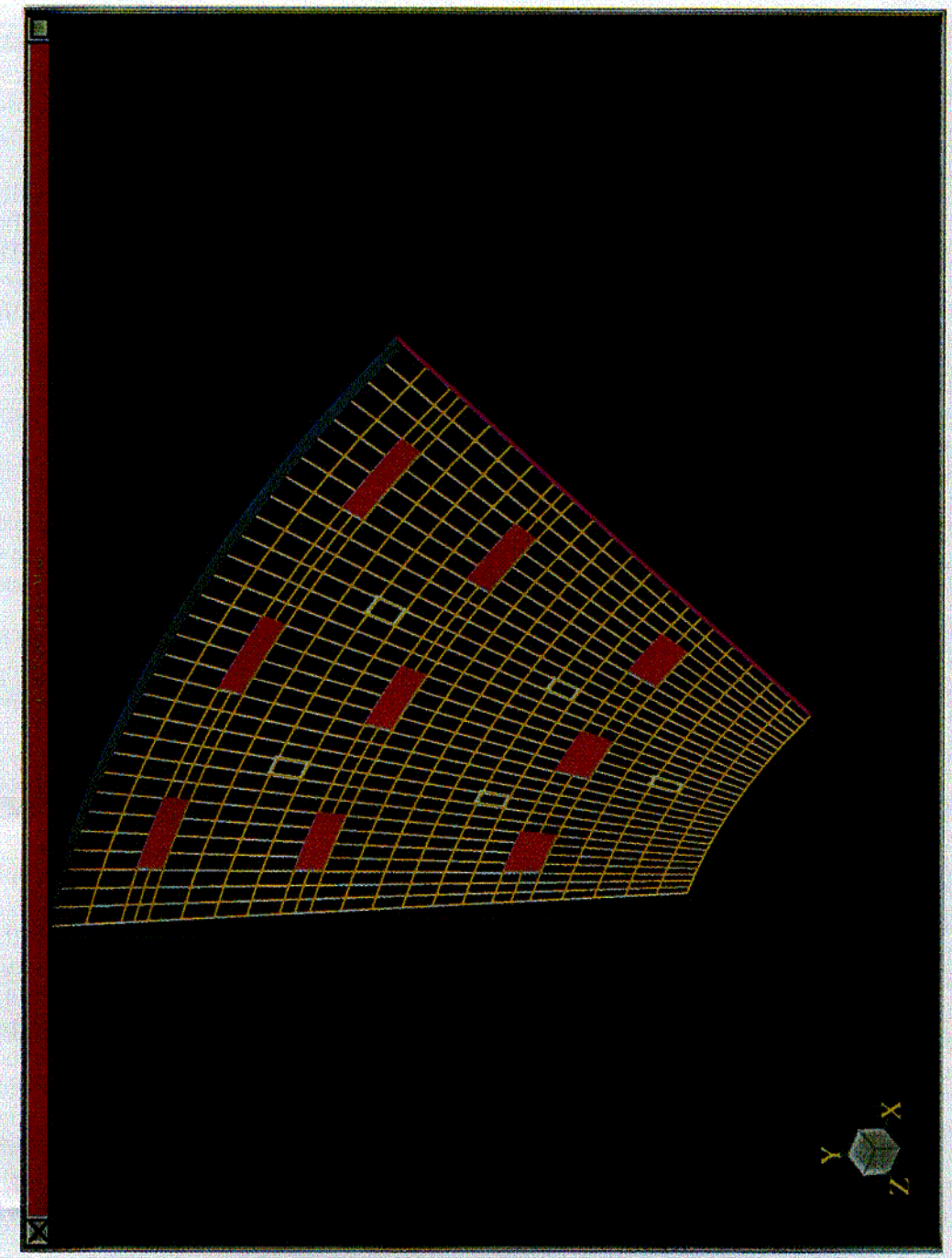

Figure 5-20: Nodalization Diagram for Containment Spray Pool in Mark II

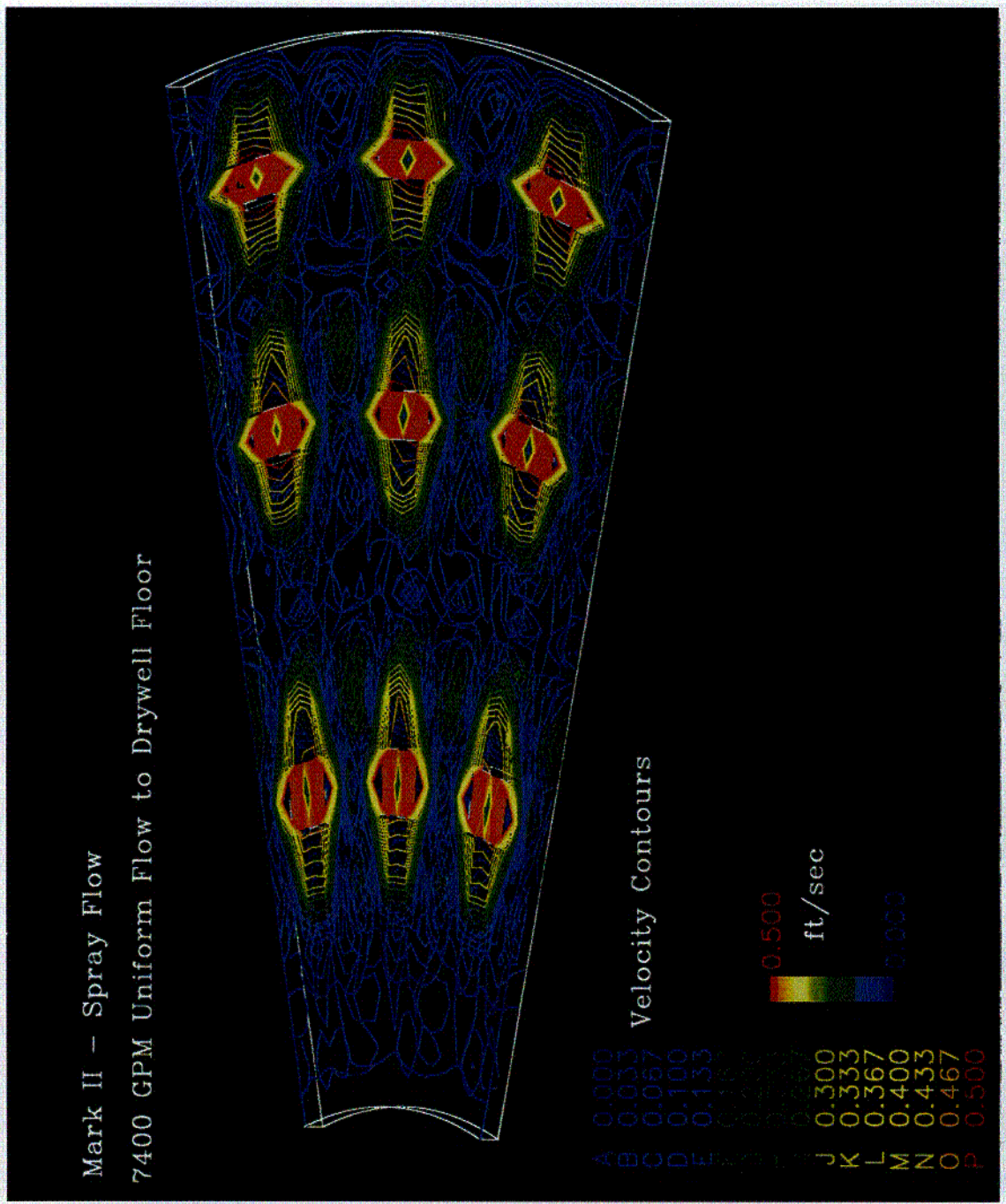

Figure 5-21: Flow Velocities for Containment Spray Pool in Mark II

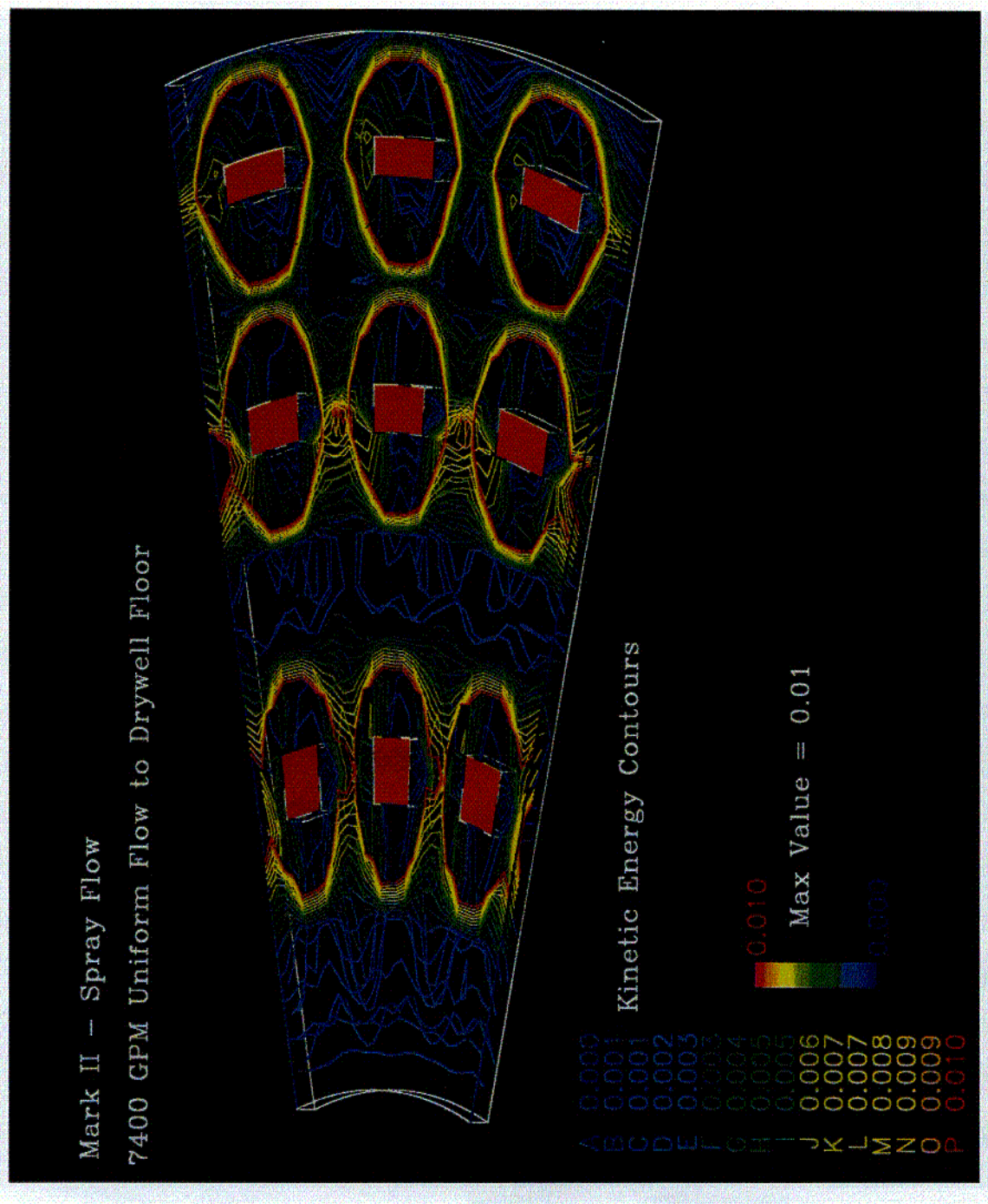

Figure 5-22: Specific Kinetic Energies for Containment Spray Pool in Mark II

C-21

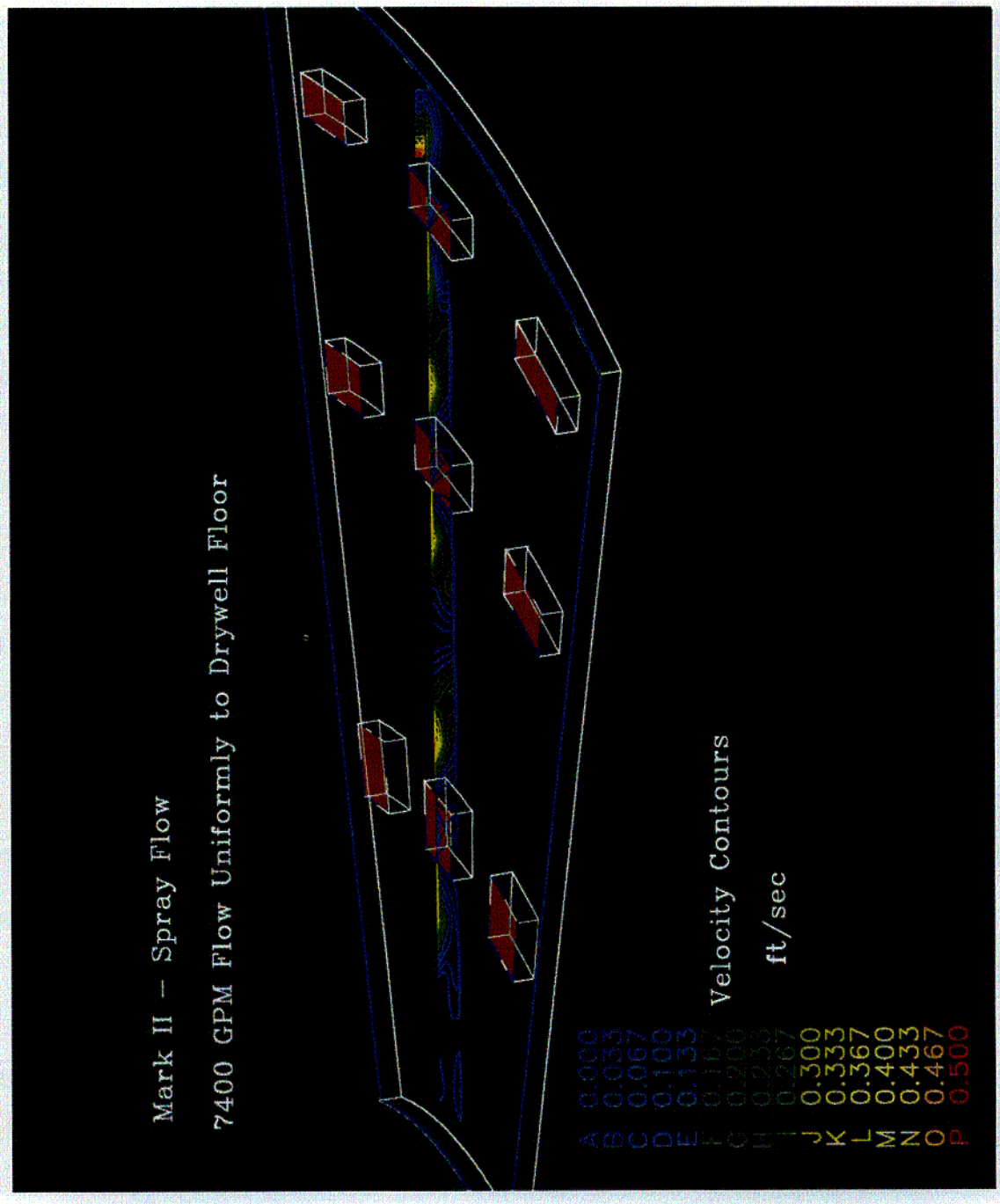

Figure 5-23: Flow Velocities in Vertical Cross-Section for Containment Spray Pool in Mark II

C-22

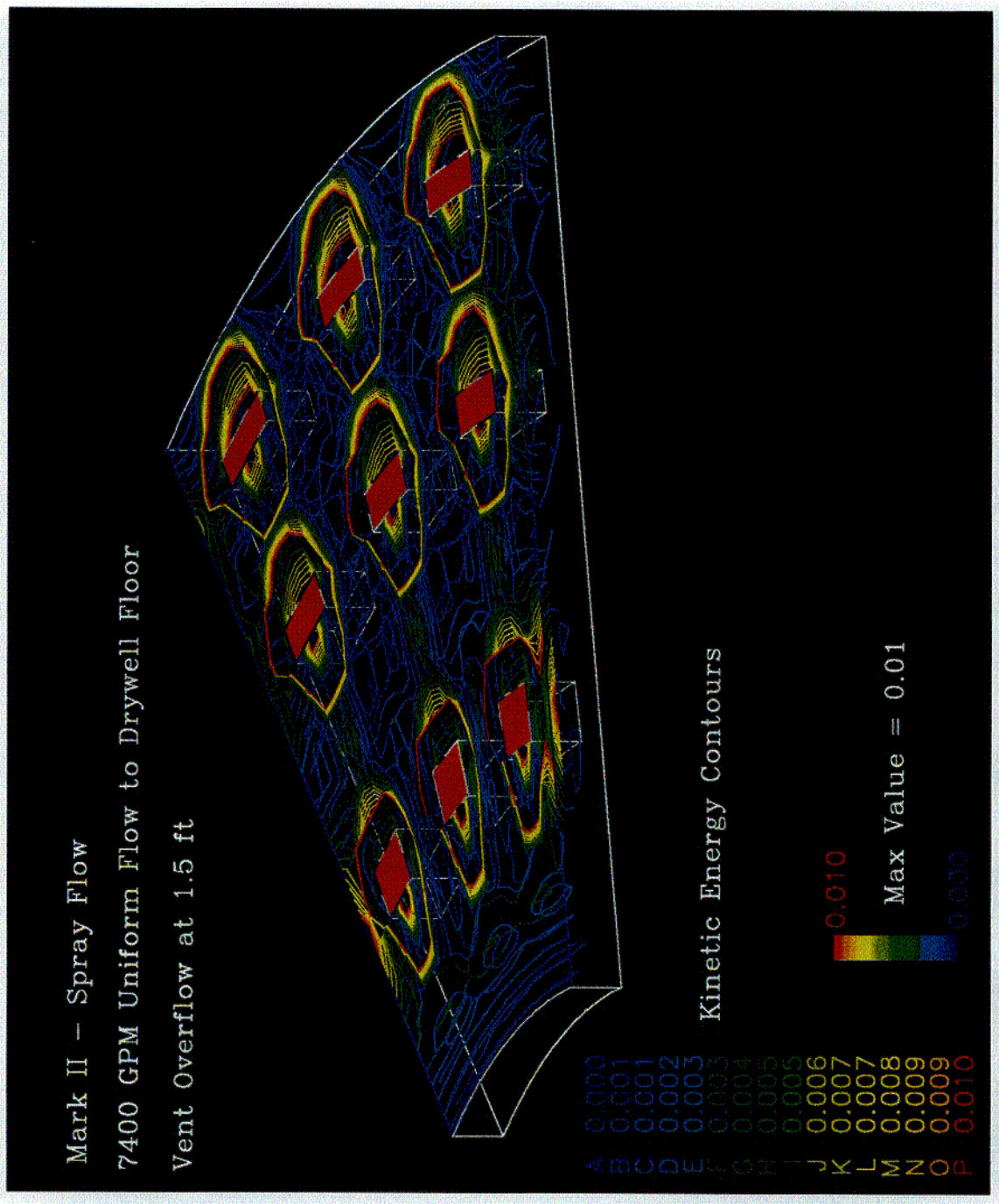

Figure 5-24: Specific Kinetic Energies for Containment Spray Pool in Mark II (18 inch Pool)

C-23

the higher turbulence levels was the effect of flows moving around the downcomer pipes. The predicted turbulence levels were low enough that large debris was expected to settle to the floor except for debris falling near a vent in an established pool. Blowdown deposited debris was not likely to be resuspended from the floor. However, the turbulence levels were generally high enough that small debris transport became very likely. When considering the extreme conservatism of the upper bound estimates, all small debris should be considered transported into the vents.

5.6 Mark III Simulations

5.6.1 Full Recirculation Flow from Break

The drywell floor pool sustained by a recirculation water flow from a broken pipe of 27,410 GPM was simulated. This flow would cascade down to the drywell floor and accumulate until the water level reached the top of the weir wall where it then would overflow into the suppression pool.

5.6.1.1 Geometrical Layout and Initial Conditions

As in the other calculations of this type, only one half of the drywell floor was simulated in the Mark III simulations because the recirculation water flows from the LOCA break would cascade down from the pipe break on one side of the drywell. The Mark III geometrical layout is illustrated in the nodalization diagram shown in Figure 5-25. There were 16 vertical calculational cells, 15 radial cells, and 80 azimuthal cells.

The height of the weir wall was 15.5 ft and an additional 3 inches were added to the height of the pool to simulate water flow over the weir. The weir overflow was modeled with a continuous outlet pressure boundary that circumvented the pool for the top 3 inches, shown as a colored strip in the nodalization diagram.

The flow was introduced into the calculation as a uniform constant velocity source over the pool surface area highlighted by blue in the nodalization diagram. The selection of this area was somewhat arbitrary but the selection was designed to focus the inlet flow over a relatively small portion of the floor area (20.2 ft^2, as it turned out) below the break. The uniform constant velocity associated with 27410 GPM of flow through this area was 1.51 ft/sec and its turbulence level was specified at 100%.

5.6.1.2 Base Case Results

The flow patterns, flow velocities, and kinetic energy levels are illustrated in Figures 5-26 through 5-30. These figures are similar to those of the preceding calculations.

Figure 5-26. This figure shows velocity contours in three dimensions. Peak velocities were a little higher than the maximum plotted of 0.25 ft/sec. The inlet flow generally continued in its downward direction until turned by the floor of the pool. A jet extending from the inlet flow can be seen extended into the central portion of the pool and still remaining relatively near the bottom. Other portions of the pool were much calmer.

Figure 5-27. This figure shows the specific kinetic energies with the maximum value plotted fixed at 0.01 ft^2/sec^2. A substantial portion of the pool near the break would likely have sufficient turbulence to keep even large debris from settling but at the other end of the pool the predicted turbulence was well below that needed to keep small debris suspended.

Figure 5-28. Flow velocities and pool pressures are shown for one specific elevation of the pool. The elevation of 15.6 ft was at the weir overflow level. Flow patterns and directions at the top of the pool are shown.

Figure 5-29. Flow velocities and pressures 1 ft above the floor are shown. The extended jet from the inlet flow can be seen as it expands out across the floor.

Figure 5-30. This figure shows the flow velocity contours and vectors in a vertical cross-section located 45° from the break end of the pool. Wall boundary effects are illustrated as well as the contorted flow pattern.

5.6.1.3 Alternate Conditions

One alternate case was performed for the Mark III recirculation line pool. This alternate case assumed that the inlet flow was widely dispersed so that it entered over a full quarter of the drywell floor at relatively low levels of turbulence. The flow rate was still 27,410 GPM but the uniform flow inlet velocity was now only 0.096 ft/sec and the

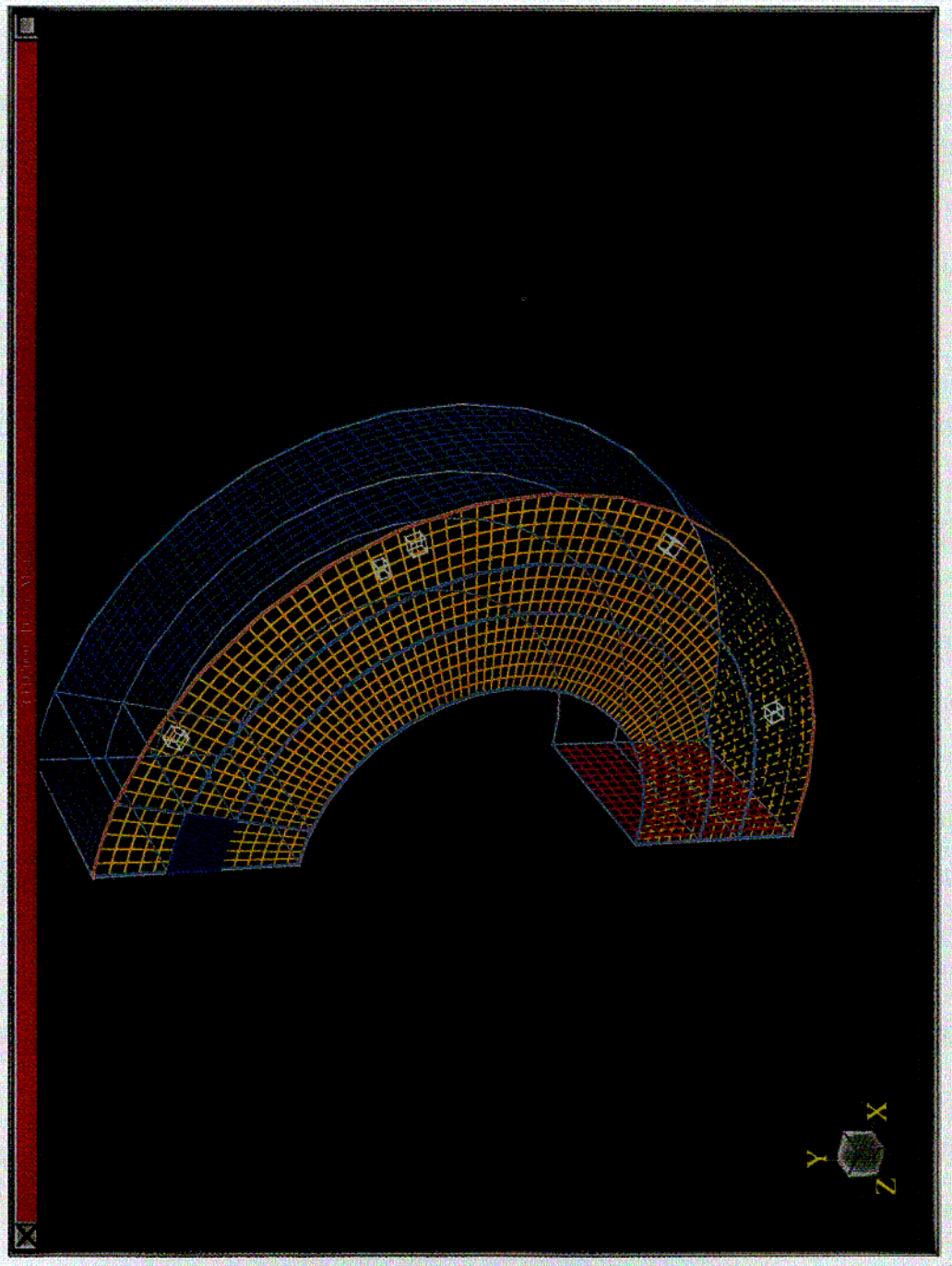

Figure 5-25: Nodalization Diagram for Full Recirculation Flow From Broken Pipe in Mark III

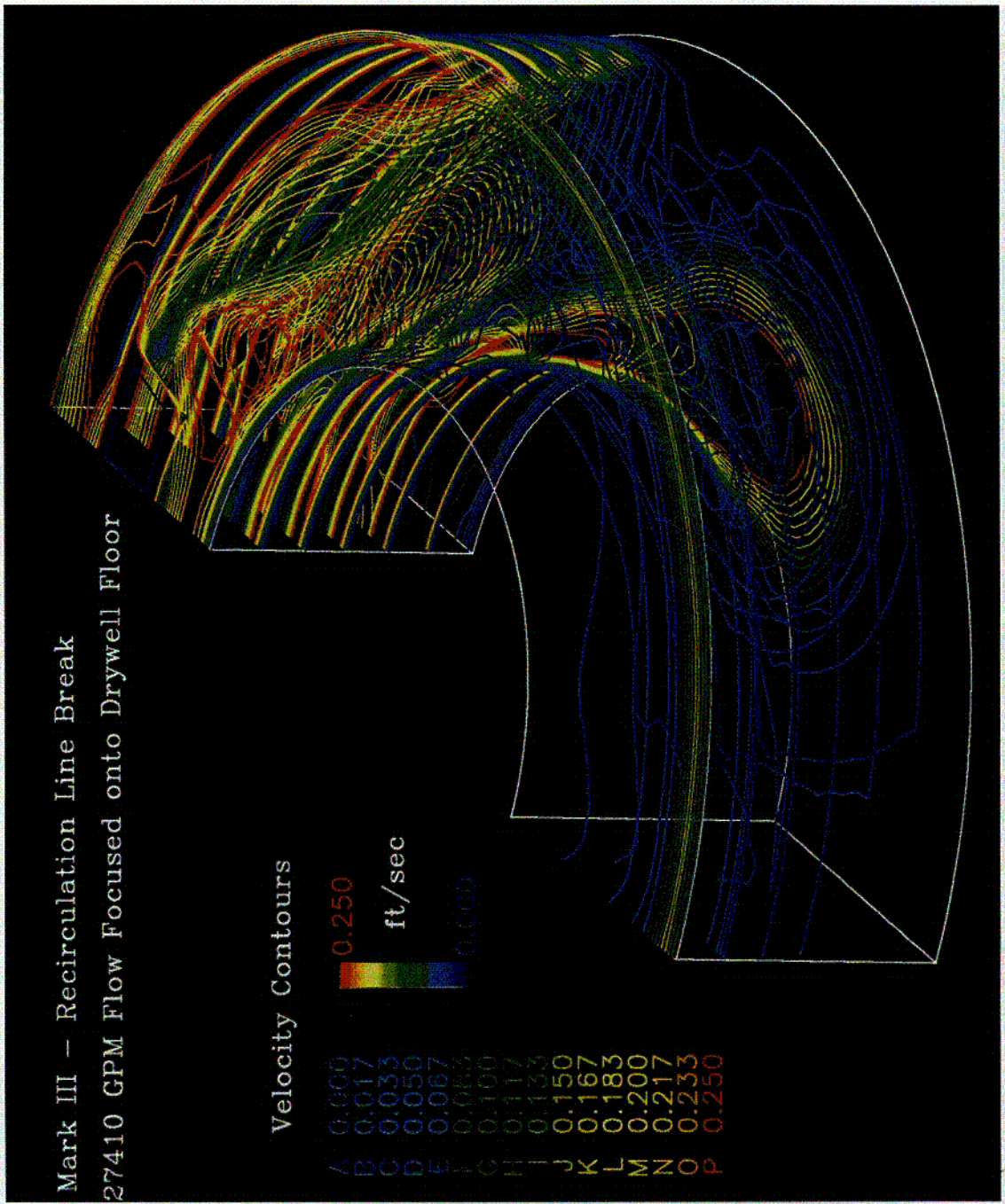

Figure 5-26: Flow Velocities for Full Recirculation Flow from Broken Pipe in Mark III

C-25

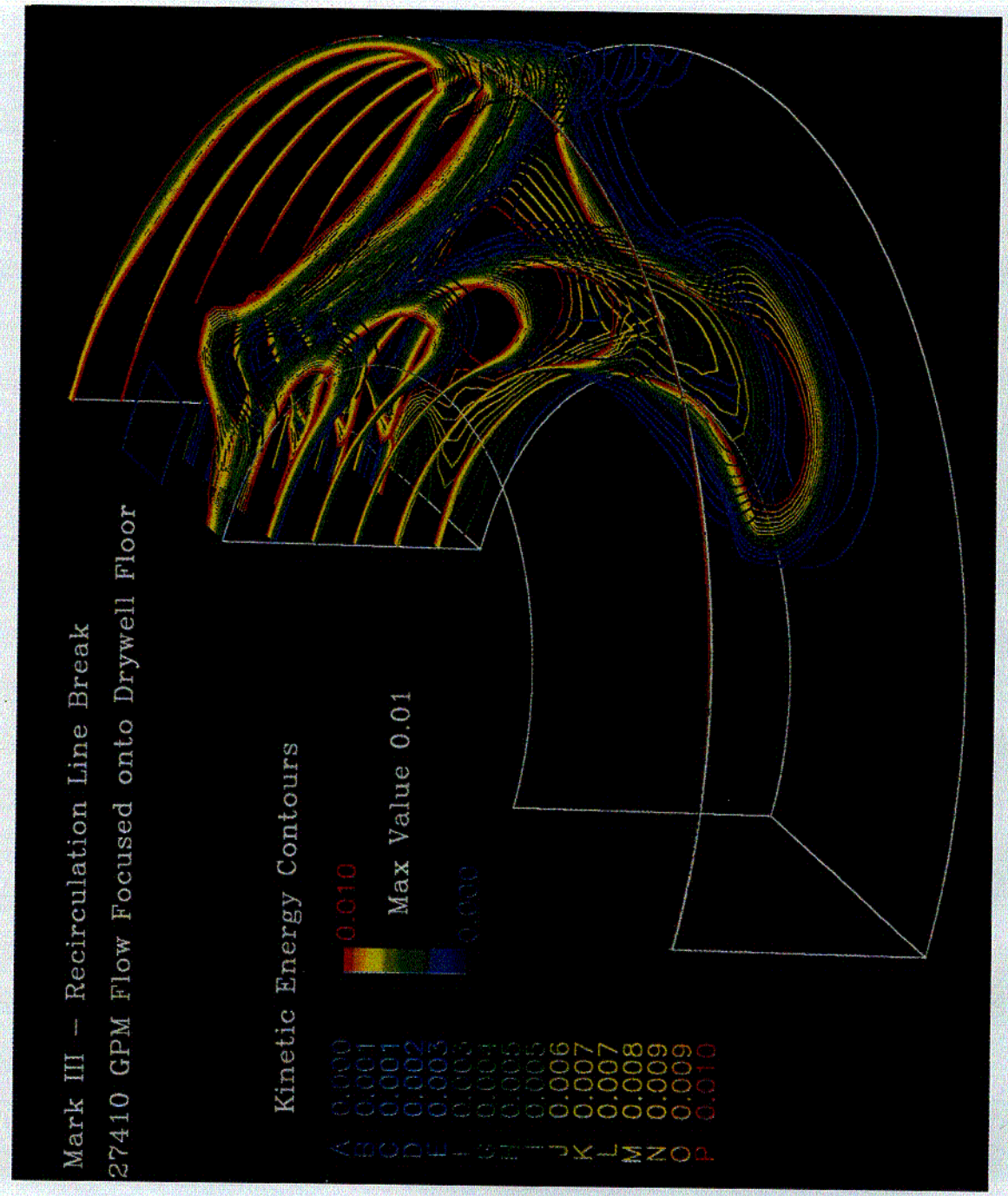

Figure 5-27: Specific Kinetic Energies for Full Recirculation Flow from Broken Pipe in Mark III

Q-26

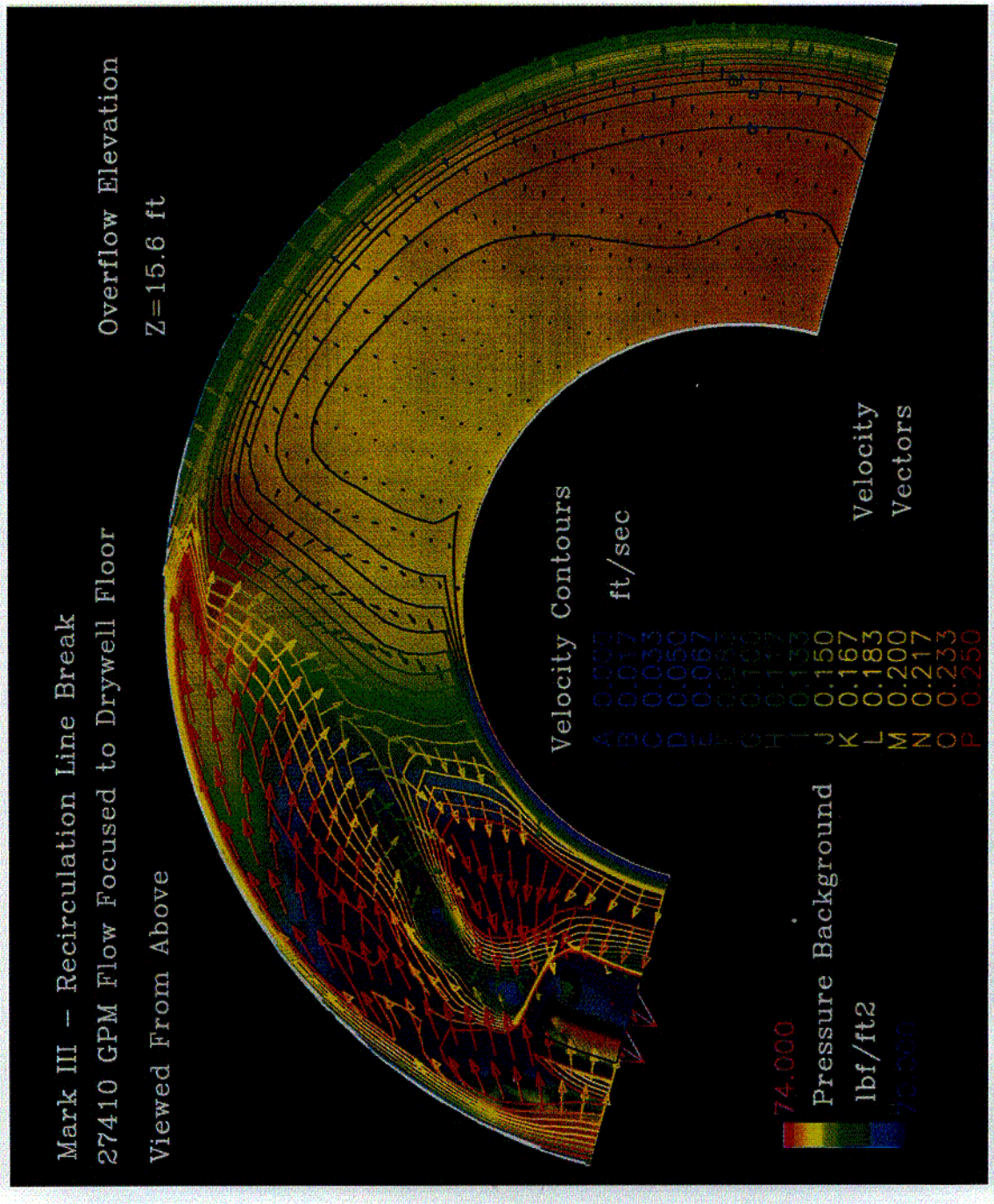

Figure 5-28: Flow Velocities at Overflow Level for Full Recirculation Flow from Broken Pipe in Mark III

C-27

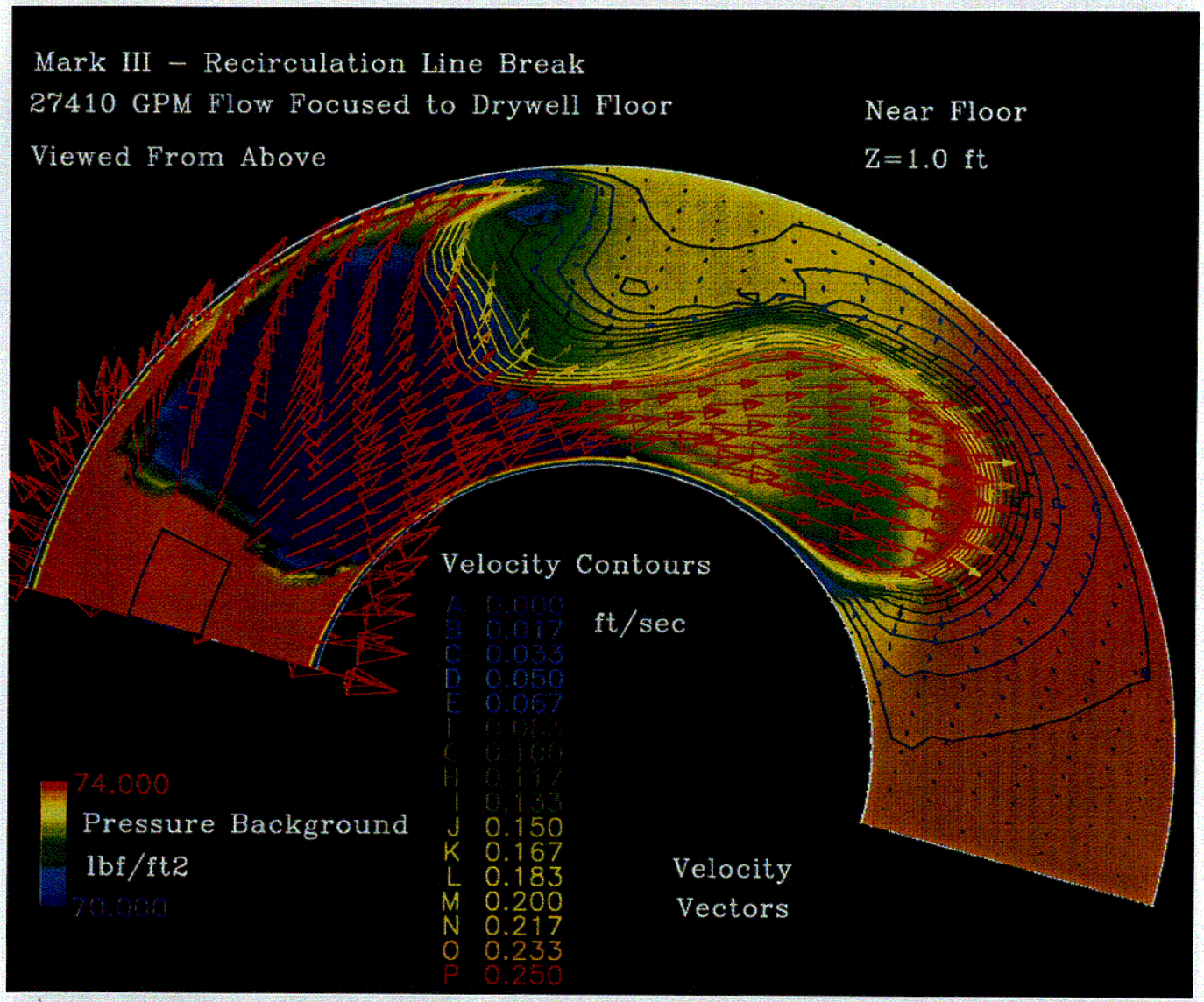

Figure 5-29: Flow Velocities Near Floor for Full Recirculation Flow from Broken Pipe in Mark III

C-28

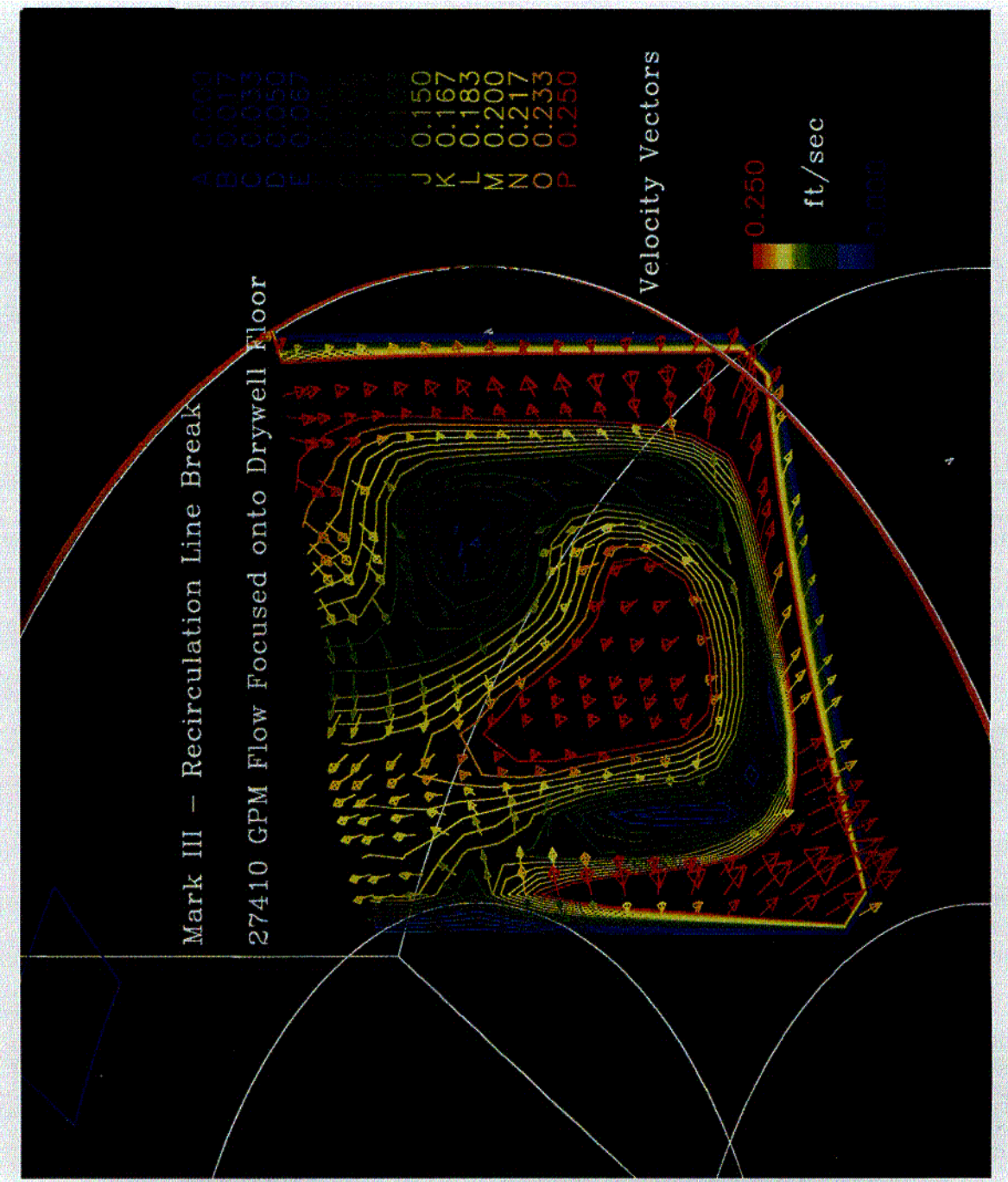

Figure 5-30: Flow Velocities in Vertical Cross-Section for Full Recirculation Flow from Broken Pipe in Mark III

C-29

turbulence was 2%. The specific kinetic energies for this case, with a maximum plotted value of 0.001 ft^2/sec^2, are shown in Figure 5-31. Here the turbulence levels in the majority of the pool were well below this maximum value.

5.6.1.4 Conclusions Regarding Debris Transport

These calculations indicate that most large debris, particularly debris deposited during blowdown, would likely settle and remain in the pool. Although, the alternate calculation with its dispersed inlet flow condition indicated a strong potential for retaining small debris, debris transport conclusions were based on the base case. The flow patterns shown in Figures 3-26 and 3-29 indicated that a large portion of small debris settling in the pool would encounter the faster flows of the extended inlet jet, whereby, the debris could be pushed back up to higher elevations. Remaining on the conservative side, a relatively high transport fraction for small debris was assumed.

5.7 Summary of CFD Turbulence and Debris Transport Results

The primary objective of this study was to examine the potential for debris to settle in drywell pools and to estimate both central and upper bound debris transport fractions. Further, the transport fractions were needed for the Mark I, II, and III designs with additional consideration for variations in the pool depth and the entrance conditions to the pools. This study accomplished the primary objective of examining the full breath of the drywell pool debris transport without delving deeply into any particular aspect.

The overall study included all aspects associated with pool debris transport including plant design data, post-LOCA thermal-hydraulic conditions, characteristics of fibrous insulation debris, and the complex flow conditions of the floor pool. Debris settling in a pool was correlated to pool turbulence using experimental debris settling data to calibrate the CFD code predicted specific kinetic energy levels with conditions that would allow debris to settle to the pool floor.

Because the overall transport process was much too complex to simulate completely, actual transport fractions were derived through the application of engineering judgment to the available data and calculational insights. Because of the uncertainties associated with this solution process, the judgments were necessarily conservative in nature to ensure safety.

The study resulted in a complete set of transport fractions. The transport fractions associated with floor pools formed by the accumulation of water from the operation of the containment sprays are shown in Table 5-5. This table lists the fractions for both small and large debris; for both debris deposited on the floor early during the blowdown process and later by the washdown process; and for both central and upper bound estimates. The corresponding transport fractions for pools formed and maintained by ECCS water flows from the broken pipe are shown in Table 5-6.

A pool would form due to the accumulation of steam condensate following a MSL break where the operator throttled the ECCS so that the effluence from the broken pipe was steam rather than water and the containment sprays were not operated. An attempt was made to simulate this pool with the CFD code but the flow velocities and turbulence levels were so low that solution convergence was not obtained. These very low flow velocities and turbulence levels and the determination that it would take an extensive period of time to accumulate a pool that would overflow into the suppression pool (approximately 9 hours for the Mark I plant simulated herein), led to the specification of no debris transport.

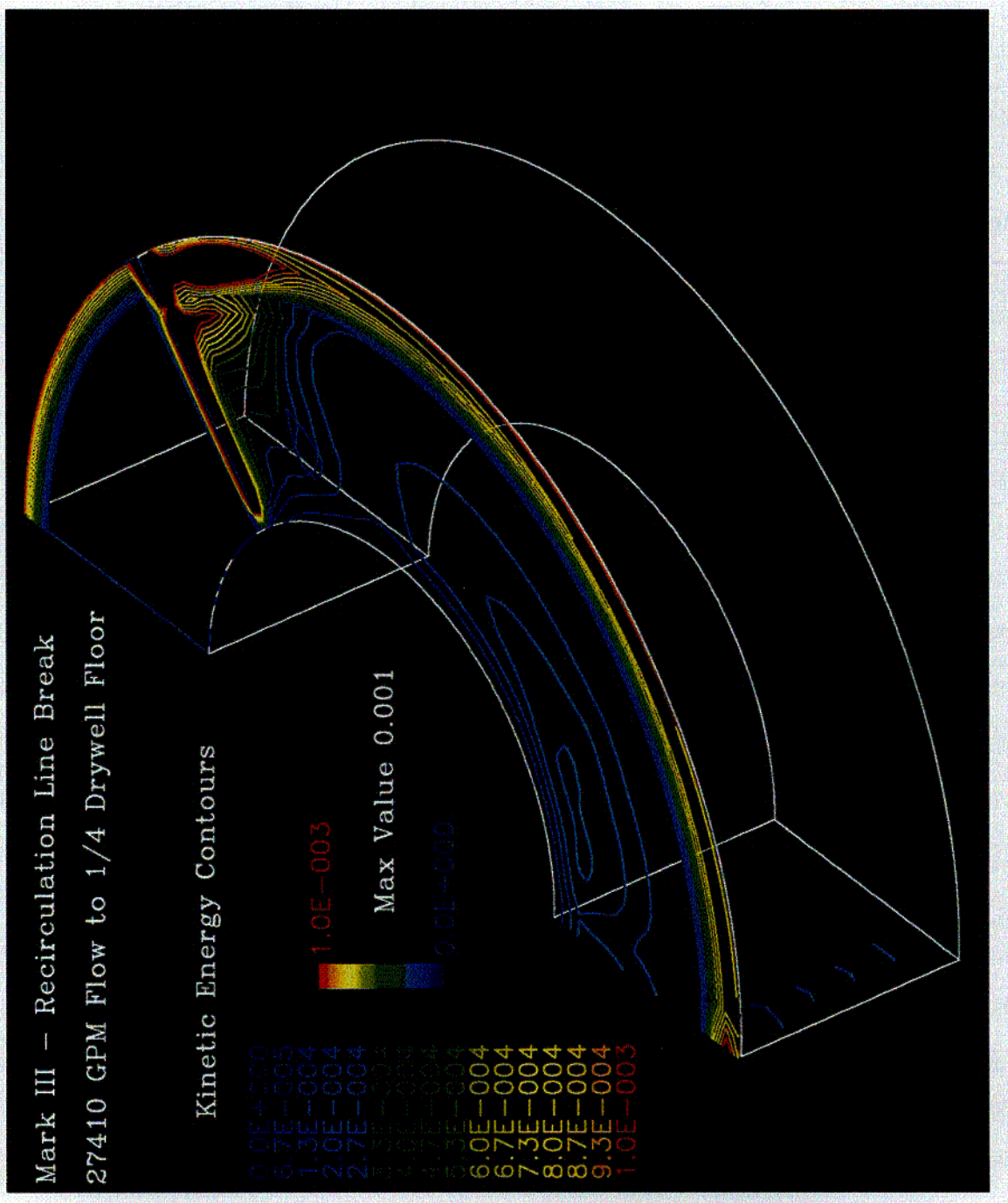

Figure 5-31: Specific Kinetic Energies for Full Recirculation Flow from Broken Pipe in Mark III (Dispersed)

Table 5-5: Drywell Pool Transport Fractions for a Pool Formed by Containment Sprays

Plant	Debris	Small Debris		Large Debris Pieces	
Design	Source	Upper	Central	Upper	Central
Mark I	Blowdown	0	0	0	0
	Washdown	0.1	0.01	0	0
Mark II	Blowdown	1	0.5	0	0
	Washdown	1	0.9	0.1	0

Table 5-6: Drywell Pool Transport Fractions for a Pool Formed by Recirculation Water Flows

Plant	Debris	Small Debris		Large Debris Pieces	
Design	Source	Upper	Central	Upper	Central
Mark I	Blowdown	1	1	1	0.9
	Washdown	1	1	1	1
Mark II	Blowdown	1	1	1	1
	Washdown	1	1	1	1
Mark III	Blowdown	1	0.8	0.1	0
	Washdown	1	0.8	0.1	0

The transport of insulation erosion products was specified as 100% under all conditions except for the condensate pool just described. These erosion products, consisting primarily of individual fibers and small groups of fibers, would settle in calm pools of water given sufficient time. However, given the pool conditions under study herein, these erosion products could only be treated as though they simply will not settle.

5.8 References

5-1 D. N. Brocard, "Buoyancy, Transport, and Head Loss of Fibrous Reactor Insulation," NUREG/CR-2982, SAND82-7205, Revision 1, July 1983.

5-2 G. Zigler, et. al., "Parametric Study of the Potential for BWR ECCS Strainer Blockage Due to LOCA Generated Debris," NUREG/CR-6224, SEA No, 93-554-06-A:1, Draft Review for Comment, July 1994.

5-3 "CFD2000 Version 2.2 User's Manual," Adaptive Research, Division of Pacific-Sierra Research Corporation, Huntsville, Alabama, Document Version V2.2UM. 1996.

5-4 K. W. Brinckman, "Results of Hydraulic Tests on ECCS Strainer Blockage and Material Transport in a BWR Suppression Pool," EC-059-1006, Revision 0, May 1994.

Appendix A

Debris Transport Plots

Appendix A

List of Figures

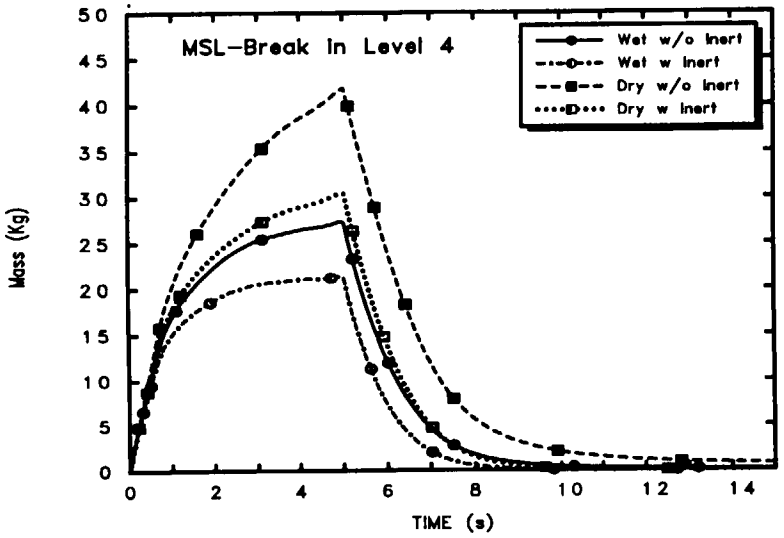

Figure A–1. Total Drywell Airborne Debris

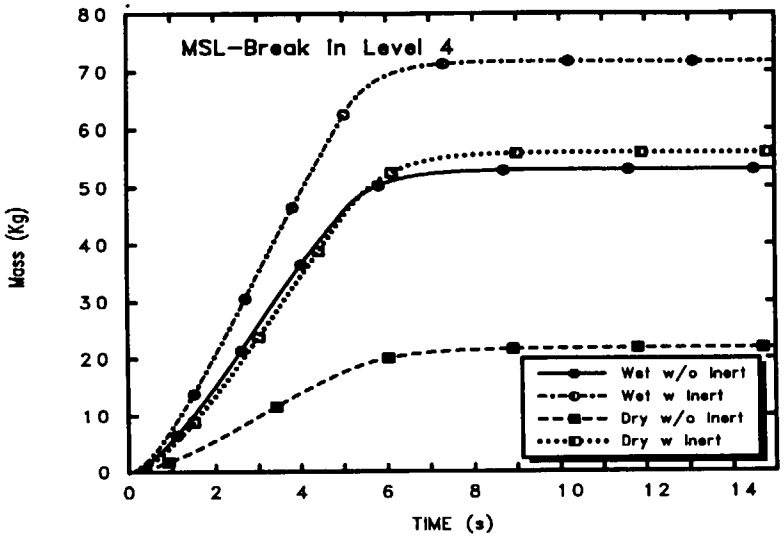

Figure A–2. Total Debris Deposited In Drywell

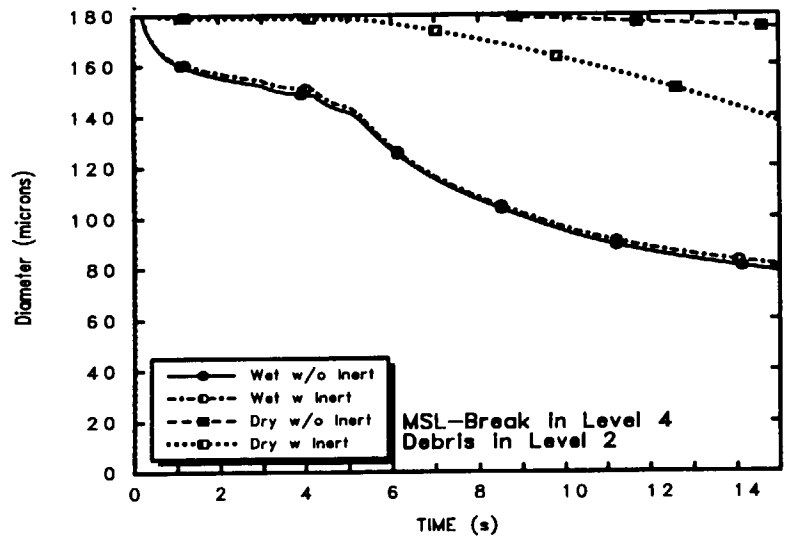

Figure A–3. Debris Mass Medium Diameter

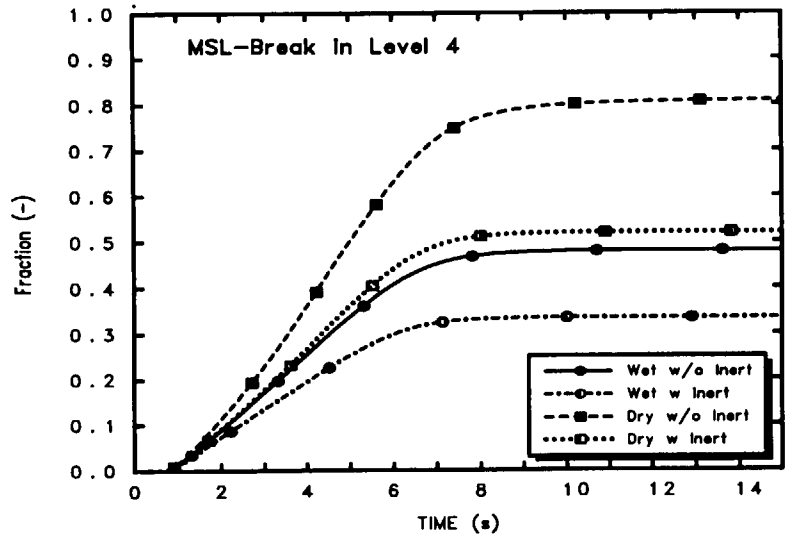

Figure A–4. Debris Transport Fraction

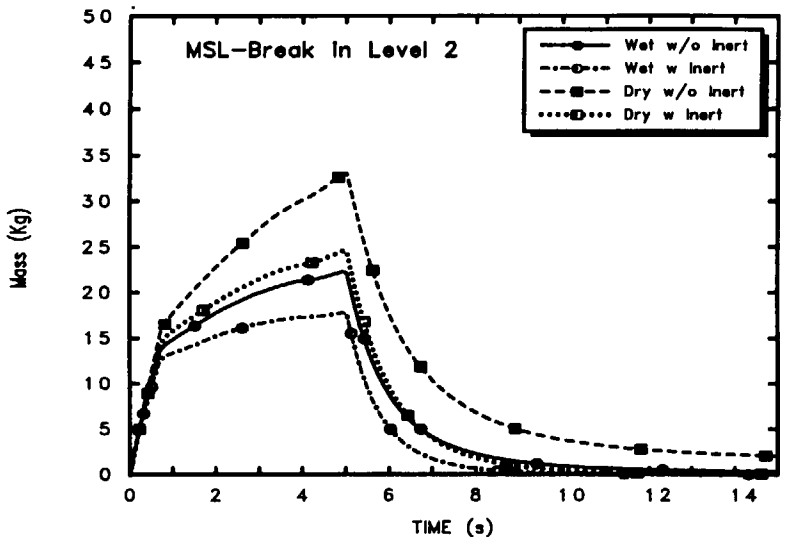

Figure A-5. Total Drywell Airborne Debris

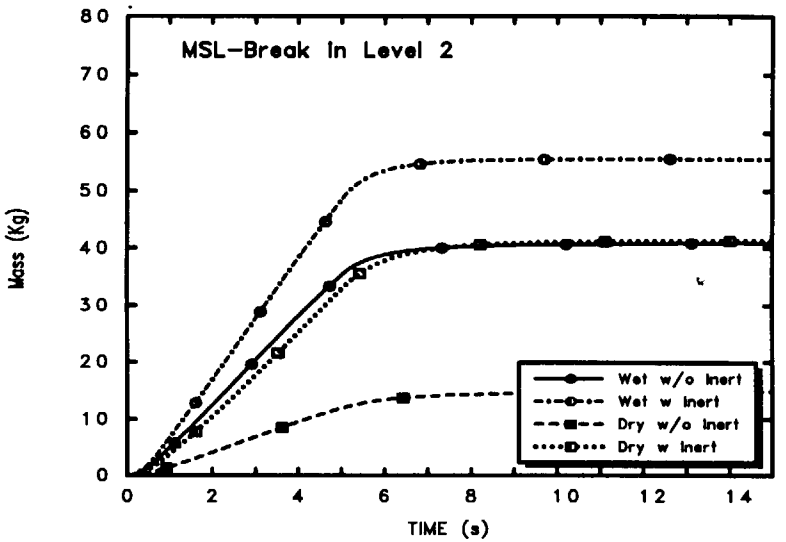

Figure A-6. Total Debris Deposited in Drywell

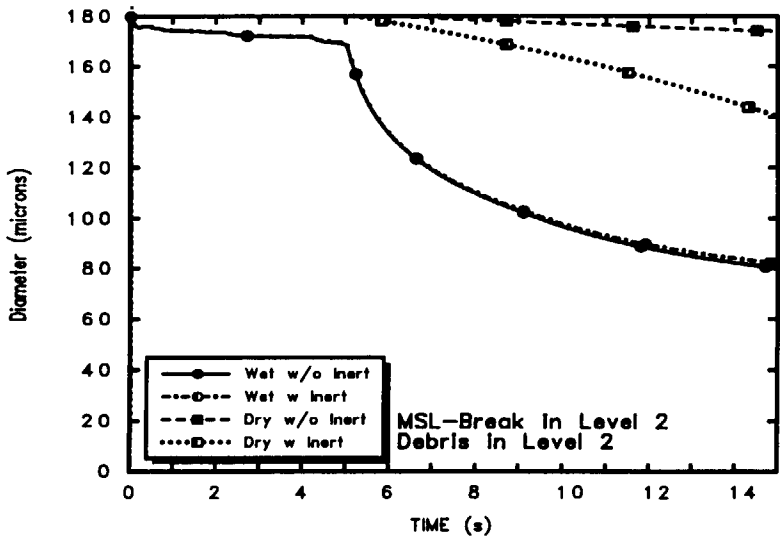

Figure A-7. Debris Mass Medium Diameter

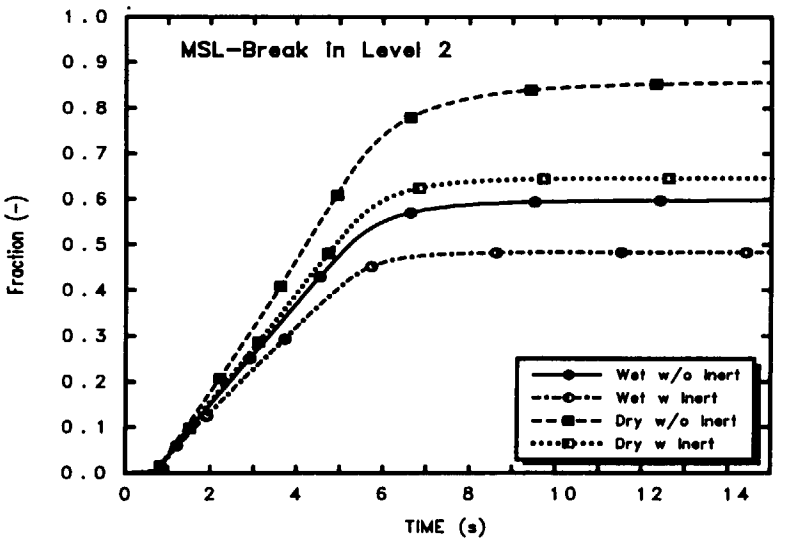

Figure A-8. MSL-2 Debris Transport Fraction

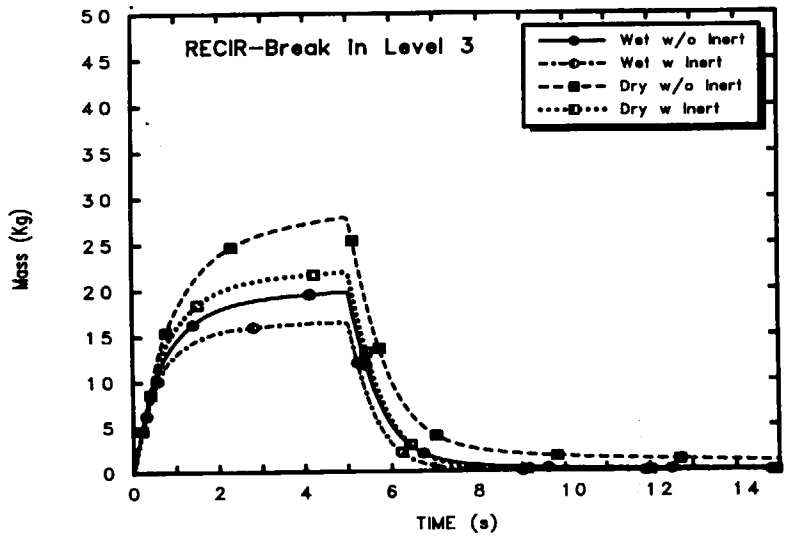

Figure A–9. Total Drywell Airborne Debris

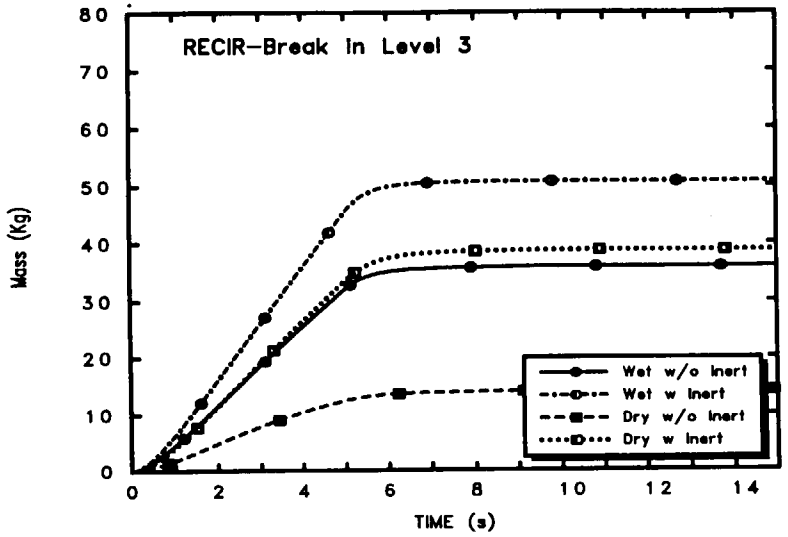

Figure A–10. Total Debris Deposited In Drywell

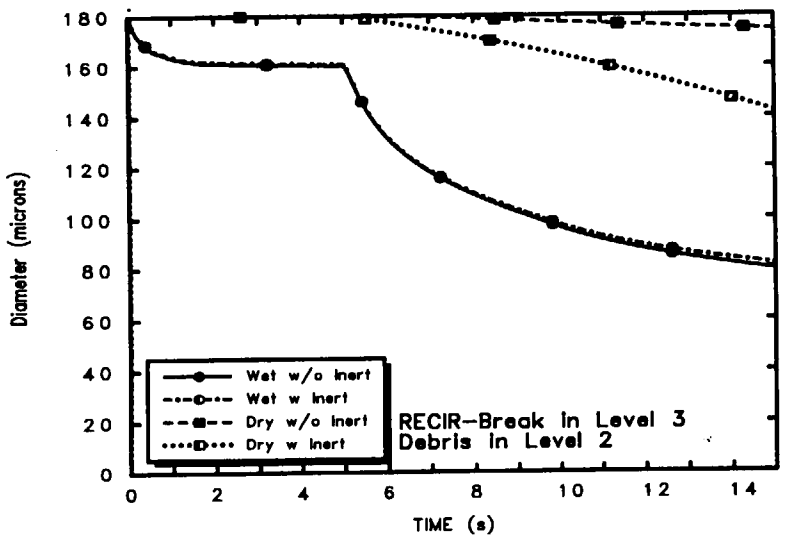

Figure A–11. Debris Mass Medium Diameter

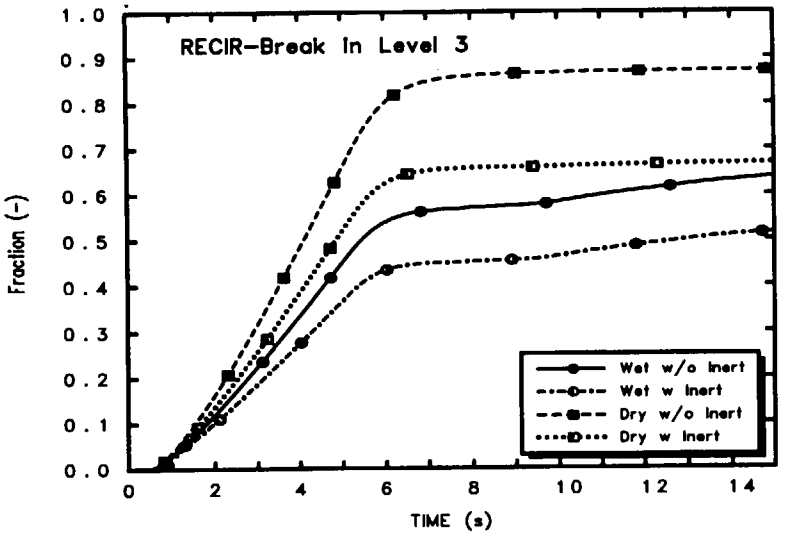

Figure A–12. Debris Transport Fraction

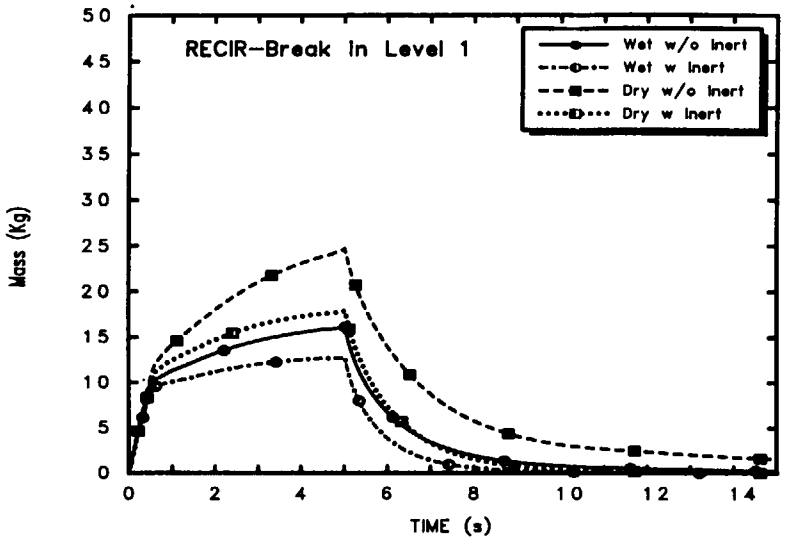

Figure A–13. Total Drywell Airborne Debris

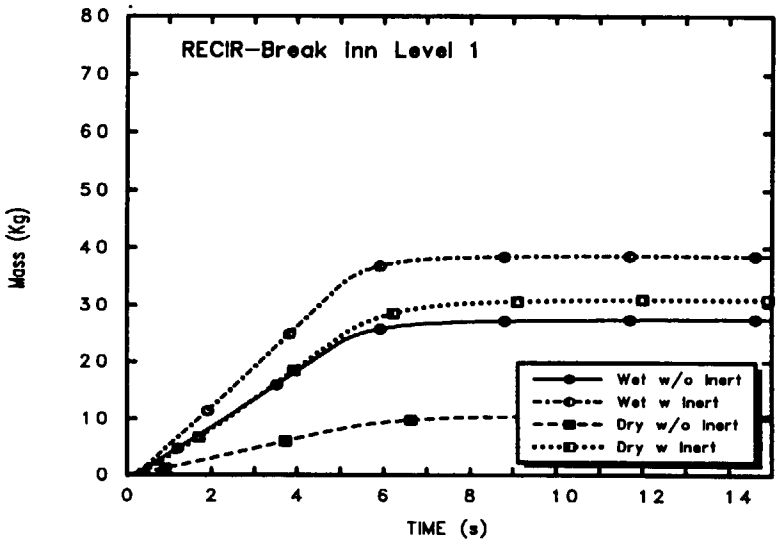

Figure A–14. Total Debris Deposited In Drywell

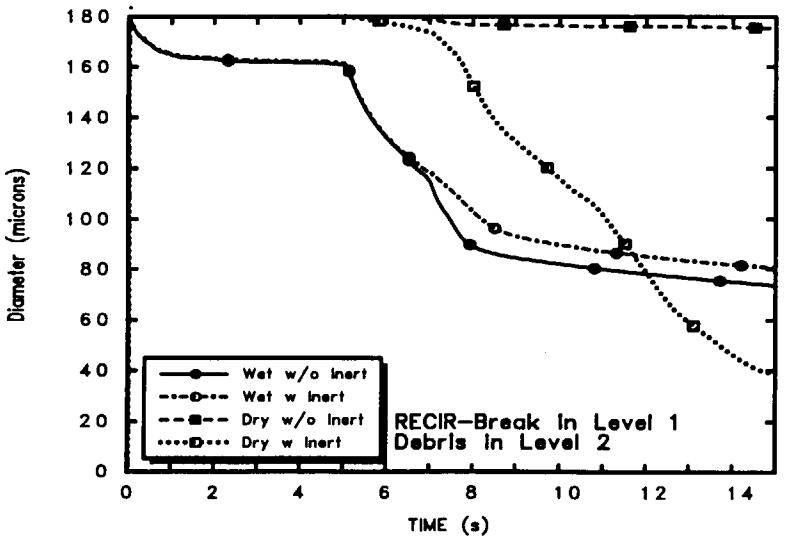

Figure A–15. Debris Mass Medium Diameter

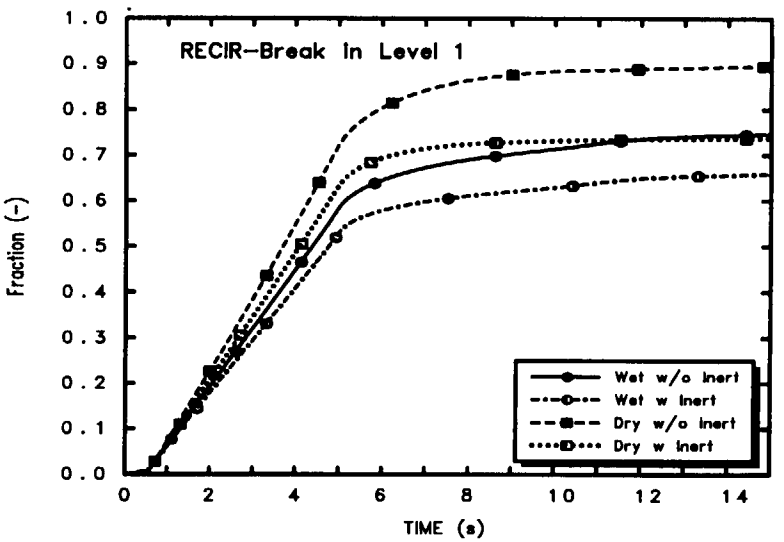

Figure A–16. Debris Transport Fraction

Appendix B

Thermal-Hydraulic Plots

Appendix B

List of Figures

Appendix B (Continued)

List of Figures

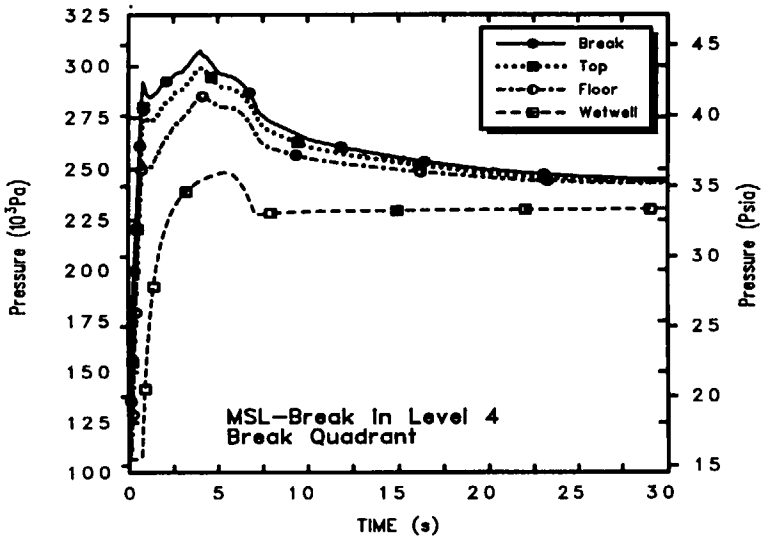

Figure B–1. Pressures

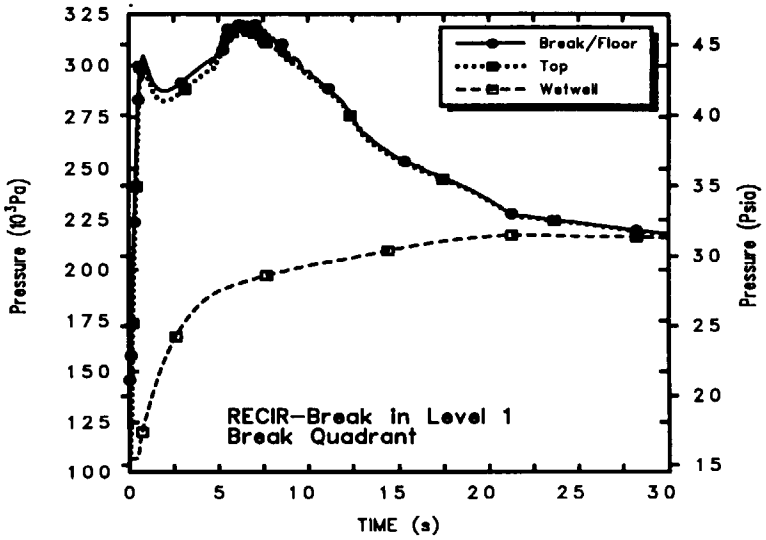

Figure B–2. Pressures

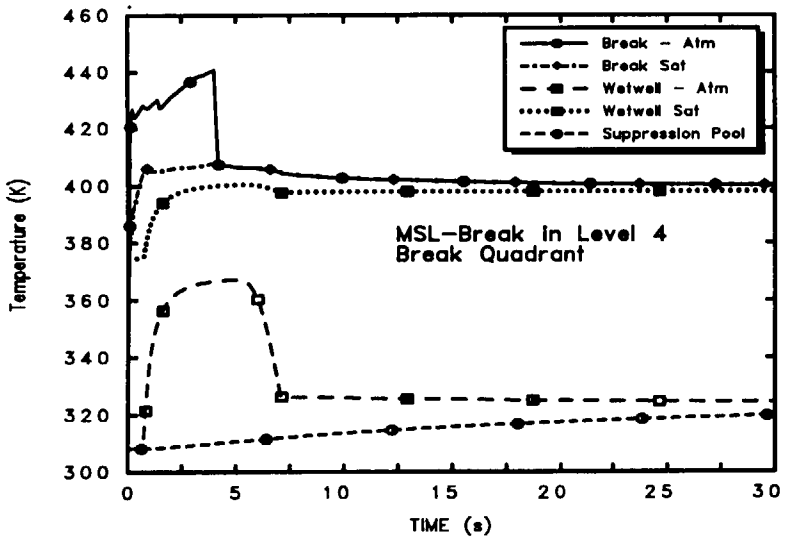

Figure B–3. Temperatures

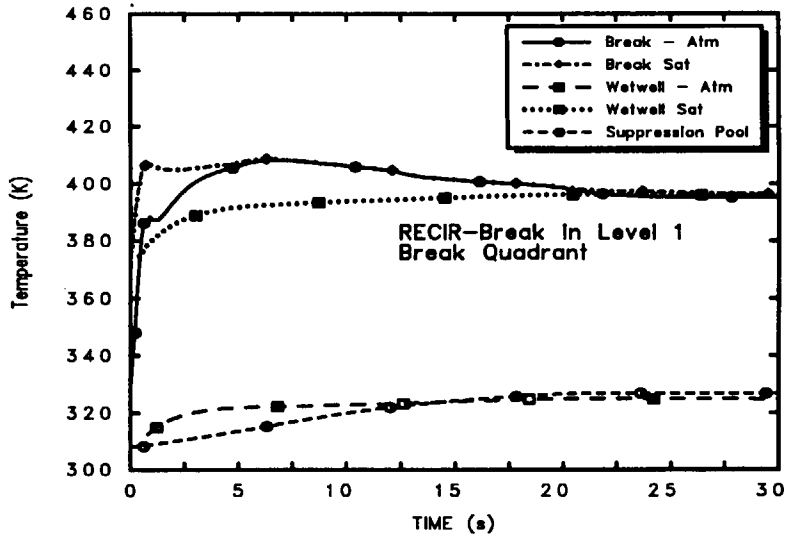

Figure B–4. Temperatures

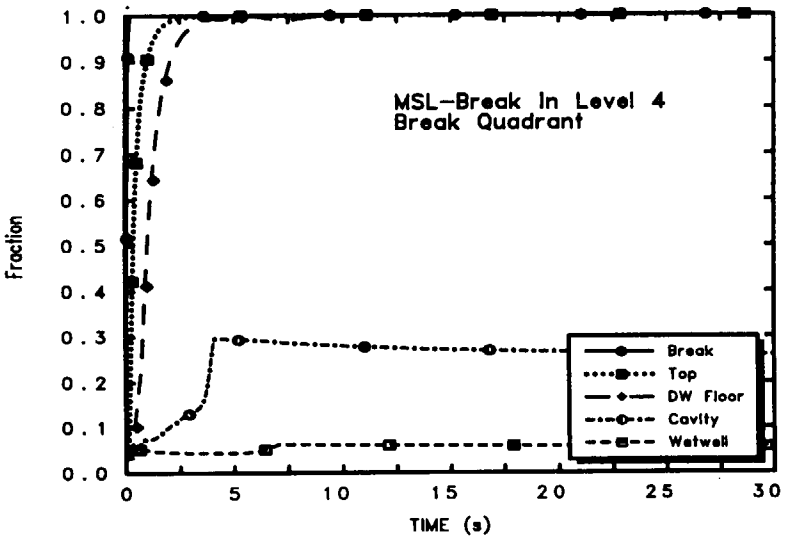

Figure B-5. Steam Mole Fractions

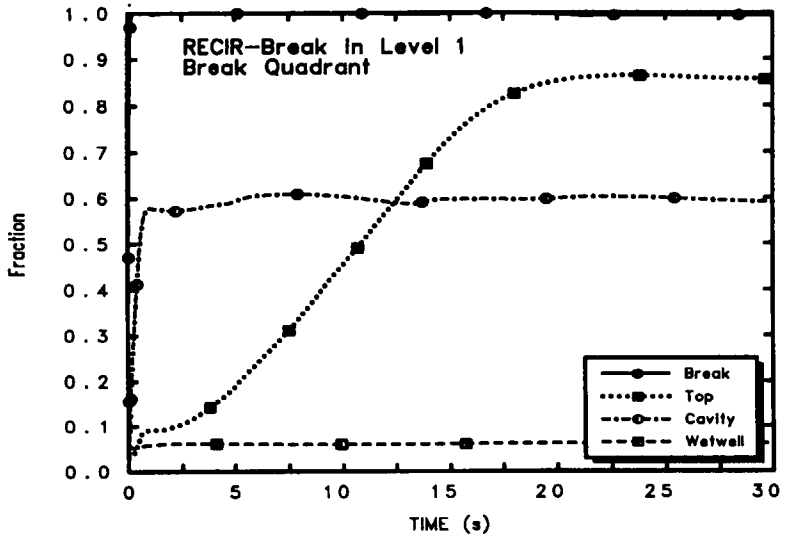

Figure B-6. Steam Mole Fractions

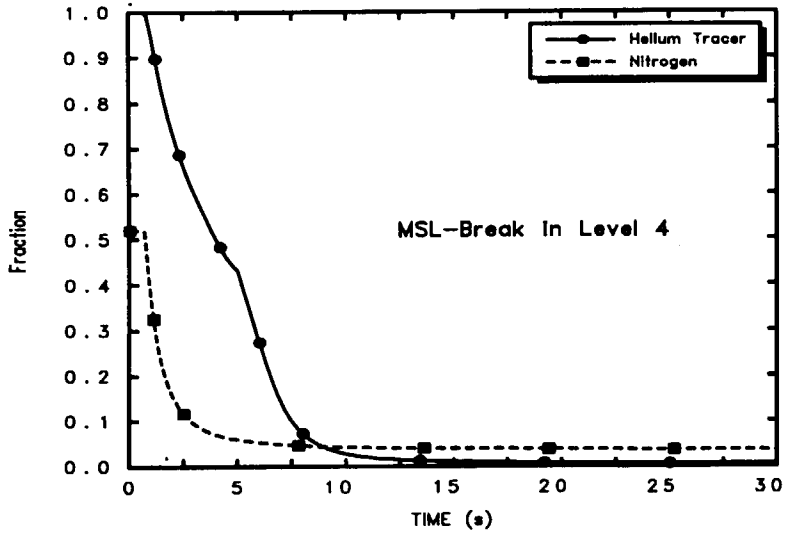

Figure B-7. DW Noncondensible Gas Mass Fractions

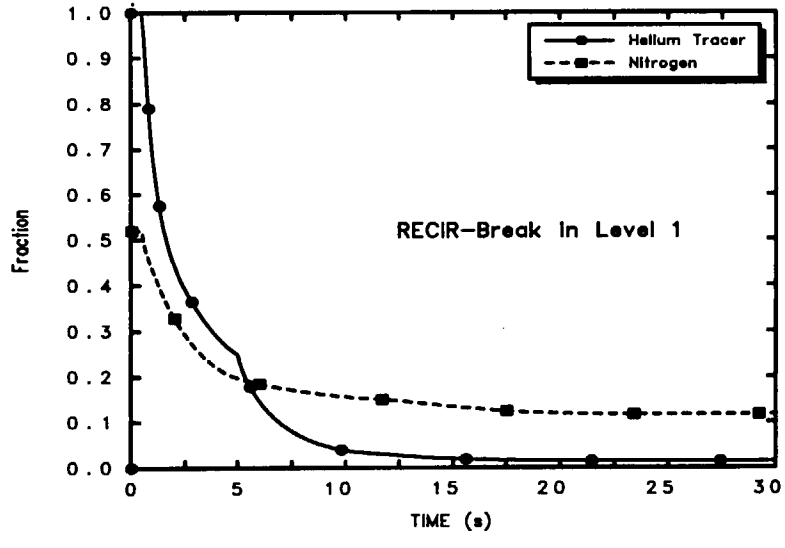

Figure B-8. DW Noncondensible Gas Mass Fractions

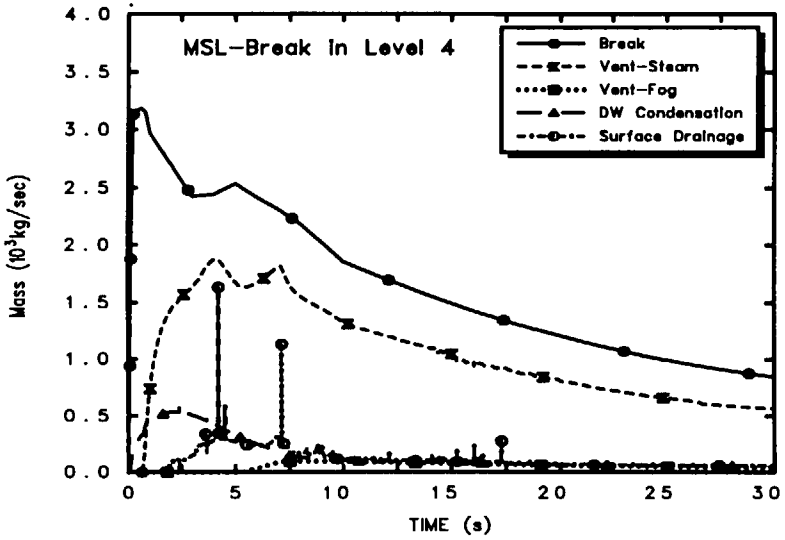

Figure B–9. Mass Flow Rates

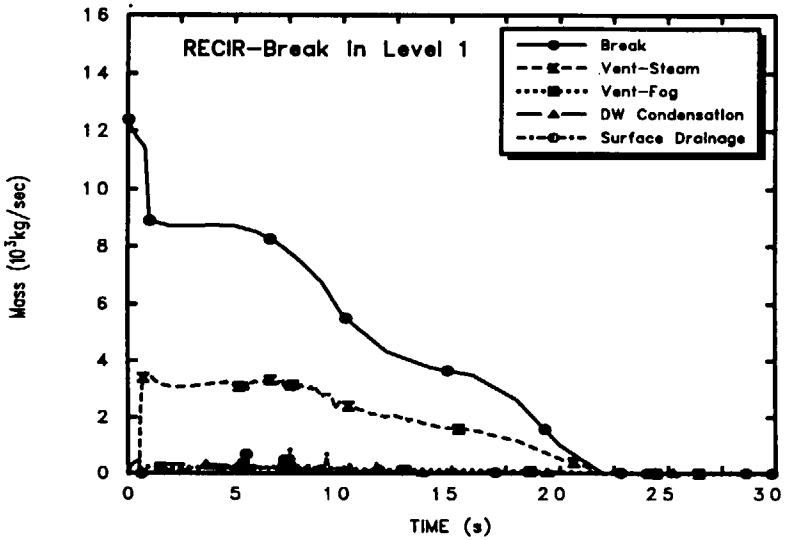

Figure B–10. Mass Flow Rates

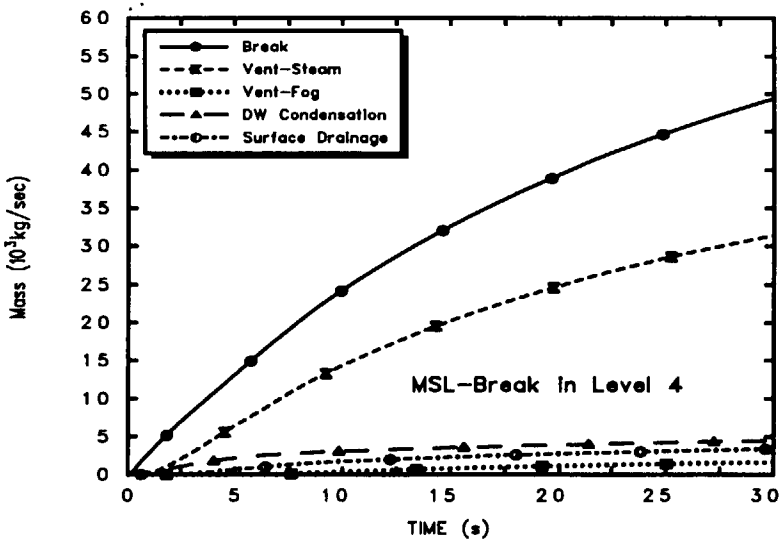

Figure B–11. Integrated Mass Flows

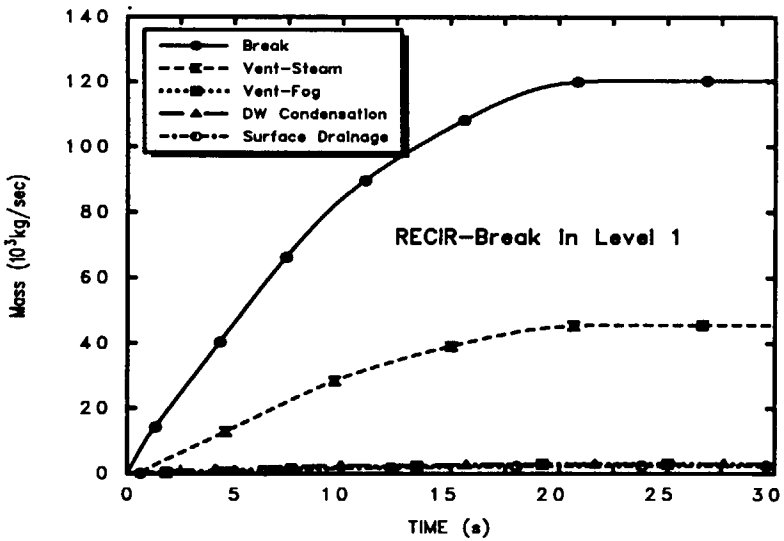

Figure B–12. Integrated Mass Flows

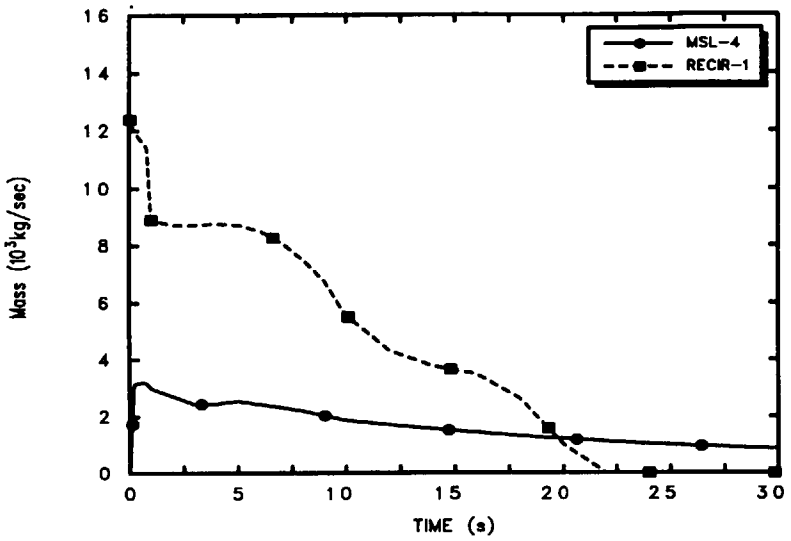

Figure B–13. Break Mass Flow Rates

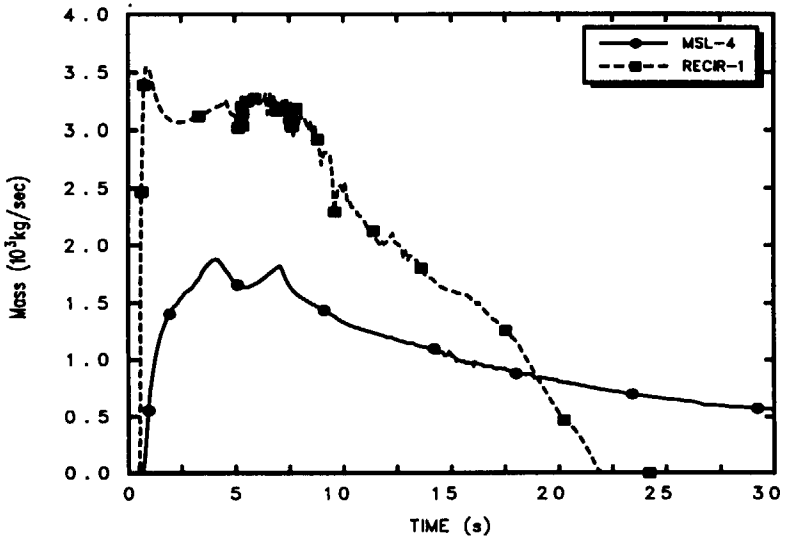

Figure B–14. Vent Steam Mass Flow Rates

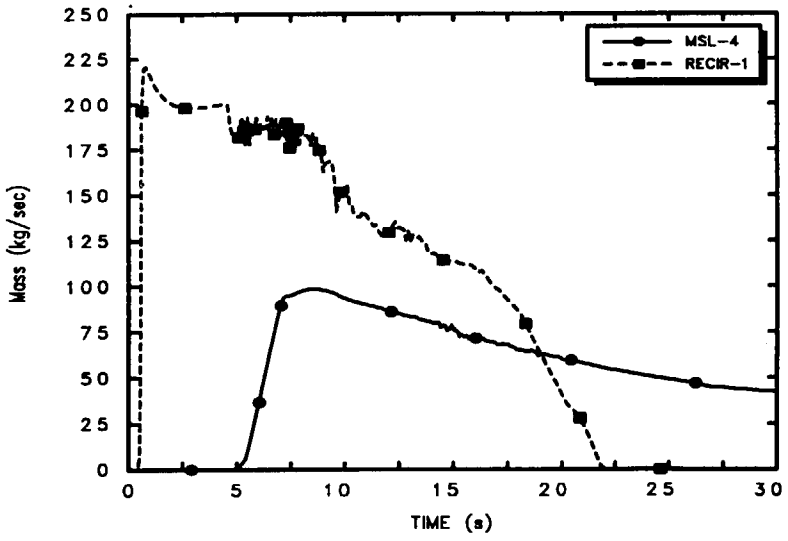

Figure B–15. Vent Fog Mass Flow Rates

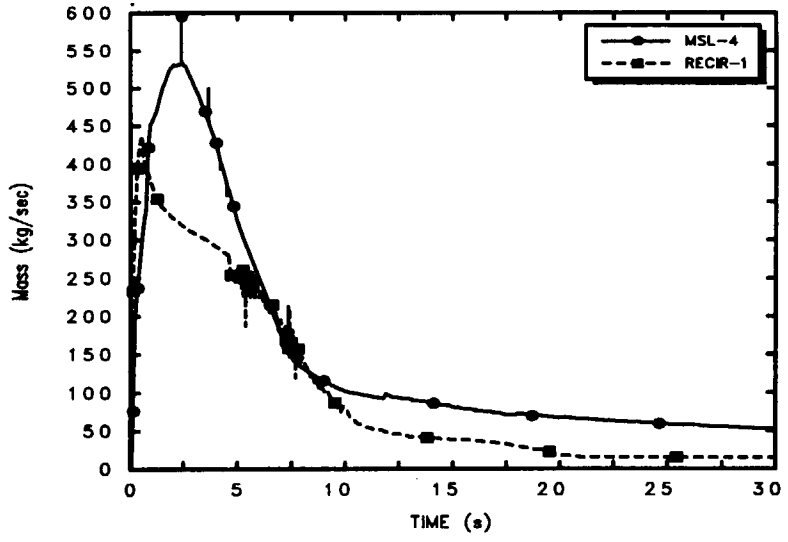

Figure B–16. Drywell Condensation Rates

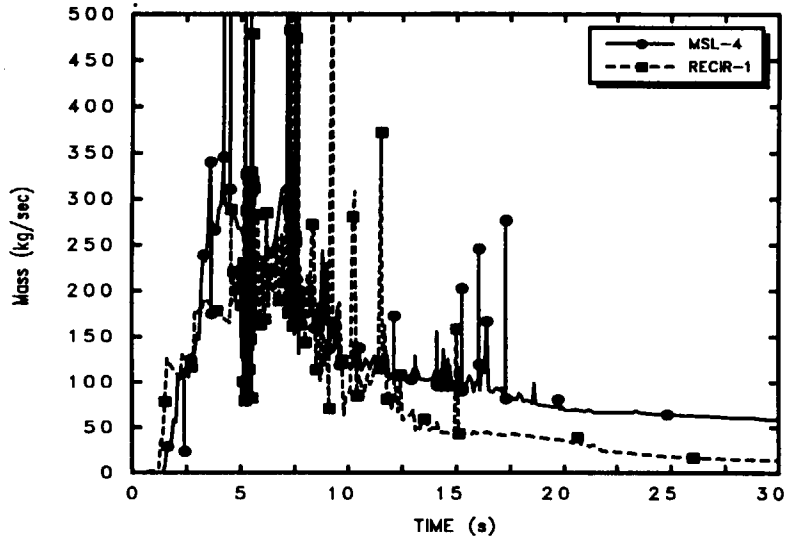

Figure B-17. Drywell Surface Drainage Rates

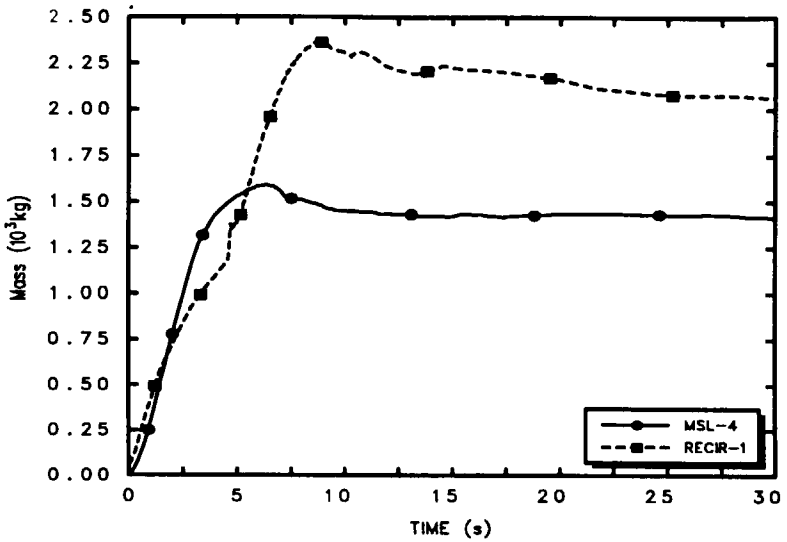

Figure B-18. Total Film Mass

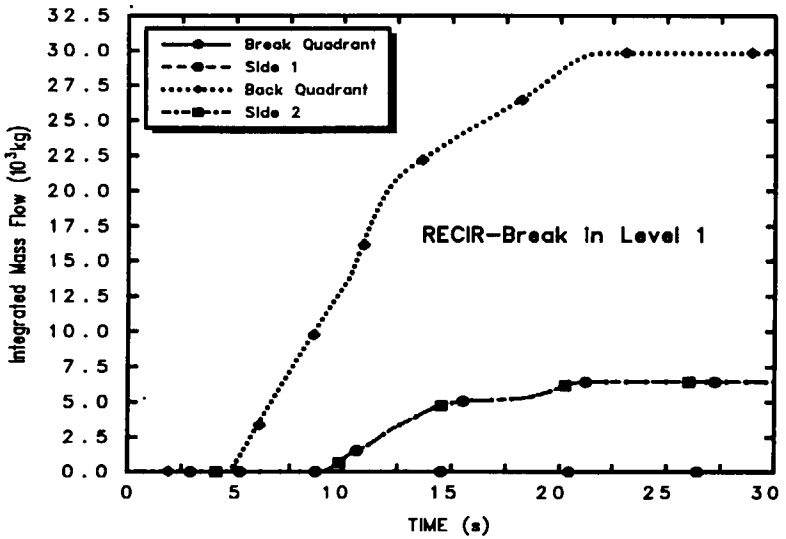

Figure B-19. Downcomer Water Flows

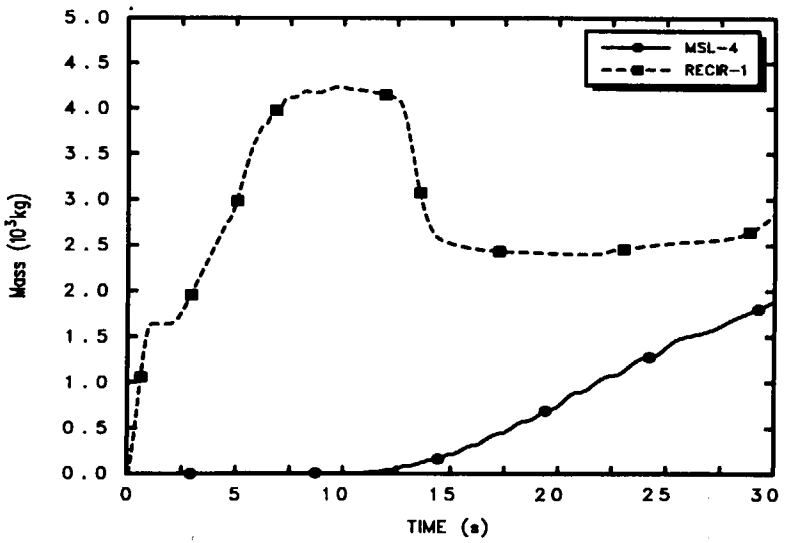

Figure B-20. Reactor Cavity Water Mass

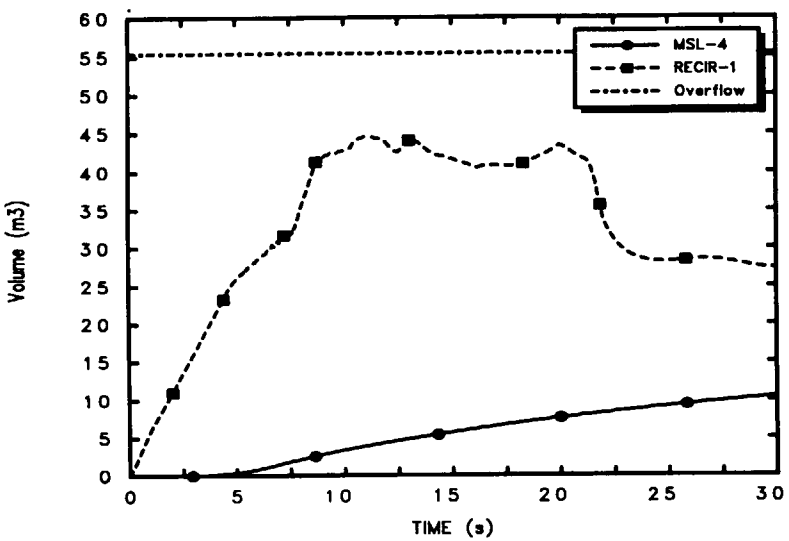

Figure B-21. Drywell Pool Volume

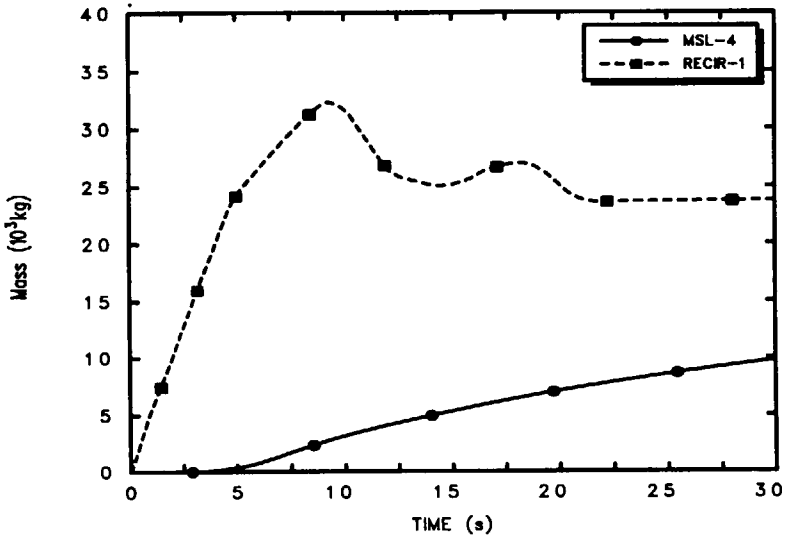

Figure B-22. Drywell Pool Mass

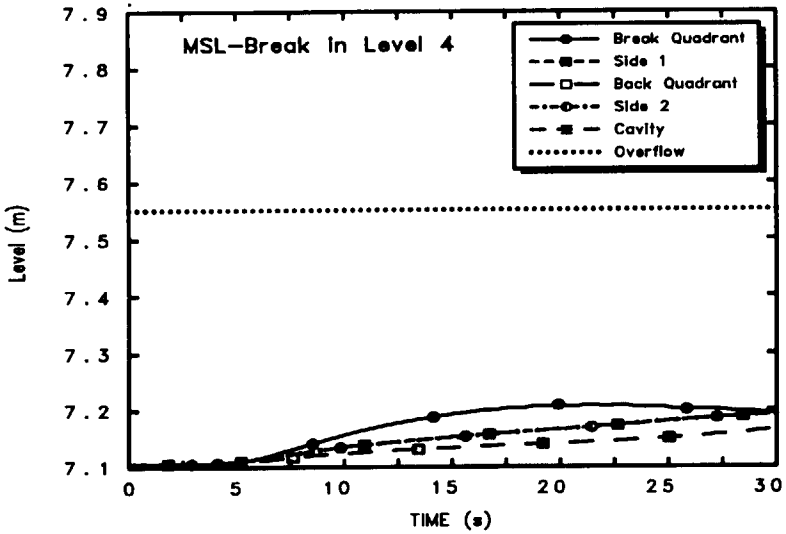

Figure B-23. Drywell Pool Levels

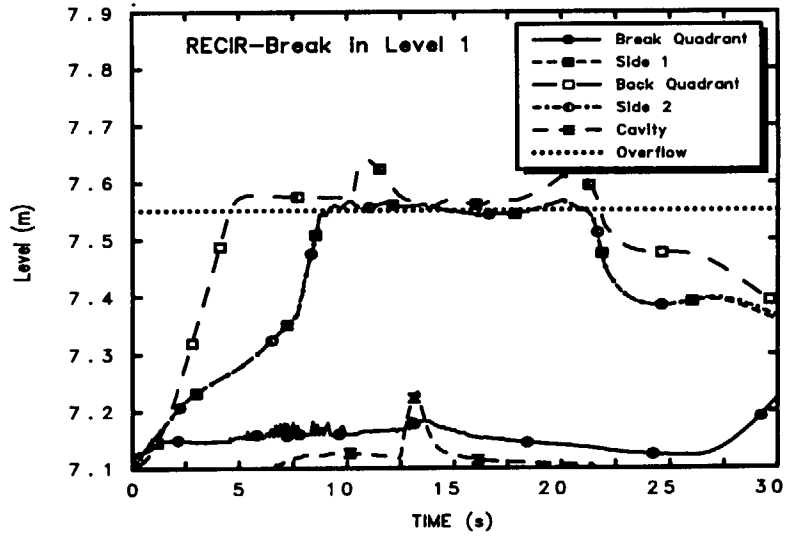

Figure B-24. Drywell Pool Levels

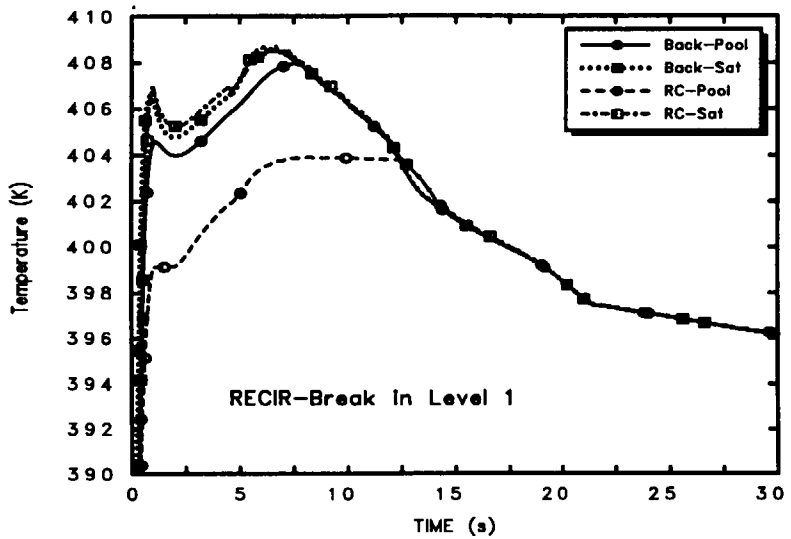

Figure B-25. DW Floor Pool Temperatures

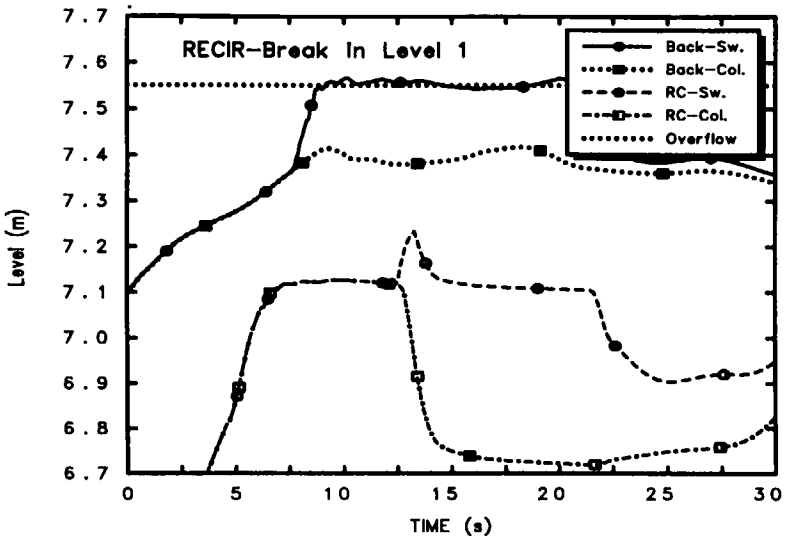

Figure B-26. DW Floor Pool Levels

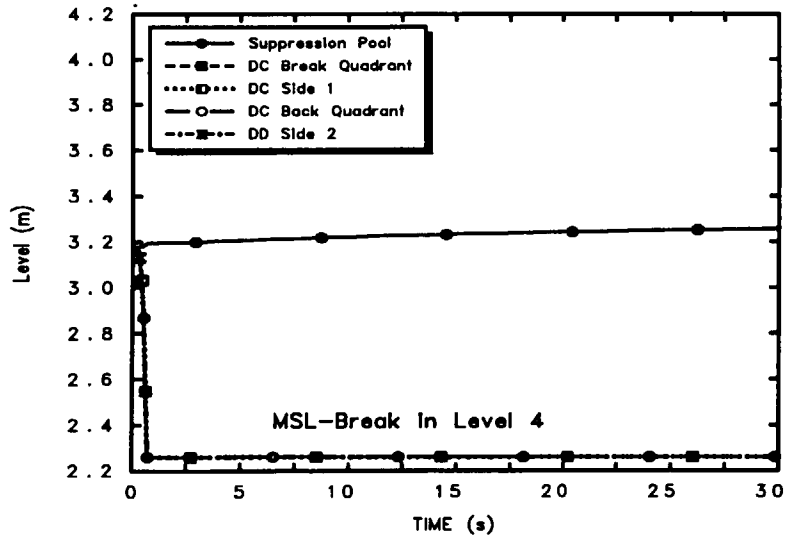

Figure B-27. Vent Downcomer Levels

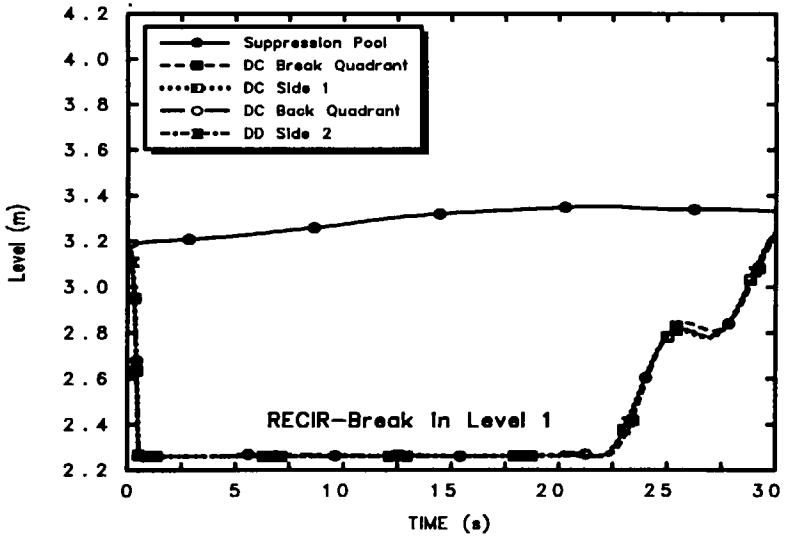

Figure B-28. Vent Downcomer Levels

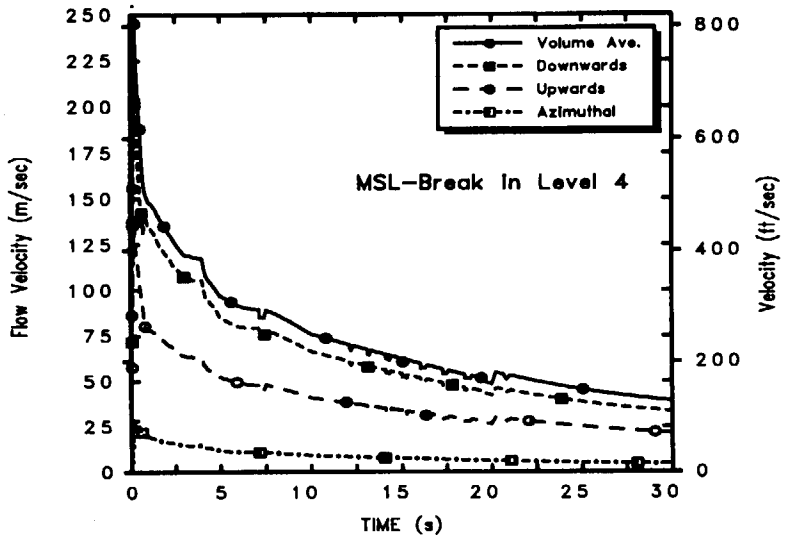

Figure B-29. Break Region Flow Velocities

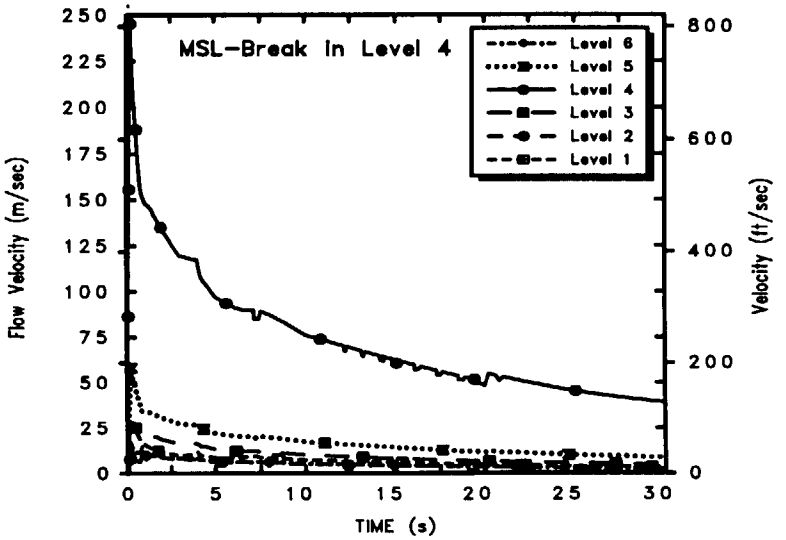

Figure B-30. Break Quadrant CV-Ave Flow Velocities

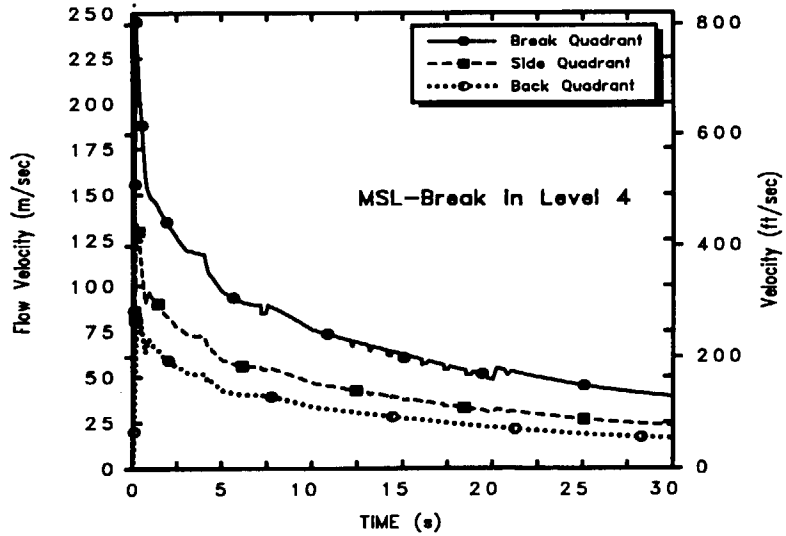

Figure B-31. Level 4 CV-Ave Flow Velocities

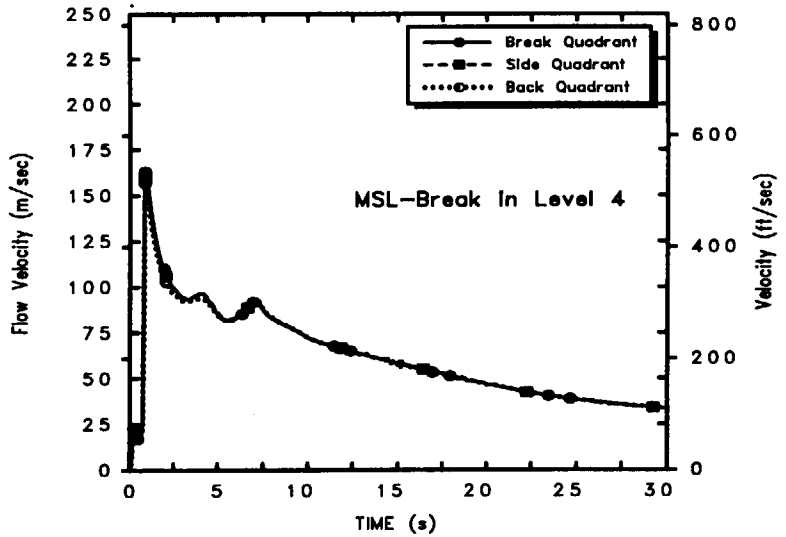

Figure B-32. Downcomer Flow Velocities

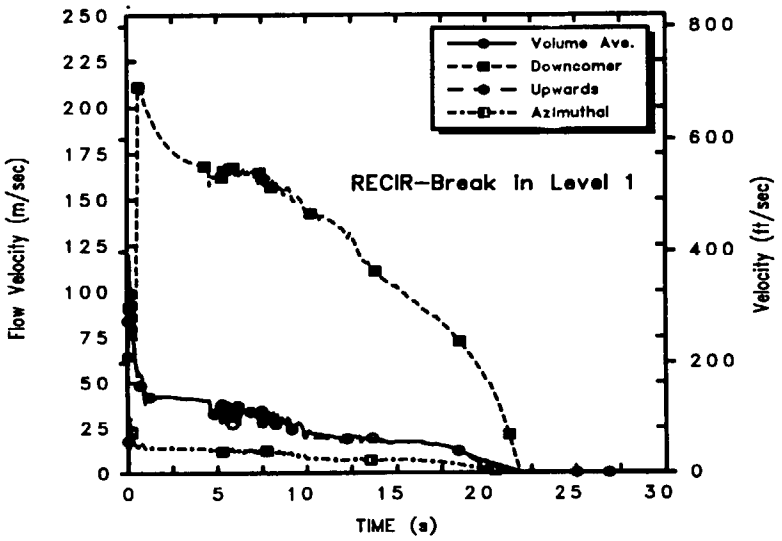

Figure B–33. Break Region Flow Velocities

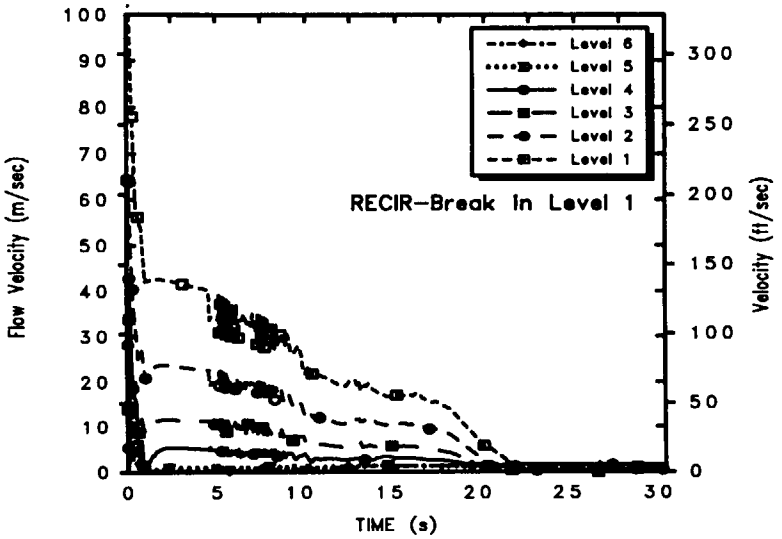

Figure B–34. Break Quadrant CV–Ave Flow Velocities

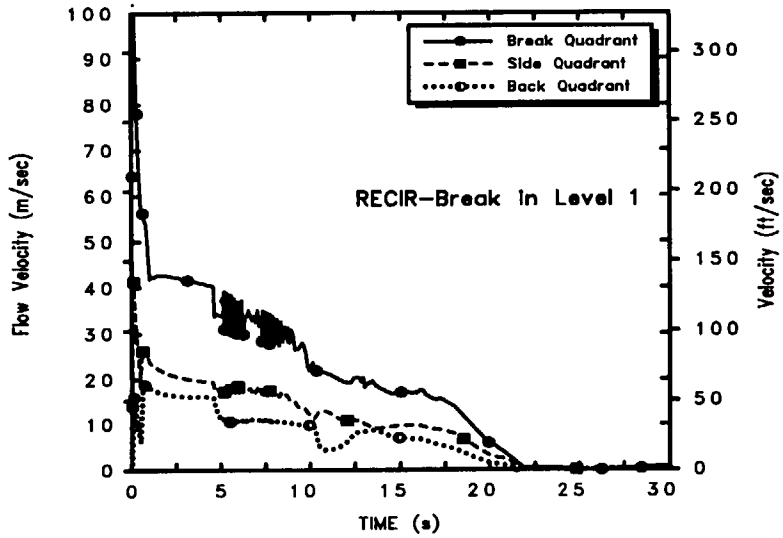

Figure B–35. Level 1 CV–Ave Flow Velocities

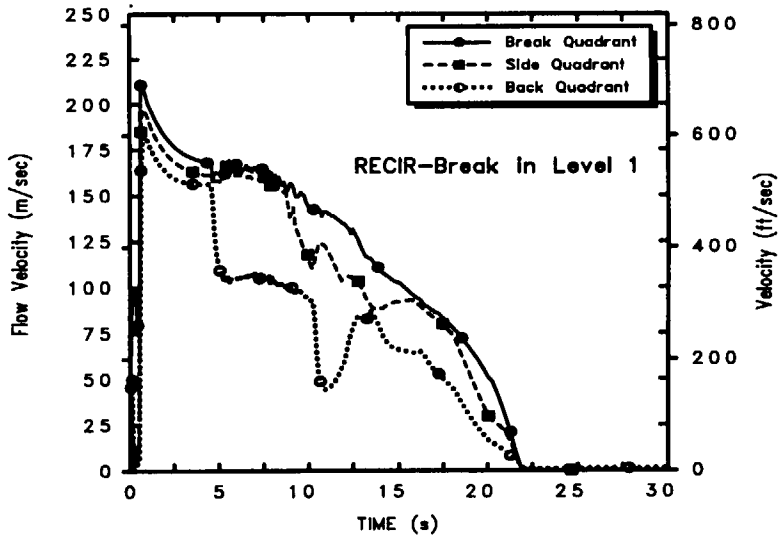

Figure B–36. Downcomer Flow Velocities

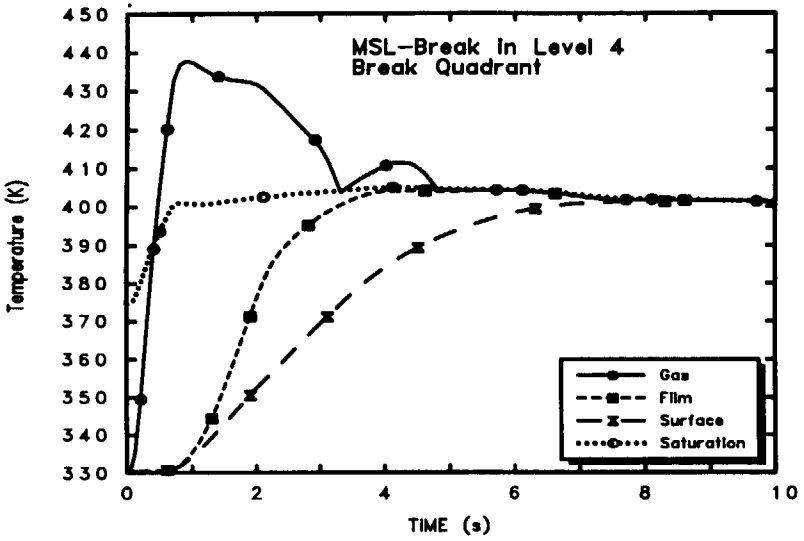

Figure B-37. Level 1 Vertical Surface Temperatures

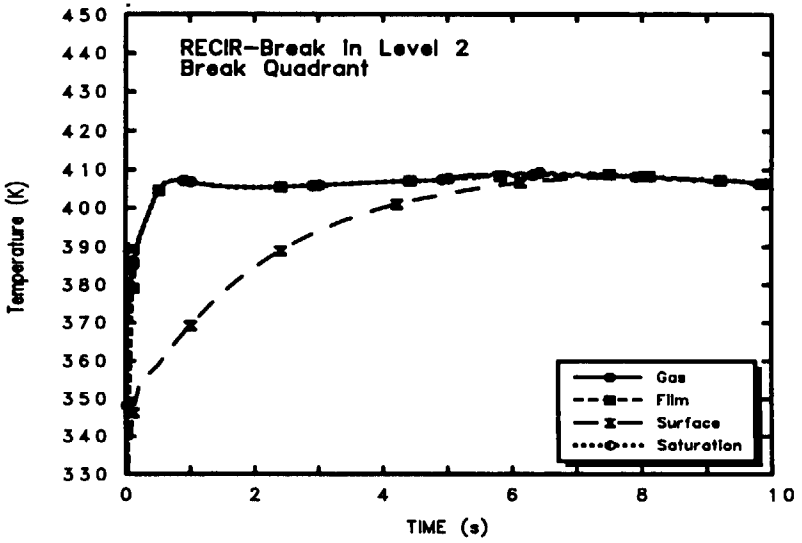

Figure B-38. Level 1 Vertical Surface Temperatures

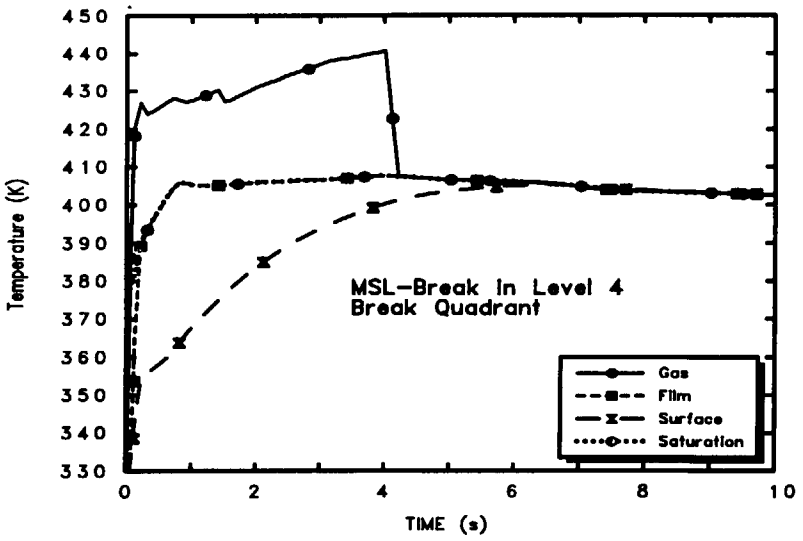

Figure B-39. Level 4 Vertical Surface Temperatures

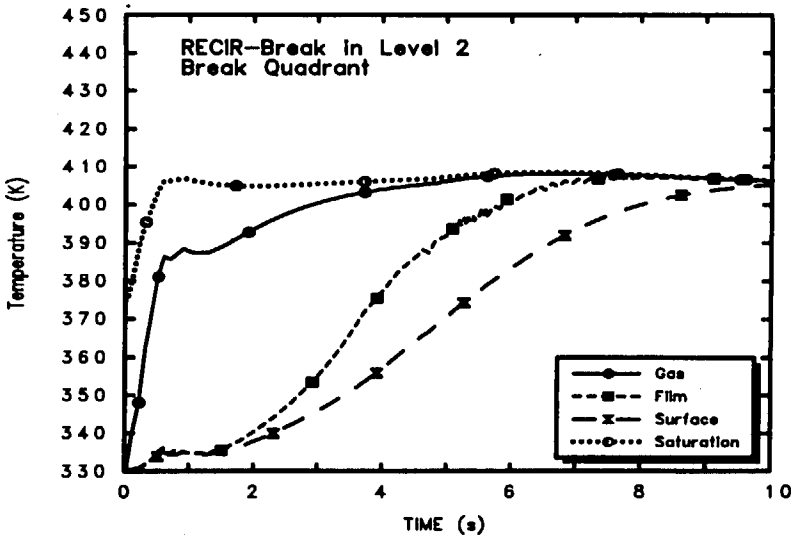

Figure B-40. Level 4 Vertical Surface Temperatures

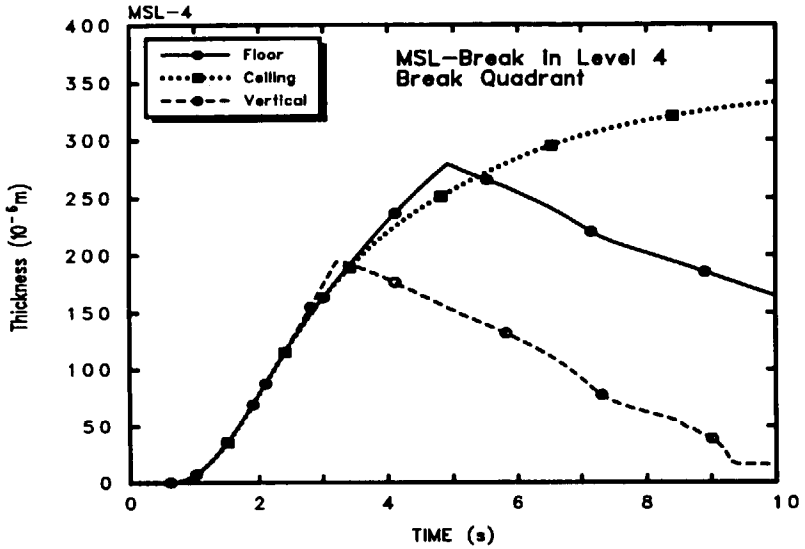

Figure B-41. Level 1 Film Thicknesses

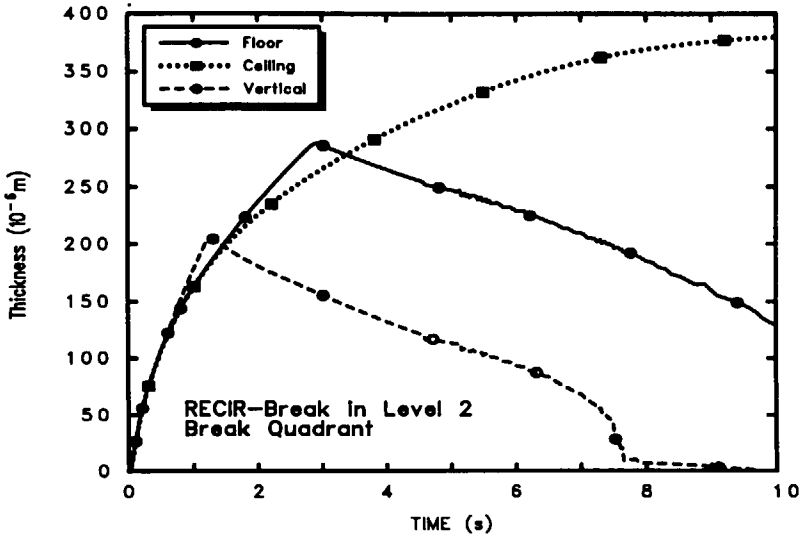

Figure B-42. Level 1 Film Thicknesses

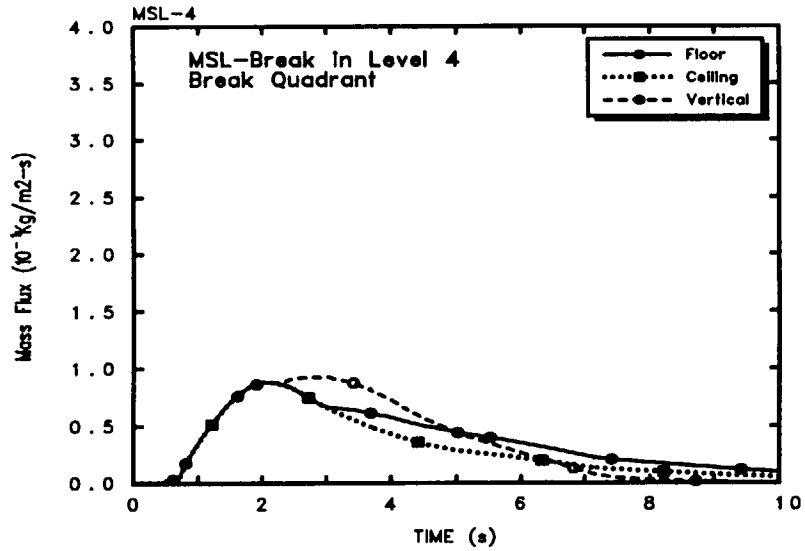

Figure B-43. Level 1 Mass Transfer Fluxes

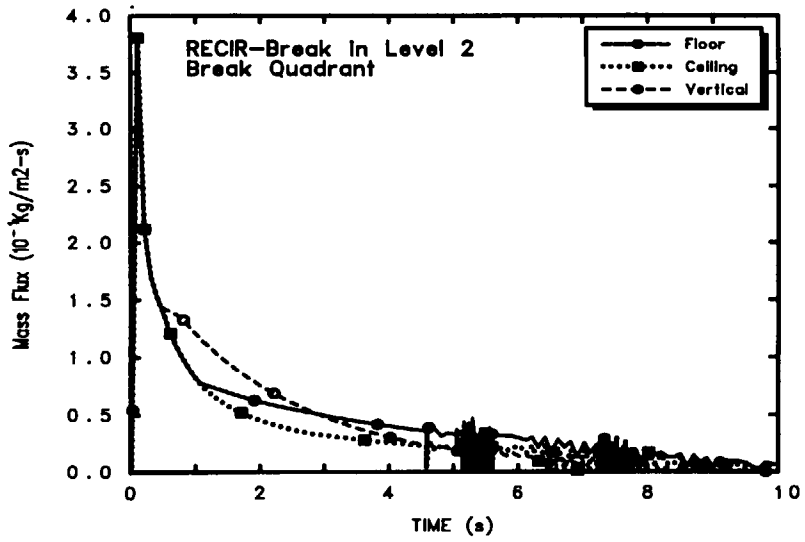

Figure B-44. Level 1 Mass Transfer Fluxes

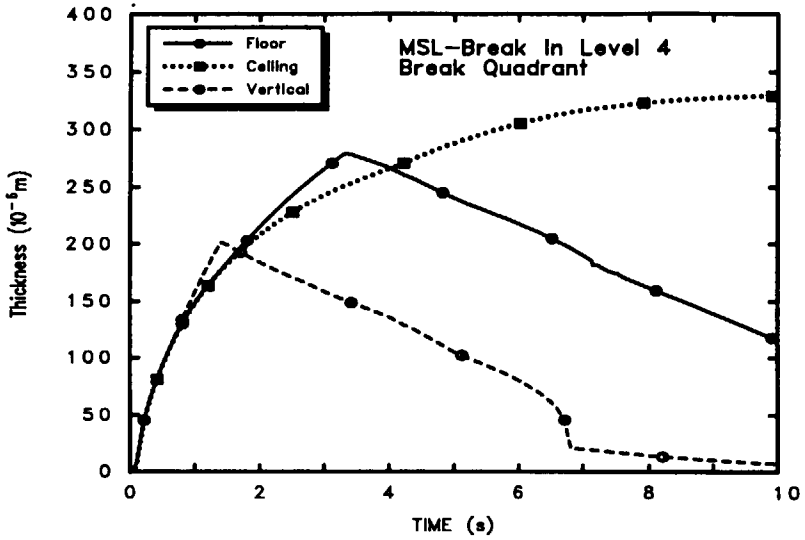

Figure B-45. Level 4 Film Thicknesses

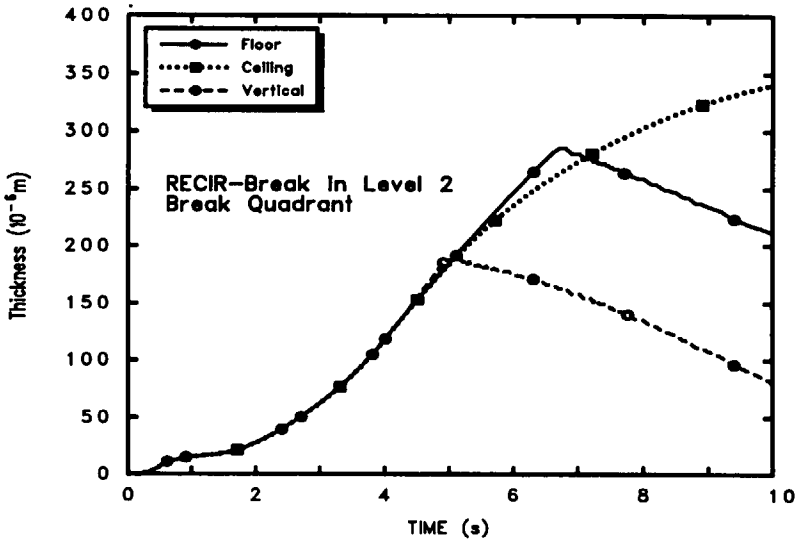

Figure B-46. Level 4 Film Thicknesses

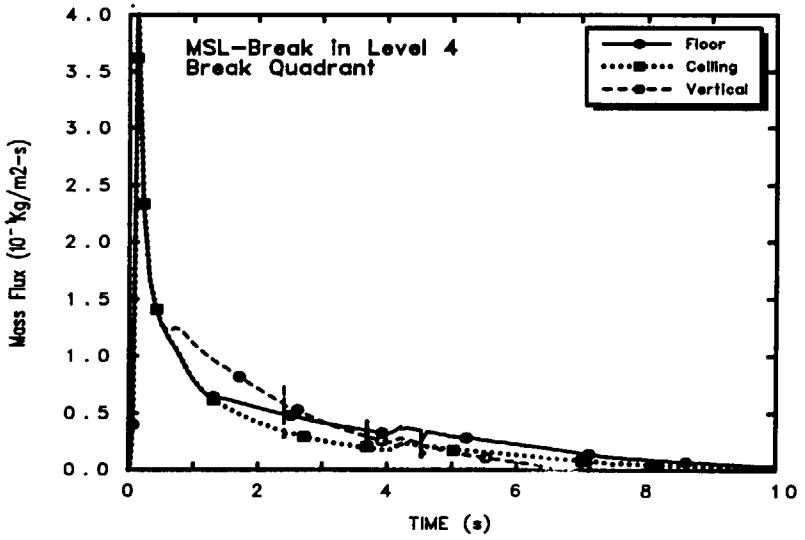

Figure B-47. Level 4 Mass Transfer Fluxes

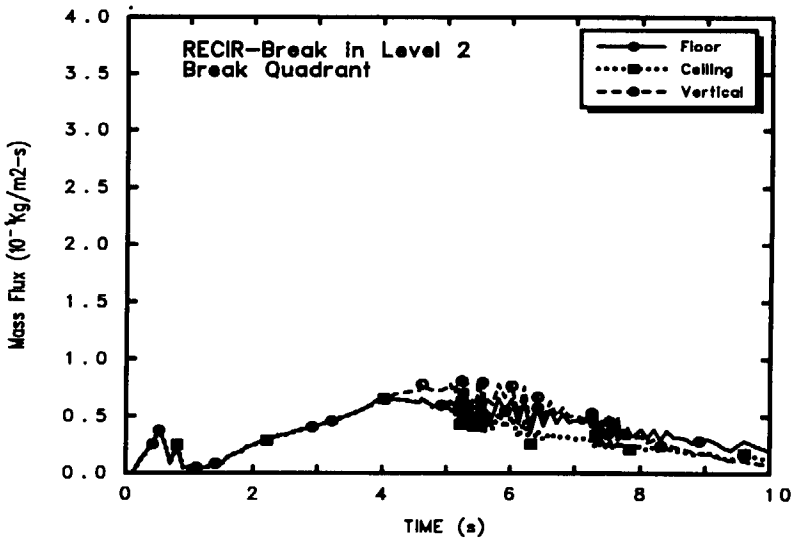

Figure B-48. Level 4 Mass Transfer Fluxes

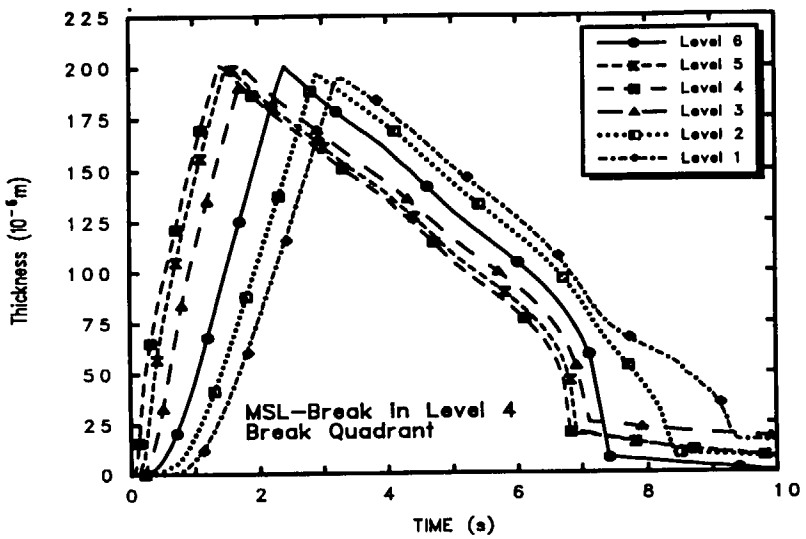

Figure B–49. Film Thickness on Vertical Surfaces

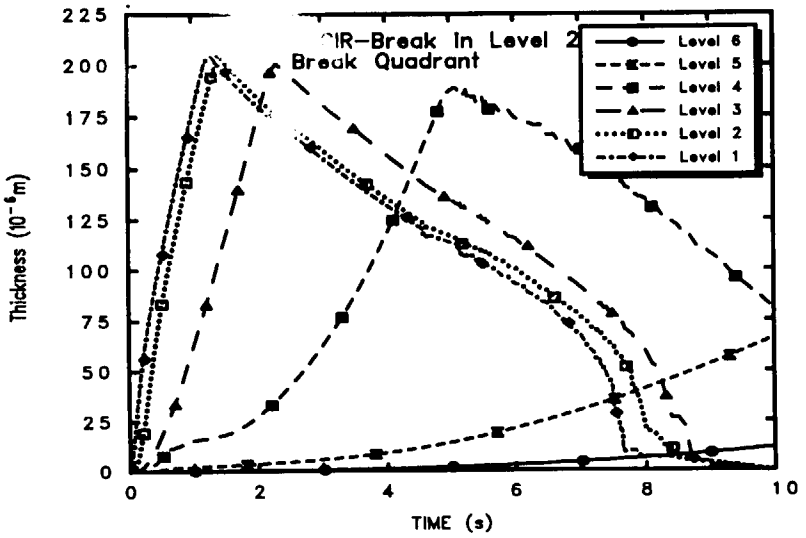

Figure B–50. Film Thickness on Vertical Surfaces

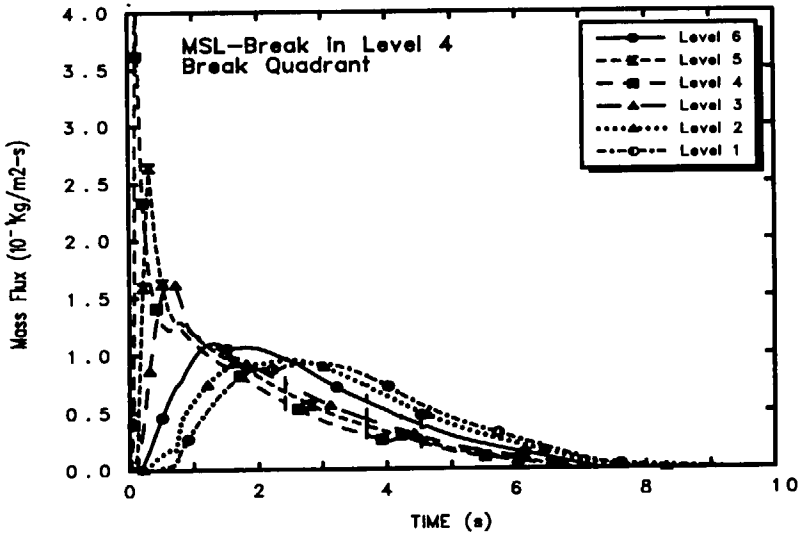

Figure B–51. Mass Transfer Flux – Vertical Surface

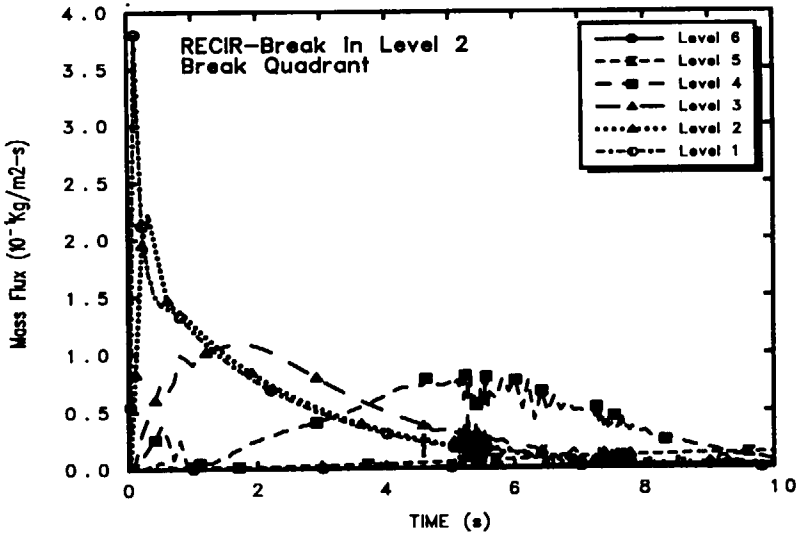

Figure B–52. Mass Transfer Flux – Vertical Surface

Appendix C
LOCA Debris Transportability in the Drywell Floor Pool: Interpretation of ARL/PPL Flume Transport Data

Table of Contents

List of Figures

List of Tables

C.1 INTRODUCTION

A Loss of Coolant Accident (LOCA) in a boiling water reactor (BWR) would destroy insulation located in the break vicinity and transport debris away from the break by blowdown and washdown flows. A fraction of this debris would reach the drywell floor where they may be deposited either by inertial capture (smaller debris) or gravitational settling (very large debris). Depending on the break location, the debris accumulated in the pool will range in size from individual fibers to undamaged blankets. The majority of the insulation debris can be categorized into three general size groups:

Small: The insulation debris of a light, loose, and well-aerated usually consisting of loose clusters of individual fibers. Typically these pieces were about 1.5-2" in size and possess little of the original structure or the chemical binding. In CEESI tests they were found to have been attached to the wet gratings. These debris were referred to as Grade-A debris in Ref. 1 and Type-E debris in Ref. 2. *The same debris are referred to as Sizes 3&4 in NUREG/CR-6224* [Ref. 3].

Medium: Insulation debris torn from the blanket by an air-jet impingement. These pieces keep some of the original structures in the inner regions, while they look torn-down or loose on the outside. Typically these pieces are about 6"x4" in dimension. In CEESI tests they were found to have been attached to the wet or dry gratings. These debris were referred to as Grade B in Reference 1 and Type D in Reference 4. *In NUREG/CR-6224, these pieces were referred to as Size 6.*

Large (L): The SEA Air-Jet tests conducted at the Colorado Engineering Experiment Station, Inc. (CEESI) have clearly demonstrated that large pieces produced from jet impingement tend to retain most of their original structure. These blanket pieces ranged in size from 10"x 10" to 18" x 18" depending on the availability of insulation. Generally they are about ¼- ½ inch in thickness. *This type of debris was not used in the ARL tests, nor were they studied as part of the NUREG/CR-6224 study.*

Depending on accident progression, a pool is expected to form on the drywell floor following blowdown as a result of water being added by either break overflow or containment spray. For Mark I and several Mark II containments, The pool is typically 6"-24" deep. For Mark III containment, the drywell pool would be several feet deep. It is important to understand transportability of debris in the drywell pool where flow is expected to be characterized by large scale anisotropic turbulence.

In 1994, Alden Research Laboratories, Inc. (ARL) conducted a series of experiments under the sponsorship of Pennsylvania Power and Light Company (PPL) to study the transportability of various sizes of fibrous insulation debris under conditions judged to be prototypical of a BWR drywell floor

[Ref. 1]. In these tests, ARL employed a flume 22-inches wide, 16-inches deep and 18-ft long. Inlet flow was forced through a series of flow straighteners that acted to reduce inlet turbulence and spread the flow uniformly across the flume flow cross-section. Figure 1 is a schematic illustration of the test facility. As shown in this figure, the test facility employed three 1-inch diameter downcomers to add higher velocity vertical flow to the flume as a means of introducing turbulence to the flume. Pre-soaked (wet) debris was introduced 2-ft upstream of the first downcomer and collected approximately 2-ft downstream of the third downcomer, which provided an active transport region of approximately 8.2-ft. In some tests a weir 12-inch in height was used to examine transportability of debris over weir-like obstacles (e.g., off-set downcomers raised from the floor etc.). Debris was collected approximately 2-ft downstream of the last downcomer using a coarse screen that allowed for measurement of vertical concentration distribution. These measurements were augmented by visual observation of debris transport. Based on the test results, transportability of debris (i.e., condition when the debris remains fully entrained with water both vertically and horizontally) was related to three parameters: a) size and type of the debris, b) transport velocity and c) specific input energy. Size and type of debris refers to the size of the debris which varied from Small to Medium (Note: ARL referred to these sizes as Grade A and Grade B). The transport velocity refers to the area averaged water velocity calculated as:

$$U_{tr} = Q_{flume}/A_{flume}$$

where,

U_{tr} = transport velocity (ft/s)

Qflume = volumetric flow rate (ft^3/s)

Aflume = Cross-sectional area of the flume (22-inch x 16-inch in ft^2)

The specific kinetic energy is defined as the energy per unit fluid volume added to the flume as a result of downcomer flow, given by:

$$E = \bullet\, Q_{dc} \bullet H/(d.w.l)$$

where,

E = Specific input energy ($lb\text{-}ft/sec/ft^3$)

• = density of water (lbm/ft^3)

Q_{dc} = down-comer flow (ft^3/s)

•H = average difference in static pressure between downcomers and the flume (ft-water)

LIST OF ITEMS

A	15 hp Centrifugal Pump	F	Downcomer flow equalizing valves
B	Total flow control valve	G	Insulation presoaking and dumping rig
C	12" x 6" Venturi flow meter	H	Flow straighteners
D	Transport flow control valve	I	Insulation collection screen
E	3" x 2" Orifice flow meter	J	Downcomer flow control valve

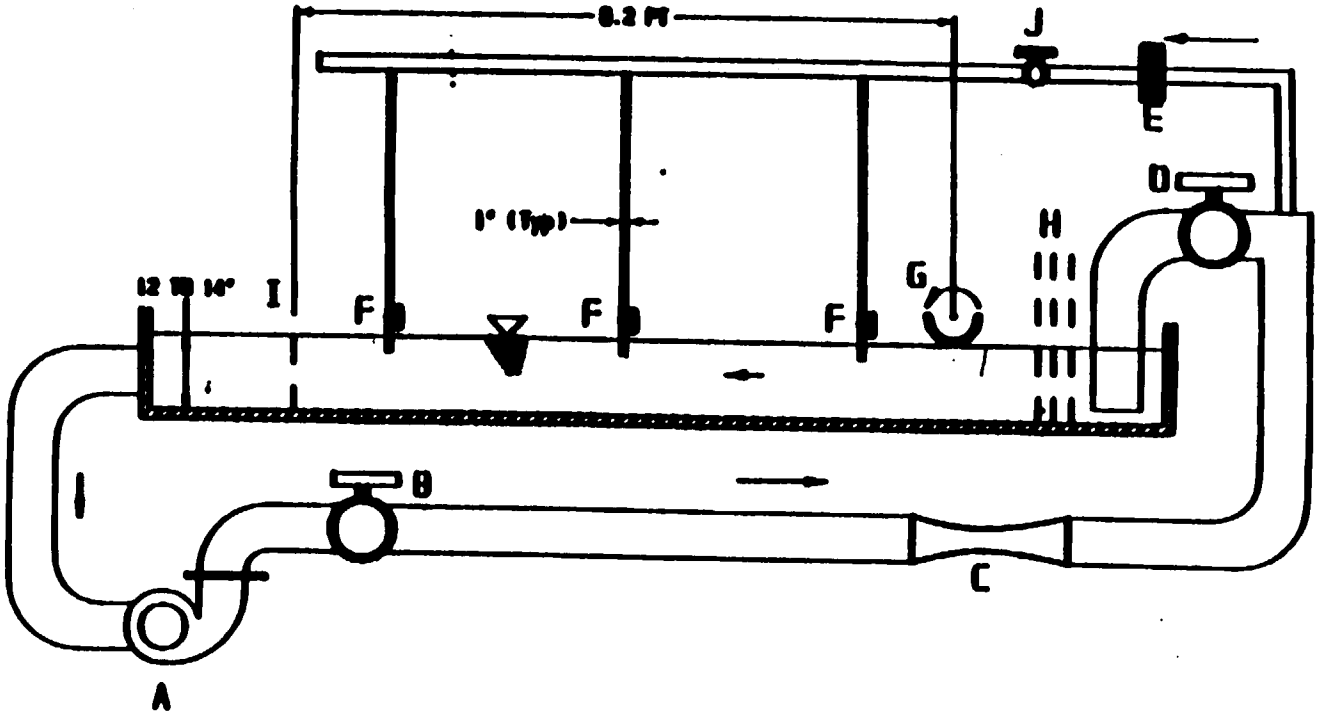

Figure 1 ARL/DPL FLUME TEST FACILITY

d, w, l = depth, width and active length of the flume (ft); active length of 8.2-ft was used to estimate E instead of the total flume length of 18-ft.

ARL's approach of relating debris transportability to specific kinetic energy is a widely used method. For example, such methods are often used to estimate levels of turbulence required to keep macro-particles in suspension in sludge pools and to estimate particle concentrations in the settling columns. In all of these applications, isotropic turbulence is expected throughout the pools, which facilitates application of first-order methods. On the other hand, turbulence in the drywell pools is not expected to be isotropic, but localized to regions closer to the location where break flow is added to the pool and possibly closer to the vent entrances. As a result, the first-order methods do not lend themselves to extrapolation to the type of flow situations where local turbulence levels govern particle settling. The objective of the present study was to use a commercially available CFD code to simulate the ARL tests and draw insights related to local turbulence energies required to fully entrain the debris and transport them with the flow. Thus determined, turbulence levels can then be used in conjunction with CFD simulation of drywell pool flow to determine whether or not debris of a particular size will transport to the downcomers.

C.2 CFD Simulation of ARL Flume Tests

A commercially available CFD code CFD-2000 was used in this study. This code has been thoroughly validated for incompressible single-phase flows, such as those of present interest. Figure 2 presents the CFD simulation of the ARL test facility. From this figure, the CFD simulation does not model the flow straighteners and other devices used by ARL to straighten the flow and dampen inlet turbulence. Instead, the similitude starts 2-ft upstream of the downcomer with an inlet boundary conditions that prescribes uniform inlet velocity and 1% turbulence (judged to be representative of ARL test conditions). The turbulence intensity was entered as the percentage of the incoming flow that is turbulent. Three downcomers (each 5.45×10^{-3} ft^2 in cross-section) were placed at 2-ft, 4-ft, and 6-ft from the entrance. In one series of simulation a wier 12-inch in height was placed 8-ft from the entrance. No slip wall-boundary condition (friction drag) was used to simulate flume bottom and two side walls. Finally, downcomers were treated as blockages with a no-slip boundary condition.

A total of 10,000 elements were used to simulate the test section, although no noticeable increase in code accuracy is noted beyond 1,000 elements. More elements were placed closer to the downcomer

and near the weir where flow is expected to undergo severe changes. Automatic time step option was used to simulate transient response. Typically time steps varied between 0.008 s to 0.3 seconds.

In each case, the code was provided with prescribed inlet velocity through all four inlets (i.e., flume inlet + 3 down-comers). Inlet turbulence levels were restricted to 1% in case of flume inlet and 2% in case of downcomers to simulate what is described as calm entrance conditions. Transient analysis was allowed to run until flow fields reached steady state, at which time the simulation was stopped and the flow fields and kinetic energy levels were output.

C.3 Selection of ARL/PPL Tests for Simulation

ARL conducted over 50 tests that simulated a variety of flow velocities and turbulence levels. A total of seven tests were simulated in this study. Table 1 provides a description of the tests simulated and the observations reported by ARL.

Table C-1. ARL/PPL Tests Selected for CFD Simulation.

ID	U_{tr} (ft/s)	V_{dc} (ft/s)	$\bullet H_{dc}$ (ft-H_2O)	Wier	Debris Transportability
1	0.27	0.0	N/A	N	All debris (Grades A ad B) settled to the floor. Smaller debris rolled on the floor. Larger debris settled within 2-ft from where it was introduced. (see Figure 5 of Ref. 1)
2	0.56	0.0	N/A	N	Same as above.
3	1.00	0.0	N/A	N	Grade A was lifted from the floor. It became fully mixed with water column. Grade B debris settled to the flume floor. (see Figure 5 of Ref. 1)
4	0.27	2.7	0.4	N	Grade A debris was fully mixed. Grade B debris settled to the flume floor. (see Figure 7 of Ref. 1)
5	0.56	5.5	1.2	N	All debris (Grades A and B) became fully mixed with water column. Paint chips also became suspended and remained in suspension till they left the active section. (see figure 7 of Ref. 1)
6	0.27	0.0	N/A	Y	All debris (Grades A and B) settled to the floor. Smaller debris rolled on the floor. None transported over the weir.
6	0.56	0.0	N/A	Y	Grade A debris was fully mixed. Grade B debris settled to the flume floor. They were not transported above the wier.

These tests were selected to represent all the conclusions drawn from the testing.

C.4 RESULTS OF THE STUDY

Figures 3 and 4 illustrate predicted flow patterns and turbulence levels for test case #1, corresponding to U_{tr} of 0.27 ft/s and no downcomer flow. The recirculating eddies shown in Figure 3 formed in the wake region of each downcomer. These eddies depart and sustain limited amounts of turbulence away from the last downcomer as shown in Figure 4. However, the turbulence levels were well below $1.25x10^{-3}$ ft^2/s^2. Although not shown here graphically, a similar trend was observed for Case 2, where once again the turbulence kinetic energy per unit mass values in most of the computational domain were well below $1.25x10^{-3}$ ft^2/s^2. The definition of the turbulence kinetic energy in ft^2/s^2 and rationale for selecting 1.25 x 10-3 ft^2/s^2 are explained in the following sections. However as the inlet velocity was increased to 1.0 ft/s, the turbulence levels increased beyond $1.25x10^{-3}$ ft^2/s^2; in fact, most of the test section was characterized by turbulence energies in excess of $1.25x10^{-3}$ ft^2/s^2 (see Figures 5 and 6).

Flow patterns and turbulence energy levels are plotted in Figures 7 through 10 for Cases 4 and 5. As shown in Figure 7 and 8, turbulence energy in Case 4 was higher than $1.25x10^{-3}$ ft^2/s^2, but lower than 1. $x10^{-2}$ ft^2/s^2. On the other hand, in Case 5 turbulence energy was higher than $1.3x10^{-2}$ ft^2/s^2 in the majority of the test geometry, especially in the mid-region where debris was added to the flume (see Figures 9 and 10).

Cases 6 and 7 are identical to Cases 1 and 2 except for the presence of the 12-inch high weir. As shown in Figure 13, this weir caused acceleration of the flow in the top regions of flume, whereas flow in the lower regioned remains at a fairly low velocity. As a result, in case 1 downstream of the flume, turbulent kinetic energy exceeded the $1.25x10^{-3}$ ft^2/s^2 required to entrain small debris. However, it was much lower than $1.25x10^{-3}$ ft^2/s^2 upstream of the weir. Although not shown here graphically, turbulence levels increased beyond 1.25x10-3 ft^2/s^2 as the flow velocity was increased to 0.56 ft/s in case 7.

Results of CFD simulations are summarized in Table 2 in terms of the turbulent kinetic energies observed corresponding to each case simulated. As shown in Table 2 turbulent energies in Cases 1, 2, and 6 are lower than $1.25x10^{-3}$ ft^2/s^2. In these case, all debris settled down to the floor of the flume. On the hand, in Cases 3, 4 and 7 turbulent energy is higher than $1.25x10^{-3}$ ft^2/s^2, but lower than 1.3 $x10^{-2}$ ft^2/s^2. In these cases, smaller debris became uniformly mixed with the water column, but the larger debris settled to the floor; where it often rolled on the floor but was not entrained and mixed with the

flow to be transported above a weir. Finally, in case 5 turbulent energy is larger than 1.3 $x10^{-2}$ ft^2/s^2 and, correspondingly, all debris was entrained.

Table C-2. Results of the CFD Simulation of Selected ARL Tests.

Case	U_{tr} (ft/s)	V_{dc} (ft/s)	Turb. K.E (ft^2/s^2)	Comments
1	0.27	0.0	$< 1.25x10^{-3}$	All debris settled to floor in ARL tests.
2	0.56	0.0	$< 1.25x10^{-3}$	All debris settled to floor in ARL tests.
3	1.00	0.0	$>1.25x10^{-3}$ $<1.4\ x10^{-2}$	Small debris mixed with flow. Large debris settled to floor.
4	0.27	2.7	$>1.25x10^{-3}$ $<1.4x10^{-2}$	Small debris mixed with flow. Large debris settled to floor.
5	0.56	5.5	$>1.4x10^{-2}$	All debris mixed with water column.
6	0.27	Weir	$<1.25x10^{-3}$	All debris settled to floor in ARL tests.
7	0.56	Weir	$>1.25x10^{-3}$ $<1.4\ x10^{-2}$	Small debris mixed with flow and was transported over the weir.

C.5 Interpretation of Results and Recommendation for Usage

As evident from the previous discussions, settling of debris is directly related to the local kinetic energy (ft^2/s^2) per unit mass, which is given as:

$$\text{K.E.} = \tfrac{1}{2}\, U^2_{rms}$$

where

U_{rms} = is root mean square of the turbulent velocity (ft/s)

This is a commonly used definition of kinetic energy [Ref. 4]. Kinetic mass per unit volume can be obtained by multiplying K.E. by density (p).

Table 3 compares the U_{rms} required to keep debris of a given size in suspension with their settling velocity in calm pool of water. As evident from that table, debris of a certain size remains suspended whenever flow U_{rms} is greater than or equal to its settling velocity in a calm pool of water. This is not a new finding, but confirms the validity of a widely-used criterion for the debris sizes of present interest.

For example, the general transport equation to estimate concentration of macro-particles in sludge pools or atmospheric plumes is:

$$dC/dt = - V_. C_o A_p/V_p$$

where

C is concentration (lbm/ft^3)

C_o is initial concentration (lbm/ft^3)

A_p is pool area for settling (ft^2)

V_p is pool volume (ft^3)

$V_.$ is settling velocity in turbulent flow (ft/s)

Turbulent settling velocity ($V_.$) is given as:

$V_. = (V_o - U_{rms})$ when $V_o > U_{rms}$

$= 0$ when $V_o \leq U_{rms}$

Table C-3. Turbulent K.E and U_{rms} Required to Keep Debris of Different Size Afloat.

Debris Size	V_o (ft/s)	Turbulent K.E. to keep in Suspension (ft^2/s^2)	Corresponding U_{rms} of flow (ft/s)
Small	0.05	$1.25x10^{-3}$	0.05
Medium	0.10-0.13	$1.4x10^{-2}$	0.10
3/16" Paint Chips	0.1	$1.4x10^{-2}$	0.10

This equation can be adopted for the application to predict transport on the drywell floor pool as discussed below:

1. Conduct CFD simulation of the pool formation by break overflow and drainage by vent pipes. Determine residual turbulence levels in the pool at different locations.
2. If turbulent kinetic energy is higher than $1.4x10^{-2}$ ft^2/s^2 over all or the majority of the pool volume, then assume that all small and large pieces would remain mixed with water and be transported to

the suppression pool. ARL data suggest that at these turbulence levels large pieces previously settled on the floor can also become re-entrained and transported over a weir.

3. If turbulent kinetic energy is higher than 1.25×10^{-3} ft^2/s^2 but lower than 1.4×10^{-2} ft^2/s^2 over all or majority of the pool volume, then assume that all smaller pieces would remain mixed with water and be transported to the suppression pool. ARL data suggest that at these turbulence levels small pieces previously settled on the floor can also become re-entrained and transported over a weir. Large pieces will likely be transported on the floor, but will not be transported over the Wiers or other obstructions.
4. For cases when turbulent kinetic energy is lower than that required to keep a debris class in suspension, allow for settling in that region after accounting for a) debris mass influx, b) turbulence (i.e., $V_t = (V_o - U_{rms})$), and c) debris mass outflow.

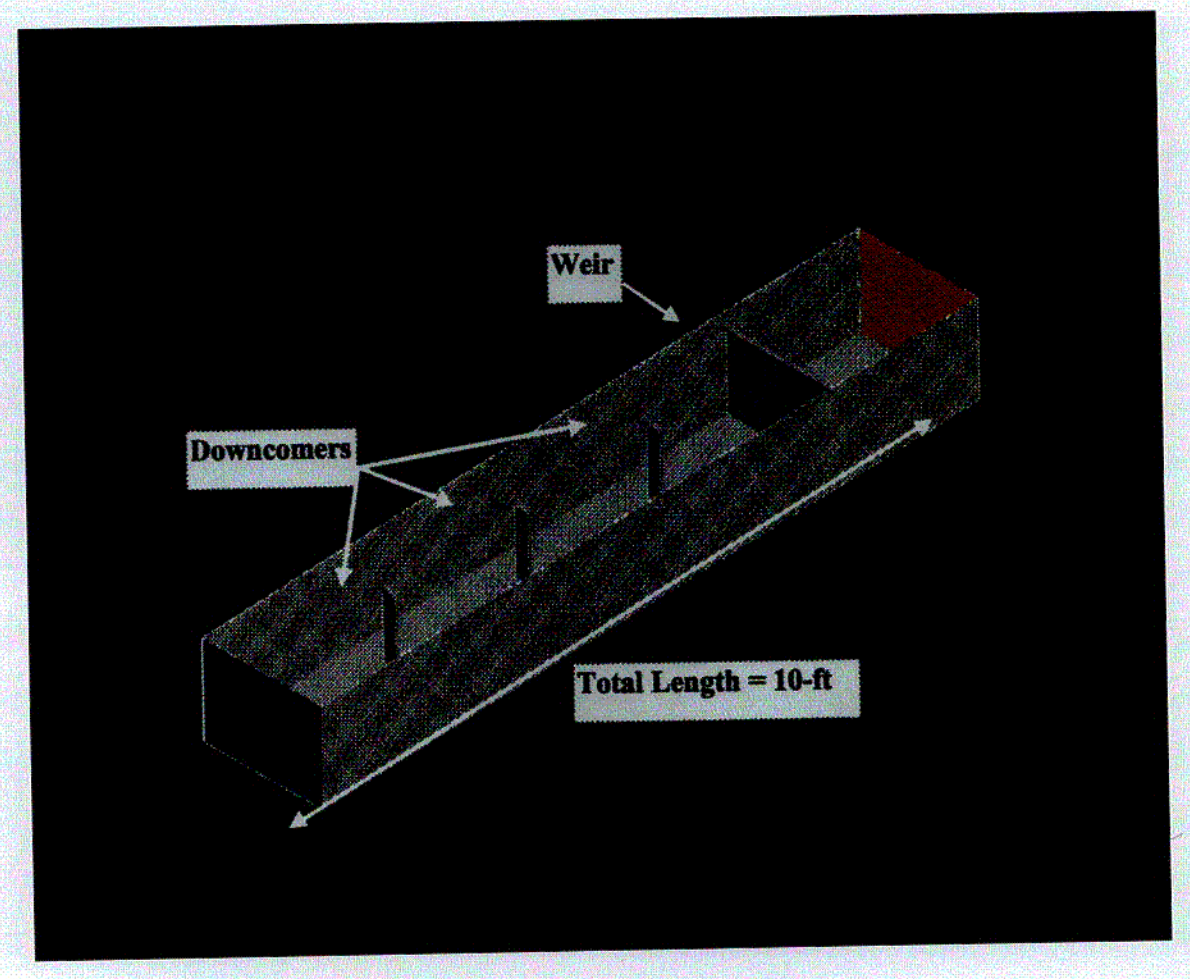

Figure 2. Schematic Illustration of the ARL Test Setup Simulated in the Study

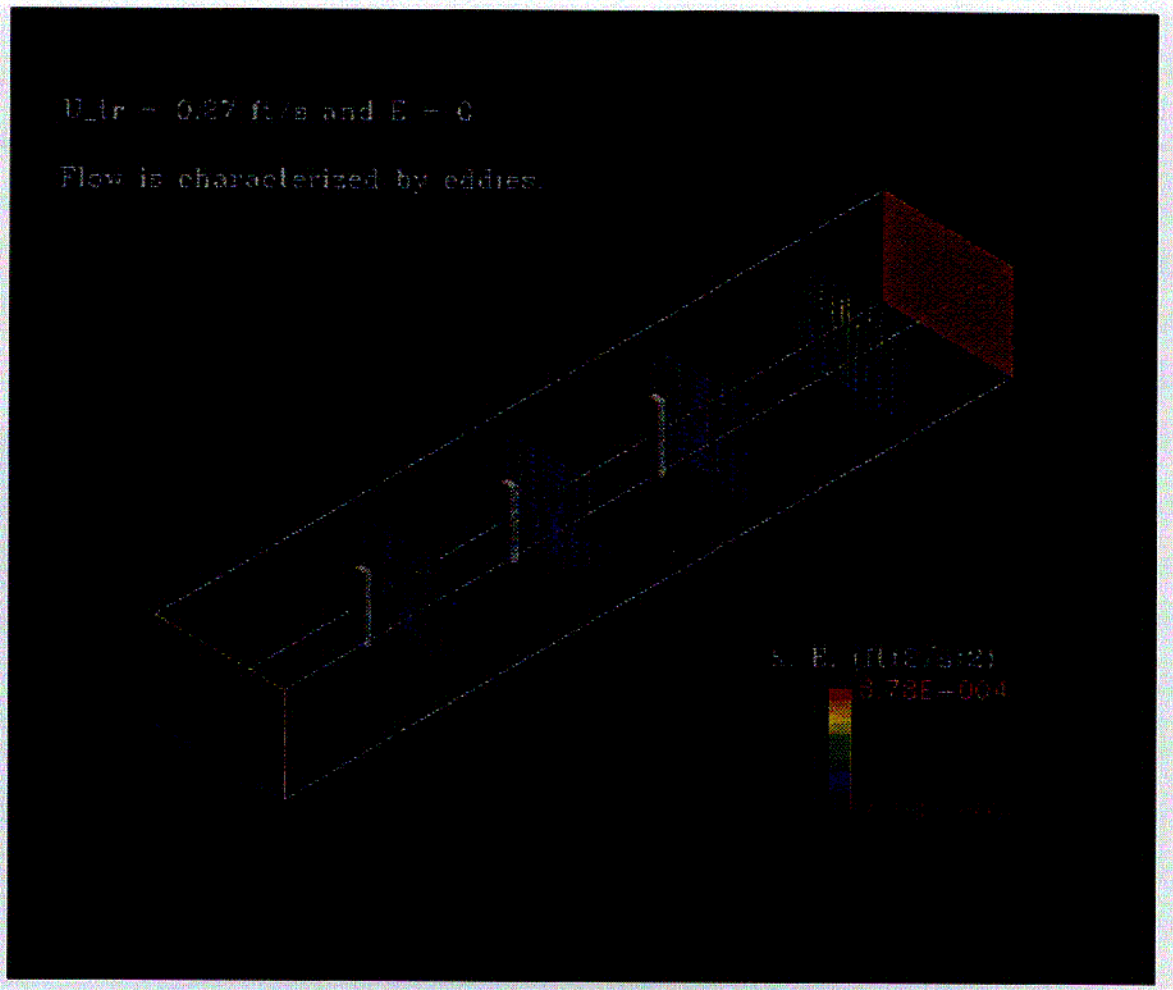

Figure 3. Predicted Flow Patterns for Case 1

C-32

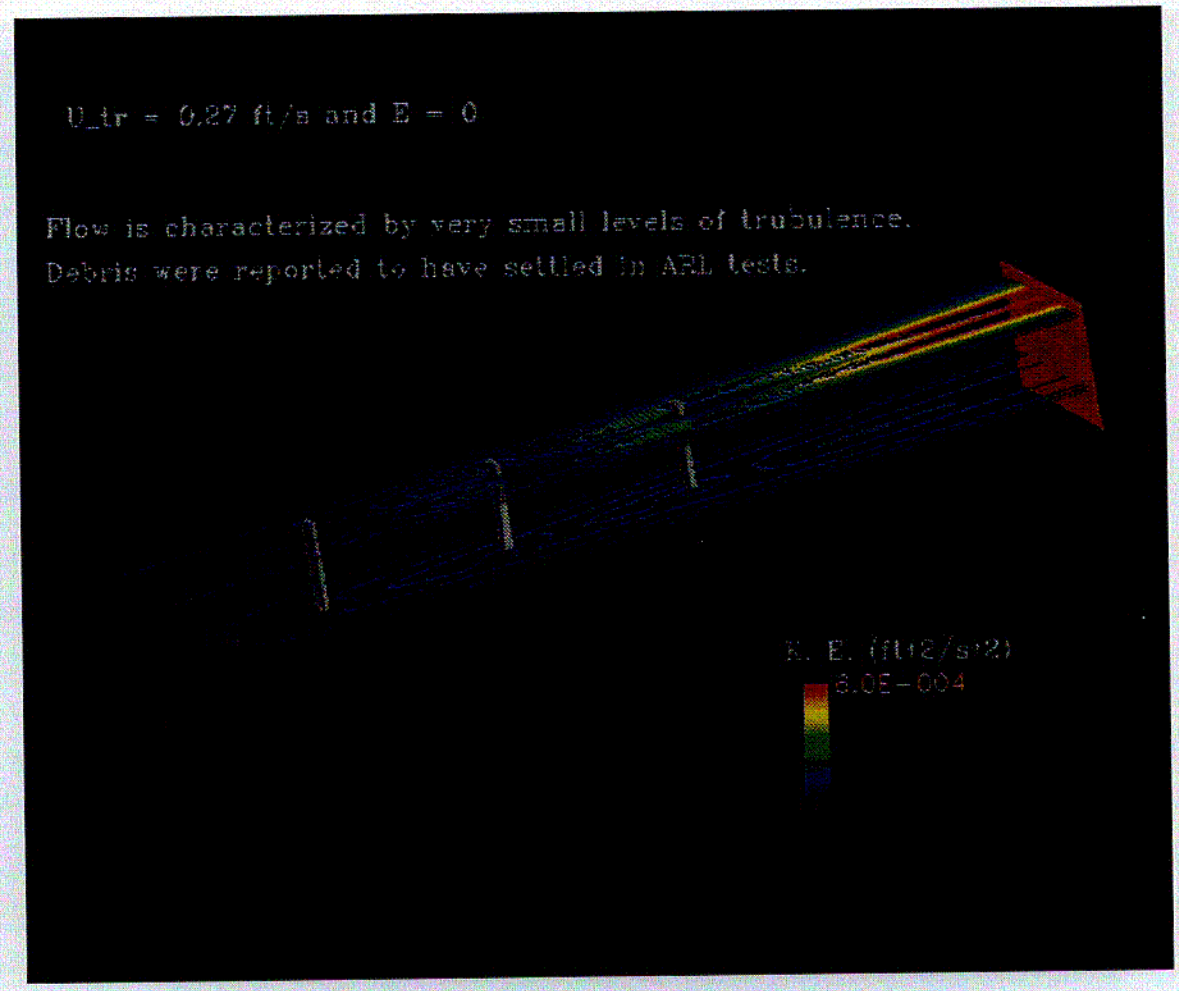

Figure 4. Kinetic Energy Contours for Two Selected Horizontal Planes

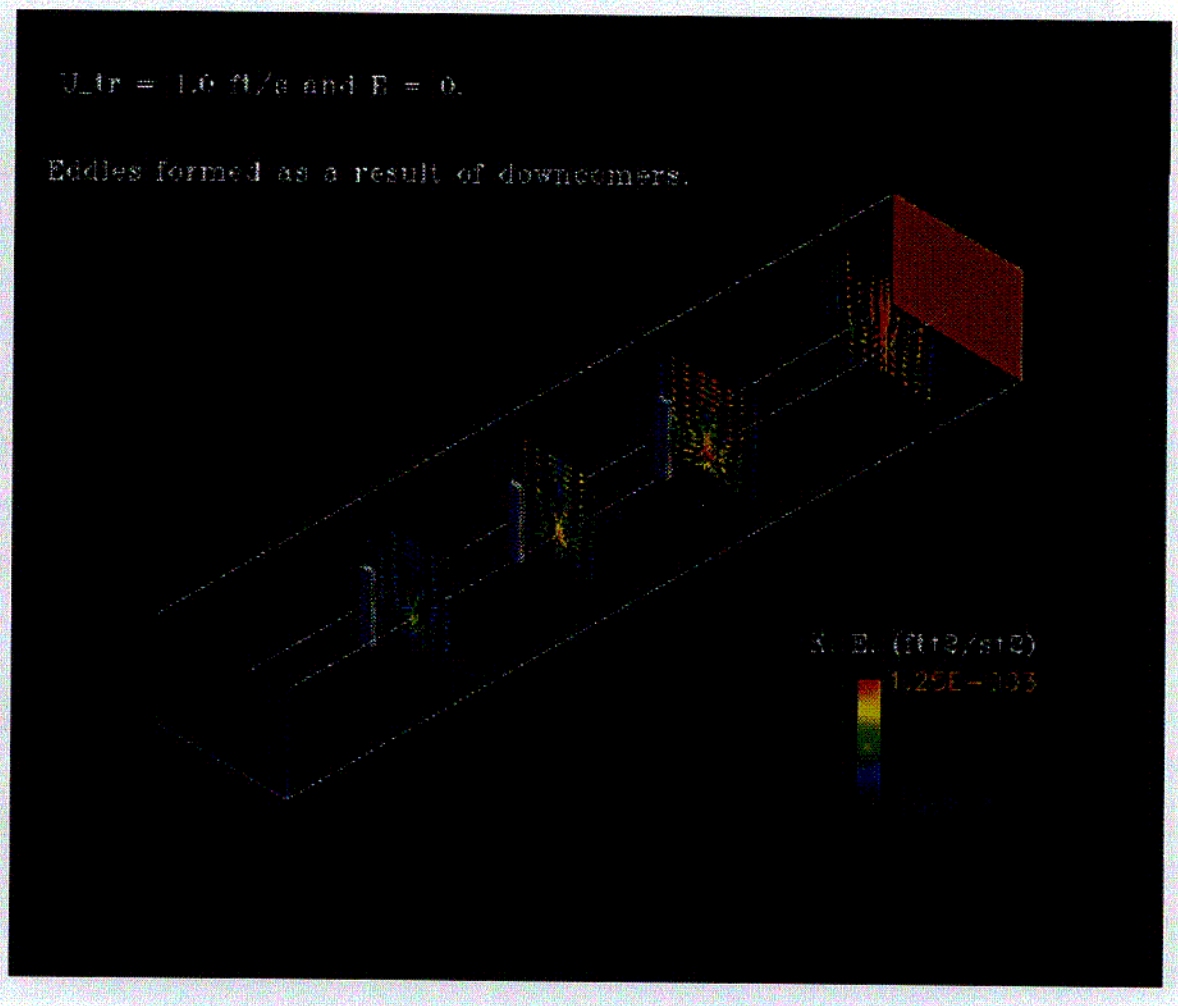

Figure 5. Flow Patterns Predicted for Case 3

C-34

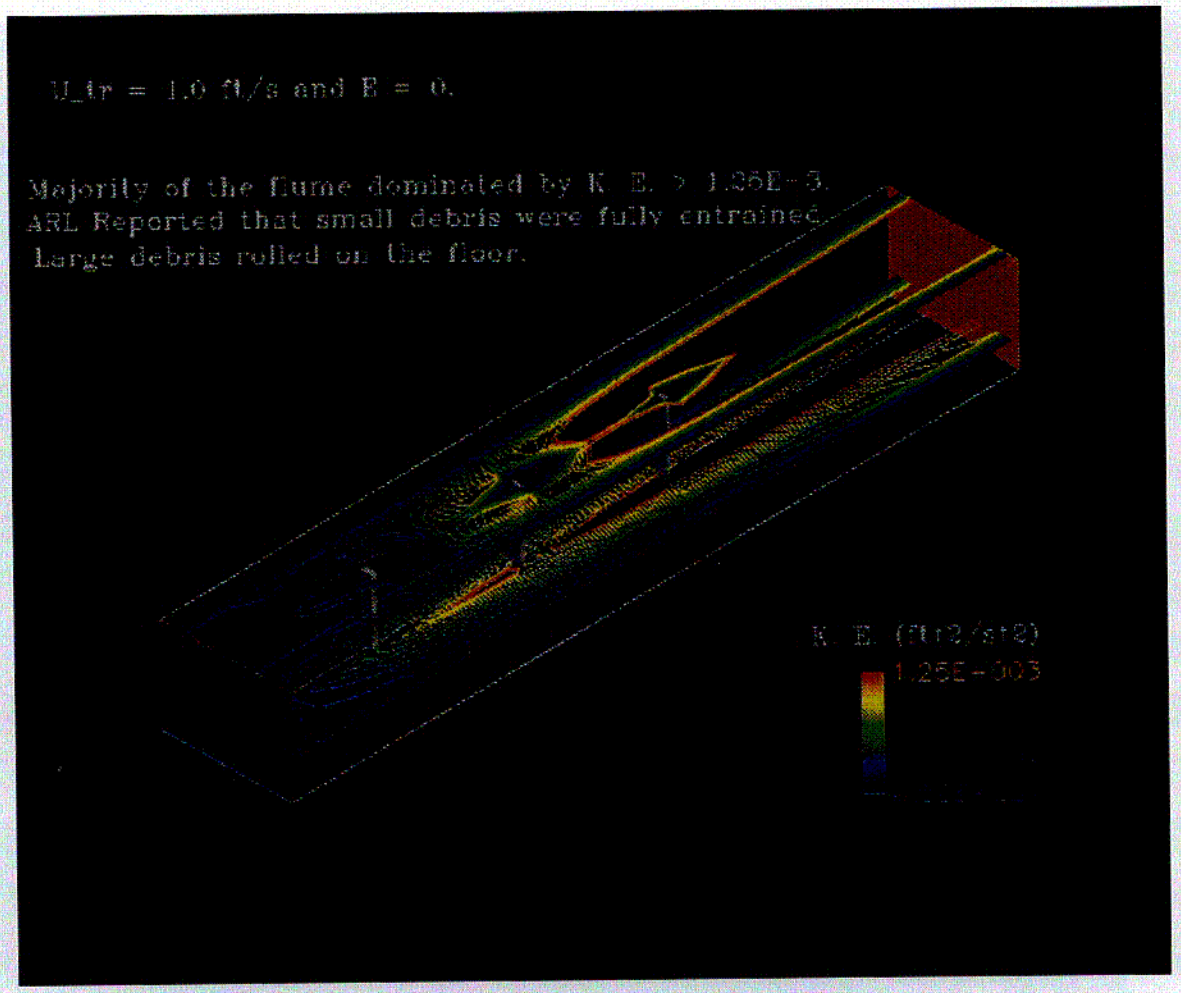

Figure 6. Kinetic Energy Contours for Two Selected Horizontal Planes for Case 3.

C-35

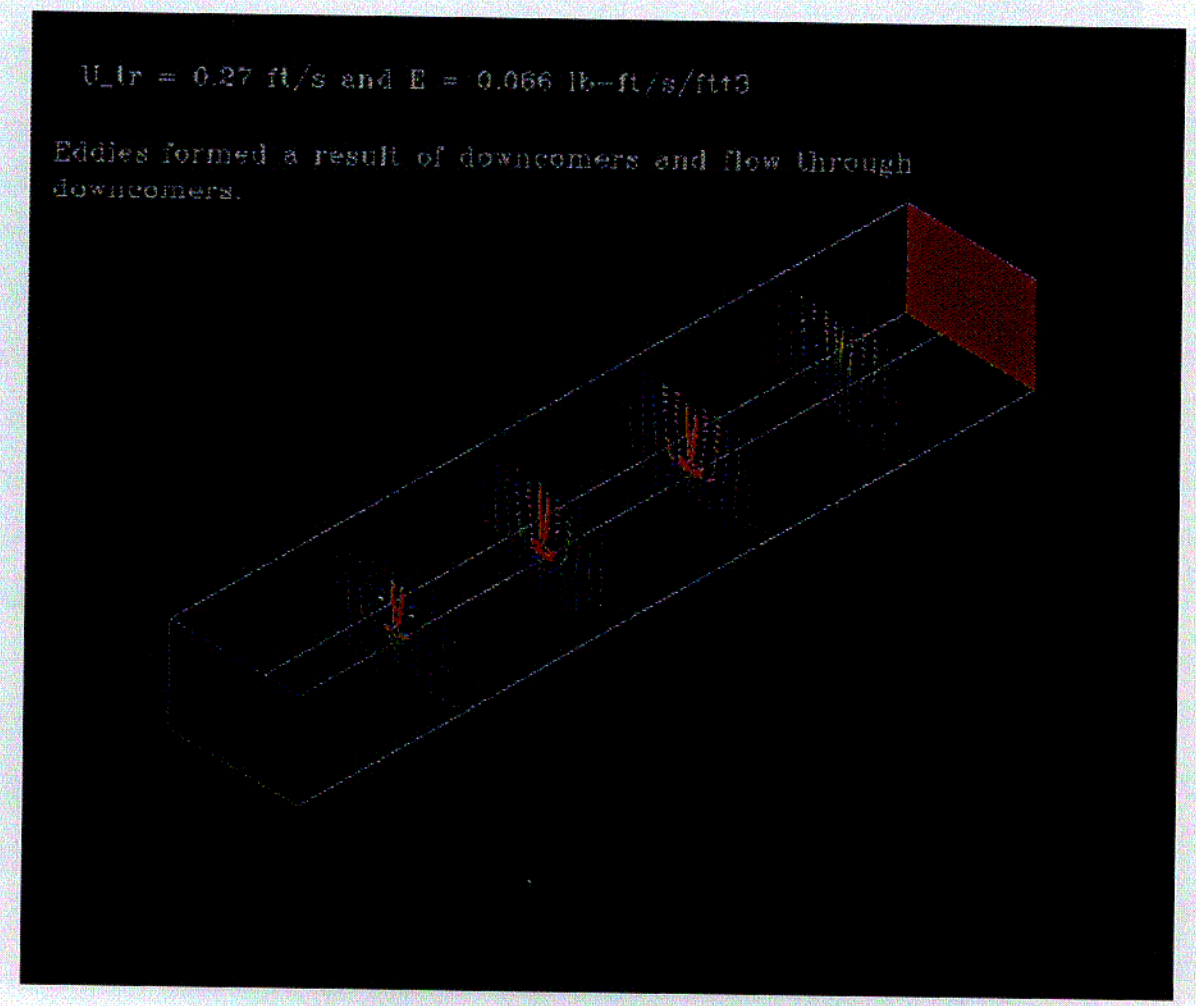

Figure 7. Flow Patterns Predicted for Case 4

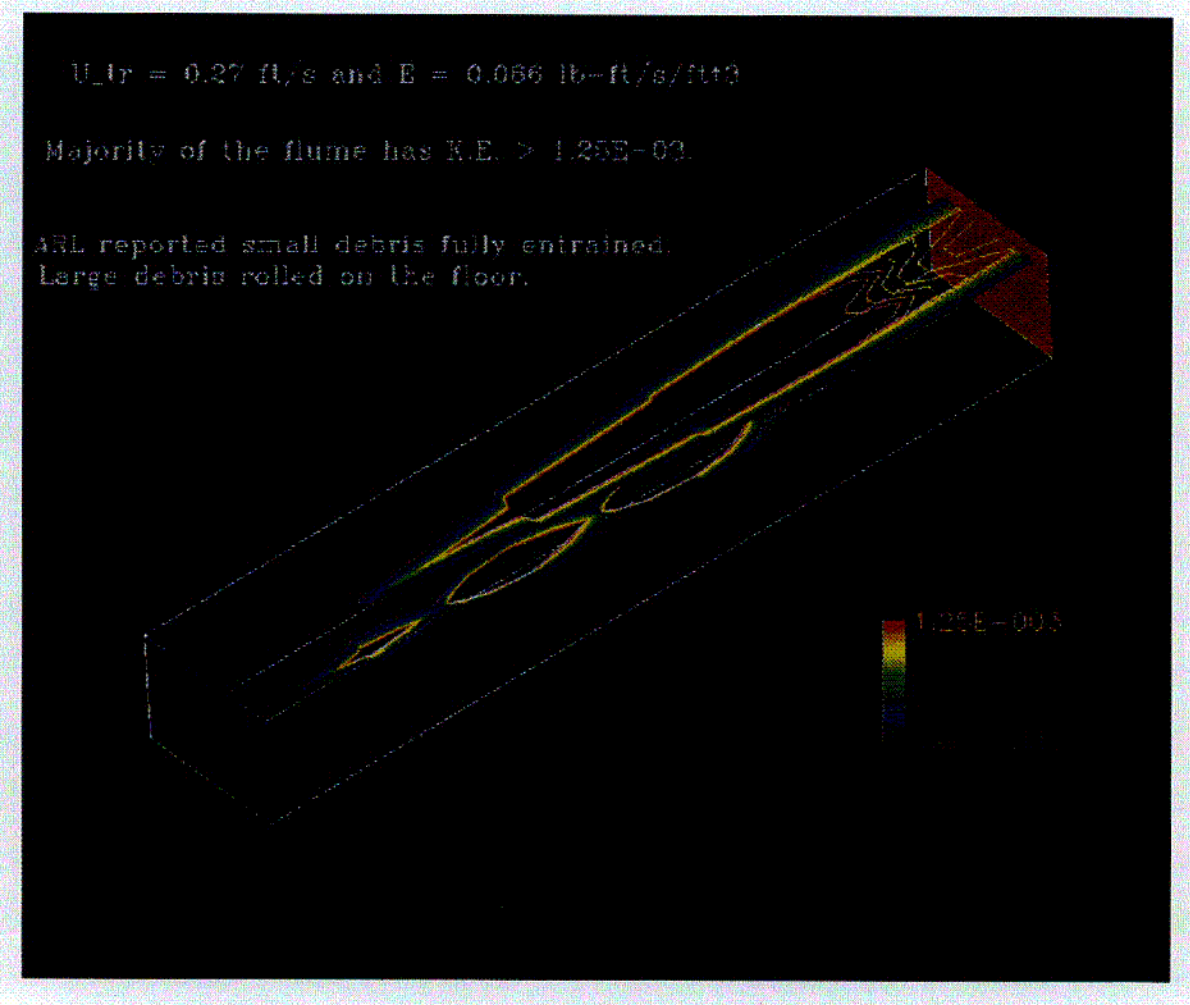

Figure 8. Kinetic Energy Contours for Two Selected Horizontal Planes for Case 4

C-37

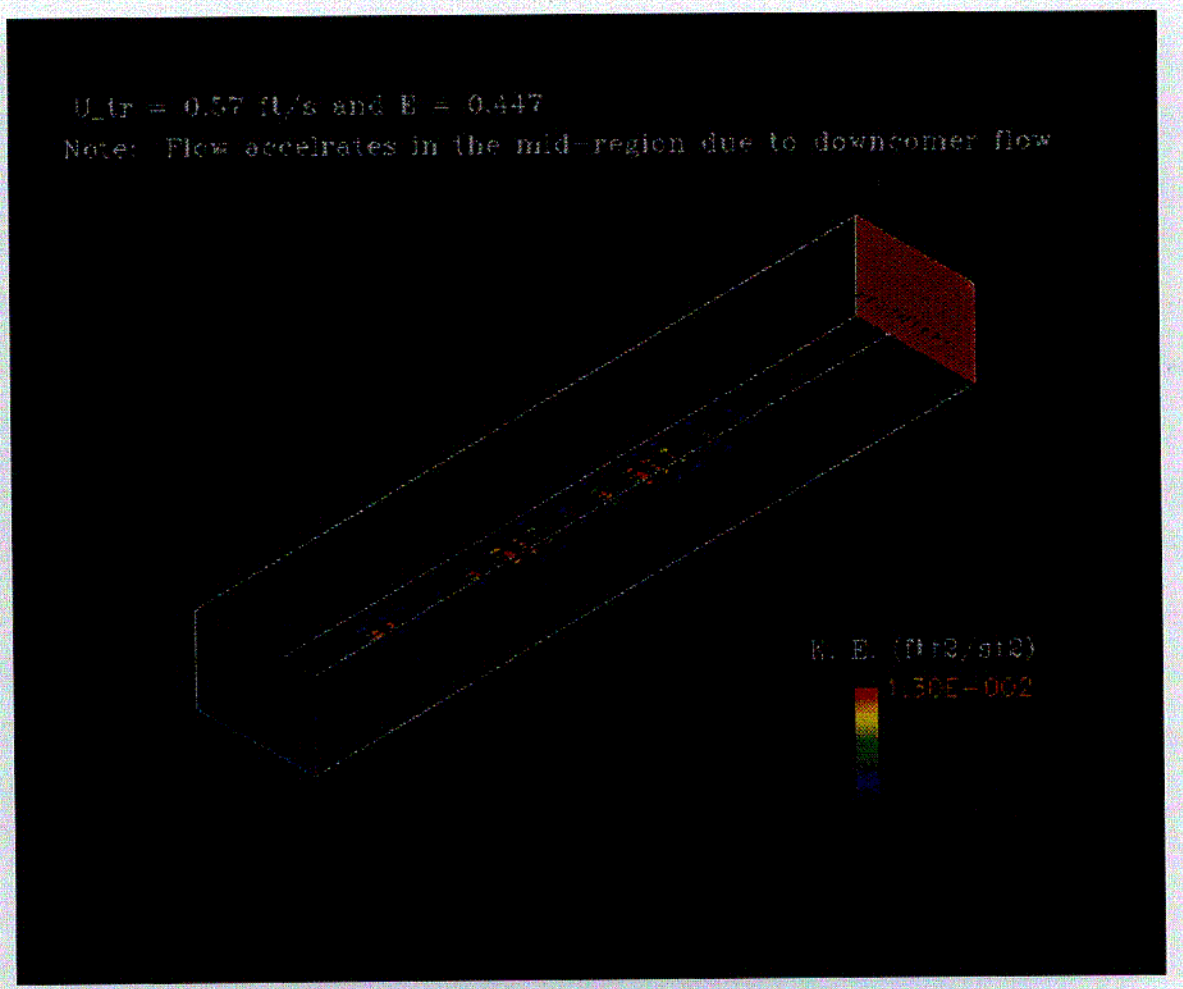

Figure 9. Flow Patterns Predicted for Case 5

C-38

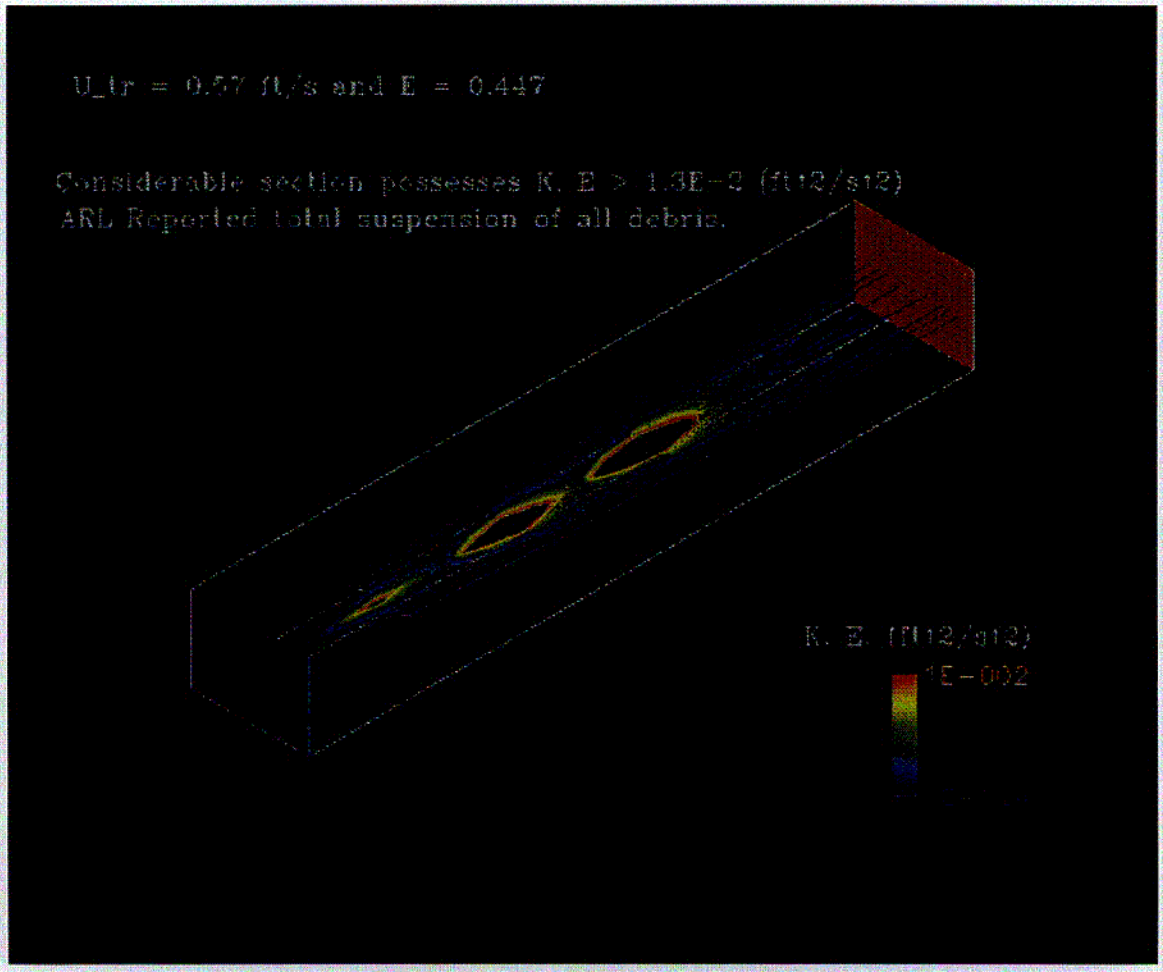

Figure 10. Kinetic Energy Contours for Two Selected Horizontal Planes for Case 5

C-39

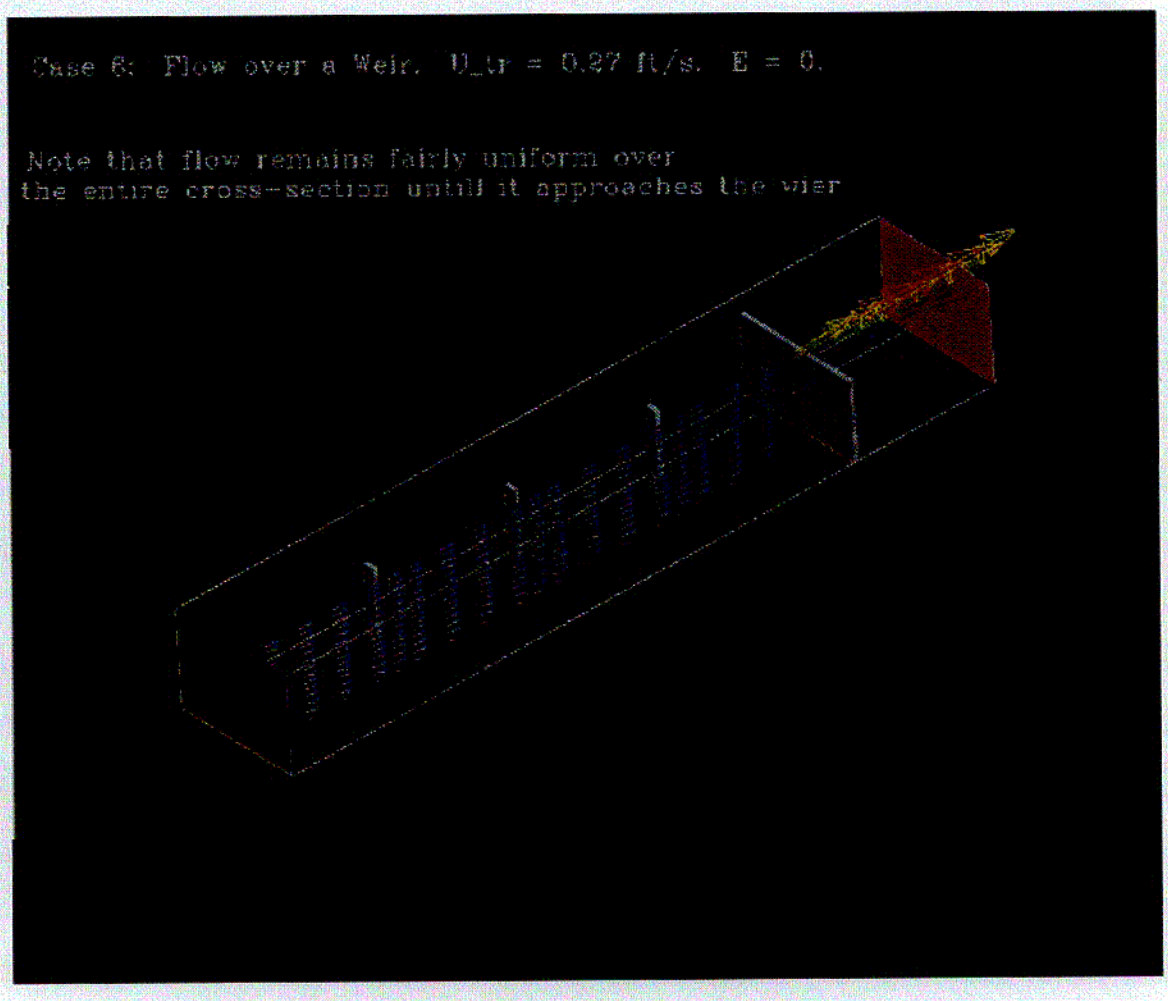

Figure 11. Flow Patterns Predicted for Case 6

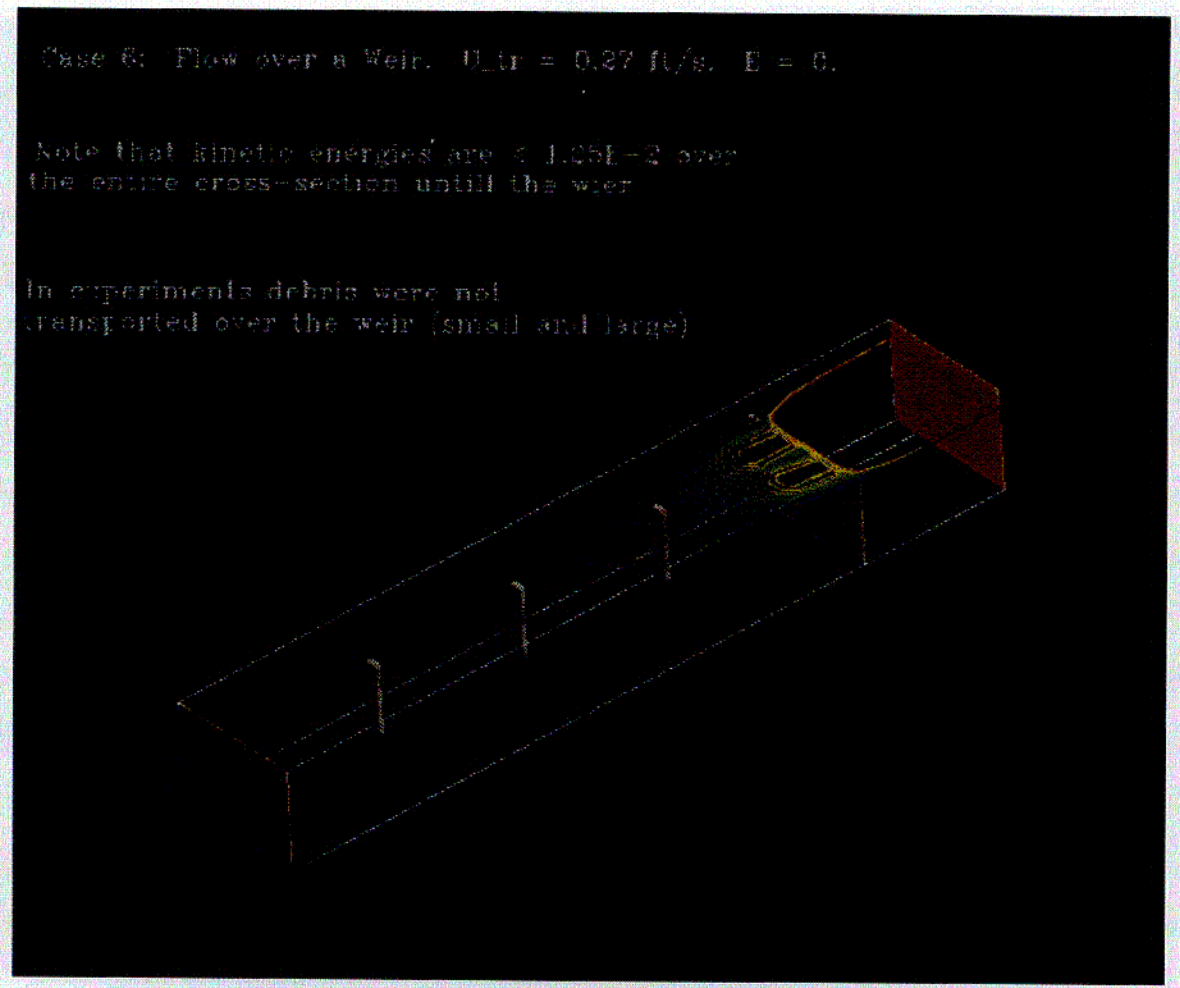

Figure 12. Kinetic Energy Contours for Two Selected Horizontal Planes for Case 6

REFERENCES

1. D. V. Rao and C. Shaffer, "Drywell Debris Transport Testing," Science and Engineering Associates, Inc., SEA 97-3105-A:8, May 1997.
2. K.W. Brinkman and P.W. Brady, "Results of Hydraulic Tests on ECCS Strainer Blockage and Material Transport in a BWR Suppression Pool," Pennsylvania Power & Light Company, EC-059-1006, Rev. 0, May 1994.
3. G. Zigler, J. Brideau, D. V. Rao, c. Shaffer, F. Souto, W. Thomas, "Parametric Study of the Potential for BWR ECCS Strainer Blockage Due to LOCA Generated Debris," NUREG/CR-6224, October 1995.
4. V. S. Arpaci and P. S. Larsen, "Convection Heat Transfer, Prentice-Hall, 1984.

NRC FORM 335 (2-89) NRCM 1102, 3201, 3202

U.S. NUCLEAR REGULATORY COMMISSION

BIBLIOGRAPHIC DATA SHEET

(See instructions on the reverse)

1. REPORT NUMBER (Assigned by NRC, Add Vol., Supp., Rev., and Addendum Numbers, if any.)

NUREG/CR-6369, Vol. 3
SEA 97-3105-A:17

2. TITLE AND SUBTITLE

Drywell Debris Transport Study: Computational Work

3. DATE REPORT PUBLISHED

MONTH	YEAR
September	1999

4. FIN OR GRANT NUMBER

W6325

5. AUTHOR(S)

C. Shaffer, D.V. Rao, and J. Brideau

6. TYPE OF REPORT

Final

7. PERIOD COVERED *(Inclusive Dates)*

8. PERFORMING ORGANIZATION - NAME AND ADDRESS *(If NRC, provide Division, Office or Region, U.S. Nuclear Regulatory Commission, and mailing address; if contractor, provide name and mailing address.)*

Science and Engineering Associates, Inc.
6100 Uptown Blvd. NE
Albuquerque, NM 87110

9. SPONSORING ORGANIZATION - NAME AND ADDRESS *(If NRC, type "Same as above"; if contractor, provide NRC Division, Office or Region, U.S. Nuclear Regulatory Commission, and mailing address.)*

Division of Engineering Technology
Officeof Nuclear Regulatory Research
U.S. Nuclear Regulatory Commission
Washington, DC 20555-0001

10. SUPPLEMENTARY NOTES

M. Marshall, NRC Project Manager

11. ABSTRACT *(200 words or less)*

This report describes various analyses conducted as part of the drywell debris transport study. The primary objective of these analyses was to identify controlling phenomena and critical data requirements. A secondary objective was to explore various options available to model debris transport in the drywell, and make judgements regarding the degree of accuracy to which each phenomenon should be modeled. These analyses decomposed the problem into several components that were amenable to resolution by well-proven analytical models. The analyses specific ally addressed the following phenomena that significantly impact debris transport: pressure vessel blowdown, containment th ermal-hydraulics (e.g., structural wetness, flow velocities in the drywell), debris removal by various capture mechanisms and de bris transport in the water pools formed on the drywell floor. The analytical tools used in the study included RELAP, MELCOR a nd CFD-2000. The results of sòme of the analyses were used tọ design the experiments conducted as part of the study and during the debris transport quantification process described in NUREG/CR-6369, Vol2.

12. KEY WORDS/DESCRIPTORS *(List words or phrases that will assist researchers in locating the report.)*

BWR Suction Strainers
Drywell Debris Transport
Analytical Models
Computational Fluid Dynamics

13. AVAILABILITY STATEMENT

unlimited

14. SECURITY CLASSIFICATION

(This Page)

unclassified

(This Report)

unclassified

15. NUMBER OF PAGES

16. PRICE

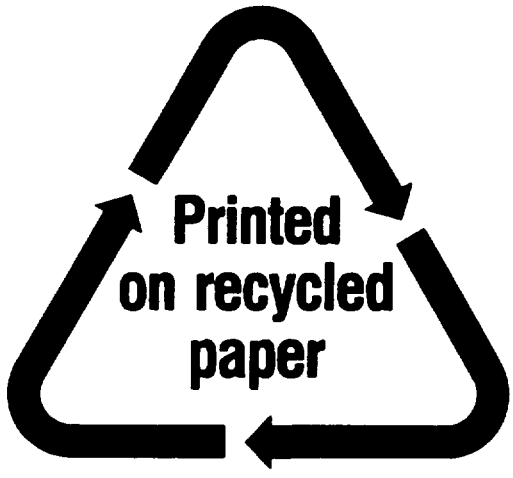

Federal Recycling Program

ISBN 0-16-050194-6

UNITED STATES
NUCLEAR REGULATORY COMMISSION
WASHINGTON, DC 20555-0001

OFFICIAL BUSINESS
PENALTY FOR PRIVATE USE, $300

SPECIAL STANDARD MAIL
POSTAGE AND FEES PAID
USNRC
PERMIT NO. G-67